論文 / 著書情報
Article / Book Information

題目(和文)	
Title(English)	SAR Matrix-Assisted Design of Curcumin Derivatives as Amyloid β Inhibitors and Their Application to MRI Contrast Agents for Alzheimer ' s Disease
著者(和文)	UTOMORohmad Yudi
Author(English)	Rohmad.Yudi Utomo
出典(和文)	学位:博士(理学), 学位授与機関:東京工業大学, 報告番号:甲第11729号, 授与年月日:2022年3月26日, 学位の種別:課程博士, 審査員:中村 浩之,田中 克典,西山 伸宏,堤 浩,藤枝 俊宣,赤間 啓之,岡田 智
Citation(English)	Degree:Doctor (Science), Conferring organization: Tokyo Institute of Technology, Report number:甲第11729号, Conferred date:2022/3/26, Degree Type:Course doctor, Examiner:,,,,,,
学位種別(和文)	博士論文
Type(English)	Doctoral Thesis

Doctoral Thesis

SAR Matrix-Assisted Design of Curcumin Derivatives as Amyloid β Inhibitors and Their Application to MRI Contrast Agents for Alzheimer's Disease

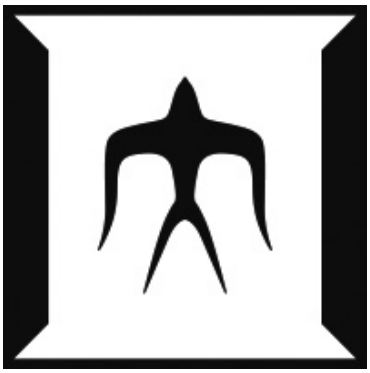

Tokyo Institute of Technology
Department of Life Science and Technology

Rohmad Yudi Utomo

Academic Supervisors: Prof. Hiroyuki Nakamura and
Assoc. Prof. Satoshi Okada

TABLE OF CONTENTS

Abbreviations

AD	Alzheimer`s disease
AICD	APP intracellular domain
APP	amyloid precursor protein
Aβ	amyloid β
$A\beta_{40}$	Aβ with 40 amino acids
$A\beta_{42}$	Aβ with 42 amino acids
BBB	blood brain barrier
CR	congo red
CTFα	C-terminal APP fragment α
CTFβ	C-terminal APP fragment β
DCC	Dicyclohexylcarbodiimide
DMAP	N,N dimethyl amino pyridine
DMEM	dulbecco's modified eagle medium
DMF	N,N dimethylformamide
DMSO	N,N dimethylsulfoxide
DOTA	1,4,7,10-tetraazacyclododecane-1,4,7,10-tetraacetic acid
DTPA	diethylenetriaminepentaacetic acid
EGCG	epigallocatechin gallate
FDA	Food Drug Administration
Gd	Gadolinium
Gd-DOTA	Gd(III)-1,4,7,10-tetraazacyclododecane-1,4,7,10-tetraacetic acid
Gd-DTPA	Gd(III)-diethylene triamine pentaacetic acid
h	hour
HCl	hydrochloric acid
HOBt	hydroxybenzotriazole
HPLC	high performance liquid chromatography
HRMS	high resolution mass spectrometry
ICD-10	international classification of disease
IVIS	in vivo imaging system
J	coupling constant
LRMS	low resolution mass spectrometry

μ	micro
M	moles per liter
MeCN	acetonitrile
MGM	molecular grid map
min	minute
MNPs	magnetic nanoparticles
MRI	magnetic resonance imaging
MTT	3-(4,5-dimethyl-2-thiazolyl)-2,5-diphenyl-2H-tetrazolium bromide
MW	microwave
NaOH	sodium hydroxide
NIA	nanoimaging agent
NMR	nuclear magnetic resonance
PAINS	pan assay interference compounds
PET	positron emission tomography
PiB	Pittsburgh compound B
PLMA	polymalic acid
QSAR	quantitative structure activity relationship
r_1	T_1 relaxivities
RPMI	roswell park memorial institute
s	second
sAPPα	soluble APPα
sAPPβ	soluble APPβ
SARM	structure activity relationship matrix
T_1	longitudinal relaxation time
TEM	transmission electron microscopy
TFA	trifluoroacetic acid
ThT	thioflavin t
UV	ultraviolet

List of Publication

Paper

1. **Utomo RY,** Asawa Y, Okada S, Ban HY, Yoshimori A, Bajorath J, Nakamura H. *Bioorg. Med.Chem.* **2021**, 46, 116357.
2. **Utomo RY,** Okada S, Sumiyoshi A, Aoki I, Nakamura H. *RSC Adv.* **2022**. 12, 5027-5030
3. **Utomo RY**, Sugie A, Okada S, Miura K, Nakamura H, *Chem. Commun.* **2022**. **2022**. 58, 2576 - 2579

Conferences

1. Novel Curcumin Derivatives Generated from SAR Matrix Possess as Amyloid βInhibitors
   Rohmad Yudi Utomo, Yasunobu Asawa, Shinichi Sato, Atsushi Yoshimori, Hiroyuki Nakamura
   日本薬学会第 140 年会, March 2020
2. Novel Curcumin Derivatives Generated from SAR Matrix Possess as Amyloid β Inhibitors for Alzheimer`s Disease
   Rohmad Yudi Utomo, Yasunobu Asawa, Atsushi Yoshimori, Hiroyuki Nakamura
   第 64 回日本薬学会関東支部大会（オンライン）, September 2020
3. Development of curcumin-based amyloid β aggregation inhibitors for Alzheimer's disease using the SAR matrix-approach
   Rohmad Yudi Utomo, Yasunobu Asawa, Satoshi Okada, Atsushi Yoshimori, Jürgen Bajorath, and Hiroyuki Nakamura
   International Conference on Chemical and Biological Sciences (ICCBS 2021), virtual, February 2021
4. Discovery of Curcumin-based Inhibitor of Amyloid β Aggregation for Alzheimer's disease using the SAR matrix approach
   Rohmad Yudi Utomo, Yasunobu Asawa, Satoshi Okada, Hyun Seung Ban, Atsushi Yoshimori, Jürgen Bajorath, Hiroyuki Nakamura
   11 回 CSJ 化学フェスタ 2021, virtual, October 2021
5. Discovery of Curcumin-Based Compounds as Amyloid β Inhibitors and Application to MRI Contrast Agents for Alzheimer`s Disease
   Rohmad Yudi Utomo, Satoshi Okada, Akira Sumiyoshi, Yasunobu Asawa, Hyun Seung Ban, Atsushi Yoshimori, Ichio Aoki, Jürgen Bajorath, Hiroyuki Nakamura
   The 7th ICPAPS 2021 and the 12th Annual Conference of ISCC, virtual, November 2021

Chapter 1
Introduction

Chapter 1. Introduction

1.1. Role of Amyloid β on Alzheimer`s Disease

Since the first report by a neuroanatomist Alois Alzheimer in 1906, Alzheimer`s disease has become one of the five primary diseases among people over 65 years old. It is predicted that the number of worldwide cases will increase from 47 million in 2015 to 132 million in 2050.[1,2] Several pathophysiological changes, such as gradual decrease of memory ability, cognitive behavior, and maintenance of daily life, are associated with the common symptom of AD.[3] The severity of AD affects the social finance of individuals and their families. It is expected that people with AD require a cost of care of up to 305 billion dollars.[4] Realizing this serious problem, several researchers worldwide try to elucidate the main cause of AD and its possible solutions.

Recent studies found the neuropathological changes involving amyloid β (Aβ) peptides contribute to the progression of AD. At physiological concentrations, Aβ modulates the nearby neuronal communication by selectively suppressing the transmission of excited synapses.[5] The precursor of Aβ, amyloid precursor protein (APP), controls the neuronal concentration of Aβ through the amyloidogenic pathway after sequential proteolysis by β-secretase and γ-secretase (Figure 1-1A). APP also undergoes a non-amyloidogenic pathway producing P3 as the response of neuronal activity through activation of the acetylcholine receptor. From the amyloidogenic proteolytic pathway, Aβ with 40 amino acids ($A\beta_{40}$) becomes the primary product while Aβ with 42 amino acids ($A\beta_{42}$) is in less concentration but possesses higher toxicity (Figure 1-1B).[6] In AD patients, the mutation of the APP gene leads to overproduction of Aβ. Furthermore, misfolded Aβ continuously aggregates into oligomers, protofibrils, and fibrils, causing extracellular senile plaques (Figure 1-1C).[7] The typical aggregation characteristic of Aβ is later indicated as the major cause of AD, which causes neurotoxicity, glial cells inactivation, and synaptotoxicity.

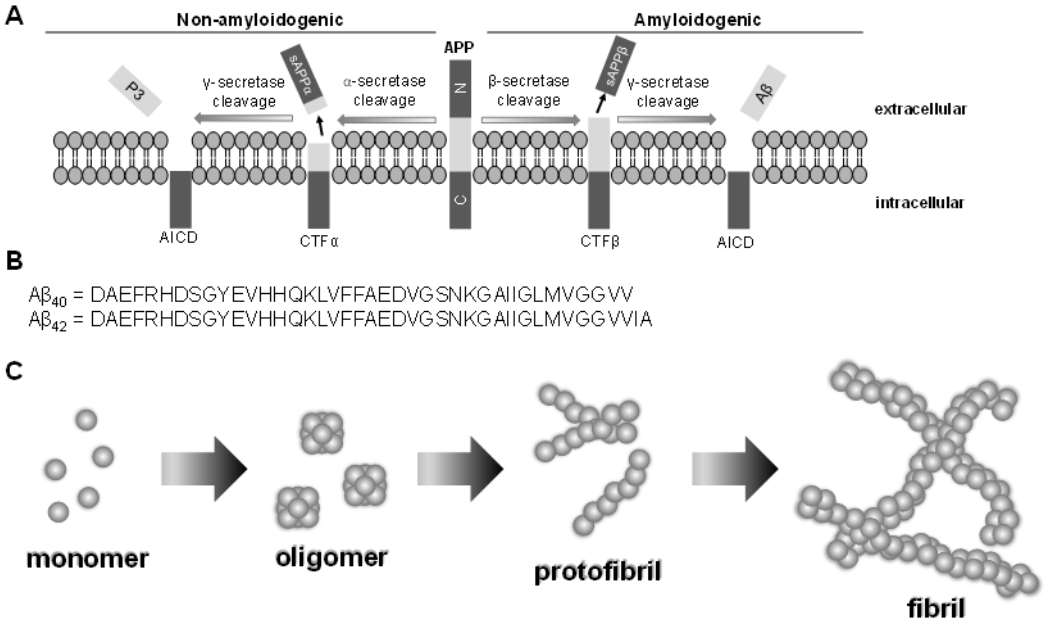

Figure 1-1. (A) Proteolytic process of human APP in neurons through the amyloidogenic and non-amyloidogenic pathway. Proteolysis of APP during amyloidogenic pathway is modulated by β-secretase to produce soluble APPβ (sAPPβ) and C-terminal APP fragment β (CTFβ), which undergoes further cleavage by γ-secretase producing Aβ and APP intracellular domain (AICD). In the non-amyloidogenic pathway, α-secretase cleaves APP producing soluble APPα (sAPPα) and C-terminal APP fragment α (CTFα) followed by the cleavage by γ-secretase to obtain P3 and AICD. (B) The full sequence of two major forms of Aβ. (C) Aggregation process of Aβ.

1.2. Drugs Targeting Aβ

Treatments of AD nowadays mainly use five approved drugs by the FDA, which sustain acetylcholine for synaptic transmission. The efficacy of those drugs however only relieves the symptoms but not overcoming the main cause of AD such as Aβ.[9] In this context, drugs targeting the leading cause of AD, such as Aβ, promote potential approaches. Despite its potency, many Aβ-targeting drugs are still in clinical trials.[2] Recently, a monoclonal antibody, aducanumab, developed by Biogen, has been approved by FDA to selectively recognize the Aβ fibrils and trigger a phagocytosis process for the removal. In clinical trials, high doses of aducanumab also improve cognitive impairment.[10,11] Beside aducanumab, other monoclonal antibodies such as solanezumab and bapineuzumab still face several

obstacles related to selectivity towards monomeric Aβ or other aggregates that affect its effectivity.[12,13] The enormous size of monoclonal antibody could also limit brain penetration which need further improvements.

The use of small molecules targeting Aβ is also potentially more eligible than macromolecules such as monoclonal antibodies in terms of brain permeability and the cost of long-term treatment of AD.[14] One of the action mechanisms by small molecules is related to inhibiting the Aβ aggregation. A pharmaceutical company, Daiichi-Sankyo Co., screened from an in-house library of 113,000 compounds and found RS0406 (Figure 1-2) inhibiting the Aβ aggregation by disrupting its misfolded β-sheet structure and improving the behavioral deficits *in vivo*.[15,16] However, results of further clinical trials of this compound have not yet been reported. Another company, Alzheon Inc., introduced ALZ-801 (Figure 1-2), the prodrug of tramiprosate, as the stabilizer of Aβ monomer to inhibit aggregations.[17] The phase III clinical trial of ALZ-801 is currently ongoing with promising pharmacokinetics and tolerability results.[18] Important notes for the current inhibitor candidates are the use of relatively high concentrations (±10 μM for *in vitro* and ±200 mg for clinical), which requires more improvements.

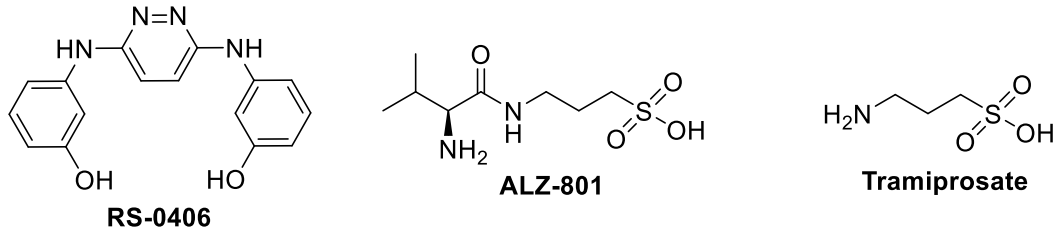

Figure 1-2. The chemical structures of the reported inhibitors of Aβ aggregations

Removing existing Aβ fibril also provides strategic treatments because large size aggregates are already observed in most AD patients.[19] Small molecules could remove the large size aggregates by inducing Aβ disaggregation into non-toxic smaller aggregates.[20] A natural compound, epigallocatechin gallate (EGCG), is the pioneer compound with Aβ disaggregation effect, which remodels the fibril into small spherical shape Aβ.[21] However, the clinical trial of EGCG shows limited efficacy with individual side effects.[22] The other candidate is resveratrol (Figure 1-

3) which remodels the Aβ fibril into disordered aggregates.[23] Although resveratrol shows promising pharmacokinetics and tolerability results, it also shows limited efficacy in clinical trials.[24,25] Considering this obstacle, finding more potent inducers of Aβ disaggregation is highly required.

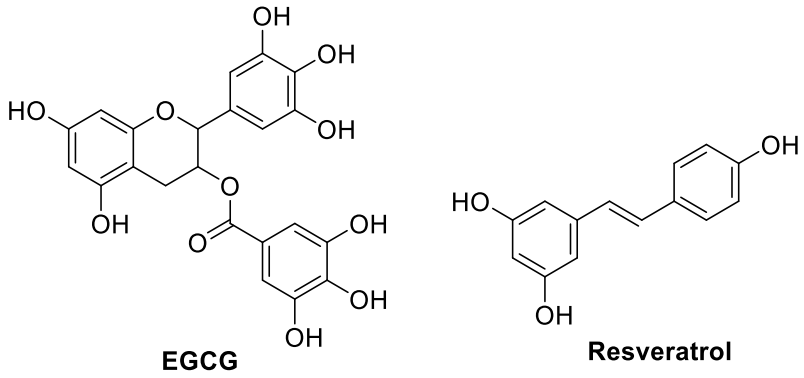

Figure 1-3. The chemical structure of the reported inducer of Aβ disaggregation

1.3. Gadolinium-based MRI Contrast Agents Targeting Aβ

Previously, the initial diagnosis of AD relied on fulfilling certain criteria as laid out in the International Classification of Disease (ICD-10), which could give presumptive results, and the definite diagnosis is only achieved until post-mortem examination.[26] Following the recent finding of several biomarkers such as Aβ, numerous imaging system was developed. Positron emission tomography (PET) emerges as a bioimaging technique that sensitively and selectively detects Aβ.[27] Several Aβ-specific ^{11}C and ^{18}F labeled PET tracers such as Pittsburgh compound B (PiB), Flumetamol, Florbetapir, and Florbetaben containing have been approved by FDA and EMA which sensitively detect Aβ deposition localized in the cerebral cortex.[28] Despite its promising Aβ detection, PET imaging limits the requirement of special equipment for radiotracer, challenging linking of isotope, and high negative predictive value.[27]

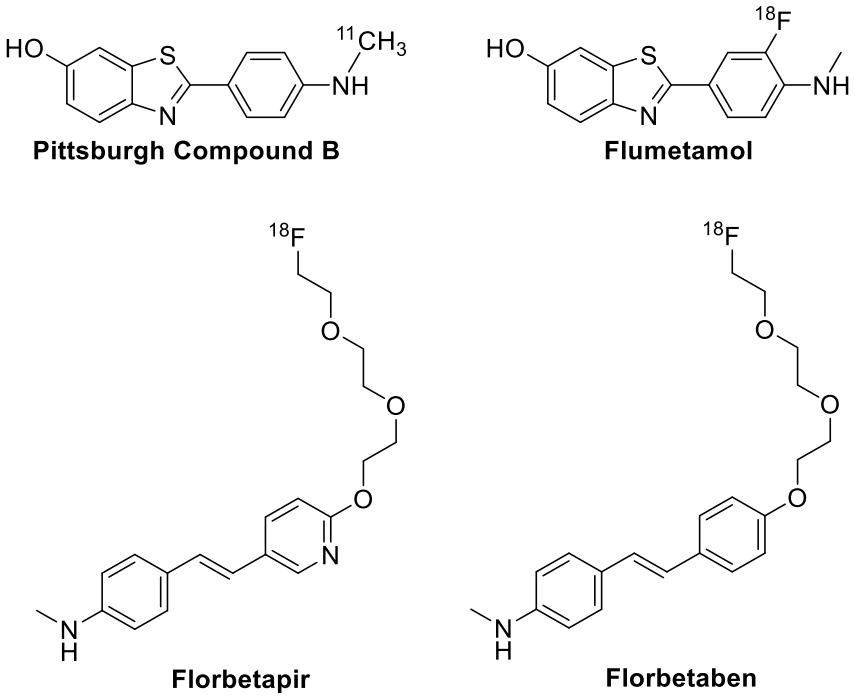

Figure 1-4. The chemical structure of reported Aβ-targeted PET ligands

Magnetic resonance imaging (MRI) is generally more accessible than PET because no radiotracer is required. The mechanism of MRI is based on the NMR relaxation of water protons.[29] Soft tissue such as brain, contains high amount of water as the main source of proton atoms making MRI is suitable for imaging the brain anatomy. Compared to other elements, Gadolinium (Gd) serves as the most commonly used MRI contrast agent due to the largest number of unpaired electrons, which efficiently decreases longitudinal relaxation time (T_1) of water protons (Figure 1-5A).[30] According to the Solomon-Bloembergen-Morgan Theory, Gd contrast agents binding to macromolecules show a slower molecular tumbling rate and can produce lower T_1 and contrast enhancement in T_1-weighted MRI (Figure 1-5B).[30]

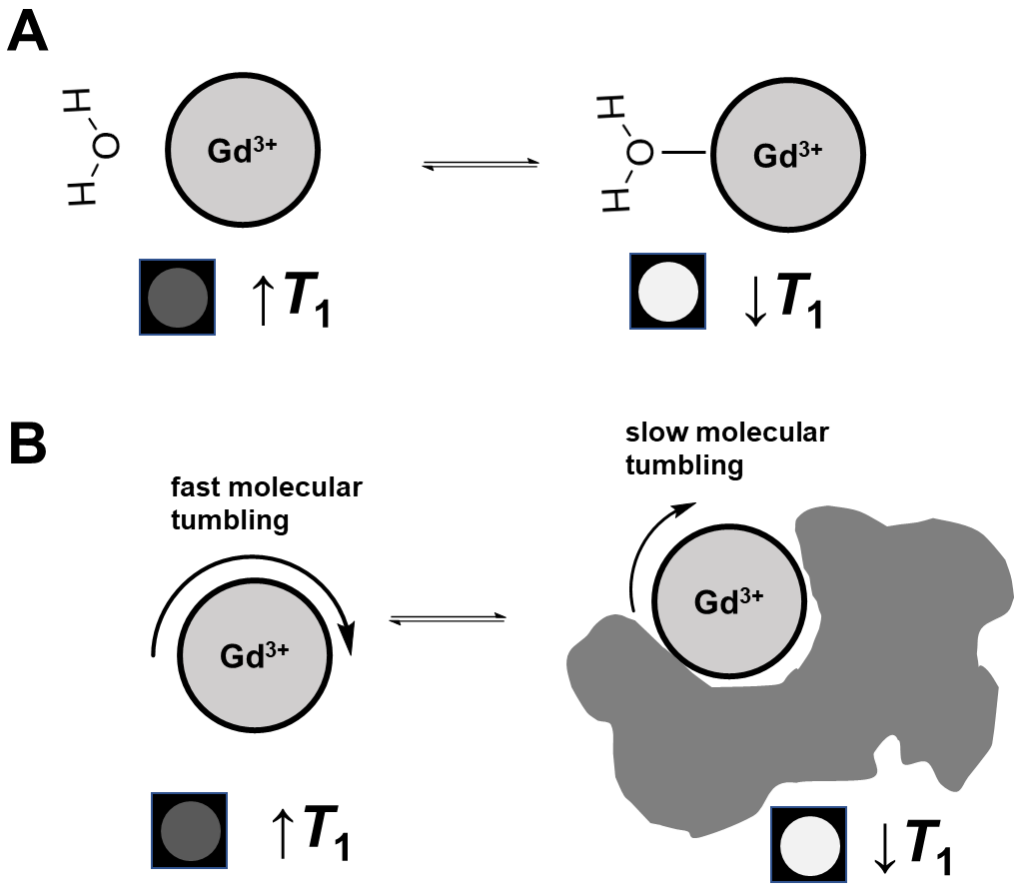

Figure 1-5. The hydration number of Gd ion (A) and slower molecular tumbling rate of Gd binding to a macromolecule (B) affect the T_1 value and MRI contrast

Because free Gd ions show significant toxicity, Gd-chelate complexes are used in clinical applications. To chelate the Gd, diethylenetriaminepentaacetic acid (DTPA) and 1,4,7,10-tetraazacyclododecane-1,4,7,10-tetraacetic acid (DOTA) remain the most commonly used chelators to prepare Gd-based MRI contrast agents. Gd(III)-diethylene triamine pentaacetic acid (Gd-DTPA, Magnevist®) and Gd(III)-1,4,7,10-tetraazacyclododecane-1,4,7,10-tetraacetic acid (Gd-DOTA, Magnescope®) are clinically used as non-targeted contrast agents to image the brain anatomy of AD patients (Figure 1-6).[31] Compare to Gd-DTPA, Gd-DOTA or other cyclic Gd complexes are more thermodynamically stable in biological conditions.[32] For selectively targeting the Aβ, several Gd complexes are conjugated with Aβ probes such as PiB, stilbene, and chalcone (Figure 1-6).[33–35] Although the *in vitro*

and *in vivo* data show promising results, those Gd-based MRI contrast agents still have no reported clinical study.

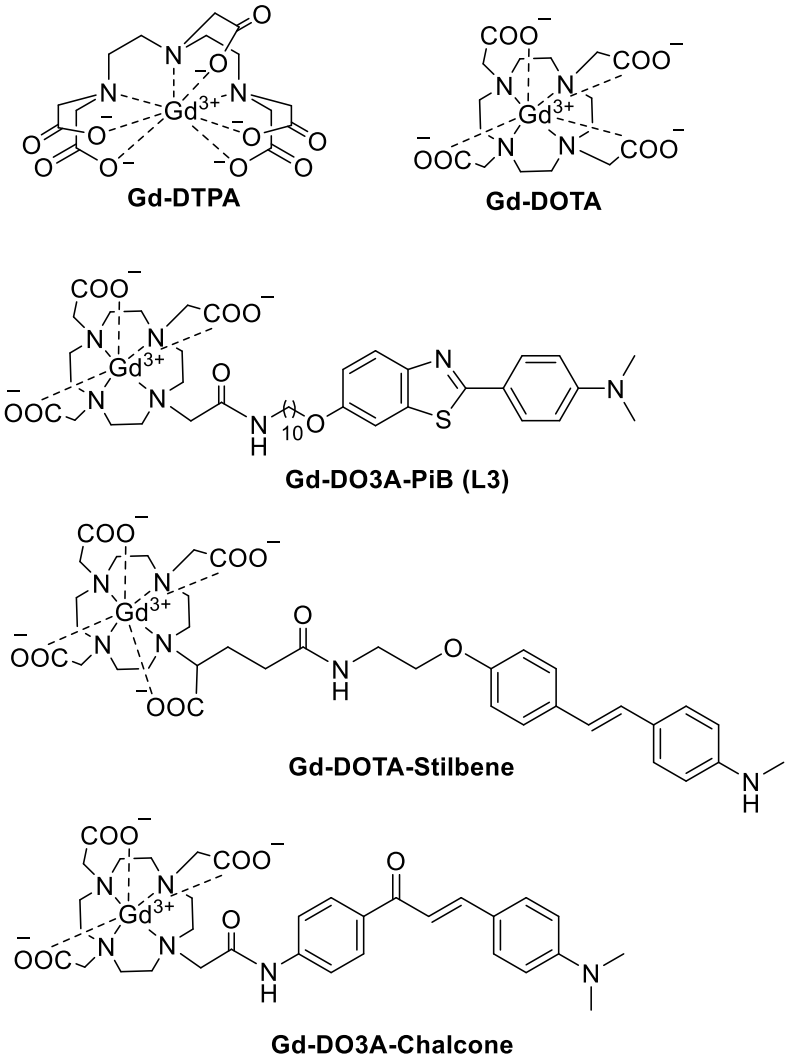

Figure 1-6. Chemical structure of reported Gd-based MRI contrast agents

1.4. Potency of Curcumin for Alzheimer`s Disease

Curcumin (Figure 1-7) is a major component of turmeric or *Curcuma longa* and has been used for over 4000 years as traditional medicine for various diseases including AD.[36] The cohort study reports that elderly people who regularly take curcumin, which is contained in Indian curry, have better cognitive functions and less incidence of AD.[37,38] Numerous studies further confirm the possibility of curcumin in treating AD by targeting the Aβ. Based on *in vitro* study using a cell-free and cell-based system, curcumin possess a good binding affinity with Aβ (Kd

= 0.20 nM), inhibits aggregation (IC_{50} = 1 μM), induces fibril disruption, and attenuates Aβ-induced toxicity.[39,40] A study using Tg2576 AD-mice expressing human APP and Sprague-Dawley rats infused by Aβ to induce its brain deposition reported a daily oral dose of curcumin (160 and 500 ppm) for 5-6 months significantly reduced the deposition of Aβ plaques and prevented the spatial memory deficits.[41–43] Intravenous administration of curcumin (7.5 mg/kg) for 7 days reduced senile plaque in APPswe/PS1dE9 mice.[44] Treatment of curcumin (0.01% w/w) in transgenic drosophila expressing human Aβ converts the Aβ fibril into non-toxic aggregates and reduces neurotoxicity.[45] Clinical trials using daily oral administration of formulated curcumin Longvida (400 mg for four weeks) and Theracumin (90 mg for 18 months) demonstrate the decrease of Aβ plaque and improvement of memory and attention performance.[46,47] Consideration from clinical results of curcumin is the gastrointestinal side effect resulting from high dose treatment, leading to the further development of curcumin derivatives.

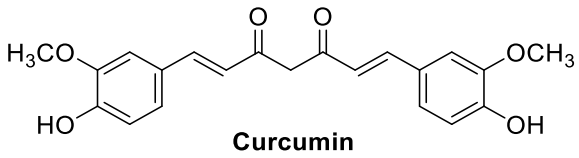

Figure 1-7. The chemical structure of curcumin

The binding affinity of curcumin with Aβ is further applied in imaging applications such as MRI. Allen et al. first reported Gd-DTPA-Curcumin (Figure 1-8), the direct conjugation of curcumin with Gd-DTPA, which binds to Aβ with four times higher relaxivity than free Gd-DTPA.[48] Furthermore, a polymalic acid (PLMA)-based nanoparticle covalently linked with curcumin and Gd-DOTA to form nanoimaging agent (NIA, Figure 1-8) which could also detect Aβ in human brain specimens by MRI.[49] Iron oxide-conjugated curcumin is also used as magnetic nanoparticles (Cur-MNPs, Figure 1-8) which could detect Aβ in the brain of Tg2576 AD-mice.[50] Learning from previous development, curcumin is potential as an Aβ probe for MRI-contrast agents.

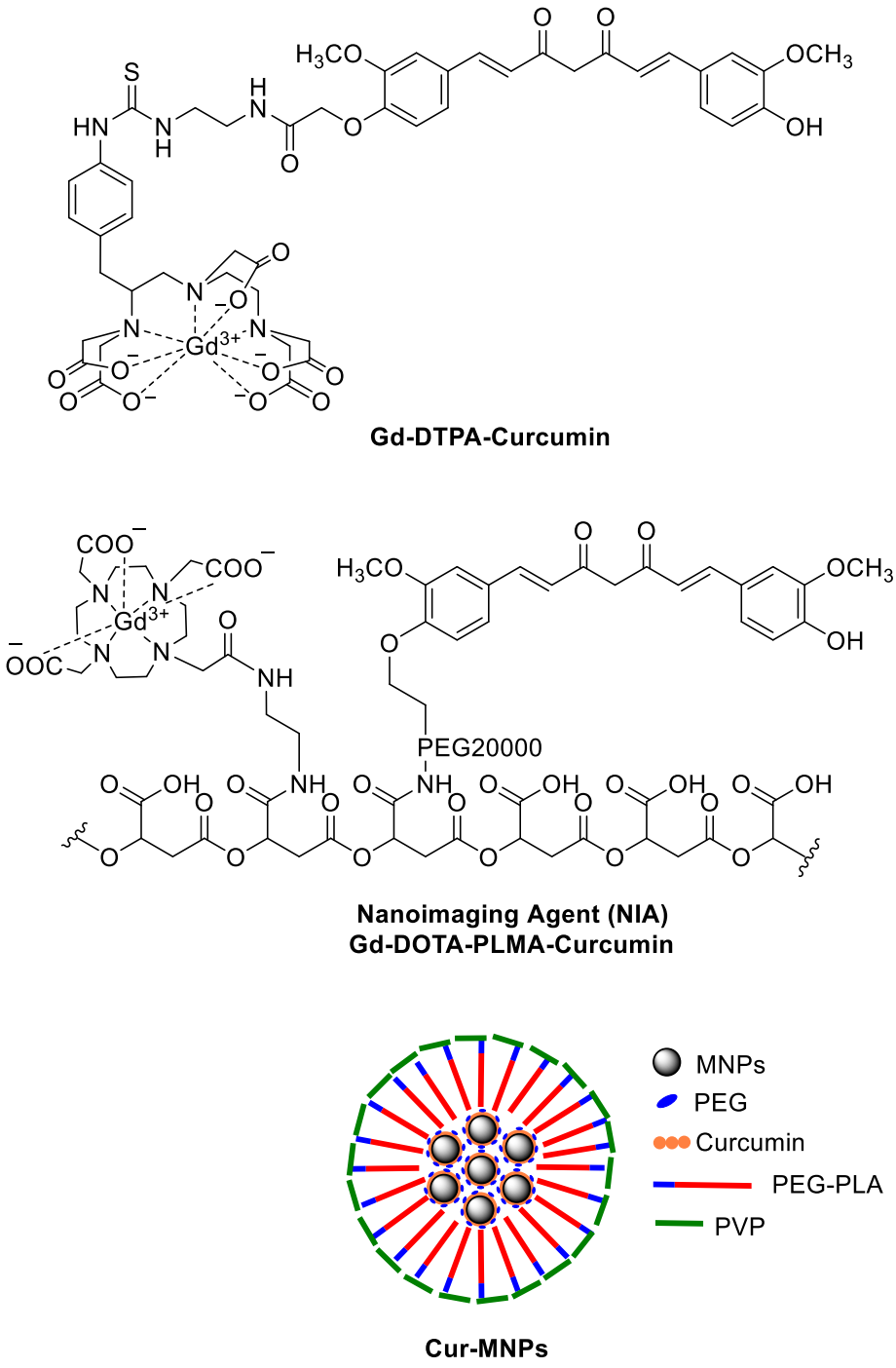

Figure 1-8. The reported MRI contrast agent containing curcumin

1.5. Possible Use of SAR Matrix for Designing Curcumin Derivatives

Over 200 curcumin derivatives are synthesized to improve the biological activity toward Aβ, but none of them are entered the clinical trials. Most drug design strategies rely on conventional ligand-based drug design using limited compounds

library or structure-based drug design combining molecular docking and molecular dynamic simulations.[51,52] Those strategies might lead to the pan assay interference compounds (PAINS), which provide assays artifacts and false-positive activity readouts.[53] Artificial activities of curcumin are intensely debated, and special care must be taken to assess apparent activities of curcuminoids.[54] Specifically, given the uncertainties associated with curcumin activities, systematic exploration of structural relationships between curcumin derivatives and its activity relationships from a large database would be less vulnerable to anticipate incidents of false positives reported in the literature than focusing on individual curcumin derivatives.

The structure-activity relationship matrix (SARM) is developed to systematically extract of analogue series from compound data sets and organize series with structurally related cores in individual matrices akin to R-group tables (Figure 1-9). Through color coding of matrix cells representing compounds, activity information can be included in the analysis. For structurally related analogue series, SARM produces virtual analogues of known active compounds that represent not yet explored combinations of existing core structures and R-groups whose potential activity can be predicted by SARM-based local Free-Wilson models.[55] In general, the activity is gradually changing with compound modifications in the presence of SAR continuity. However, in the presence of SAR discontinuity, the activity can drastically change with slight chemical modifications, leading to the formation of an activity cliff (i.e., a pair of structural analogues with a large difference in potency).[56] Local Free-Wilson type QSAR predictions are generally confined to compound subsets forming continuous SARs, but SARMs also detect of activity cliffs in regions of SAR discontinuity. As the proof of concept, SARM successfully generates new compounds possessing more potent inhibitory activity toward MMP-1. Learning from these success results, SARM could generate novel curcumin derivatives targeting Aβ, avoiding the possible PAINS profile.

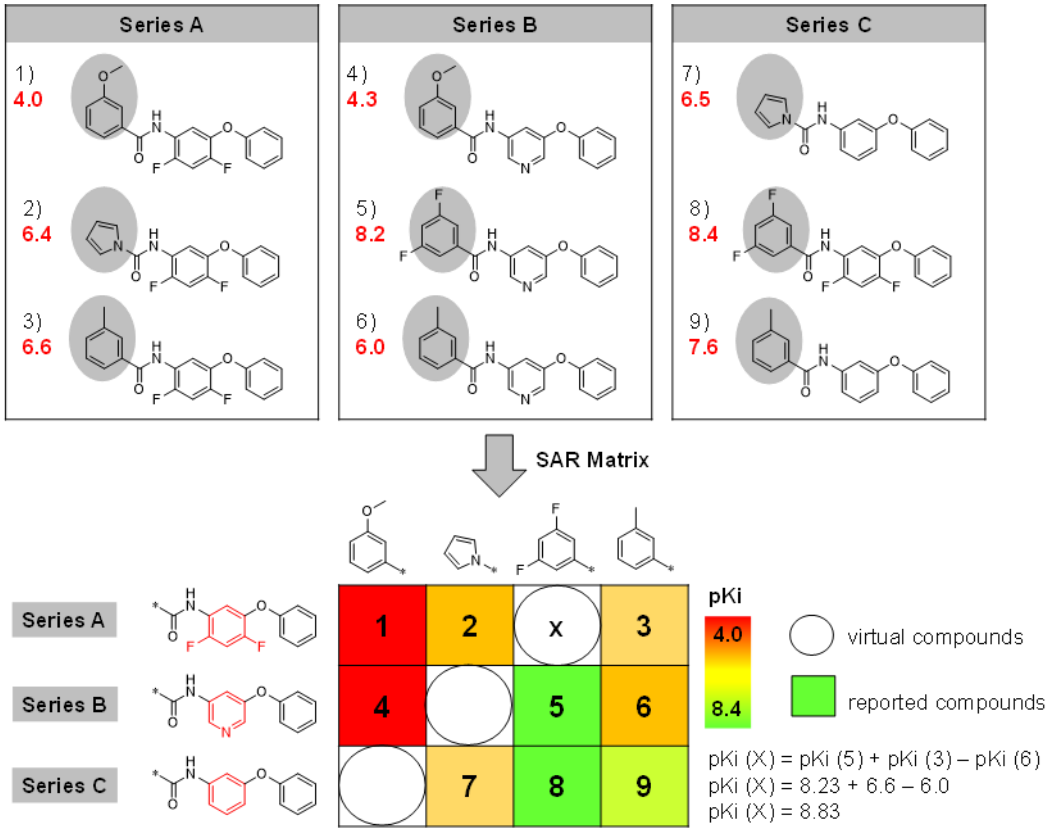

Figure 1-9. Workflow of SARM for compound generations and activity prediction (adopted from reference no 56).

1.6. Purpose of Study

For the development of drug targeting Aβ, this study reported the application of SARM for generating curcumin derivatives as the potent inhibitor of Aβ. Furthermore, this study also demonstrated the conjugation of curcumin derivatives generated from SARM with Gd complex MRI contrast agent with high MRI sensitivity toward Aβ fibril and detected inhibition of Aβ aggregation. Further optimization of curcumin derivatives purposing as the inducer of Aβ disaggregation with brain penetration ability was also described.

1.7. References

(1) Hippius, H.; Neundörfer, G. The Discovery of Alzheimer's Disease. *Dialogues Clin Neurosci* **2003**, *5* (1), 101–108.

(2) Cummings, J.; Lee, G.; Zhong, K.; Fonseca, J.; Taghva, K. Alzheimer's Disease Drug Development Pipeline: 2021. *Alzheimers Dement (N Y)* **2021**, *7* (1), e12179.

(3) Dubois, B.; Feldman, H. H.; Jacova, C.; Cummings, J. L.; DeKosky, S. T.; Barberger-Gateau, P.; Delacourte, A.; Frisoni, G.; Fox, N. C.; Galasko, D.; Gauthier, S.; Hampel, H.; Jicha, G. A.; Meguro, K.; O'Brien, J.; Pasquier, F.; Robert, P.; Rossor, M.; Salloway, S.; Sarazin, M.; de Souza, L. C.; Stern, Y.; Visser, P. J.; Scheltens, P. Revising the Definition of Alzheimer's Disease: A New Lexicon. *Lancet Neurol.* **2010**, *9* (11), 1118–1127.

(4) Winston Wong, P. Economic Burden of Alzheimer Disease and Managed Care Considerations. *Am J Manag Care* **2020**. 26, S177-S183.

(5) Kamenetz, F.; Tomita, T.; Hsieh, H.; Seabrook, G.; Borchelt, D.; Iwatsubo, T.; Sisodia, S.; Malinow, R. APP Processing and Synaptic Function. *Neuron* **2003**, *37* (6), 925–937.

(6) Chen, G.; Xu, T.; Yan, Y.; Zhou, Y.; Jiang, Y.; Melcher, K.; Xu, H. E. Amyloid Beta: Structure, Biology and Structure-Based Therapeutic Development. *Acta Pharmacol Sin* **2017**, *38* (9), 1205–1235.

(7) Bloom, G. S. Amyloid-β and Tau: The Trigger and Bullet in Alzheimer Disease Pathogenesis. *JAMA Neurol.* **2014**, *71* (4), 505–508.

(8) Giorgetti, S.; Greco, C.; Tortora, P.; Aprile, F. A. Targeting Amyloid Aggregation: An Overview of Strategies and Mechanisms. *Int J Mol Sci* **2018**, *19* (9), 2677.

(9) Cummings, J.; Aisen, P. S.; DuBois, B.; Frölich, L.; Jack, C. R.; Jones, R. W.; Morris, J. C.; Raskin, J.; Dowsett, S. A.; Scheltens, P. Drug Development in Alzheimer's Disease: The Path to 2025. *Alzheimers Res Ther* **2016**, *8* (1), 39.

(10) Sevigny, J.; Chiao, P.; Bussière, T.; Weinreb, P. H.; Williams, L.; Maier, M.; Dunstan, R.; Salloway, S.; Chen, T.; Ling, Y.; O'Gorman, J.; Qian, F.; Arastu, M.; Li, M.; Chollate, S.; Brennan, M. S.; Quintero-Monzon, O.; Scannevin, R. H.; Arnold, H. M.; Engber, T.; Rhodes, K.; Ferrero, J.; Hang, Y.; Mikulskis, A.; Grimm, J.; Hock, C.; Nitsch, R. M.; Sandrock, A. The Antibody Aducanumab Reduces Aβ Plaques in Alzheimer's Disease. *Nature* **2016**, *537* (7618), 50–56.

(11) Alexander, G. C.; Emerson, S.; Kesselheim, A. S. Evaluation of Aducanumab for Alzheimer Disease: Scientific Evidence and Regulatory Review Involving Efficacy, Safety, and Futility. *JAMA* **2021**, *325* (17), 1717–1718.

(12) Watt, A. D.; Crespi, G. A. N.; Down, R. A.; Ascher, D. B.; Gunn, A.; Perez, K. A.; McLean, C. A.; Villemagne, V. L.; Parker, M. W.; Barnham, K. J.; Miles, L. A. Do Current Therapeutic Anti-Aβ Antibodies for Alzheimer's Disease Engage the Target? *Acta Neuropathol* **2014**, *127* (6), 803–810.

(13) Feinberg, H.; Saldanha, J. W.; Diep, L.; Goel, A.; Widom, A.; Veldman, G. M.; Weis, W. I.; Schenk, D.; Basi, G. S. Crystal Structure Reveals Conservation of Amyloid-β Conformation Recognized by 3D6 Following Humanization to Bapineuzumab. *Alzheimers Res Ther* **2014**, *6* (3), 31.

(14) Nagashima, N.; Ozawa, S.; Furuta, M.; Oi, M.; Hori, Y.; Tomita, T.; Sohma, Y.; Kanai, M. Catalytic Photooxygenation Degrades Brain Aβ in Vivo. *Sci. Adv.* **2021**, *7* (13).
(15) Nakagami, Y.; Nishimura, S.; Murasugi, T.; Kubo, T.; Kaneko, I.; Meguro, M.; Marumoto, S.; Kogen, H.; Koyama, K.; Oda, T. A Novel Compound RS-0466 Reverses β-Amyloid-Induced Cytotoxicity through the Akt Signaling Pathway *in Vitro*. *Eur J Pharmacol* **2002**, *457* (1), 11–17.
(16) O'Hare, E.; Scopes, D. I. C.; Treherne, J. M.; Norwood, K.; Spanswick, D.; Kim, E.-M. RS-0406 Arrests Amyloid-β Oligomer-Induced Behavioural Deterioration *In Vivo*. *Behav Brain Res* **2010**, *210* (1), 32–37.
(17) Hey, J. A.; Kocis, P.; Hort, J.; Abushakra, S.; Power, A.; Vyhnálek, M.; Yu, J. Y.; Tolar, M. Discovery and Identification of an Endogenous Metabolite of Tramiprosate and Its Prodrug ALZ-801 That Inhibits Beta Amyloid Oligomer Formation in the Human Brain. *CNS Drugs* **2018**, *32* (9), 849–861.
(18) Hey, J. A.; Yu, J. Y.; Versavel, M.; Abushakra, S.; Kocis, P.; Power, A.; Kaplan, P. L.; Amedio, J.; Tolar, M. Clinical Pharmacokinetics and Safety of ALZ-801, a Novel Prodrug of Tramiprosate in Development for the Treatment of Alzheimer's Disease. *Clin Pharmacokinet* **2018**, *57* (3), 315–333.
(19) Ke, P. C.; Zhou, R.; Serpell, L. C.; Riek, R.; Knowles, T. P. J.; Lashuel, H. A.; Gazit, E.; Hamley, I. W.; Davis, T. P.; Fändrich, M.; Otzen, D. E.; Chapman, M. R.; Dobson, C. M.; Eisenberg, D. S.; Mezzenga, R. Half a Century of Amyloids: Past, Present and Future. *Chem. Soc. Rev.* **2020**, *49* (15), 5473–5509.
(20) Chuang, E.; Hori, A. M.; Hesketh, C. D.; Shorter, J. Amyloid Assembly and Disassembly. *J Cell Sci* **2018**, *131* (8).
(21) Bieschke, J.; Russ, J.; Friedrich, R. P.; Ehrnhoefer, D. E.; Wobst, H.; Neugebauer, K.; Wanker, E. E. EGCG Remodels Mature α-Synuclein and Amyloid-β Fibrils and Reduces Cellular Toxicity. *PNAS* **2010**, *107* (17), 7710–7715.
(22) Levin, J.; Maaß, S.; Schuberth, M.; Respondek, G.; Paul, F.; Mansmann, U.; Oertel, W. H.; Lorenzl, S.; Krismer, F.; Seppi, K.; Poewe, W.; Wenning, G.; Giese, A.; Bötzel, K.; Höglinger, G.; The PROMESA study group. The PROMESA-Protocol: Progression Rate of Multiple System Atrophy under EGCG Supplementation as Anti-Aggregation-Approach. *J Neural Transm* **2016**, *123* (4), 439–445.
(23) Ladiwala, A. R. A.; Lin, J. C.; Bale, S. S.; Marcelino-Cruz, A. M.; Bhattacharya, M.; Dordick, J. S.; Tessier, P. M. Resveratrol Selectively Remodels Soluble Oligomers and Fibrils of Amyloid Aβ into Off-Pathway Conformers. *J Biol Chem* **2010**, *285* (31), 24228–24237.
(24) Turner, R. S.; Thomas, R. G.; Craft, S.; van Dyck, C. H.; Mintzer, J.; Reynolds, B. A.; Brewer, J. B.; Rissman, R. A.; Raman, R.; Aisen, P. S. A Randomized, Double-Blind, Placebo-Controlled Trial of Resveratrol for Alzheimer Disease. *Neurology* **2015**, *85* (16), 1383–1391.
(25) Zhu, C. W.; Grossman, H.; Neugroschl, J.; Parker, S.; Burden, A.; Luo, X.; Sano, M. A Randomized, Double-Blind, Placebo-Controlled Trial of Resveratrol with Glucose and Malate (RGM) to Slow the Progression of

Alzheimer's Disease: A Pilot Study. *Alzheimers Dement (N Y)* **2018**, *4* (1), 609–616.
(26) Adlard, P. A.; Tran, B. A.; Finkelstein, D. I.; Desmond, P. M.; Johnston, L. A.; Bush, A. I.; Egan, G. F. A Review of β-Amyloid Neuroimaging in Alzheimer's Disease. *Front. Neurosci.* **2014**, *8*.
(27) Salerno, M.; Santo Domingo Porqueras, D. Alzheimer's Disease: The Use of Contrast Agents for Magnetic Resonance Imaging to Detect Amyloid Beta Peptide inside the Brain. *Coord. Chem. Rev.* **2016**, *327–328*, 27–34.
(28) Scheltens, P.; Blennow, K.; Breteler, M. M. B.; de Strooper, B.; Frisoni, G. B.; Salloway, S.; Van der Flier, W. M. Alzheimer's Disease. *Lancet* **2016**, *388* (10043), 505–517.
(29) Sedgwick, A. C.; Brewster, J. T.; Harvey, P.; Iovan, D. A.; Smith, G.; He, X.-P.; Tian, H.; Sessler, J. L.; James, T. D. Metal-Based Imaging Agents: Progress towards Interrogating Neurodegenerative Disease. *Chem. Soc. Rev.* **2020**, *49* (10), 2886–2915.
(30) Lauffer, R. B. Paramagnetic Metal Complexes as Water Proton Relaxation Agents for NMR Imaging: Theory and Design. *Chem. Rev.* **1987**, *87* (5), 901–927.
(31) Wahsner, J.; Gale, E. M.; Rodríguez-Rodríguez, A.; Caravan, P. Chemistry of MRI Contrast Agents: Current Challenges and New Frontiers. *Chem. Rev.* **2019**, *119* (2), 957–1057.
(32) Ersoy, H.; Rybicki, F. J. Biochemical Safety Profiles of Gadolinium-Based Extracellular Contrast Agents and Nephrogenic Systemic Fibrosis. *J Magn Reson Imaging* **2007**, *26* (5), 1190–1197.
(33) Majdoub, S.; Garda, Z.; Oliveira, A. C.; Relich, I.; Pallier, A.; Lacerda, S.; Hureau, C.; Geraldes, C. F. G. C.; Morfin, J.-F.; Tóth, É. Concentration-Dependent Interactions of Amphiphilic PiB Derivative Metal Complexes with Amyloid Peptides Aβ and Amylin. *Chemistry – A European Journal* **2021**, *27* (6), 2009–2020.
(34) Bort, G.; Catoen, S.; Borderies, H.; Kebsi, A.; Ballet, S.; Louin, G.; Port, M.; Ferroud, C. Gadolinium-Based Contrast Agents Targeted to Amyloid Aggregates for the Early Diagnosis of Alzheimer's Disease by MRI. *Eur J Med Chem* **2014**, *87*, 843–861.
(35) Choi, G.; Kim, H.-K.; Baek, A. R.; Kim, S.; Kim, M. J.; Kim, M.; Cho, A. E.; Lee, G.-H.; Jung, H.; Yang, J.; Lee, T.; Chang, Y. Multifunctional Imaging of Amyloid-Beta Peptides with a New Gadolinium-Based Contrast Agent in Alzheimer's Disease. *J. Ind. Eng. Chem.* **2020**, *83*, 214–223.
(36) Wanninger, S.; Lorenz, V.; Subhan, A.; Edelmann, F. T. Metal Complexes of Curcumin – Synthetic Strategies, Structures and Medicinal Applications. *Chem. Soc. Rev.* **2015**, *44* (15), 4986–5002.
(37) Ng, T.-P.; Chiam, P.-C.; Lee, T.; Chua, H.-C.; Lim, L.; Kua, E.-H. Curry Consumption and Cognitive Function in the Elderly. *Am J Epidemiol* **2006**, *164* (9), 898–906.
(38) Ganguli, M.; Chandra, V.; Kamboh, M. I.; Johnston, J. M.; Dodge, H. H.; Thelma, B. K.; Juyal, R. C.; Pandav, R.; Belle, S. H.; DeKosky, S. T. Apolipoprotein E Polymorphism and Alzheimer Disease: The Indo-US Cross-National Dementia Study. *Arch Neurol* **2000**, *57* (6), 824–830.

(39) Ono, K.; Hasegawa, K.; Naiki, H.; Yamada, M. Curcumin Has Potent Anti-Amyloidogenic Effects for Alzheimer's β-Amyloid Fibrils *in Vitro*. *J Neurosci Res* **2004**, *75* (6), 742–750.
(40) Thapa, A.; Jett, S. D.; Chi, E. Y. Curcumin Attenuates Amyloid-β Aggregate Toxicity and Modulates Amyloid-β Aggregation Pathway. *ACS Chem. Neurosci.* **2016**, *7* (1), 56–68.
(41) Yang, F.; Lim, G. P.; Begum, A. N.; Ubeda, O. J.; Simmons, M. R.; Ambegaokar, S. S.; Chen, P. P.; Kayed, R.; Glabe, C. G.; Frautschy, S. A.; Cole, G. M. Curcumin Inhibits Formation of Amyloid β Oligomers and Fibrils, Binds Plaques, and Reduces Amyloid in Vivo. *J. Biol. Chem.* **2005**, *280* (7), 5892–5901.
(42) Lim, G. P.; Chu, T.; Yang, F.; Beech, W.; Frautschy, S. A.; Cole, G. M. The Curry Spice Curcumin Reduces Oxidative Damage and Amyloid Pathology in an Alzheimer Transgenic Mouse. *J. Neurosci.* **2001**, *21* (21), 8370–8377.
(43) Frautschy, S. A.; Hu, W.; Kim, P.; Miller, S. A.; Chu, T.; Harris-White, M. E.; Cole, G. M. Phenolic Anti-Inflammatory Antioxidant Reversal of Aβ-Induced Cognitive Deficits and Neuropathology. *Neurobiol Aging* **2001**, *22* (6), 993–1005.
(44) Garcia-Alloza, M.; Borrelli, L. A.; Rozkalne, A.; Hyman, B. T.; Bacskai, B. J. Curcumin Labels Amyloid Pathology in Vivo, Disrupts Existing Plaques, and Partially Restores Distorted Neurites in an Alzheimer Mouse Model. *J Neurochem* **2007**, *102* (4), 1095–1104.
(45) Caesar, I.; Jonson, M.; Nilsson, K. P. R.; Thor, S.; Hammarström, P. Curcumin Promotes A-Beta Fibrillation and Reduces Neurotoxicity in Transgenic Drosophila. *PLoS ONE* **2012**, *7* (2), e31424.
(46) Cox, K. H.; Pipingas, A.; Scholey, A. B. Investigation of the Effects of Solid Lipid Curcumin on Cognition and Mood in a Healthy Older Population. *J Psychopharmacol* **2015**, *29* (5), 642–651.
(47) Small, G. W.; Siddarth, P.; Li, Z.; Miller, K. J.; Ercoli, L.; Emerson, N. D.; Martinez, J.; Wong, K.-P.; Liu, J.; Merrill, D. A.; Chen, S. T.; Henning, S. M.; Satyamurthy, N.; Huang, S.-C.; Heber, D.; Barrio, J. R. Memory and Brain Amyloid and Tau Effects of a Bioavailable Form of Curcumin in Non-Demented Adults: A Double-Blind, Placebo-Controlled 18-Month Trial. *Am J Geriatr Psychiatry* **2018**, *26* (3), 266–277.
(48) Vithanarachchi, S. M.; Allen, M. J. A Multimodal, β-Amyloid-Targeted Contrast Agent. *Chem. Commun.* **2013**, *49* (39), 4148–4150.
(49) Patil, R.; Gangalum, P. R.; Wagner, S.; Portilla-Arias, J.; Ding, H.; Rekechenetskiy, A.; Konda, B.; Inoue, S.; Black, K. L.; Ljubimova, J. Y.; Holler, E. Curcumin Targeted, Polymalic Acid-Based MRI Contrast Agent for the Detection of Aβ Plaques in Alzheimer's Disease. *Macromol Biosci* **2015**, *15* (9), 1212–1217.
(50) Cheng, K. K.; Chan, P. S.; Fan, S.; Kwan, S. M.; Yeung, K. L.; Wáng, Y.-X. J.; Chow, A. H. L.; Wu, E. X.; Baum, L. Curcumin-Conjugated Magnetic Nanoparticles for Detecting Amyloid Plaques in Alzheimer's Disease Mice Using Magnetic Resonance Imaging (MRI). *Biomaterials* **2015**, *44*, 155–172.

(51) Chainoglou, E.; Hadjipavlou-Litina, D. Curcumin in Health and Diseases: Alzheimer's Disease and Curcumin Analogues, Derivatives, and Hybrids. *Int. J. Mol. Sci.* **2020**, *21* (6), 1975.
(52) Shabbir, U.; Rubab, M.; Tyagi, A.; Oh, D.-H. Curcumin and Its Derivatives as Theranostic Agents in Alzheimer's Disease: The Implication of Nanotechnology. *Int. J. Mol. Sci.* **2021**, *22* (1), 196.
(53) Baell, J. B.; Holloway, G. A. New Substructure Filters for Removal of Pan Assay Interference Compounds (PAINS) from Screening Libraries and for Their Exclusion in Bioassays. *J. Med. Chem.* **2010**, *53* (7), 2719–2740.
(54) Nelson, K. M.; Dahlin, J. L.; Bisson, J.; Graham, J.; Pauli, G. F.; Walters, M. A. The Essential Medicinal Chemistry of Curcumin. *J. Med. Chem.* **2017**, *60* (5), 1620–1637.
(55) Wassermann, A. M.; Haebel, P.; Weskamp, N.; Bajorath, J. SAR Matrices: Automated Extraction of Information-Rich SAR Tables from Large Compound Data Sets. *J. Chem. Inf. Model.* **2012**, *52* (7), 1769–1776.
(56) Gupta-Ostermann, D.; Shanmugasundaram, V.; Bajorath, J. Neighborhood-Based Prediction of Novel Active Compounds from SAR Matrices. *J. Chem. Inf. Model.* **2014**, *54* (3), 801–809.

Chapter 2
Development of Curcumin-based Amyloid β Aggregation Inhibitors for Alzheimer's Disease using the SAR Matrix Approach

Chapter 2. Development of Curcumin-based Amyloid β Aggregation Inhibitors for Alzheimer's Disease using the SAR Matrix Approach

2.1. Introduction

Inhibiting the Aβ aggregation provides the strategic approach to overcome the progression of Alzheimer`s Disease.[1] Curcumin, a natural polyphenol, possesses a promising candidate with considerable apparent efficacy, however as mentioned in Chapter 1.4, non-negligible side effects such as gastrointestinal symptoms were observed in phase II clinical trials.[2] So far, over 200 curcumin derivatives have been synthesized to find stronger Aβ inhibitors, but none of them enter the clinical trial due to the possible PAINS profile (also see Chapter 1.5).[3,4]

SARM provides a promising approach for drug design by systematically analyzing analogue series from compound data sets, generating series with structurally related cores in individual matrices, and predicting the biological activity.[5] Previously, SARM successfully generates a compound with 60-times higher inhibitory activity toward MMP-1.[6] Those finding enlightens the possible use of SARM to avoid compounds with PAINS profile.

This study demonstrates the use of SARM to generate inhibitors of Aβ aggregation by systematic analysis from large data set in the ChEMBL database. After synthesizing the generated compounds and evaluating their inhibitory activity, the results from the first screening could be updated in the SARM to generate the other curcumin derivatives, and then the second screening could be performed. The strongest inhibitor among candidates was further confirmed by TEM image and cell-based assay.

2.2. Results and Discussion

2.2.1. Novel Curcumin Derivatives Generated from SAR Matrix

To construct SARM for analysis, 697 known Aβ inhibitors with available IC_{50} values were retrieved from ChEMBL (data set 2487). After the existing curcumin derivatives or analogues were fragmented by systematic cleavage of

exocyclic bonds using the SARM methodology, SARM analysis was obtained, including novel curcumin derivatives, and the activity of several of these derivatives was predicted. (Figure 2-1). Analyzing the compound distribution using the Molecular Grid Map (MGM), SARM generated a putative activity cliff associated with compounds **A**–**C** in Figure 2-1. An activity cliff is formed by any of these compounds and the known weakly active analogs at adjacent positions in the MGM. All compounds in this activity cliff region possessed distinct benzene substitution patterns with a combination of several functional groups such as hydroxyl, methoxy, methyl methoxyacetate, methyl hydroxyacetate, and trifluoromethyl groups. In addition to compounds **A**–**C**, compound **D** as a new curcumin derivative not originating from the SARM and compounds **E** and **F** as the reported curcumin derivatives with Aβ-inhibitory activity were synthesized.

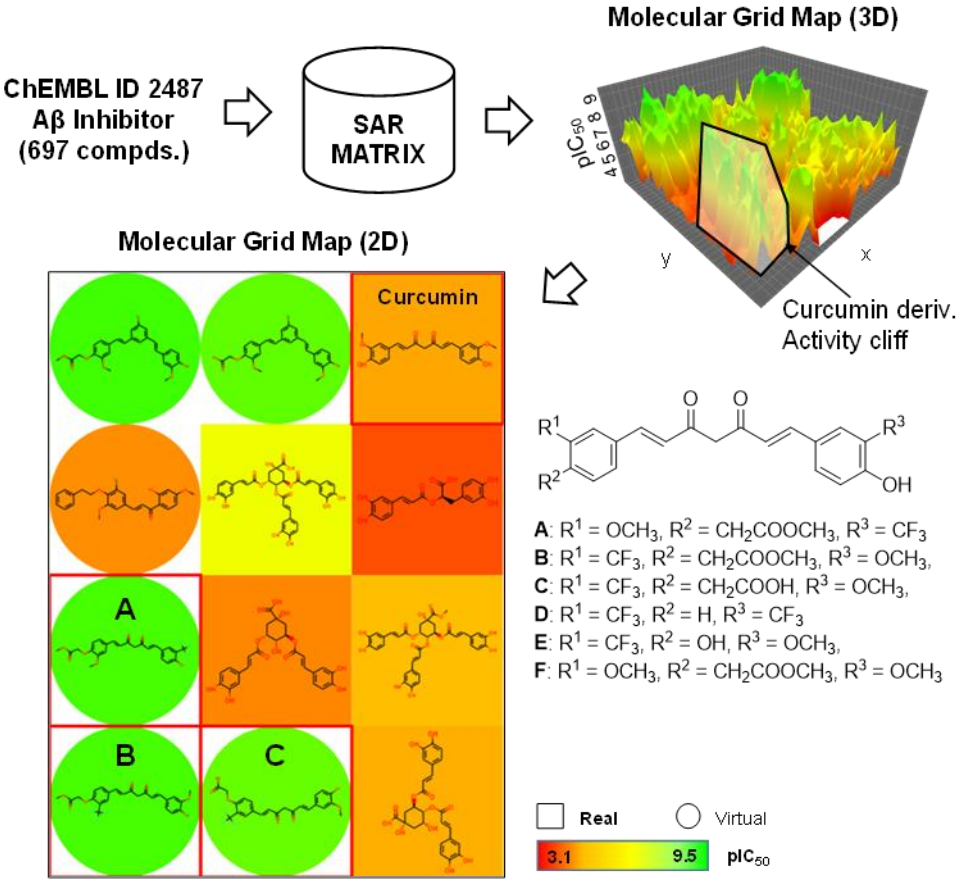

Figure 2-1. Activity cliff prediction from SAR Matrix (SARM) method.

2.2.2. Synthesis of Curcumin Derivatives

Synthesis of curcumin derivatives **A**–**F** is shown in Scheme 2-1. Aldehydes **1a**–**b** were chosen as starting materials and reacted with methyl bromoacetate under basic conditions. The resulting aldehyde **2a** underwent the condensation reaction with acetylacetone to give the corresponding conjugated ketone **3a** in 61% yield. The microwave (MW) irradiated condition is essential for this condensation reaction, and the desired product **3a** was obtained only in 5% yield without MW irradiation. Further condensation reaction was performed between compound **3a** with compound **1b** to obtain asymmetric curcumin derivative **A**. For obtaining other asymmetric curcumins, compound **1a** was first reacted with acetylacetone to give compound **4a**. Further condensation reaction with various aldehydes, such as compounds **1b**, **2a-b**, and 3-trifluoromethyl benzaldehyde, produced asymmetric curcumin derivatives **E**, **F**, **B**, and **D**, respectively. Compound **C** was obtained from the condensation reaction between compound **2c** (obtained by hydrolysis of compound **2b**) with compound **4a.**

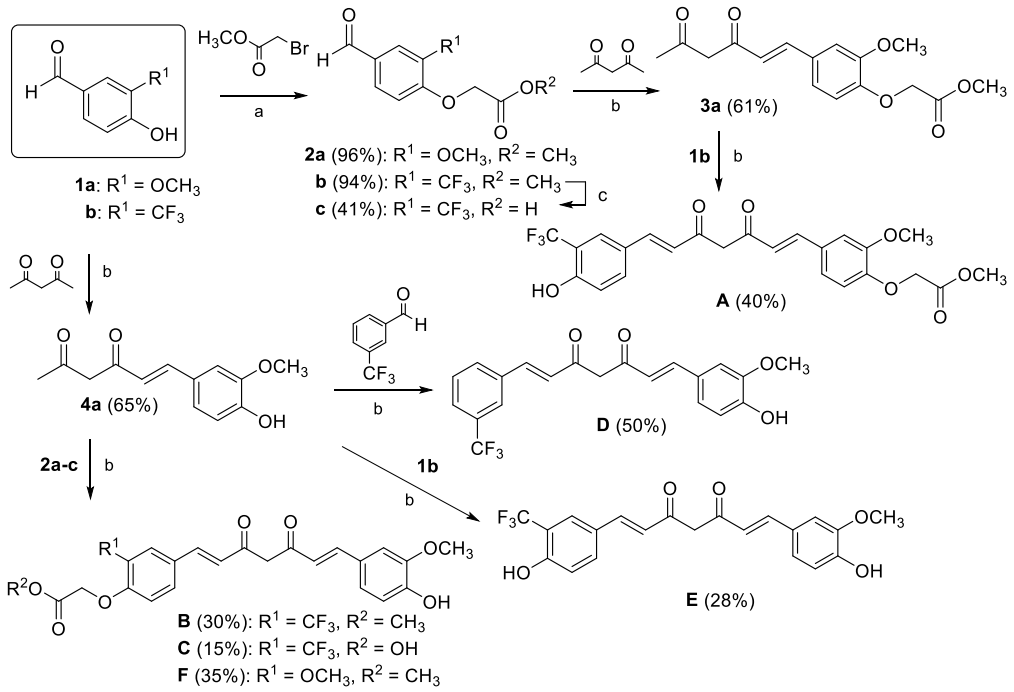

Scheme 2-1. Synthetic scheme of curcumin derivatives **A**–**F**. Reaction conditions: (a) DMF, K_2CO_3, 80 ^oC, 2h; (b) DMF, $B(OH)_3$, morpholine, MW 150 ^oC, 15 min; (c) NaOH, H_2O, 100 ^oC, 30 min

2.2.3. First Screening of Inhibitory Activity toward Aβ Aggregation

The synthesized curcumin derivatives were further screened for their *in vitro* inhibitory activity of Aβ aggregation. In this study, Aβ containing 42-amino acid residue was used, considered as the most neurotoxic Aβ isoform.[7] The aggregation of Aβ occurred immediately under the biological conditions (pH 7.4), thus it could be detected by thioflavin t (ThT), which is known to interact on the hydrophobic site of Aβ.[8] In this assay, an Aβ inhibitor was defined by the ability of the compound to competitively interact at the binding site of ThT, resulting in the decreasing of fluorescence intensity during detection. The IC_{50} values of curcumin derivatives obtained from the ThT assay were summarized in Table 2-1. Curcumin dose-dependently inhibited the aggregation with the IC_{50} $A\beta_{42}$ value of 0.693 ± 0.013 μM. Further screening using the ThT fluorescence assay revealed that several compounds containing a hydroxyl group and a methoxycarbonylmethyloxy group on different positions on their benzene ring such as compounds **A**, **B**, and **F** displayed stronger inhibitory activity than curcumin with IC_{50} values of 0.022 ± 0.004, 0.007 ± 0.001, and 0.029 ± 0.005, respectively. In addition, compounds **D** and **E**, which did not contain a methoxycarbonylmethyloxy group but contained a hydroxyl group, also exhibited comparable inhibitory activity to compound **F**, indicating a crucial role for the trifluoromethyl and hydroxyl groups. Although the presence of the carboxymethyloxy group and hydroxyl group on different benzene rings decreased the inhibitory activity, the activity was still comparable to curcumin as shown by compound **C**. Based on the results of this screening, SARM analysis was continued in search of other promising derivatives.

Table 2-1. Inhibition of Aβ aggregation using ThT assay[a]

Compound	IC_{50} (μM) [b]
A	0.022 ± 0.013
B	0.007 ± 0.001
C	0.698 ± 0.010
D	0.013 ± 0.002
E	0.052 ± 0.006
F	0.029 ± 0.005
Curcumin	0.693 ± 0.013
Tacrine	0.022 ± 0.043

[a] The ThT fluorescence assay was carried out by incubating 20 μM of Aβ with serial concentrations of curcumin derivatives in PBS pH 7.4 at 37 °C. [b] The drug concentration

required to inhibit Aβ aggregation by 50% (IC_{50}) was determined from semi-logarithmic dose–response plots, and results represent the mean ± s.d. of triplicate samples.

2.2.4. Updating the SAR Matrix to Generate Other Curcumin Derivatives

The results observed from the ThT fluorescence assay revealed that several curcumin derivatives possessed higher inhibitory activity of Aβ aggregation than curcumin. Therefore, SARM analysis was further updated by including the experimental IC_{50} values of all compounds to find other more potent curcumin derivatives. The revised SARM analysis revealed several other curcumin derivatives, including novel compounds **G**, **H**, **I**, and **J**, possessing more potent inhibitory activity than curcumin and comparable with compound **B** (Figure 2-2).

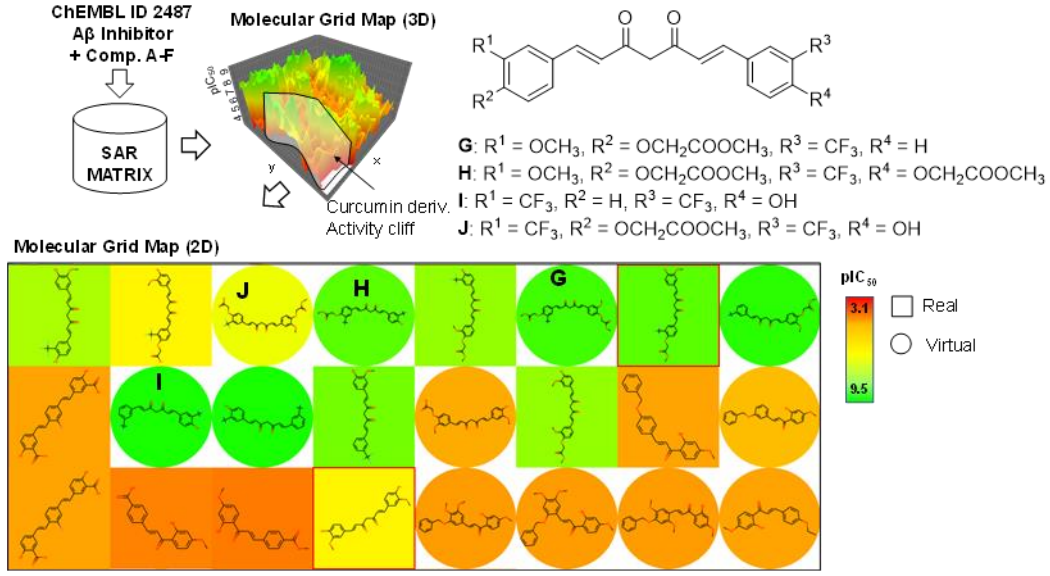

Figure 2-2. Activity cliff prediction after SAR matrix update.

2.2.5. Synthesis of Curcumin Derivatives from SAR Matrix Update

Synthetic routes for the preparation of compounds **G**, **H**, **I**, and **J**, which were derived from the updated-SARM analysis, are shown in Scheme 2-2. The compounds **G** and **H** were prepared by reacting compound **3a** with 3-trifluoromethyl benzaldehyde and compound **2b**, respectively. Compounds **I** and **J** were obtained from the condensation reaction between compound **4b** with 3-trifluoromethyl benzaldehyde or compound **2b**. Furthermore, compound **K**, a derivative of compound **B**, in which the tert-butyl ester replaced the methyl ester,

was synthesized. The *tert*-butyl group was first introduced on compound **1b**, and the resulting compound **5** was treated with **4a** to afford compound **K**.

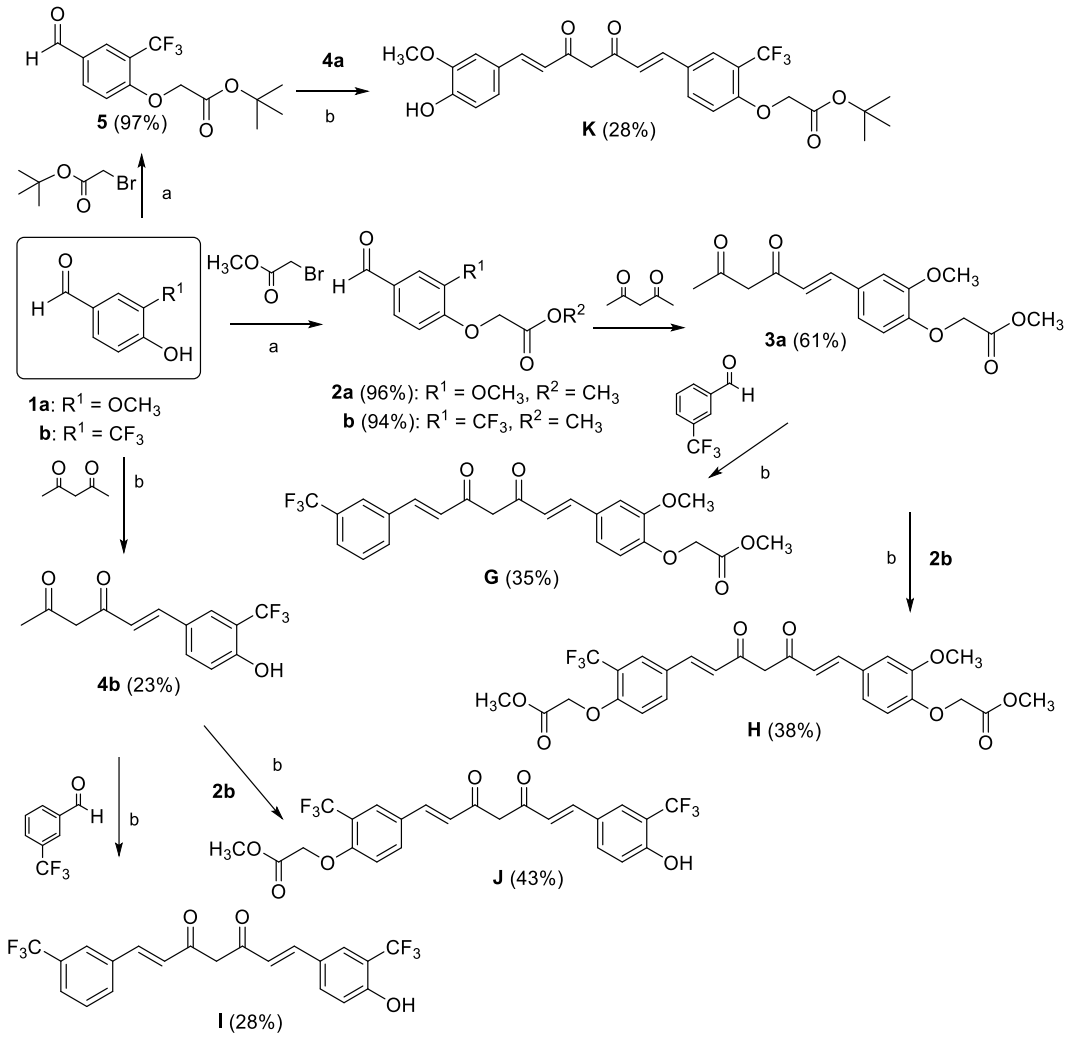

Scheme 2-2. Synthetic scheme of curcumin derivatives **G**–**K**. Reaction conditions: (a) DMF, K_2CO_3, 80 °C, 2h; (b) DMF, $B(OH)_3$, morpholine, MW 150 °C, 15 min; (c) NaOH, H_2O, 100 °C, 30 min

2.2.6. Second Screening of Inhibitory Activity toward Aβ Aggregation

To further assess SARM predictions, compounds **G**, **H**, **I**, and **J** were tested in the ThT assay. The dose-dependent ThT assay showed these curcumin derivatives were more potent than curcumin: their IC_{50} values were 0.018-0.109 μM, whereas the IC_{50} of curcumin was 0.693 μM (Table 2-2). Compound **G** and **H**, which have one or two methoxycarbonylmethyloxy groups in the para-position and a 3-trifluoromethylphenyl group or a methoxy group in the meta-position, showed

lower inhibitory activity than compound **A**, which has a hydroxyl group in the para-position, indicating that the hydroxyl group is more important than the methoxycarbonylmethyloxy group. In addition, compound **I**, which has two 3-trifluoromethyl on the meta-position and one hydroxyl group, exhibited the strongest inhibitor in the second screening and comparable with compound **B**. However, the methoxycarbonylmethyloxy group decreased the inhibitory activity as seen in compound **J**. These data revealed the importance of the trifluoromethyl group for the amyloid inhibition activity followed by methoxy, hydroxyl, and methoxycarbonylmethyloxy group. Compound **K**, a derivative of compound **B**, showed considerable inhibitory activity, suggesting the possibility of further modification on the ester group.

Table 2-2. Inhibition of Aβ aggregation using ThT assay

compound	IC_{50} (μM)
G	0.046 ± 0.012
H	0.055 ± 0.009
I	0.018 ± 0.001
J	0.109 ± 0.037
K	0.055 ± 0.006

2.2.7. Morphological Change of Aβ Treated by Curcumin Derivatives

The ThT assay revealed the effectiveness of the curcumin derivatives, especially compound **B**, to inhibit Aβ aggregation. The inhibitory activity was further confirmed by negative staining transmission electron microscopy (TEM) imaging with similar conditions in ThT assay by examining the morphological change after the treatment of Aβ monomer with compound **B**. As shown in Figure 2-3, Aβ formed fibrils and oligomers as indicated by long-filament surrounded by spherical-shape species.[15] The addition of compound **B** induced shortening of Aβ fibrils and increased the generation of Aβ oligomers in a concentration-dependent manner, resulting in the inhibition of the fibril formation from oligomers. These findings strongly support the validity of the detected activity of the new curcumin derivatives.

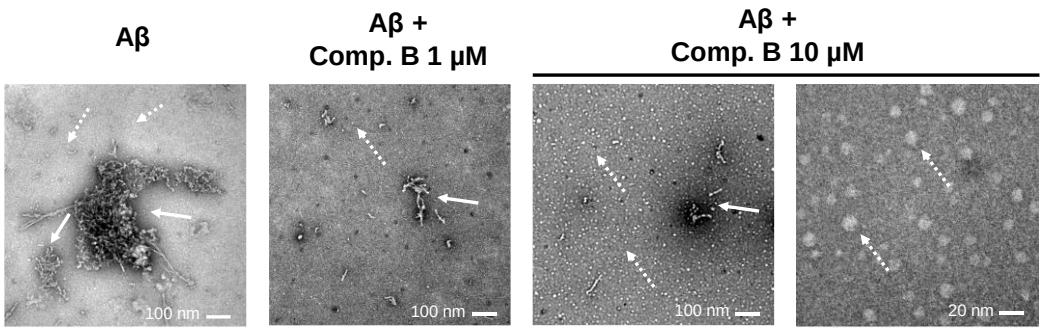

Figure 2-3. Negative staining TEM images of Aβ incubated at 37 °C in the absence and presence of Compound B. Fibril (→), oligomer (-->).

2.2.8. Effect of Curcumin Derivatives against Aβ-induced Toxicity

Aggregation of Aβ monomer to oligomers or fibrils has been reported to cause neurotoxicity in Alzheimer's disease.[10] Therefore, it is also important to evaluate whether the synthesized curcumin derivatives prevented neurotoxicity by inhibiting Aβ aggregation. Compounds **B** and **D** were chosen as the most potent inhibitors and compound **K** as a derivative of compound **B** for comparison. Murine neuroblastoma (N2a) and human glioblastoma (U87MG) cells were used as the models which have been reported for the Aβ cytotoxicity study of Alzheimer's disease.[11,12] First, the effect of selected curcumin derivatives toward N2a and U87MG cells was examined using 3-(4,5-dimethyl-2-thiazolyl)-2,5-diphenyl-2H-tetrazolium bromide (MTT) assay. The results are summarized in Table 2-3. Curcumin induced a cytotoxic effect on N2a and U87MG cells with IC_{50} values of 22.6 ±1.48 and 18.4 ± 3.59, respectively, which were similar to those previously reported.[13] In contrast, the curcumin derivatives **B**, **D**, and **K** were less cytotoxic toward both cell lines than curcumin. Especially, compound **K** did not show significant cytotoxicity at 100 μM concentration.

Table 2-3. Cell viability of selected compounds toward N2A and U87MG cells using MTT assay[a]

compound	IC_{50} (μM)[b]	
	N2a	U87MG
B	38.7 ± 8.47	90.0 ± 5.93
D	65.7 ± 7.44	88.7 ± 2.78
K	>100	>100
Curcumin	22.6 ± 1.48	18.4 ± 3.59

[a] The MTT assay was carried out after treating the cells with serial concentrations of curcumin derivatives for 24h. [b] The drug concentration required to inhibit the cell growth by 50% (IC_{50}) was determined from semi-logarithmic dose–response plots, and results represent the mean ± s.d. of three independent experiments in triplicate.

The effect of curcumin derivatives **B** and **K** were further evaluated toward Aβ-induced cytotoxicity in N2a cells. As expected, Aβ caused a dose-dependent cytotoxic effect on N2a cells, as reported (Figure 2-4A).[14] Next, the effects of compounds **B** and **K** on the viability of N2a cells stimulated by Aβ were evaluated (Figure 2-4B). The cell viability was reduced to ca. 55% by Aβ (10 μM). In the presence of compound **B** at 1 μM concentration, the cell viability was reduced to ca. 70% with or without Aβ, indicating that compound **B** attenuates the Aβ-induced cytotoxicity. Indeed, these reductions in cell viability were caused by the cytotoxicity of compound **B**. Surprisingly, compound **K** was found not only to possess low cytotoxicity but also a significant protective ability against the Aβ-induced cytotoxicity, and more than 90% of cell viability was observed in the Aβ-stimulated cells treated with compound **K**. These results indicated that compound **K** would be able to prevent neurotoxicity caused by Aβ aggregation.

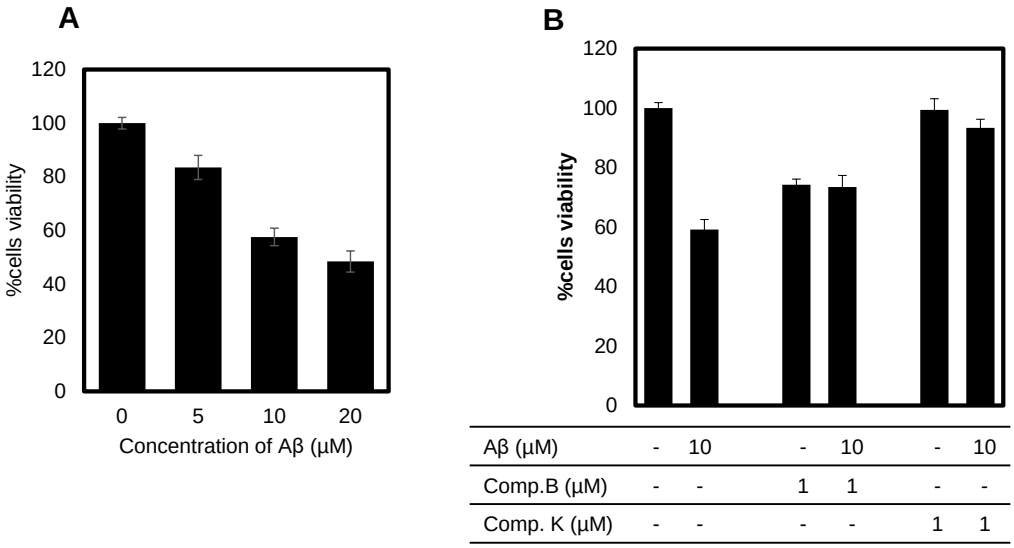

Figure 2-4. Curcumin derivatives attenuate Aβ-induced cytotoxicity. (A) Cytotoxic effect of Aβ on N2a cells. (B) Effect of compounds **B** and **K** on the cell viability of Aβ-stimulated N2A cells.

2.3. Summary of Chapter 2

This study identified compound **B** as a potent Aβ inhibitor from a curcumin-based activity cliff region originating from SARM analysis and revealed by MGM. Compound **B** possessed low cytotoxicity on N2a cells and attenuated Aβ-induced cytotoxicity. Negative staining TEM images indicated that compound **B** induced the shortening of Aβ fibrils and increased the generation of Aβ oligomers in a concentration-dependent manner. Furthermore, compound **K**, in which the tert-butyl ester group replaced the methyl ester group of compound **B**, possessed lower cytotoxicity on N2a cells and attenuated Aβ-induced cytotoxicity than compound **B**, indicating that compound **K** could prevent neurotoxicity caused by Aβ aggregation. Taken together, the results provide several lines of evidence for the relevance of the activities of curcumin derivatives observed in this study, although curcumin has PAINS character and is prone to eliciting assay artifacts.

2.4. Experimental section

SAR Matrix software beta version was provided under the license from Dr. Atsushi Yoshimori from Institute for Theoretical Medicine, Inc, Japan. All the solvents used

were in analytical standard grade. The NMR spectra were measured on a Bruker biospin AVANCE II (400 MHz for ^{1}H and 100 MHz for ^{13}C) or a Bruker biospin AVANCE III (500 MHz for ^{1}H, 125 MHz for ^{13}C, and 470 MHz for ^{19}F). Chemical shifts (δ) was reported in ppm relative to internal tetramethylsilane. The HRMS data were recorded on the Bruker ESI-TOF-MS micrOTOF II instrument with sodium formate as the calibration standard. Transmission electron microscopy was performed using Hitachi H-8100 operated at 200 kV. Vanillin was purchased from Wako (Japan). Acetyl acetone and methyl bromoacetate were purchased from Sigma (USA). Morpholine was purchased from Wako (Japan). The 4-hydroxy-3-(trifluoromethyl) benzaldehyde was purchased from Fluorochem (UK). The 3-(trifluoromethyl) benzaldehyde was purchased from Combi-Blocks (USA). The 4-fluoro-3-(trifluoromethyl) benzaldehyde and tert-butyl bromoacetate were purchased from Tokyo Chemical Industry (Japan). Tacrine hydrochloride was purchased from Cayman Chemical (USA). Microwave for synthesis was conducted on Biotage® Initiator+ instrument. Column chromatography was performed on silica gel Chromatorex (Japan). Purity analysis of compound **A-K** was determined by HPLC analysis using Inertsil ODS-3 5 μm (4.6 × 75 mm; GL Science) with a linear gradient of 0.1% formic acid in water/0.1% formic acid in MeCN detected by a UV lamp for 25 min. The amyloid β containing 42-amino acid residue was purchased from Peptide Institute (Japan). The ThT for fluorescence detection of Aβ was purchased from Sigma (USA). The fluorescence intensity was measured on Tecan Infinite 200.

Synthesis of Compounds

General Procedure to Synthesis Compound 2a and 2b

Compound **1a** or **1b** (1 mmol) and potassium carbonate (1 mmol) were dissolved in DMF 10 mL. Methyl bromoacetate (1.1 mmol) was added then the mixture was refluxed for 2 h at 80 ^{o}C. The reaction was quenched by HCl 0.1 M then extracted by ethyl acetate. The organic layer was dried using $MgSO_4$ then, purified by column chromatography (silica gel, hexane:ethyl acetate 2:1). **Methyl 2-(4-formyl-2-methoxyphenoxy) acetate (2a).** Yield: 96%. ^{1}H-NMR (400 MHz, $CDCl_3$): δ (ppm) 3.86 (-OCH_3, s, 3H), 4.01 (-OCH_3, s, 3H), 4.84 (-CH_2, s, 2H), 6.92 (=CH, *J*=8.1, d,

1H), 7.46 (=CH, *J*=5.5, 1.8 Hz, dd, 1H), 7.49 (=CH, *J*=1.7, d, 1H), 9.92 (-CHO, s, 1H). ^{13}C-NMR (100 MHz, $CDCl_3$): δ (ppm) 52.89, 56.52, 66.24, 110.34, 112.78, 126.62, 131.59, 150.37, 152.89, 169.01, 190.38. LRMS-ESI (*m/z*): calcd for $C_{11}H_{13}O_5^+$ 225.08; found 225.09 $[M+H]^+$. **Methyl 2-(4-formyl-2-(trifluoromethyl)phenoxy)acetate (2b).** Yield: 94%. ^{1}H-NMR (400 MHz, $CDCl_3$): δ (ppm) 3.82 (-OCH_3, s, 3H), 4.01 (-OCH_3, s, 3H), 4.76 (-CH_2, s, 2H), 6.88 (=CH, *J*=8.8, d, 1H), 8.05 (=CH, *J*=8.4, d, 1H), 8.18 (=CH, s, 1H), 9.96 (-OH, s, 1H). ^{13}C-NMR (100 MHz, $CDCl_3$): δ (ppm) 52.15, 65.21, 112.86, 119.55 (J_{C-F}=30.7 Hz, d), 122.69 (J_{C-F}=271.4 Hz, d), 128.81 (J_{C-F}=5.2 Hz, d), 129.59, 134.92, 159.97, 159.98, 167.66, 189.54. LRMS-ESI (*m/z*): calcd for $C_{11}H_9F_3O_4Na^+$ 285.03; found 285.09 $[M+Na]^+$.

General Procedure to Synthesis Compound 2c

Compound **2b** (0.26 mmol) was dissolved in 0.5 mL methanol, then 2 mL of NaOH 1 M was added. The mixture was stirred for 1 h at 100 ^{o}C. The reaction was quenched by adding of HCl 0.1 M, then was extracted using ethyl acetate. The desired compound was purified by column chromatography (silica gel, hexane:ethyl acetate 2:1). **2-(4-formyl-2-(trifluoromethyl)phenoxy)acetic acid (2c).** Yield: 41%. ^{1}H-NMR (400 MHz, $CDCl_3$): 4.94 (=CH, *J*=8.6 Hz, d, 1H) 7.08 (=CH, *J*=8.6 Hz, d, 1H), 8.09 (=CH, *J*=8.7 Hz, d, 1H), 8.21 (=CH, *J*=1.6, d, 1H), 9.99 (-CHO, s, 1H). ^{13}C-NMR (125 MHz, DMSO-d_6): δ (ppm) 65.43, 68.99, 113.89, 117.19 (J_{C-F}=30.9 Hz, q), 123.30 (J_{C-F}=270.9 Hz, q), 123.33, 128.09 (J_{C-F}=5.7 Hz, q), 128.84 (J_{C-F}=5.6 Hz, q), 129.31, 135.41, 159.15, 166.04, 169.25, 191.02. LRMS-ESI (*m/z*): calcd for $C_{10}H_6F_3O_4^-$ 247.02; found 247.12 $[M-H]^-$.

General Procedure to Synthesis Compound 3a

Compound **3a** was synthesized using microwave-assisted reaction. Acetylacetone (20 mmol) and boric acid (20 mmol) were dissolved in DMF. Compound **2a** (2 mmol) was added, followed by morpholine (0.6 mmol). The mixture was irradiated in the microwave at 150 ^{o}C for 10 min. The reaction was stopped by adding HCl 0.1 M. Crude product was extracted by ethyl acetate then the organic phase was dried using $MgSO_4$. Purification to obtain the desired compound was conducted

using column chromatography (silica gel, hexane:ethyl acetate 2:1). **Methyl 2-{4-[(1E)-3,5-dioxohex-1-en-1-yl]-2-methoxyphenoxy}acetate (3a).** Yield: 61%. ^{1}H-NMR (400 MHz, $CDCl_3$): δ (ppm) 3.85 (-OCH_3, s, 3H), 3.97 (-OCH_3, s, 3H), 4.78 (-CH_2, s, 2H), 5.69 (-CH_2, s, 2H), 6.39 (=CH, *J*=15.6 Hz, d, 1H), 6.83 (=CH, *J*=8.8 Hz, d, 1H), 7.10 (=CH, *J*=6.8 Hz, d, 1H), 7.12 (=CH, *J*=6.8 Hz, d, 1H), 7.57 (=CH, *J*=16.0 Hz, d, 1H).). ^{13}C-NMR (125 MHz, CD_3CN): δ (ppm) 27.00, 52.66, 56.42, 66.25, 101.72, 111.66, 114.10, 118.32, 122.18, 122.87, 130.09, 149.94, 150.45, 169.98, 178.59, 198.89. LRMS-ESI (*m/z*): calcd for $C_{16}H_{19}O_6^+$ 307.12; found 307.02 $[M+H]^+$.

General Procedure to Synthesis Compound A and G

Compound **A** and **G** was synthesized using microwave-assisted reaction. Compound **3a** (0.26 mmol) and boric acid (0.26 mmol) was suspended in DMF. Compound **1b** or compound 3-trifluoromethyl benzaldehyde (0.26 mmol) was added followed by morpholine (0.1 mmol). The mixture was irradiated in microwave at 150 ^{o}C for 10 min. HCl 0.1 M was added to quench the reaction. Crude product was extracted by ethyl acetate then dried using $MgSO_4$. The desired compound was purified by column chromatography (silica gel, hexane:ethyl acetate 2:1). **Methyl 2-(4-((1E,6E)-7-(4-hydroxy-3-(trifluoromethyl)phenyl)-3,5-dioxohepta-1,6-dien-1-yl)-2-methoxyphenoxy)acetate (A)**. Yield: 40%. ^{1}H-NMR (400 MHz, CD_3CN): δ (ppm) 3.76 (-OCH_3, s, 3H), 3.91 (-OCH_3, s, 3H), 4.76 (-CH_2, s, 2H), 5.47 (-CH_2, s, 2H), 5.47 (=CH, s, 1H), 5.97 (=CH, s, 1H), 6.72 (=CH, *J*=16.0 Hz, d, 1H), 6.76 (=CH, *J*=16.0 Hz, d, 1H), 6.91 (=CH, *J*=8.4 Hz, d, 1H), 7.09 (=CH, *J*=8.4 Hz, d, 1H), 7.18 (=CH, *J*=8.4 Hz, d, 1H), 7.30 (=CH, *J*=1.9 Hz, d, 1H), 7.62 (=CH, *J*=16.0 Hz, d, 1H), 7.64 (=CH, *J*=16.0 Hz, d, 1H), 7.76 (=CH, *J*=8.4, 2.0 Hz, dd, 1H), 7.86 (=CH, *J*=1.6 Hz, d, 1H), 8.34 (=CH, s, 1H). ^{13}C-NMR (125 MHz, DMSO-d_6): δ (ppm) 52.16, 55.99, 58.75, 65.28, 101.67, 111.32, 112.35 (J_{C-F}=270.3 Hz, q), 116.36 (J_{C-F}=32.1 Hz, q), 117.95, 122.90, 125.95, 127.62, (J_{C-F}=4.4 Hz, q), 128.28, 128.50 (J_{C-F}=3.8 Hz, q), 128.74, 133.66, 135.82, 139.35, 140.63, 149.37, 157.94, 169.29, 183.31, 183.65. ^{19}F-NMR (470 MHz, DMSO-d_6): δ 61.2. HRMS-ESI (*m/z*): calcd for $C_{24}H_{20}F_3O_7^-$ 477.1239; found 477.1241 $[M-H]^-$.HPLC purity 94.3%, retention time 5.74 min. **Methyl 2-(4-((1E,6E)-3,5-**

dioxo-7-(3-(trifluoromethyl)phenyl)hepta-1,6-dien-1-yl)-2-methoxyphenoxy)acetate (G). Yield: 35%. ^{1}H-NMR (400 MHz, $CDCl_3$): δ (ppm) 3.83 (-OCH_3, s, 3H), 3.97 (-OCH_3, s, 3H), 4.77 (-CH_2, s, 2H), 5.85 (-CH_2, s, 1H), 6.55 (=CH, *J*=15.8 Hz, d, 1H), 6.69 (=CH, *J*=15.8 Hz, d, 1H), 6.83 (=CH, *J*=8.7 Hz, d, 1H), 7.13 (=CH, s, 1H), 7.15 (=CH, *J*=7.2, 1.8 Hz, dd, 1H), 7.55 (=CH, *J*=8.0 Hz, t, 1H), 7.65 (=CH, *J*=15.8 Hz, d, 1H), 7.69 (=CH, *J*=15.8 Hz, d, 1H), 7.73 (=CH, *J*=7.8 Hz, d, 1H), 7.82 (=CH, s, 1H). ^{13}C-NM`R (125 MHz, DMSO-d_6): δ (ppm) 52.01, 55.87, 65.14, 102.08, 111.27, 113.25, 122.71, 122.95, 124.19 (J_{C-F}=270.9 Hz, q), 124.82, 126.40, 128.49, 130.02 (J_{C-F}=32.8 Hz, q), 130.16, 132.05, 136.11, 138.01, 141.33, 149.27, 149.39, 169.11, 181.21, 185.28. ^{19}F-NMR (470 MHz, DMSO-d_6): δ 61.2. HRMS-ESI (*m/z*): calcd for $C_{24}H_{20}F_3O_6^-$ 462.1290; found 461.1280 $[M-H]^-$. HPLC purity 90.7%, retention time 6.76 min.

General Procedure to Synthesis Compound 4a and 4b

Compound **4a** and **4b** was synthesized using microwave-assisted reaction. Acetylacetone (20 mol) and boric acid (20 mmol) were suspended in DMF. Compound **1a** or **1b** (2 mmol) was added then followed by morpholine (0.6 mmol). The mixture was irradiated in microwave at 150 ^{o}C for 10 min. The reaction mixture was quenched by HCl 0.1 M and extracted using ethyl acetate. The organic phase was dried using $MgSO_4$. The crude product was purified by column chromatography (silica gel, hexane:ethyl acetate 2:1) to obtain the desired compound and curcumin. **(4-hydroxy-3-methoxyphenyl) hex-5-ene-2,4-dione (4a)**. Yield: 65%. ^{1}H-NMR (400 MHz, $CDCl_3$): δ (ppm) 2.20 (-CH_3, s, 3H), 3.98 (-OCH_3, s, 3H), 5.68 (=CH, s, 1H), 5.87 (=CH, s, 1H), 6.37 (=CH, *J*=15.8, d, 1H), 6.97 (=CH, *J*=8.2, d, 1H), 7.06 (=CH, *J*=1.8 Hz, d, 1H), 7.13 (=CH, *J*=8.2, 1.8 Hz, dd, 1H), 7.58 (=CH, *J*=15.8 Hz, d, 1H). ^{13}C-NMR (125 MHz, $CDCl_3$): δ (ppm) 26.59, 55.86, 100.69, 111.39, 115.88, 119.87, 123.09, 126.55, 140.47, 148.19, 149.41, 178.48, 196.85. LRMS-ESI (*m/z*): calcd for $C_{13}H_{15}O_4^+$ 235.10; found 235.13 $[M+H]^+$. **(E)-6-(4-hydroxy-3-(trifluoromethyl)phenyl)hex-5-ene-2,4-dione (4b).** Yield: 23%. ^{1}H-NMR (400 MHz, $CDCl_3$): δ (ppm) 2.20 (-CH_3, s, 3H), 5.67 (-CH_2, s, 1H), 6.41 (=CH, *J*=16.0 Hz, d, 1H), 7.01 (=CH, *J*=8.4 Hz, d, 1H), 7.57 (=CH, *J*=16.0 Hz, d, 1H), 7.61 (=CH, *J*=8.4, 1.6 Hz, dd, 1H), 7.70 (=CH, s,

1H). ^{13}C-NMR (125 MHz, DMSO-d_6): δ (ppm) 26.79, 101.24, 101.32, 116.53 (J_{C-F}=30.1 Hz, q), 117.94, 121.48, 124.15 (J_{C-F}=270.9 Hz, q), 125.99, 127.33, 128.24 (J_{C-F}=5.2 Hz, q), 133.37, 138.59, 157.93, 177.59, 197.78. LRMS-ESI (*m/z*): calcd for $C_{13}H_{10}F_3O_3^-$ 271.05; found 271.03 $[M-H]^+$.

General Procedure to Synthesis Compound B, C, F, and J

Compounds **B**, **C**, **F**, and **J** were synthesized using microwave-assisted reaction. Compounds **4a** or **4b** (0.26 mmol) and boric acid (0.26 mmol) were suspended in DMF. Compounds **2a**, **2b**, and **2c** (0.26 mmol) were added followed by morpholine (0.1 mmol). The mixture was irradiated in microwave at 150 ^{o}C for 10 min. The HCl 0.1 M was added to quench the reaction. Crude product was extracted by ethyl acetate then dried using $MgSO_4$. The desired compound was purified by column chromatography (silica gel, hexane:ethyl acetate 2:1). **(1E,6E)-1-(4-hydroxy-3-methoxyphenyl)-7-[3-(trifluoromethyl)phenyl]hepta-1,6-diene-3,5-dione (B)**. Yield: 30%. ^{1}H-NMR (400 MHz, DMSO-d_6): 3.72 (-OCH_3, s, 3H), 3.85 (-OCH_3, s, 3H), 5.07 (-CH_2, s, 2H), 6.12 (=CH, s, 1H), 6.81 (=CH, *J*=15.8 Hz, d, 1H), 6.83 (=CH, *J*=8.1 Hz, d, 1H), 6.93 (=CH, *J*=15.9 Hz, d, 1H), 7.18 (=CH, *J*=8.1 Hz, d, 1H), 7.2% (=CH, *J*=8.8 Hz, d, 1H), 7.34 (=CH, s, 1H), 7.58 (=CH, *J*=15.8, d, 1H), 7.63 (=CH, *J*=15.9, d, 1H), 7.98 (=CH, *J*=8.6, d, 1H), 8.01 (=CH, s, 1H).). ^{13}C-NMR (125 MHz, DMSO-d_6): δ (ppm) 52.19, 55.88, 65.29, 101.64, 111.59, 114.36, 115.94, 118.01 (J_{C-F}=30.9 Hz, q), 121.29, 123.54, 123.54 (J_{C-F}=270.4 Hz, q), 124.19, 126.45, 127.09 (J_{C-F}=4.7 Hz, q), 128.17, 133.81, 137.99, 141.68, 148.23, 149.78, 156.70, 168.55, 181.73, 184.89. ^{19}F-NMR (470 MHz, DMSO-d_6): δ 60.9. HRMS-ESI (*m/z*): calcd for $C_{24}H_{20}F_3O_7^-$ 477.1239; found 477.1235 $[M-H]^-$. HPLC purity 96.1%, retention time 5.88 min. **2-(4-((1E,6E)-7-(4-hydroxy-3-methoxyphenyl)-3,5-dioxohepta-1,6-dien-1-yl)-2-(trifluoromethyl)phenoxy)acetic acid (C).** Yield: 15%. ^{1}H-NMR (400 MHz, CD_3CN): 3.98 (-OCH_3, s, 3H), 4.84 (-CH_2, s, 2H), 5.98 (=CH, s, 1H), 6.72 (=CH, *J*=16.0 Hz, d, 1H), 6.78 (=CH, *J*=16.0 Hz, d, 1H), 6.89 (=CH, *J*=8.0 Hz, d, 1H), 7.10 (=CH, *J*=8.8 Hz, d, 1H), 7.18 (=CH, *J*=8.2, 1.9 Hz, dd, 1H), 7.29 (=CH, *J*=1.8 Hz, d, 1H), 7.65 (=CH, *J*=15.6 Hz, d, 2H), 7.84 (=CH, *J*=8.6 Hz, d, 1H), 7.94 (=CH, *J*=1.9 Hz, d, 1H). ^{13}C-NMR (125 MHz, DMSO-d6): δ (ppm) 55.92, 66.81, 101.58,

111.59, 114.52, 115.99, 117.66 (J_{C-F}=30.2 Hz, q), 121.29, 122.67, 123.58, 123.74 (J_{C-F}=270.7 Hz, q), 126.40, 126.62, 126.74, 127.04 (J_{C-F}=4.7 Hz, q), 127.22, 127.49 (J_{C-F}=5.2 Hz, q), 133.61, 138.37, 141.62, 141.98, 148.28, 157.84, 170.25, 182.01, 184.68, 198.26. ^{19}F-NMR (470 MHz, DMSO-d_6): δ 60.8. HRMS-ESI (*m/z*): calcd for $C_{23}H_{18}F_3O_7^-$ 463.1083; found 463.1087 $[M-H]^-$. HPLC purity 96.2%, retention time 5.69 min. **methyl 2-(4-((1E,6E)-7-(4-hydroxy-3-methoxyphenyl)-3,5-dioxohepta-1,6-dien-1-yl)-2-methoxyphenoxy)acetate (F).** Yield: 35%. ^{1}H-NMR (400 MHz, $CDCl_3$): δ (ppm) 3.82 (-OCH_3, s, 3H), 3.94 (-OCH_3, s, 3H), 3.94 (-OCH_3, s, 3H), 4.75 (-CH_2, s, 2H), 5.82 (-CH_2, s, 1H), 6.47 (=CH, *J*=15.8 Hz, d, 1H), 6.52 (=CH, *J*=15.8 Hz, d, 1H), 6.82 (=CH, *J*=8.8 Hz, d, 1H), 6.94 (=CH, *J*=8.2 Hz, d, 1H), 7.04-7.13 (=CH, m, 4H), 7.58 (=CH, *J*=15.8 Hz, d, 1H), 7.62 (=CH, *J*=15.8 Hz, d, 1H). ^{13}C-NMR (100 MHz, $CDCl_3$): δ (ppm) 52.29, 55.96, 66.15, 101.28, 109.75, 110.87, 113.77, 114.89, 121.76, 122.74, 127.63, 129.65, 139.89, 140.79, 146.86, 147.98, 149.03, 149.75, 169.03, 182.69, 183.78. HRMS-ESI (*m/z*): calcd for $C_{24}H_{23}O_8^-$ 439.1471; found 439.1471 $[M-H]^-$. HPLC purity 94.9%, retention time 5.15 min. **methyl 2-(4-((1E,6E)-7-(4-hydroxy-3-(trifluoromethyl)phenyl)-3,5-dioxohepta-1,6-dien-1-yl)-2-(trifluoromethyl)phenoxy)acetate (J).** Yield: 43%. ^{1}H-NMR (400 MHz, DMSO-d_6): δ (ppm) 3.72 (-CH_3, s, 3H), 5.07 (-CH_2, s, 2H), 6.14 (-CH_2, s, 1H), 6.89 (=CH, *J*=16.0 Hz, d, 1H), 6.98 (=CH, *J*=16.0 Hz, d, 1H), 7.10 (=CH, *J*=8.4 Hz, d, 1H), 7.27 (=CH, *J*=8.8 Hz, d, 1H), 7.62-7.68 (=CH, m, 2H), 7.87 (=CH, *J*=8.8 Hz, d, 1H), 7.90 (=CH, s, 1H), 7.99 (=CH, *J*=8.7 Hz, d, 1H), 8.02 (=CH, s, 1H). ^{13}C-NMR (125 MHz, DMSO-d_6): δ (ppm) 52.20, 65.29, 101.86, 114.41, 116.26 (J_{C-F}=30.1 Hz, q), 117.79, 117.96 (J_{C-F}=30.5 Hz, q), 122.83, 123.51 (J_{C-F}=271.3 Hz, q), 123.92 (J_{C-F}=272.5 Hz, q), 124.16, 125.83, 127.18, 127.61 (J_{C-F}=4.1 Hz, q), 128.07, 133.70, 133.96, 138.48, 139.65, 156.78, 157.83, 168.55, 182.63, 183.99. ^{19}F-NMR (470 MHz, DMSO-d_6): δ 60.9, 61.2. HRMS-ESI (*m/z*): calcd for $C_{24}H_{17}F_6O_6^-$ 515.1008; found 515.1008 $[M-H]^-$. HPLC purity 93.4%, retention time 6.33 min.

General Procedure to Synthesis Compound D and I

Compound **D** was synthesized using microwave-assisted reaction. Compound **4a** (0.26 mmol) and boric acid (0.26 mmol) were suspended in DMF. 3-

Trifluoromethyl benzaldehyde (0.26 mmol) was added followed by morpholine (0.1 mmol). The mixture was irradiated in microwave at 150 ºC for 10 min. The HCl 0.1 M was added to quench the reaction. Crude product was extracted by ethyl acetate then dried over $MgSO_4$. The desired compound was purified by column chromatography (silica gel, hexane:ethyl acetate 2:1). **(1E,6E)-1-(4-hydroxy-3-methoxyphenyl)-7-[3-(trifluoromethyl) phenyl]hepta-1,6-diene-3,5-dione (D)**. Yield: 50%. ^{1}H-NMR (400 MHz, $CDCl_3$): 3.98 (-OCH_3, s, 3H), 5.88 (-CH_2, s, 2H), 6.53 (=CH, *J*=15.8 Hz, d, 1H), 6.68 (=CH, *J*=15.9 Hz, d, 1H), 6.97 (=CH, *J*=8.2, d, 1H), 7.09 (=CH, *J*=1.5 Hz, d, 1H), 7.17 (=CH, *J*=8.2, 1.6 Hz, dd, 1H), 7.55 (=CH, *J*=7.8 Hz, t, 1H), 7.65 (=CH, *J*=15.8 Hz, d, 1H), 7.68 (=CH, *J*=15.9 Hz, d, 1H), 7.73 (=CH, *J*=7.8 Hz, d, 1H), 7.82 (=CH, s, 1H). ^{13}C-NMR (125 MHz, DMSO-d_6): δ (ppm) 55.89, 102.12, 116.02, 121.38, 123.69, 124.26 (J_{C-F}=271.1 Hz, q), 125.78 (J_{C-F}=4.1 Hz, q), 126.29, 126.44 (J_{C-F}=4.8 Hz, q), 129.58 (J_{C-F}=32.1 Hz, q), 129.98, 130.12, 130.27, 131.94, 133.36, 136.25, 137.69, 142.20, 148.31, 150.01, 180.54, 185.96. ^{19}F-NMR (470 MHz, DMSO-d_6): δ 61.4. HRMS-ESI (*m/z*): calcd for $C_{21}H_{16}F_3O_4^-$ 389.1079; found 389.1069 $[M-H]^-$. HPLC purity 98.8%, retention time 6.78 min. **(1E,6E)-1-(4-hydroxy-3-(trifluoromethyl)phenyl)-7-(3-(trifluoromethyl)phenyl)hepta-1,6-diene-3,5-dione (I)** Yield: 28%. ^{1}H-NMR (400 MHz, CD_3CN): δ (ppm) 6.05 (-CH_2, s, 2H), 6.81 (=CH, *J*=16.0 Hz, d, 1H), 6.96 (=CH, *J*=16.0 Hz, d, 1H), 7.09 (=CH, *J*=8.8 Hz, d, 1H), 7.65-7.74 (=CH, m, 3H), 7.78 (=CH, *J*=8.4, 2.0 Hz, dd, 1H), 7.88 (=CH, *J*=2.1 Hz d, 1H), 7.92 (=CH, *J*=7.7 Hz, d, 1H), 7.99 (=CH, s, 1H). ^{13}C-NMR (125 MHz, DMSO-d_6): δ (ppm) 48.83, 102.33, 116.39 (J_{C-F}=30.1 Hz, q), 117.89, 122.83, 123.99 (J_{C-F}=271.3 Hz, q), 124.26 (J_{C-F}=270.7 Hz, q), 124.87, 125.72, 126.42, 127.72, 130.14 (J_{C-F}=31.6 Hz, q), 130.17, 132.07, 133.72, 136.17, 138.14, 140.16, 158.12, 181.41, 185.11. ^{19}F-NMR (470 MHz, DMSO-d_6): δ 61.32, 61.37. HRMS-ESI (*m/z*): calcd for $C_{21}H_{13}F_6O_3^-$ 427.0847; found 427.0849 $[M-H]^-$. HPLC purity 93.7%, retention time 7.28 min.

General Procedure to Synthesis Compound E

Compound **E** was synthesized using microwave-assisted reaction. Compound **4a** (0.26 mmol) and boric acid (0.26 mmol) were suspended in DMF. Compound **1**b

(0.26 mmol) was added followed by morpholine (0.1 mmol). The mixture was irradiated in microwave at 150 ^{o}C for 10 min. The HCl 0.1 M was added to quench the reaction. Crude product was extracted by ethyl acetate then dried over $MgSO_4$. The desired compound was purified by column chromatography (silica gel, hexane:ethyl acetate 2:1). **(1E,6E)-1-(4-hydroxy-3-(trifluoromethyl)phenyl)-7-(4-hydroxy-3-methoxyphenyl)hepta-1,6-diene-3,5-dione (E).** Yield: 28%. Yield: 28%. ^{1}H-NMR (400 MHz, CD_3CN): δ (ppm) 3.94 (-OCH_3, s, 3H), 5.96 (-CH_2, s, 1H), 6.70 (=CH, *J*=15.6 Hz, d, 1H), 6.74 (=CH, *J*=15.6 Hz, d, 1H), 6.89 (=CH, *J*=8.0 Hz, d, 1H), 7.08 (=CH, *J*=8.4 Hz, d, 1H), 7.17 (=CH, *J*=8.4, 1.8 Hz, dd, 1H), 7.28 (=CH, *J*=1.8 Hz, d, 1H), 7.61 (=CH, *J*=15.6 Hz, d, 2H), 7.75 (=CH, *J*=8.6, 1.8 Hz, dd, 1H), 7.86 (=CH, *J*=1.6 Hz, d, 1H). ^{13}C-NMR (125 MHz, DMSO-d_6): δ (ppm) 55.85, 101.32, 115.86, 116.19 (J_{C-F}=30.0 Hz, q), 117.75, 121.22, 121.98 (J_{C-F}=271.3 Hz, q), 122.88, 123.46, 124.99, 125.90, 126.42, 127.41 (J_{C-F}=4.7 Hz, q), 133.54, 138.84, 141.35, 148.16, 149.63, 157.66, 182.42, 184.22. ^{19}F-NMR (470 MHz, DMSO-d_6): δ 61.2. HRMS-ESI (*m/z*): calcd for $C_{21}H_{16}F_3O_5^-$ 405.1028; found 405.1022 $[M-H]^-$. HPLC purity 94.1%, retention time 5.63 min.

General Procedure to Synthesis Compound H

Compound **H** was synthesized using microwave-assisted reaction. Compound **3a** (0.26 mmol) and boric acid (0.26 mmol) were suspended in DMF. Compound **2b** (0.26 mmol) was added followed by morpholine (0.1 mmol). The mixture was irradiated in microwave at 150 ^{o}C for 10 min. The HCl 0.1 M was added to quench the reaction. Crude product was extracted by ethyl acetate then dried over $MgSO_4$. The desired compound was purified by column chromatography (silica gel, hexane:ethyl acetate 2:1). **Methyl 2-(2-methoxy-4-((1E,6E)-7-(4-(2-methoxy-2-oxoethoxy)-3-(trifluoromethyl)phenyl)-3,5-dioxohepta-1,6-dien-1-yl)phenoxy)acetate (H).** Yield: 38%. ^{1}H-NMR (400 MHz, CD_3CN): δ (ppm) 3.77 (-OCH_3, s, 3H), 3.79 (-OCH3, s, 3H), 3.91 (-OCH_3, s, 3H), 4.76 (-CH_2, s, 2H), 4.89 (-CH_2, s, 2H), 6.00 (-CH_2, s, 1H), 6.77 (=CH, *J*=15.8 Hz, d, 1H), 6.81 (=CH, *J*=15.8 Hz, d, 1H), 6.90 (=CH, *J*=8.4 Hz, d, 1H), 7.12 (=CH, *J*=8.7 Hz, d, 1H), 7.21 (=CH, *J*=8.4, 1.9 Hz, dd, 1H), 7.32 (=CH, *J*=1.9 Hz, d, 1H), 7.62 (=CH, *J*=15.8 Hz, d, 1H), 7.67 (=CH, *J*=15.8 Hz, d, 1H), 7.85 (=CH, *J*=8.8, 1.9 Hz, dd, 1H), 7.96 (=CH, *J*=1.9

Hz, d, 1H). ^{13}C-NMR (125 MHz, DMSO-d_6): δ (ppm) 52.04, 52.20, 55.89, 65.16, 65.28, 101.71, 111.25, 113.28, 143.39, 117.93 (J_{C-F}=30.4 Hz, q), 122.42, 122.69, 123.51 (J_{C-F}=271.0 Hz, q), 124.19, 127.14 (J_{C-F}=4.9 Hz, q), 128.07, 128.59, 133.91, 138.34, 140.86, 149.29, 156.75, 168.54, 169.15, 182.45, 184.22. ^{19}F-NMR (470 MHz, DMSO-d_6): δ 60.9. HRMS-ESI (*m/z*): calcd for $C_{27}H_{24}F_3O_9^-$ 549.1451; found 549.1449 $[M-H]^-$. HPLC purity 99.8%, retention time 6.52 min.

General Procedure to Synthesis Compound 5

Compound **1b** (1 mmol) and potassium carbonate (1 mmol) were dissolved in DMF 10 mL. Tert-butyl bromoacetate (1.1 mmol) was added then was refluxed for 2 h at 80 ^oC. The reaction was quenched by HCl 0.1 M then extracted by ethyl acetate. The organic layer was dried using $MgSO_4$ then, purified by column chromatography (silica gel, hexane:ethyl acetate 2:1). **Synthesis of (E)-6-(3-(trifluoromethyl)phenyl)hex-5-ene-2,4-dione.** Yield: 97%. ^{1}H-NMR (400 MHz, $CDCl_3$): δ (ppm) 1.48 (3x-CH_3, s, 9H), 4.75 (-CH_2, s, 2H), 7.02 (=CH, *J*=8.6 Hz, d, 1H), 8.05 (=CH, *J*=8.6, 2.0 Hz, dd, 1H), 8.16 (=CH, *J*=1.8 Hz, d, 1H), 9.95 (-CHO, s, 1H). ^{13}C-NMR (125 MHz, $CDCl_3$): δ (ppm) 27.46, 65.62, 82.69, 112.74, 119.34 (J_{C-F}=31.6 Hz, q), 122.71 (J_{C-F}=271.1 Hz, q), 128.61 (J_{C-F}=5.0 Hz, q), 134.79, 160.10, 166. 06, 189.36. LRMS-ESI (*m/z*): calcd for $C_{14}H_{14}F_3O_4^-$ 303.09; found 303.07 $[M-H]^-$.

General Procedure to Synthesis Compound K

Compound **K** was synthesized using microwave-assisted reaction. Compound **4a** (0.26 mmol) and boric acid (0.26 mmol) were suspended in DMF. Compound **5** (0.26 mmol) was added followed by morpholine (0.1 mmol). The mixture was irradiated by microwave at 150 ^oC for 10 min. The HCl 0.1 M was added to quench the reaction. Crude product was extracted by ethyl acetate then dried using $MgSO_4$. The desired compound was purified by column chromatography (silica gel, hexane:ethyl acetate 2:1. **tert-butyl 2-(4-((1E,6E)-7-(4-hydroxy-3-methoxyphenyl)-3,5-dioxohepta-1,6-dien-1-yl)-2-(trifluoromethyl)phenoxy)acetate (K).** Yield: 28%. ^{1}H-NMR (400 MHz, $CDCl_3$): δ (ppm) 1.51 (-CH_3, s, 9H), 3.99 (-CH_3, s, 3H), 4.70 (-CH_2, s, 2H), 5.86 (-CH_2, S,

2H), 6.53 (=CH, *J*=16.0 Hz, d, 1H), 6.57 (=CH, *J*=16.0 Hz, d, 1H) 6.92 (=CH, *J*=8.6 Hz, d, 1H), 6.99 (=CH, *J*=8.0 Hz, d, 1H), 7.11 (=CH, s, 1H), 7.19 (=CH, *J*=7.9 Hz, d, 1H), 7.61-7.69 (=CH, m, 3H), 7.85 (=CH, s, 1H). ^{13}C-NMR (125 MHz, DMSO-d_6): δ (ppm) 27.82, 55.87, 65.61, 81.98, 101.58, 111.56, 114.18, 115.82, 117.89 (J_{C-F}=30.5 Hz, q), 121.26, 123.53 (J_{C-F}=271.3 Hz, q), 123.56, 124.09, 126.39, 127.11 (J_{C-F}=5.5 Hz, q), 127.96, 133.74, 141.66, 148.18, 149.71, 167.06, 181.77, 184.84. ^{19}F-NMR (470 MHz, DMSO-d_6): δ 60.9. HRMS-ESI (*m/z*): calcd for $C_{27}H_{26}F_3O_7^-$ 519.1709; found 519.1713 $[M-H]^-$. HPLC purity 98.4%, retention time 6.79 min.

ThT Fluorescence Assay

The procedure for solubilizing the Aβ was slightly modified according to the known literature.[16] To prepare the Aβ monomer stock solution, 0.5 mg of the lyophilized Aβ was dissolved in NaOH 2 mM by gently mixing without vortexing to obtain 500 µM as the final concentration. The solution was centrifuged at 13,200 rpm, 4°C, and 10 min. The supernatant was collected and stored at -80 °C. This assay was conducted in 96-well plate full black non-binding with frequent 15s of linear shaking every 5 min and constant heating at 37 °C for 3 h. The ThT stock at concentration 200 µM was freshly prepared in tris glycine 10 mM pH 8.5. For the assay system, the ThT was diluted by PBS 7.4 to reach a concentration of 40 µM in each well. Curcumin stock 10 mM was diluted in each well to obtain 10-fold dilution (1, 0.1, 0.01, 0.001, 0.0001, and 0.00001 µM). The Aβ stock solution was transferred to each well to reach a final concentration of 20 µM. The fluorescence intensity was immediately measured with an excitation of 430 nm and emission of 480 nm using a microplate reader (Tecan Infinite F200, Tecan, Switzerland). The fluorescence intensity data were corrected toward blank containing PBS and ThT, while the IC_{50} values were obtained by plotting the intensity at half V_{max} of each group toward concentration.

MTT Assay

The N2a and U87 MG cells were suspended in Dulbecco's Modified Eagle Medium (DMEM) medium supplemented with 10% fetal bovine serum. Briefly, N2a cells ($8x10^3$ cells/well) and U87MG ($8x10^3$ cells/well) were grown on a 96-well plate

overnight at 37 ^{o}C CO_2 5%. For the single treatment on N2a and U87MG using curcumin derivatives, cells were treated by serial concentrations of curcumin, compound **B**, **D**, and **K** (1, 5, 10, 25, 50, 100, and 200 µM). To screen the toxicity of Aβ, N2a cells were treated by Aβ at a concentration of 5, 10, and 20 µM. Evaluation of protective effect was conducted by treating the N2a cells with Aβ 10 µM with or without curcumin derivatives (1 µM). An MTT reduction assay was conducted as described previously.[17] Briefly, MTT powder was dissolved in PBS pH 7.4 to obtain 5 mg/mL concentration stock, then was diluted into 0.5 mg/mL in DMEM medium. After removing the medium on a 96-well plate containing-treated cell, each well was added by 100 µL MTT 0.5 mg/mL and incubated at 37 ^{o}C CO_2 5%. After 3 h incubation, 100 µL DMSO was added following the absorbance measurement at a wavelength of 550 nm using a microplate reader (Tecan Infinite F200, Tecan, Switzerland). Calculation of % cells viability was measured by dividing the absorbance of untreated cells with the absorbance of curcumin-treated cells.

Negative Staining TEM Imaging

The negative-staining TEM images were obtained according to the following procedure. Elastic carbon grids (ELS-C10, STEM, Japan) was made hydrophilic using an ion coater (IB-2, Eiko, Japan) with 3 mA of plasma current for 40 s before applying sample solution. 5 µM of Aβ only or combined with compound **B** was incubated on PBS pH 7.4 at 37 ^{o}C for 30 min. Briefly, 5 µL of the Aβ sample was applied to a hydrophilic grid and incubated for 1 min at RT. After gently dried with filter paper, the grid sample was washed with Milli-Q water and dried again with filter paper three times. Finally, the grid was incubated with 5 µL of 1% Nano-W negative staining solution (NY, USA) for 1 min followed by complete drying using filter paper. The negative staining sample was observed using TEM H-8100 (Hitachi) operated at 200 kV.

2.5. References

(1) Cummings, J.; Lee, G.; Zhong, K.; Fonseca, J.; Taghva, K. Alzheimer's Disease Drug Development Pipeline: 2021. *Alzheimers Dement (N Y)* **2021**, *7* (1), e12179.

(2) Ringman, J. M.; Frautschy, S. A.; Teng, E.; Begum, A. N.; Bardens, J.; Beigi, M.; Gylys, K. H.; Badmaev, V.; Heath, D. D.; Apostolova, L. G.; Porter, V.; Vanek, Z.; Marshall, G. A.; Hellemann, G.; Sugar, C.; Masterman, D. L.; Montine, T. J.; Cummings, J. L.; Cole, G. M. Oral Curcumin for Alzheimer's Disease: Tolerability and Efficacy in a 24-Week Randomized, Double Blind, Placebo-Controlled Study. *Alzheimers Res Ther.* **2012**, *4* (5), 43.

(3) Bairwa, K.; Grover, J.; Kania, M.; Jachak, S. M. Recent Developments in Chemistry and Biology of Curcumin Analogues. *RSC Adv.* **2014**, *4* (27), 13946.

(4) Chen, M.; Du, Z.-Y.; Zheng, X.; Li, D.-L.; Zhou, R.-P.; Zhang, K. Use of Curcumin in Diagnosis, Prevention, and Treatment of Alzheimer's Disease. *Neural Regen Res* **2018**, *13* (4), 742.

(5) Gupta-Ostermann, D.; Shanmugasundaram, V.; Bajorath, J. Neighborhood-Based Prediction of Novel Active Compounds from SAR Matrices. *J. Chem. Inf. Model.* **2014**, *54* (3), 801–809.

(6) Asawa, Y.; Yoshimori, A.; Bajorath, J.; Nakamura, H. Prediction of an MMP-1 Inhibitor Activity Cliff Using the SAR Matrix Approach and Its Experimental Validation. *Sci Rep* **2020**, *10* (1), 14710.

(7) Pike, C. J.; Burdick, D.; Walencewicz, A. J.; Glabe, C. G.; Cotman, C. W. Neurodegeneration Induced by Beta-Amyloid Peptides in Vitro: The Role of Peptide Assembly State. *J. Neurosci.* **1993**, *13* (4), 1676–1687.

(8) Sulatskaya, A. I.; Sulatsky, M. I.; Antifeeva, Iu. A.; Kuznetsova, I. M.; Turoverov, K. K. Structural Analogue of Thioflavin T, DMASEBT, as a Tool for Amyloid Fibrils Study. *Anal. Chem.* **2019**, *91* (4), 3131–3140.

(9) Nelson, K. M.; Dahlin, J. L.; Bisson, J.; Graham, J.; Pauli, G. F.; Walters, M. A. The Essential Medicinal Chemistry of Curcumin. *J. Med. Chem.* **2017**, *60* (5), 1620–1637.

(10) Um, J. W.; Nygaard, H. B.; Heiss, J. K.; Kostylev, M. A.; Stagi, M.; Vortmeyer, A.; Wisniewski, T.; Gunther, E. C.; Strittmatter, S. M. Alzheimer Amyloid-β Oligomer Bound to Postsynaptic Prion Protein Activates Fyn to Impair Neurons. *Nat Neurosci* **2012**, *15* (9), 1227–1235.

(11) Bettayeb, K.; Oumata, N.; Zhang, Y.; Luo, W.; Bustos, V.; Galons, H.; Greengard, P.; Meijer, L.; Flajolet, M. Small-Molecule Inducers of Aβ-42 Peptide Production Share a Common Mechanism of Action. *FASEB J* **2012**, *26* (12), 5115–5123.

(12) Li, Y.; Cheng, D.; Cheng, R.; Zhu, X.; Wan, T.; Liu, J.; Zhang, R. Mechanisms of U87 Astrocytoma Cell Uptake and Trafficking of Monomeric versus Protofibril Alzheimer's Disease Amyloid-β Proteins. *PLoS ONE* **2014**, *9* (6), e99939.

(13) Sidhar, H.; Giri, R. K. Induction of Bex Genes by Curcumin Is Associated with Apoptosis and Activation of P53 in N2a Neuroblastoma Cells. *Sci. Rep.* **2017**, *7* (1), 41420.

(14) Yang, T.; Zhu, Z.; Yin, E.; Wang, Y.; Zhang, C.; Yuan, H.; Zhang, H.; Jin, S.; Guo, Z.; Wang, X. Alleviation of Symptoms of Alzheimer's Disease by Diminishing Aβ Neurotoxicity and Neuroinflammation. *Chem. Sci.* **2019**, *10* (43), 10149–10158.
(15) Xiao, Y.; Matsuda, I.; Inoue, M.; Sasahara, T.; Hoshi, M.; Ishii, Y. NMR-Based Site-Resolved Profiling of β-Amyloid Misfolding Reveals Structural Transitions from Pathologically Relevant Spherical Oligomer to Fibril. *J. Biol. Chem.* **2020**, *295* (2), 458–467.
(16) Mohamed, T.; Shakeri, A.; Tin, G.; Rao, P. P. N. Structure–Activity Relationship Studies of Isomeric 2,4-Diaminoquinazolines on β-Amyloid Aggregation Kinetics. *ACS Med. Chem. Lett.* **2016**, *7* (5), 502–507.
(17) Mosmann, T. Rapid Colorimetric Assay for Cellular Growth and Survival: Application to Proliferation and Cytotoxicity Assays. *J Immunol Methods* **1983**, *65* (1), 55–63.

^{1}H-NMR Profile of methyl 2-(4-formyl-2-methoxyphenoxy) acetate (2a)

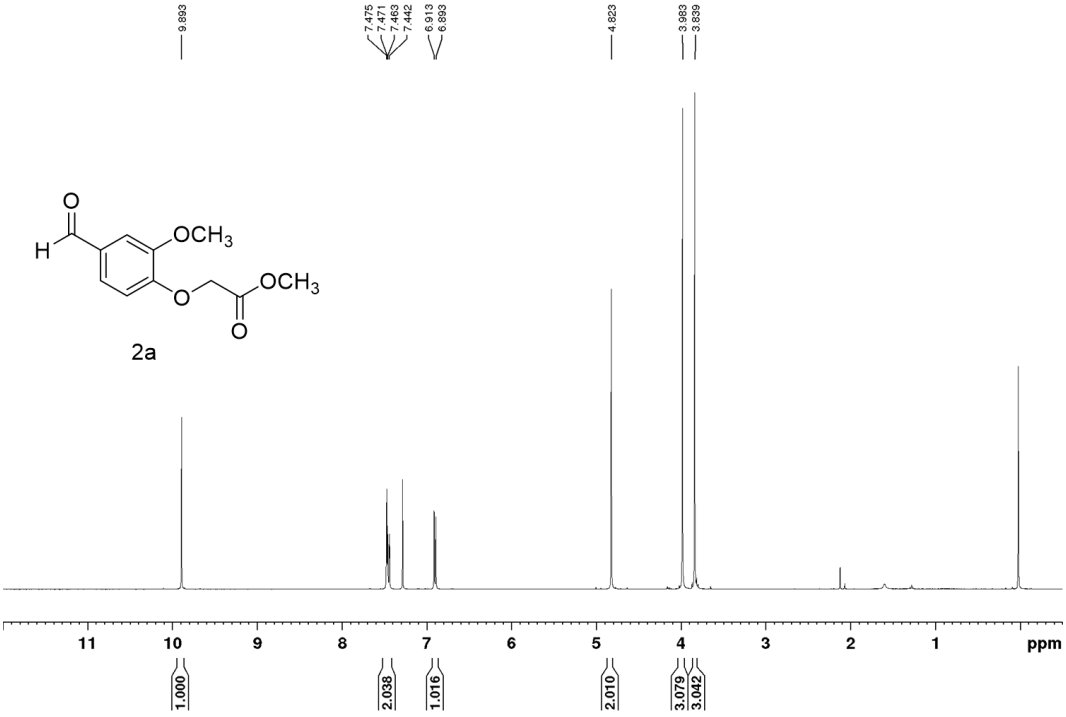

^{13}C-NMR Profile of methyl 2-(4-formyl-2-methoxyphenoxy) acetate (2a)

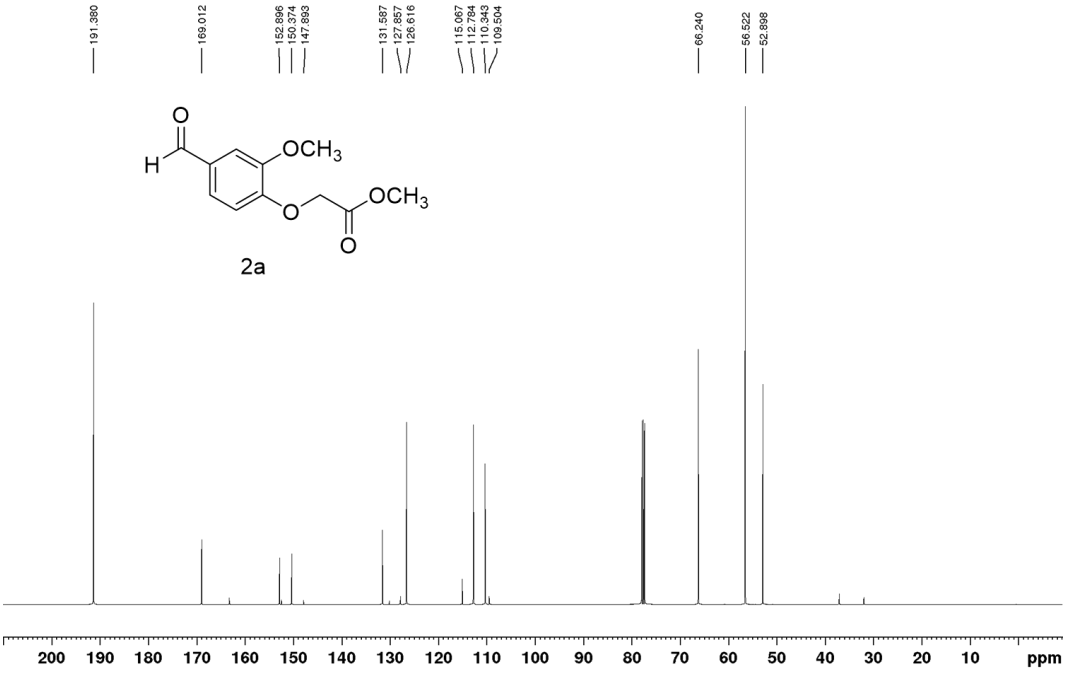

^{1}H-NMR Profile of methyl 2-{4-[(1E)-3,5-dioxohex-1-en-1-yl]-2-methoxyphenoxy}acetate (3a)

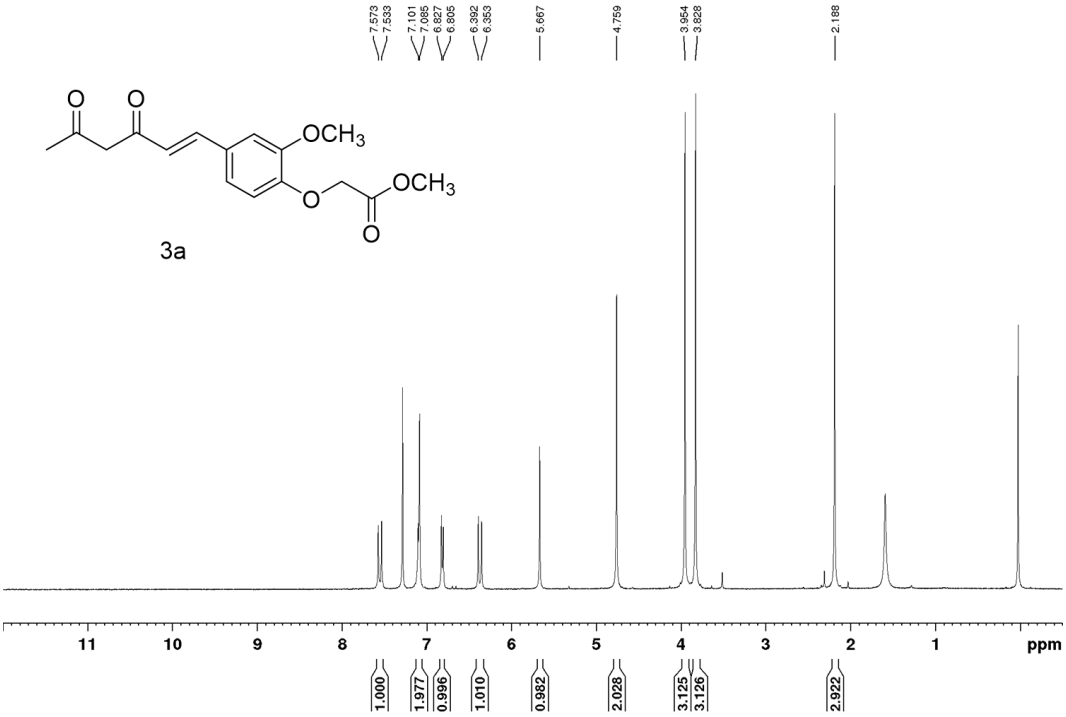

^{13}C-NMR Profile of methyl 2-{4-[(1E)-3,5-dioxohex-1-en-1-yl]-2-methoxyphenoxy}acetate (3a)

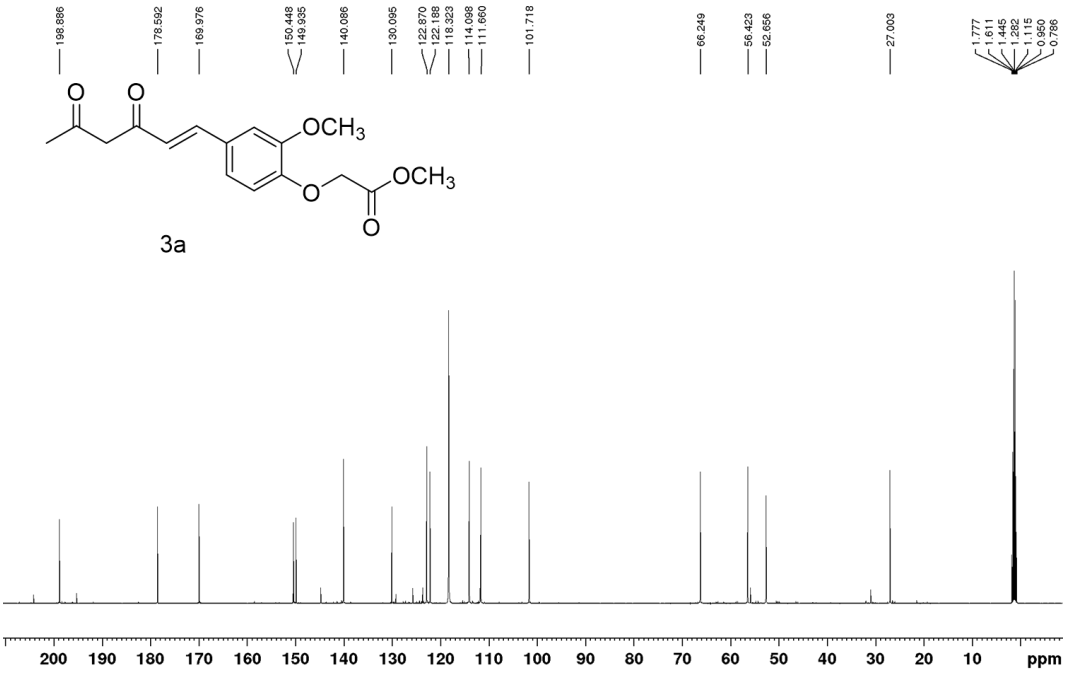

[1]H-NMR Profile of methyl 2-(4-((1E,6E)-7-(4-hydroxy-3-(trifluoromethyl)phenyl)-3,5-dioxohepta-1,6-dien-1-yl)-2-methoxyphenoxy)acetate (Compound A)

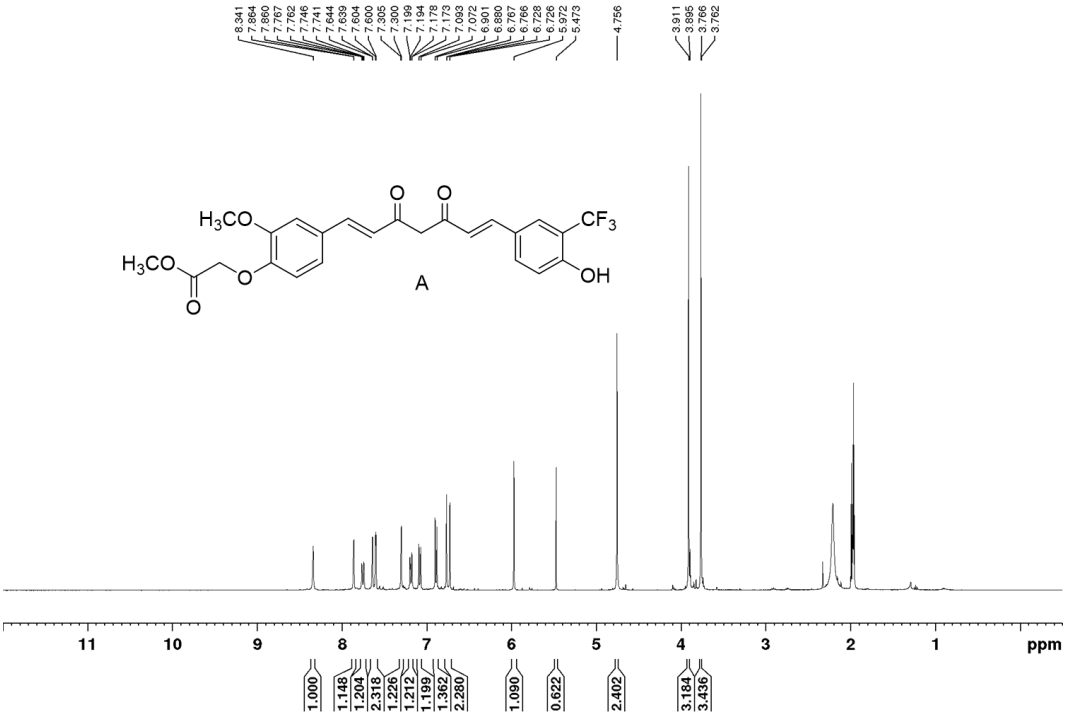

[13]C-NMR Profile of methyl 2-(4-((1E,6E)-7-(4-hydroxy-3-(trifluoromethyl)phenyl)-3,5-dioxohepta-1,6-dien-1-yl)-2-methoxyphenoxy)acetate (Compound A)

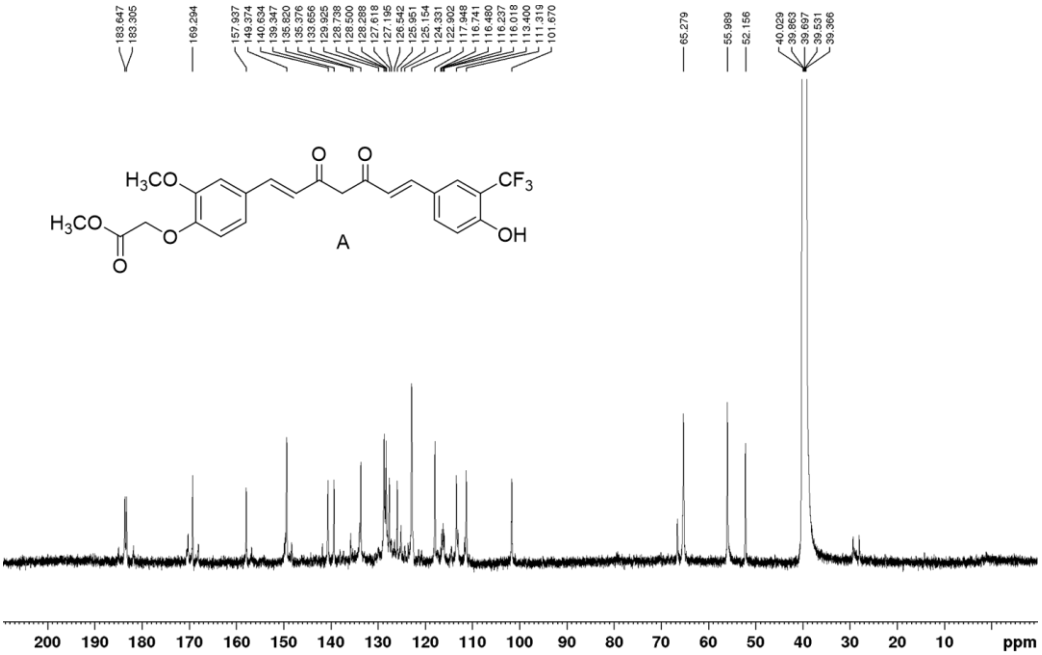

^{19}F-NMR Profile of methyl 2-(4-((1E,6E)-7-(4-hydroxy-3-(trifluoromethyl)phenyl)-3,5-dioxohepta-1,6-dien-1-yl)-2-methoxyphenoxy)acetate (Compound A)

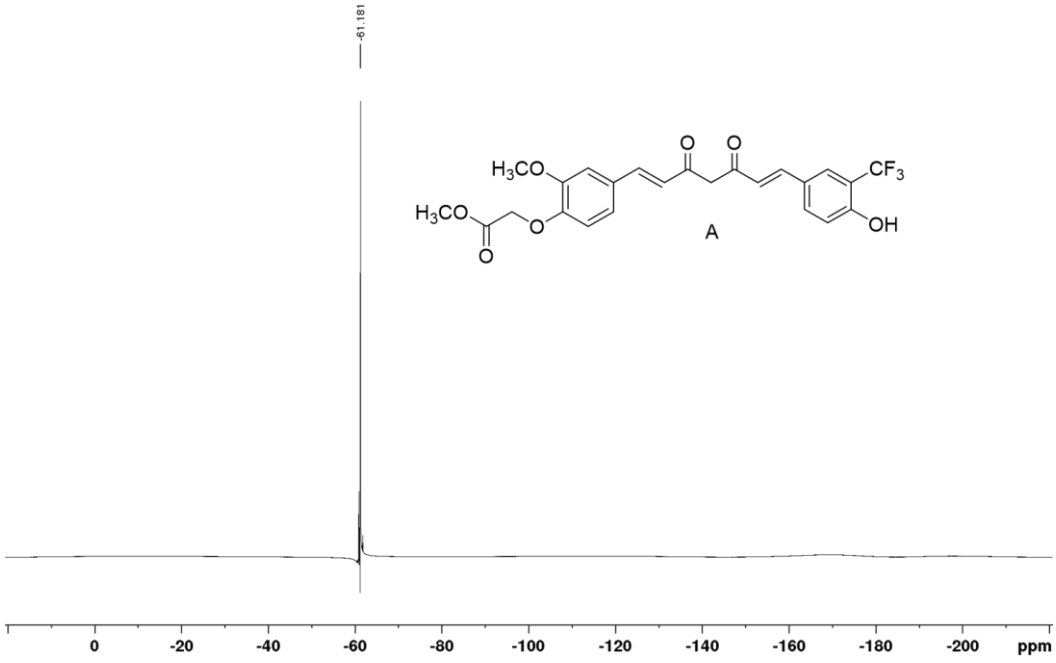

^{1}H-NMR Profile of (4-hydroxy-3-methoxyphenyl)hex-5-ene-2,4-dione (4a)

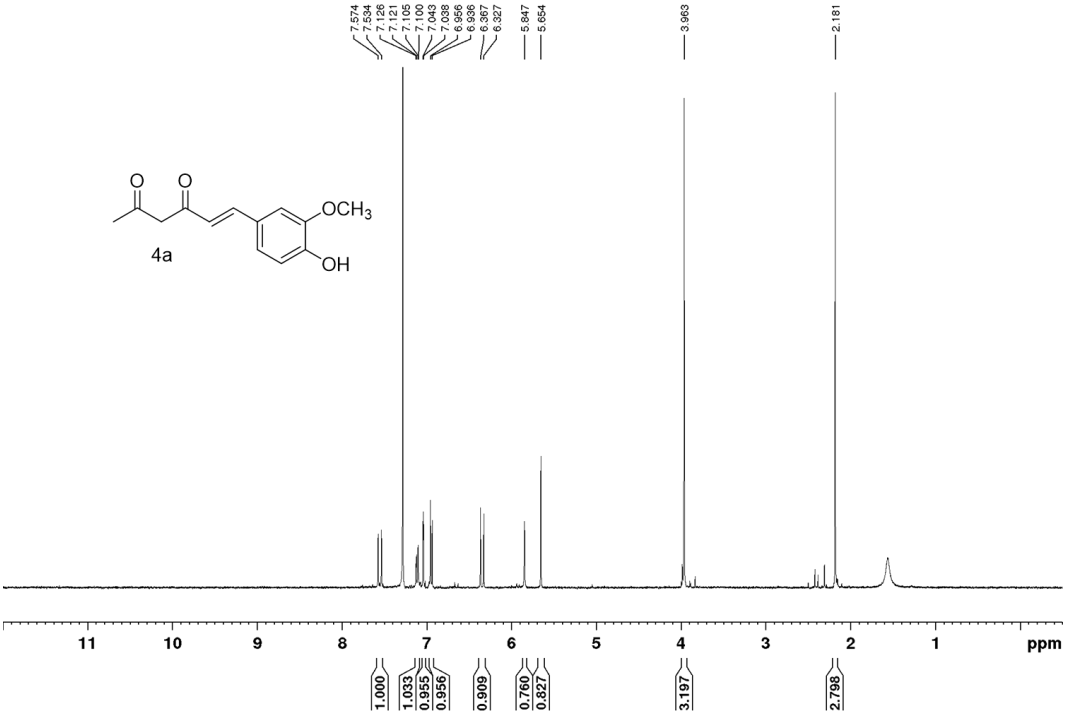

^{13}C-NMR Profile of (4-hydroxy-3-methoxyphenyl)hex-5-ene-2,4-dione (4a)

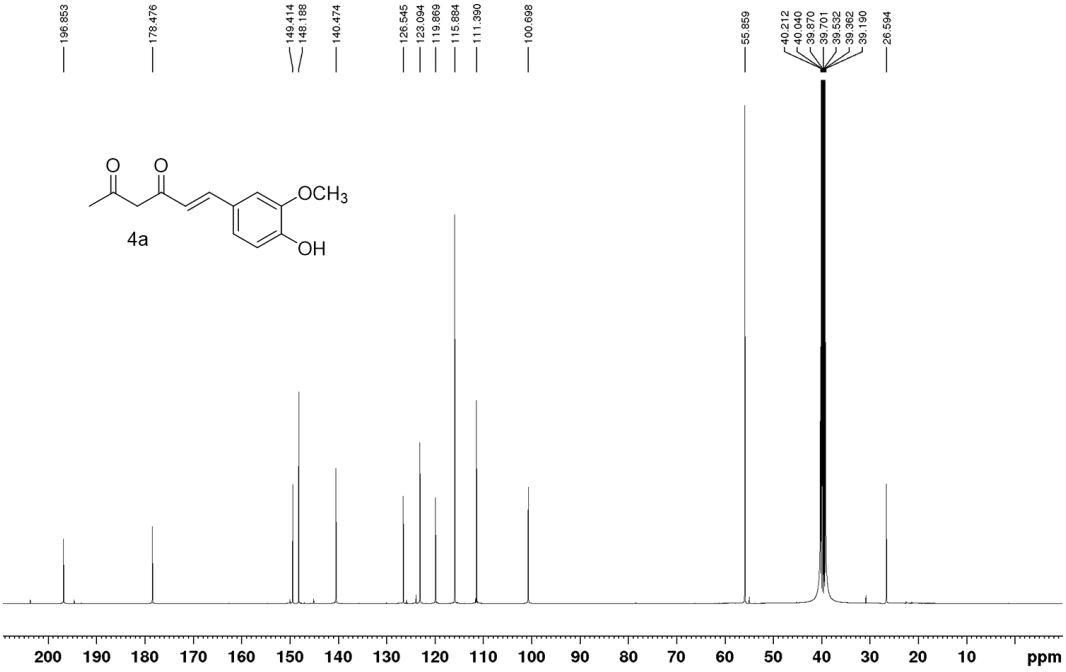

^{1}H-NMR Profile of methyl 2-(4-formyl-2-(trifluoromethyl)phenoxy)acetate (2b)

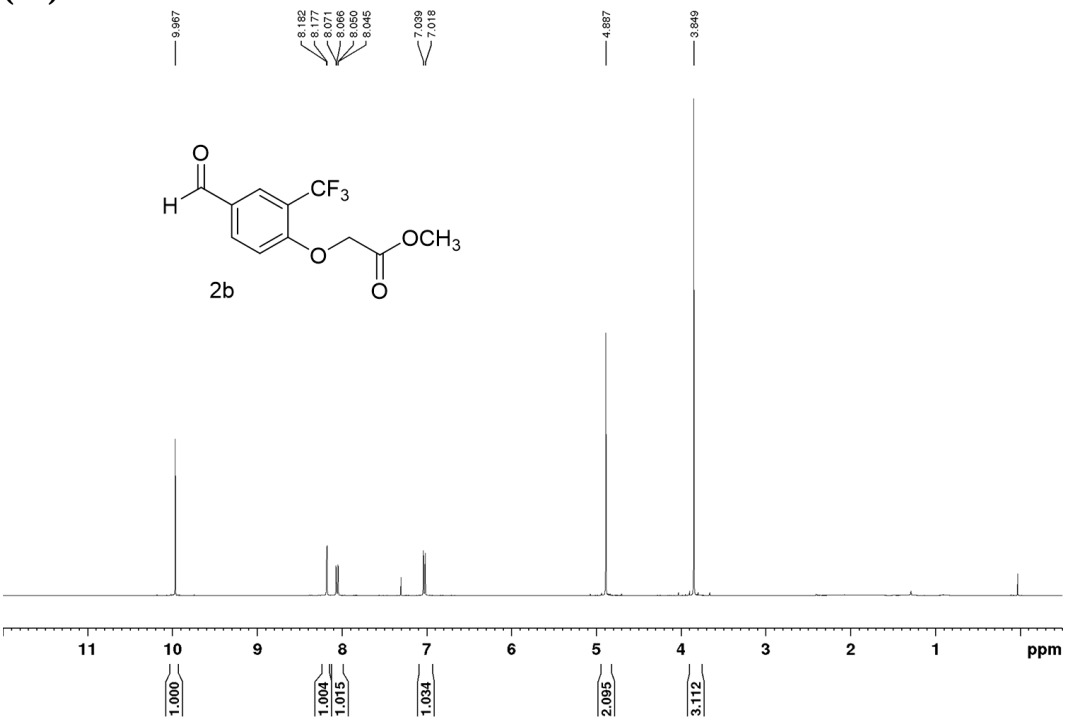

^{13}C-NMR Profile of methyl 2-(4-formyl-2-(trifluoromethyl)phenoxy)acetate (2b)

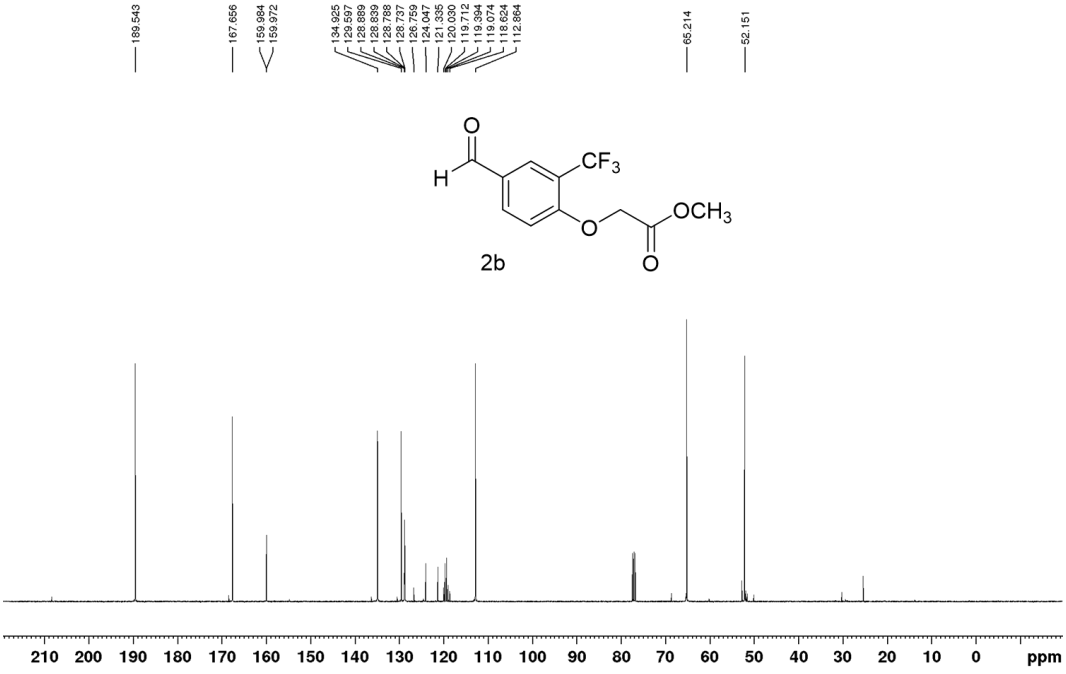

[1]H-NMR Profile of methyl 2-(4-((1E,6E)-7-(4-hydroxy-3-methoxyphenyl)-3,5-dioxohepta-1,6-dien-1-yl)-2-(trifluoromethyl)phenoxy)acetate (Compound B)

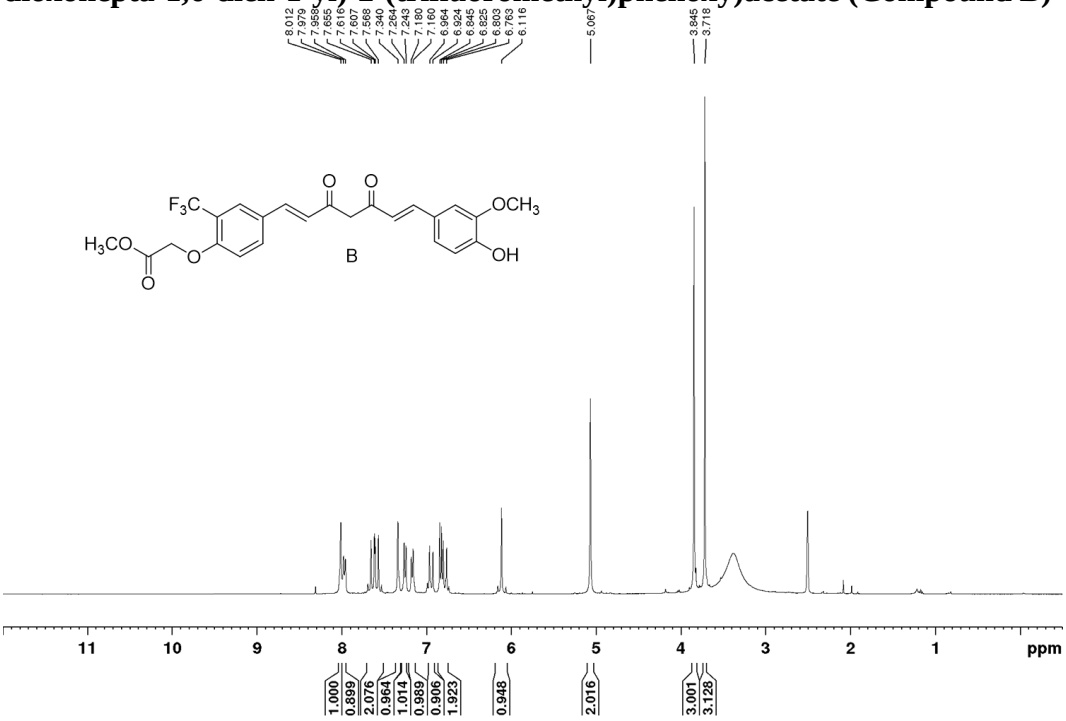

[13]C-NMR Profile of methyl 2-(4-((1E,6E)-7-(4-hydroxy-3-methoxyphenyl)-3,5-dioxohepta-1,6-dien-1-yl)-2-(trifluoromethyl)phenoxy)acetate (Compound B)

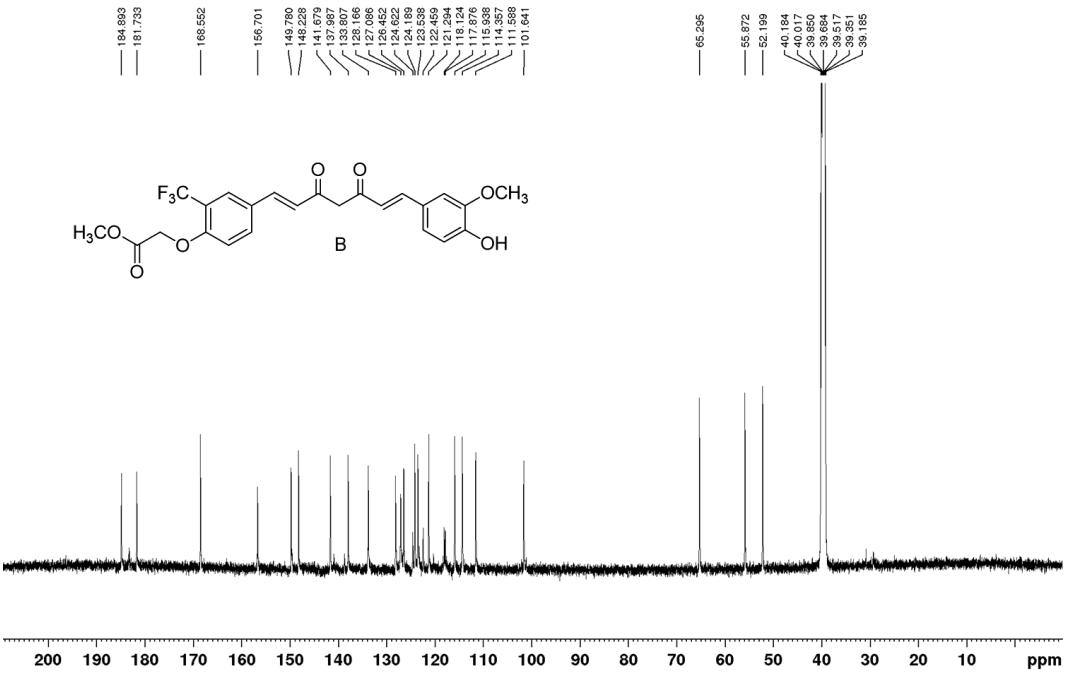

^{19}F-NMR Profile of methyl 2-(4-((1E,6E)-7-(4-hydroxy-3-methoxyphenyl)-3,5-dioxohepta-1,6-dien-1-yl)-2-(trifluoromethyl)phenoxy)acetate (Compound B)

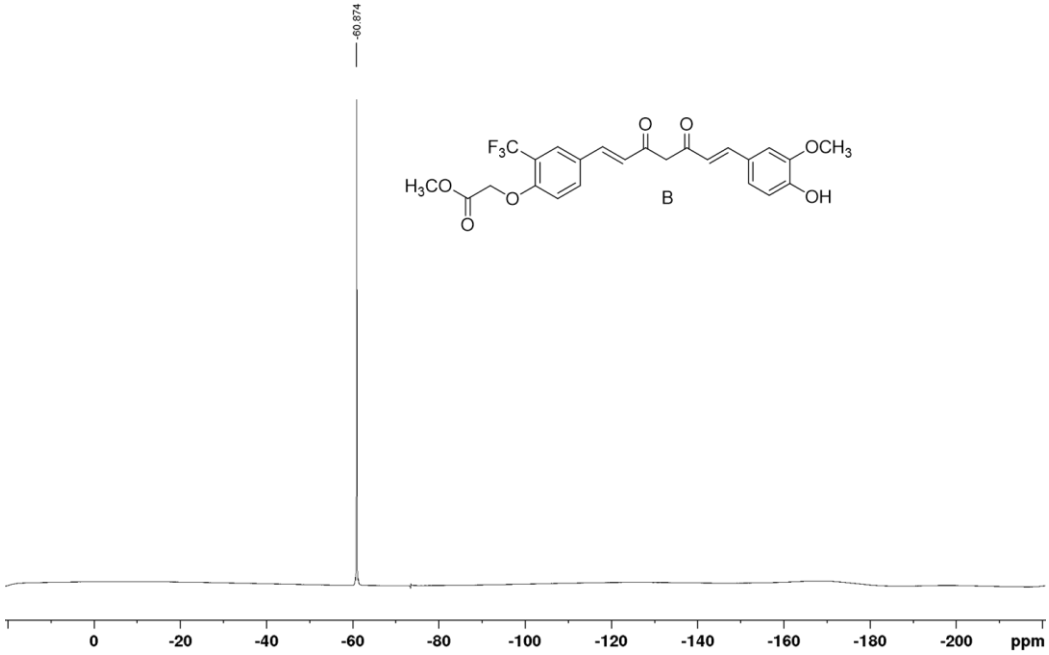

^{1}H-NMR Profile of 2-(4-formyl-2-(trifluoromethyl)phenoxy)acetic acid (2c)

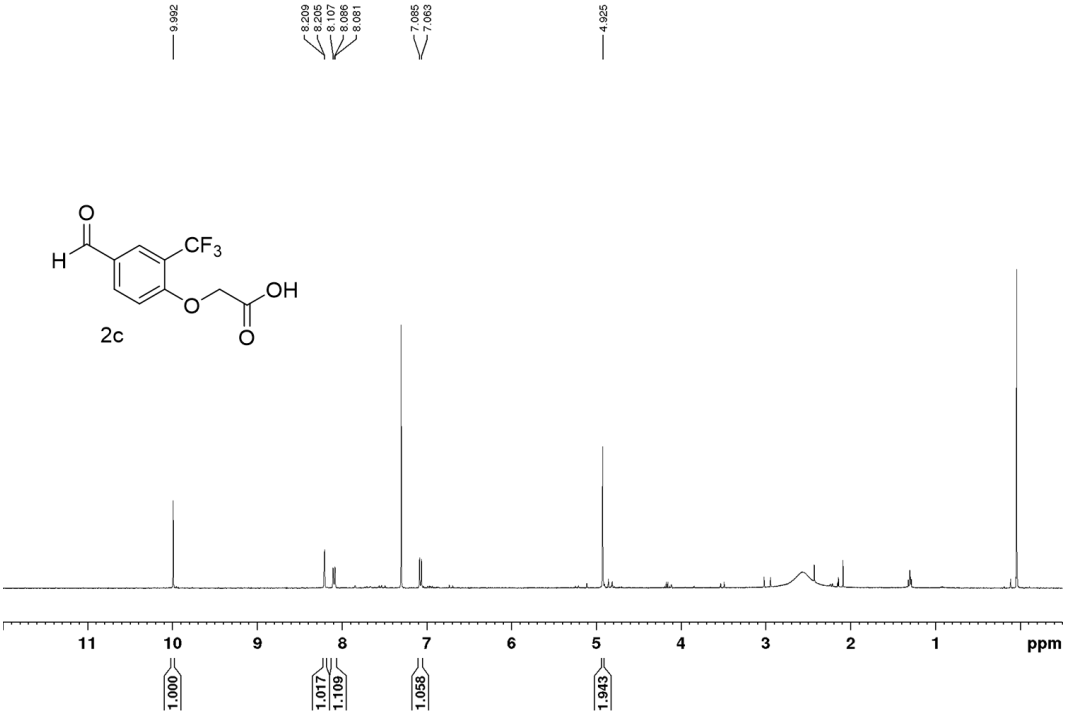

^{13}C-NMR Profile of 2-(4-formyl-2-(trifluoromethyl)phenoxy)acetic acid (2c)

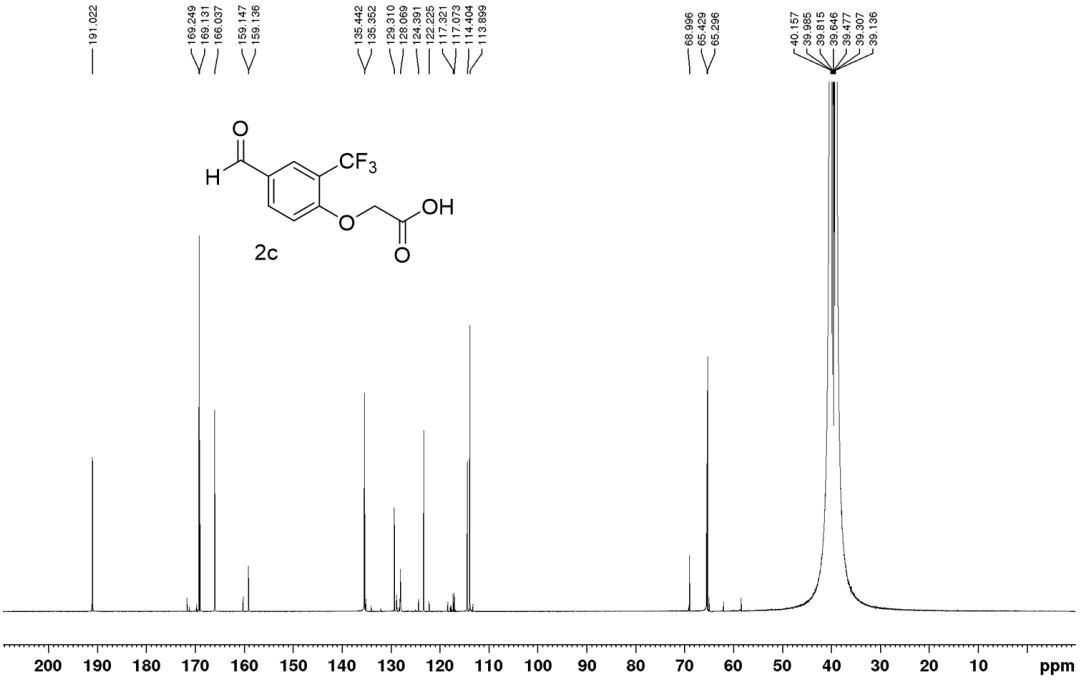

^{1}H-NMR Profile of 2-(4-((1E,6E)-7-(4-hydroxy-3-methoxyphenyl)-3,5-dioxohepta-1,6-dien-1-yl)-2-(trifluoromethyl)phenoxy)acetic acid (Compound C)

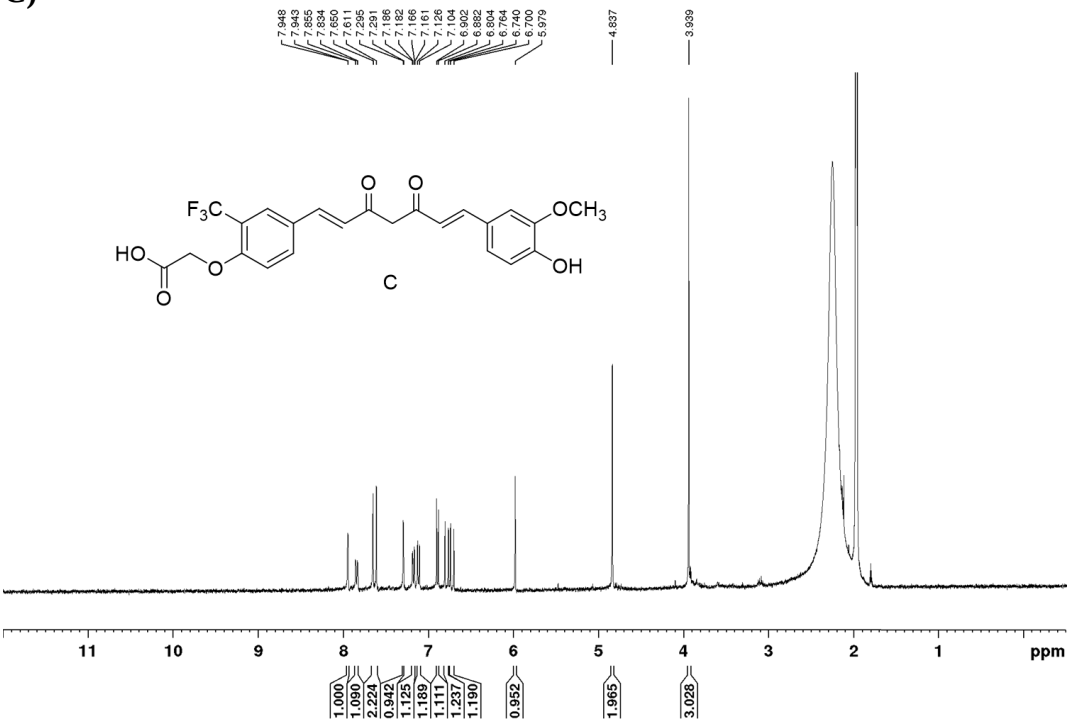

^{13}C-NMR Profile of 2-(4-((1E,6E)-7-(4-hydroxy-3-methoxyphenyl)-3,5-dioxohepta-1,6-dien-1-yl)-2-(trifluoromethyl)phenoxy)acetic acid (Compound C)

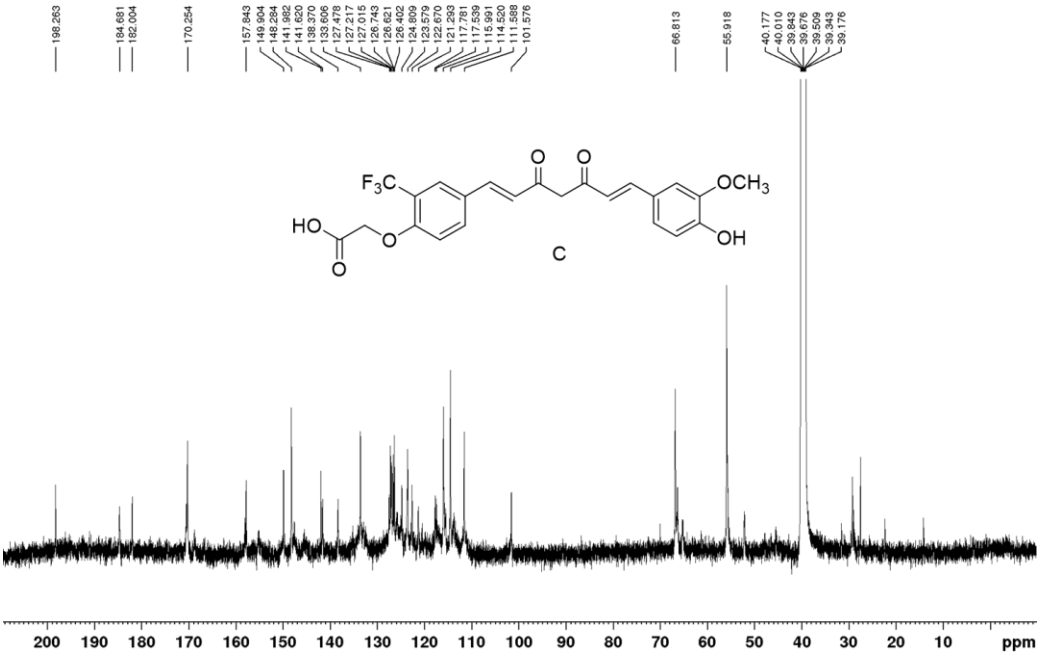

^{19}F-NMR Profile of 2-(4-((1E,6E)-7-(4-hydroxy-3-methoxyphenyl)-3,5-dioxohepta-1,6-dien-1-yl)-2-(trifluoromethyl)phenoxy)acetic acid (Compound C)

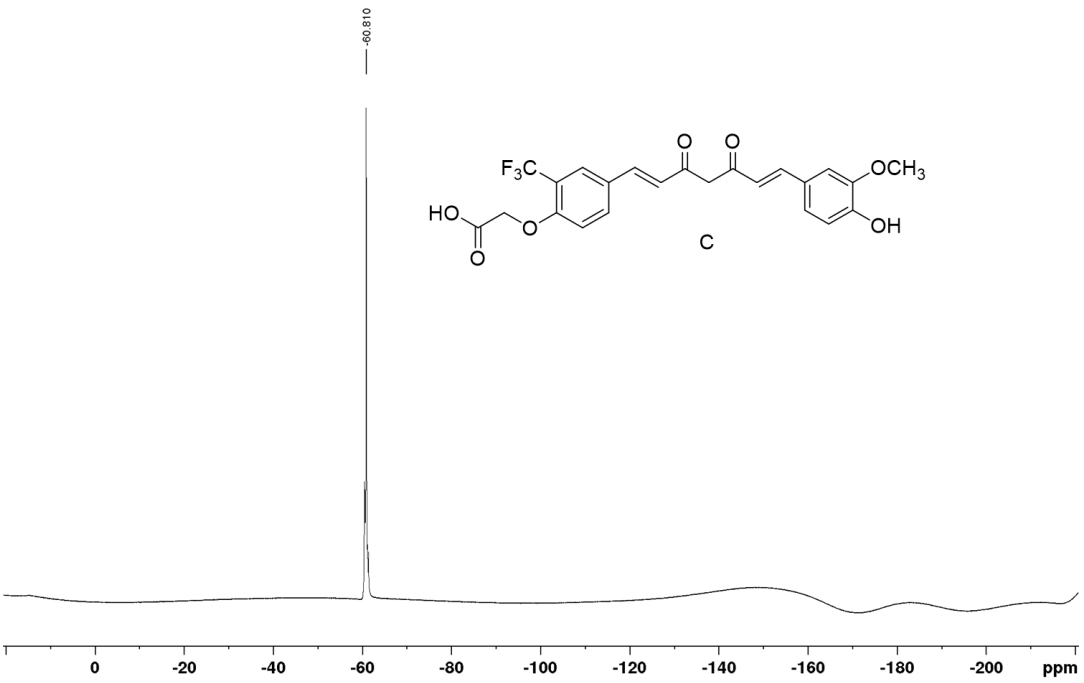

[1]H-NMR Profile of 1E,6E)-1-(4-hydroxy-3-methoxyphenyl)-7-[3-(trifluoromethyl)phenyl]hepta-1,6-diene-3,5-dione (Compound D)

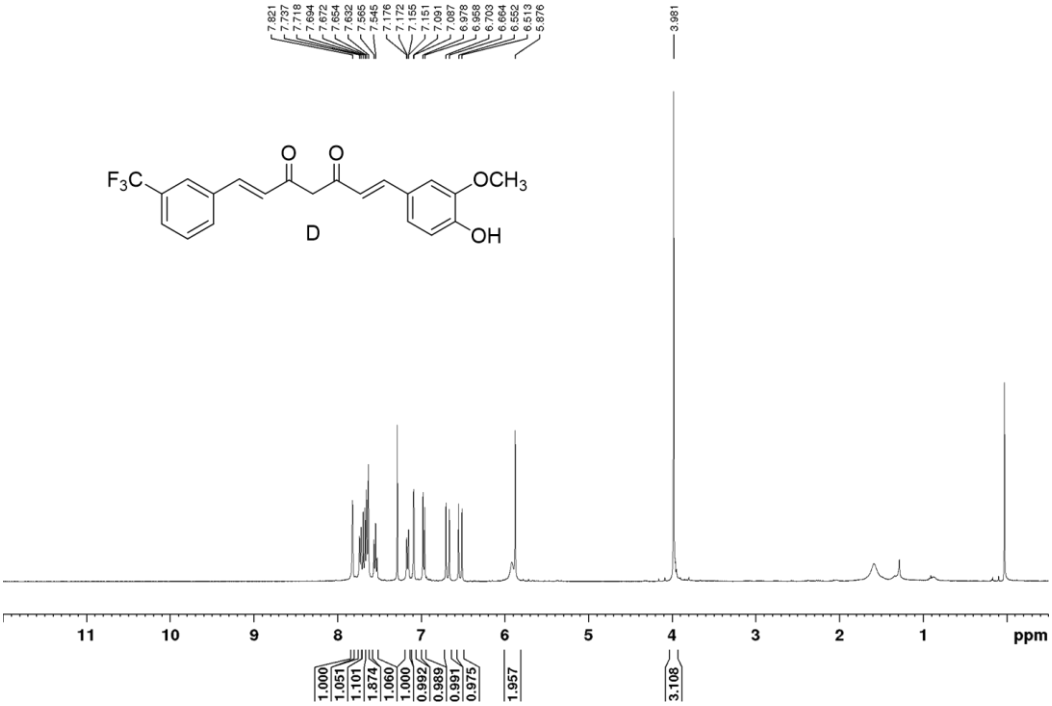

[13]C-NMR Profile of 1E,6E)-1-(4-hydroxy-3-methoxyphenyl)-7-[3-(trifluoromethyl)phenyl]hepta-1,6-diene-3,5-dione (Compound D)

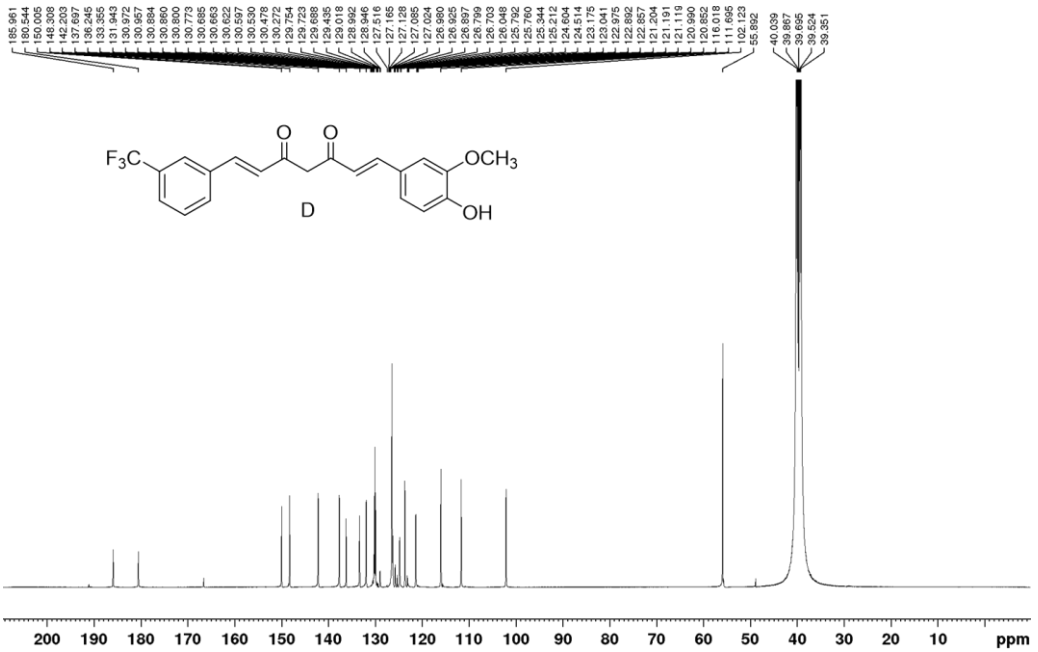

^{19}F-NMR Profile of 1E,6E)-1-(4-hydroxy-3-methoxyphenyl)-7-[3-(trifluoromethyl)phenyl]hepta-1,6-diene-3,5-dione (Compound D)

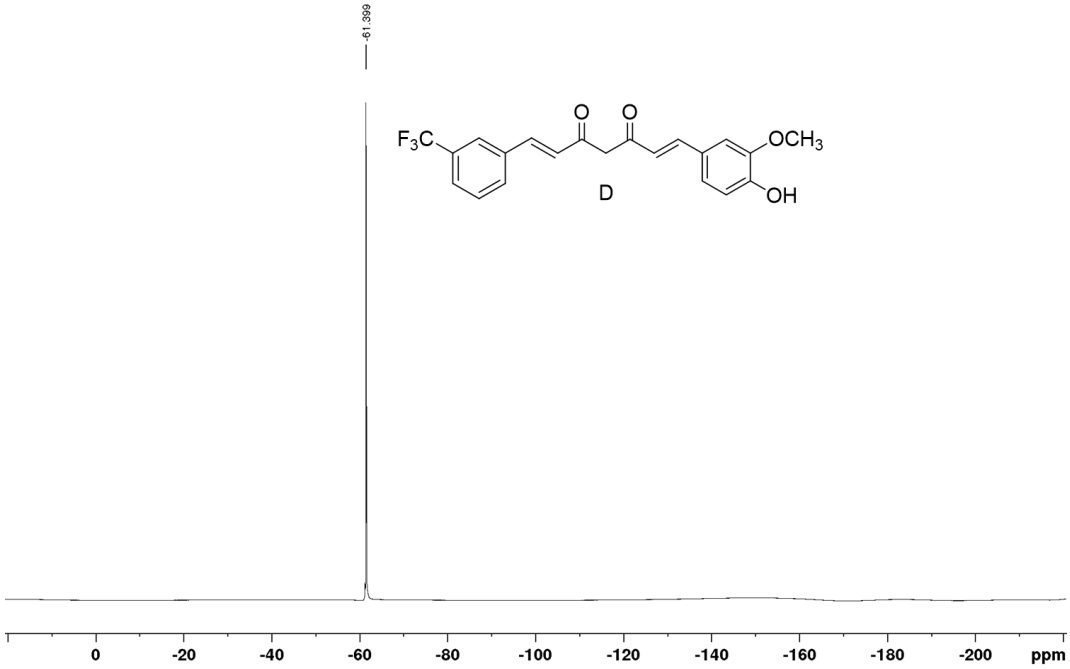

[1]H-NMR Profile of (1E,6E)-1-(4-hydroxy-3-(trifluoromethyl)phenyl)-7-(4-hydroxy-3-methoxyphenyl)hepta-1,6-diene-3,5-dione (Compound E)

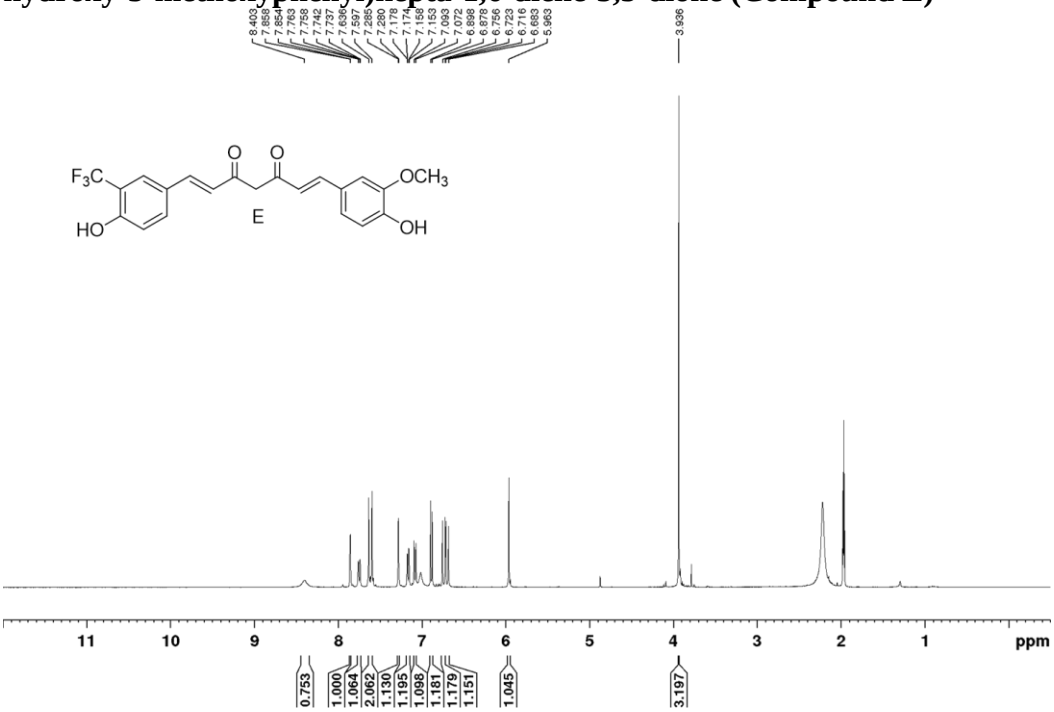

[13]C-NMR Profile of (1E,6E)-1-(4-hydroxy-3-(trifluoromethyl)phenyl)-7-(4-hydroxy-3-methoxyphenyl)hepta-1,6-diene-3,5-dione (Compound E)

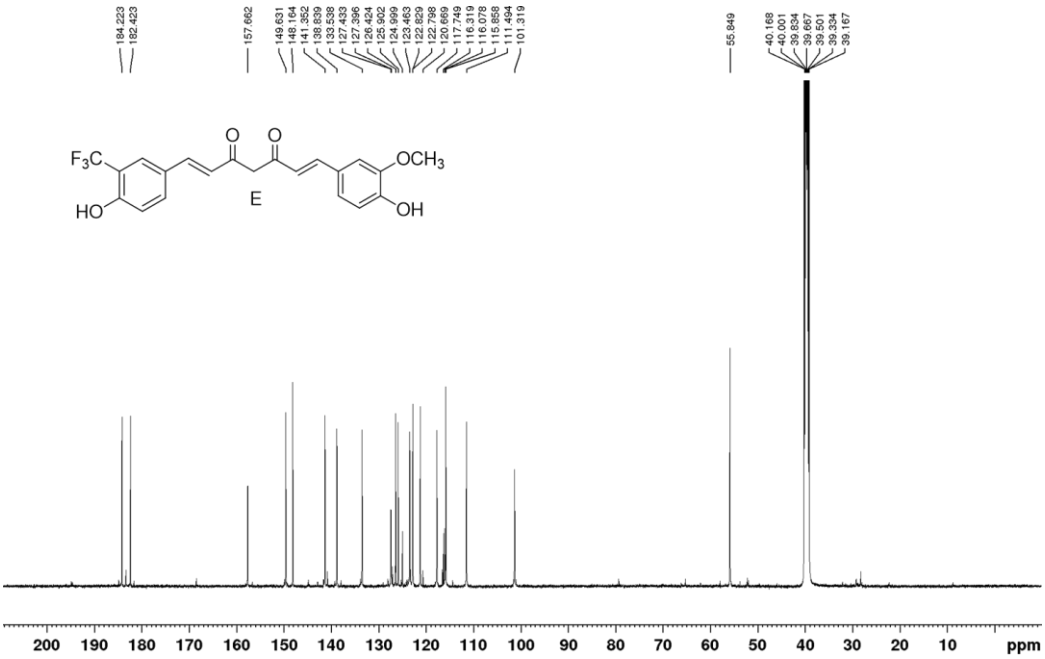

^{19}F-NMR Profile of (1E,6E)-1-(4-hydroxy-3-(trifluoromethyl)phenyl)-7-(4-hydroxy-3-methoxyphenyl)hepta-1,6-diene-3,5-dione (Compound E)

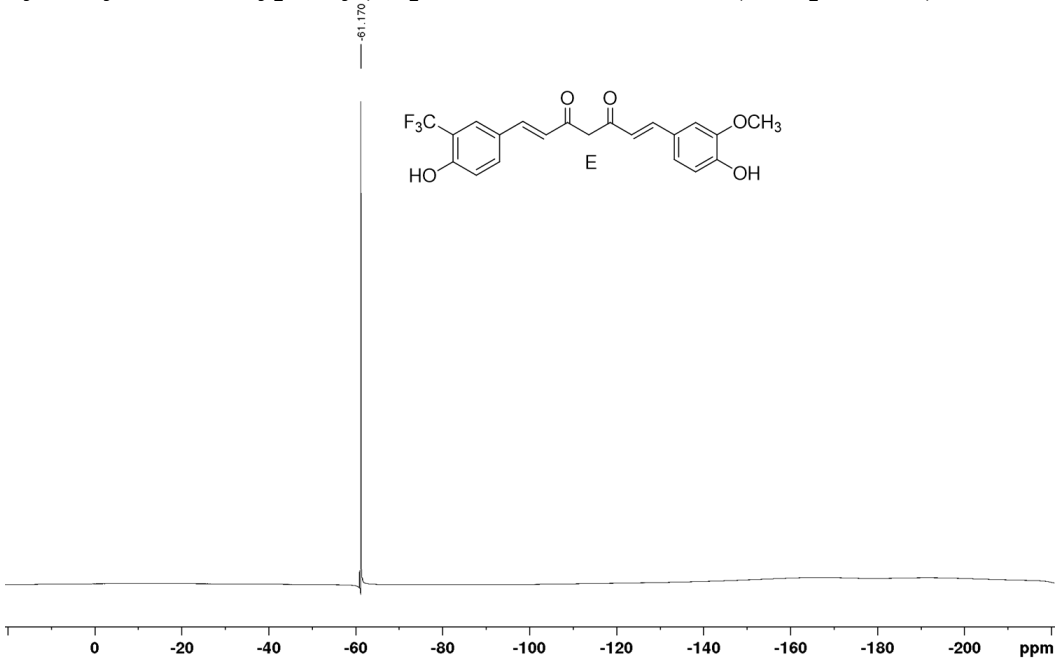

[1]H-NMR Profile of methyl 2-(4-((1E,6E)-7-(4-hydroxy-3-methoxyphenyl)-3,5-dioxohepta-1,6-dien-1-yl)-2-methoxyphenoxy)acetate (Compound F)

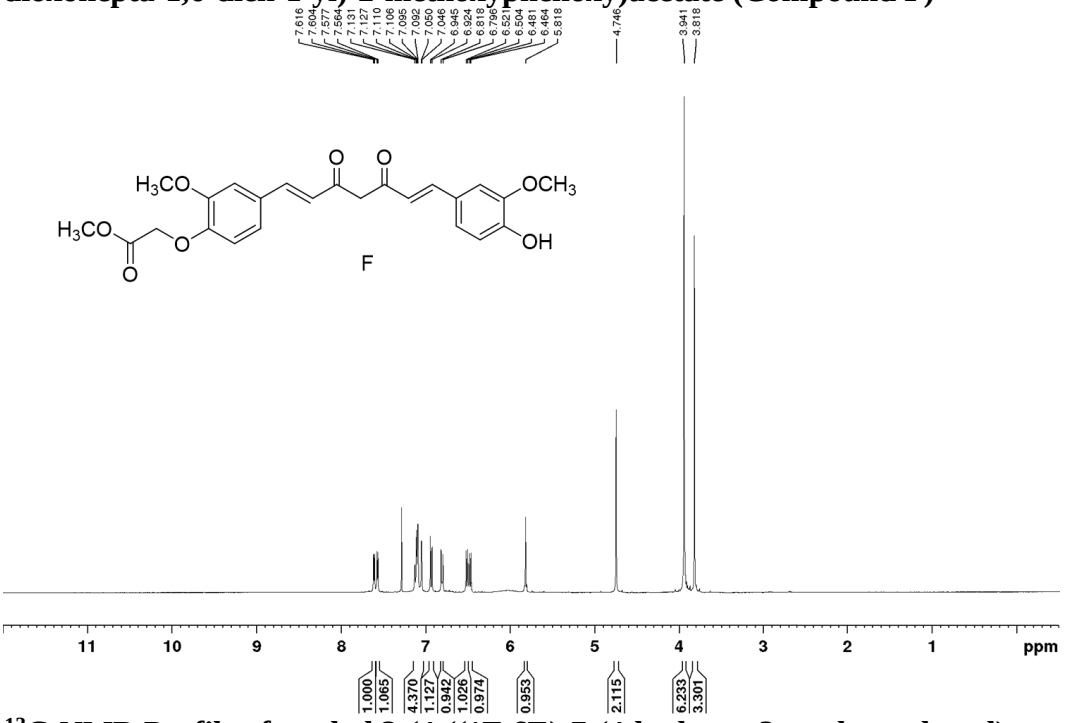

[13]C-NMR Profile of methyl 2-(4-((1E,6E)-7-(4-hydroxy-3-methoxyphenyl)-3,5-dioxohepta-1,6-dien-1-yl)-2-methoxyphenoxy)acetate (Compound F)

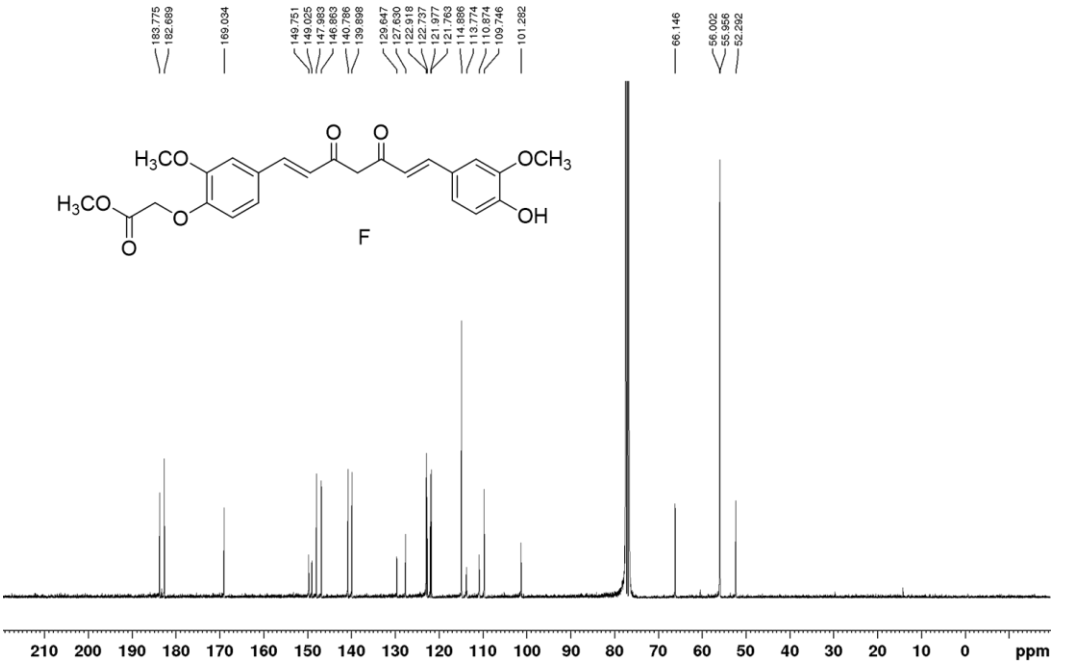

[1]H-NMR Profile of methyl 2-(4-((1E,6E)-3,5-dioxo-7-(3-(trifluoromethyl)phenyl)hepta-1,6-dien-1-yl)-2-methoxyphenoxy)acetate (Compound G)

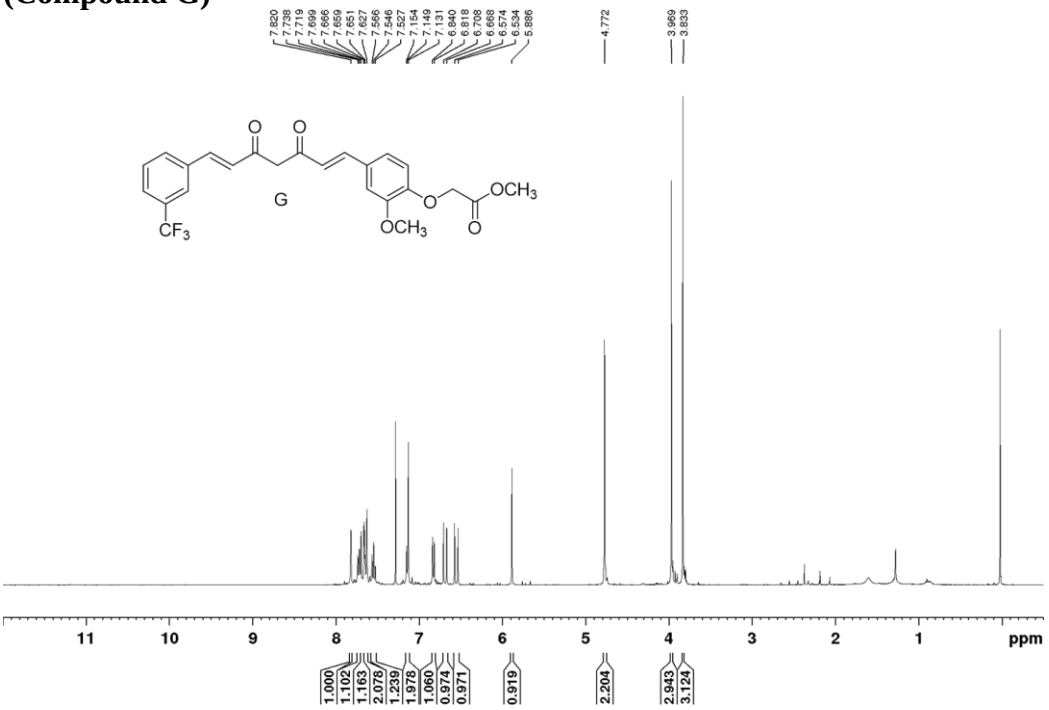

[13]C-NMR Profile of methyl 2-(4-((1E,6E)-3,5-dioxo-7-(3-(trifluoromethyl)phenyl)hepta-1,6-dien-1-yl)-2-methoxyphenoxy)acetate (Compound G)

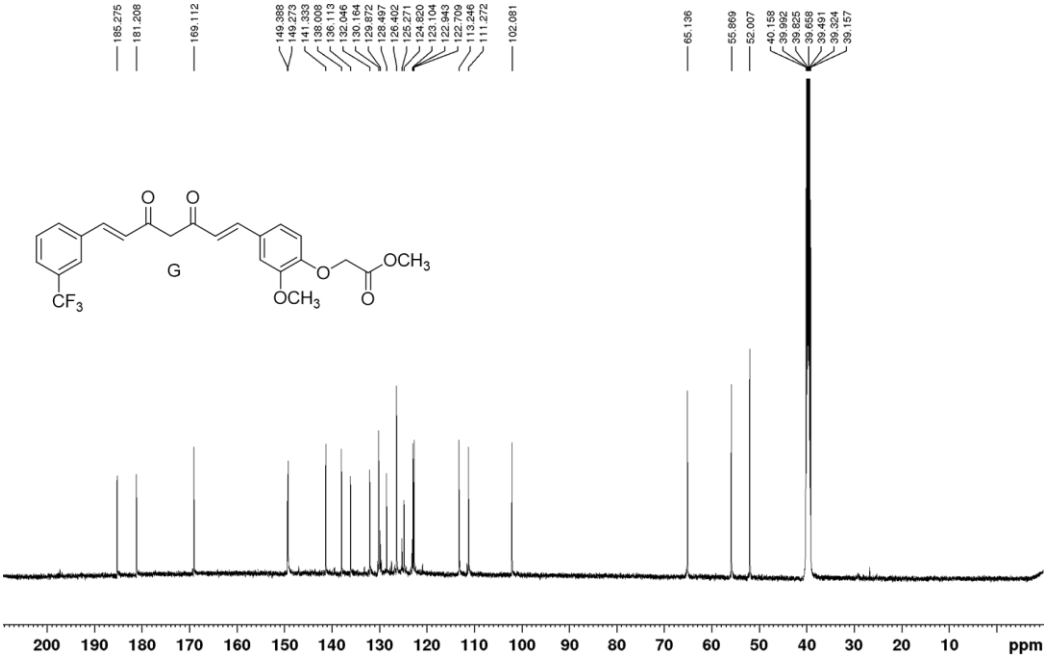

^{19}F-NMR Profile of methyl 2-(4-((1E,6E)-3,5-dioxo-7-(3-(trifluoromethyl)phenyl)hepta-1,6-dien-1-yl)-2-methoxyphenoxy)acetate (Compound G)

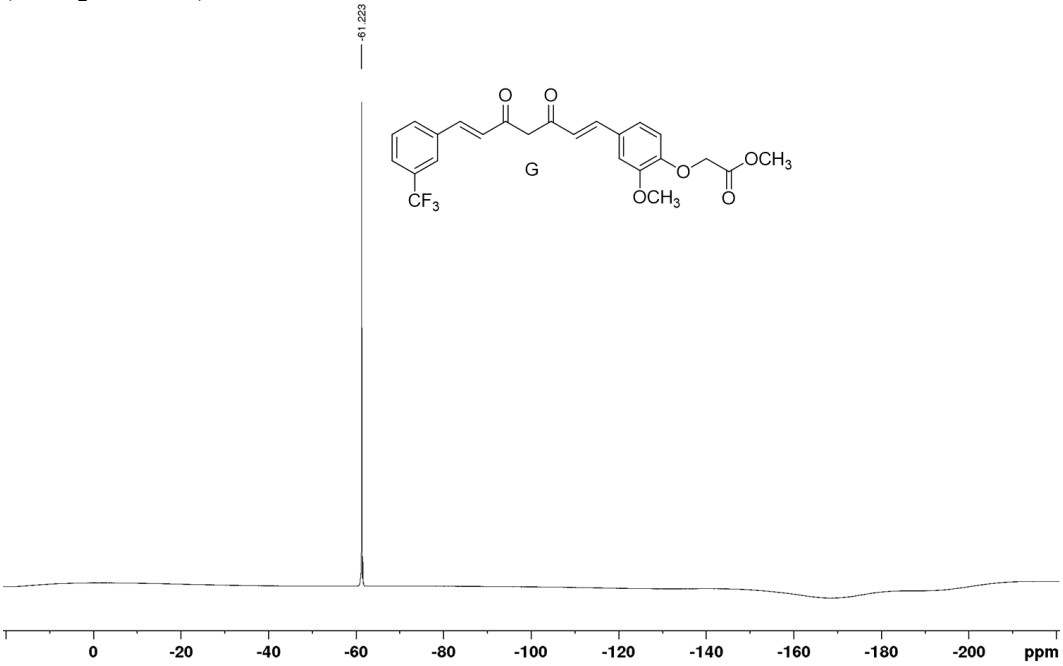

[1]H-NMR Profile of methyl 2-(2-methoxy-4-((1E,6E)-7-(4-(2-methoxy-2-oxoethoxy)-3-(trifluoromethyl)phenyl)-3,5-dioxohepta-1,6-dien-1-yl)phenoxy)acetate (Compound H)

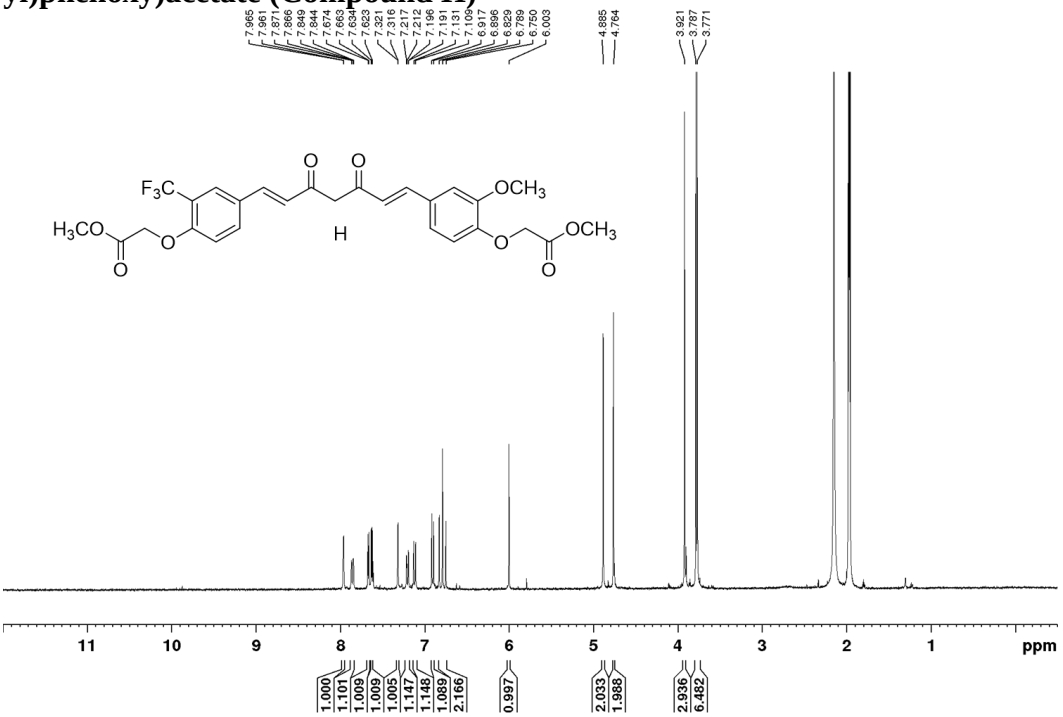

[13]C-NMR Profile of methyl 2-(2-methoxy-4-((1E,6E)-7-(4-(2-methoxy-2-oxoethoxy)-3-(trifluoromethyl)phenyl)-3,5-dioxohepta-1,6-dien-1-yl)phenoxy)acetate (Compound H)

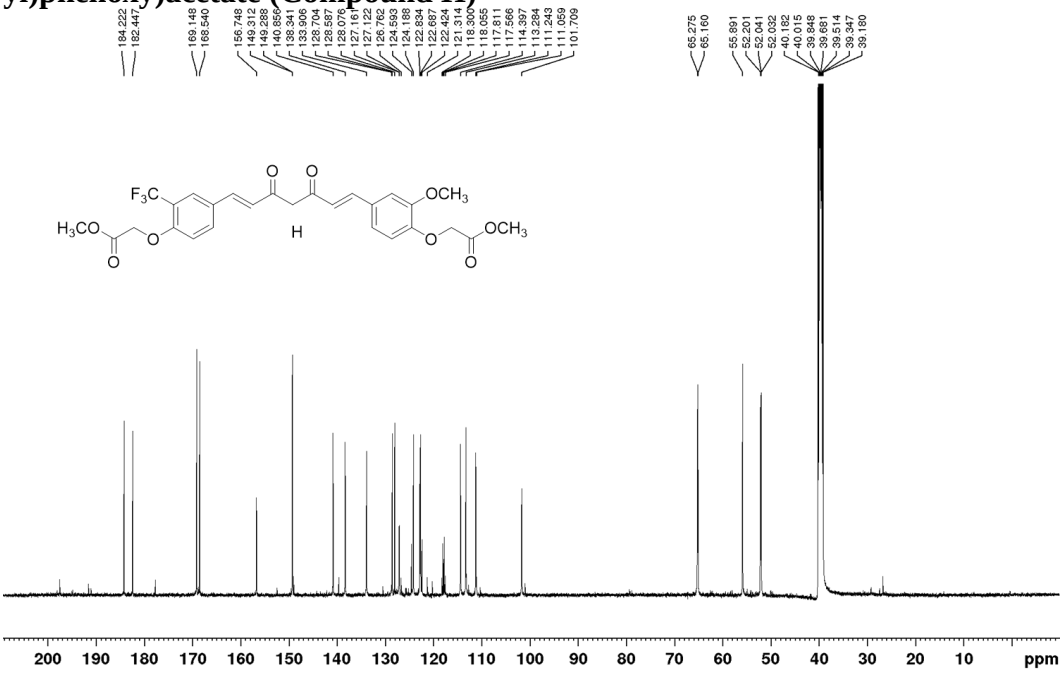

^{19}F-NMR Profile of methyl 2-(2-methoxy-4-((1E,6E)-7-(4-(2-methoxy-2-oxoethoxy)-3-(trifluoromethyl)phenyl)-3,5-dioxohepta-1,6-dien-1-yl)phenoxy)acetate (Compound H)

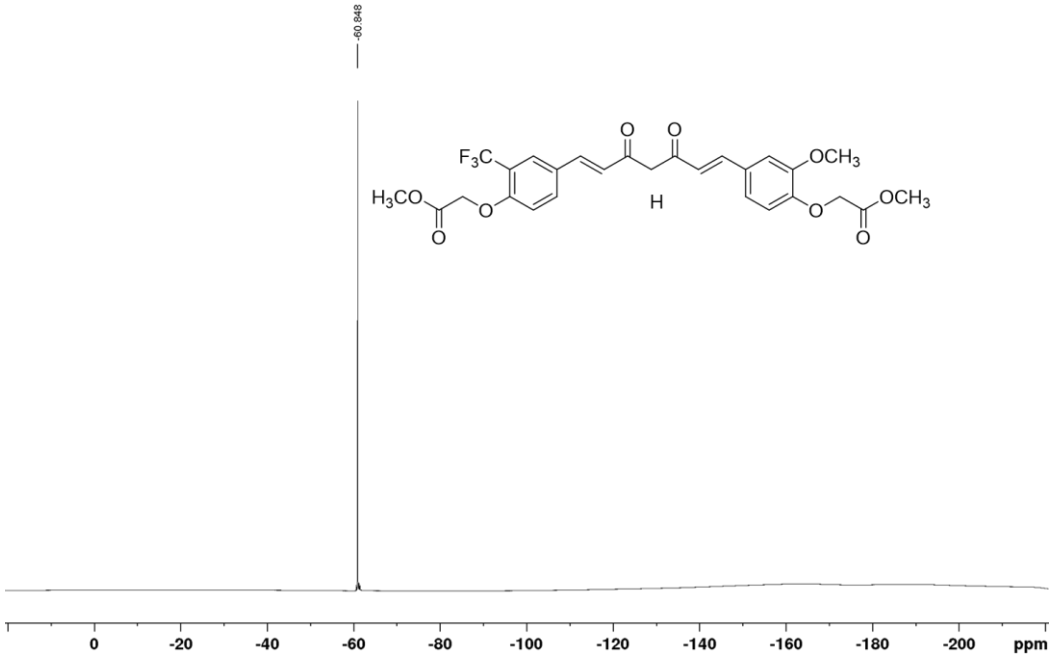

^{1}H-NMR Profile of (E)-6-(4-hydroxy-3-(trifluoromethyl)phenyl)hex-5-ene-2,4-dione (4b)

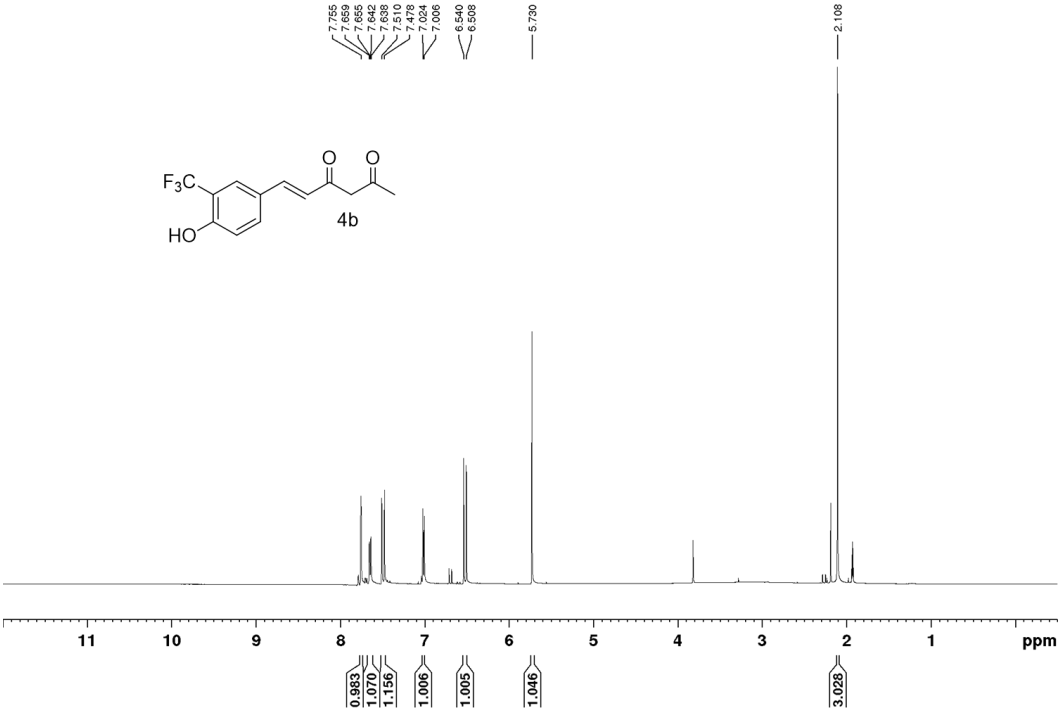

^{13}C-NMR Profile of (E)-6-(4-hydroxy-3-(trifluoromethyl)phenyl)hex-5-ene-2,4-dione (4b)

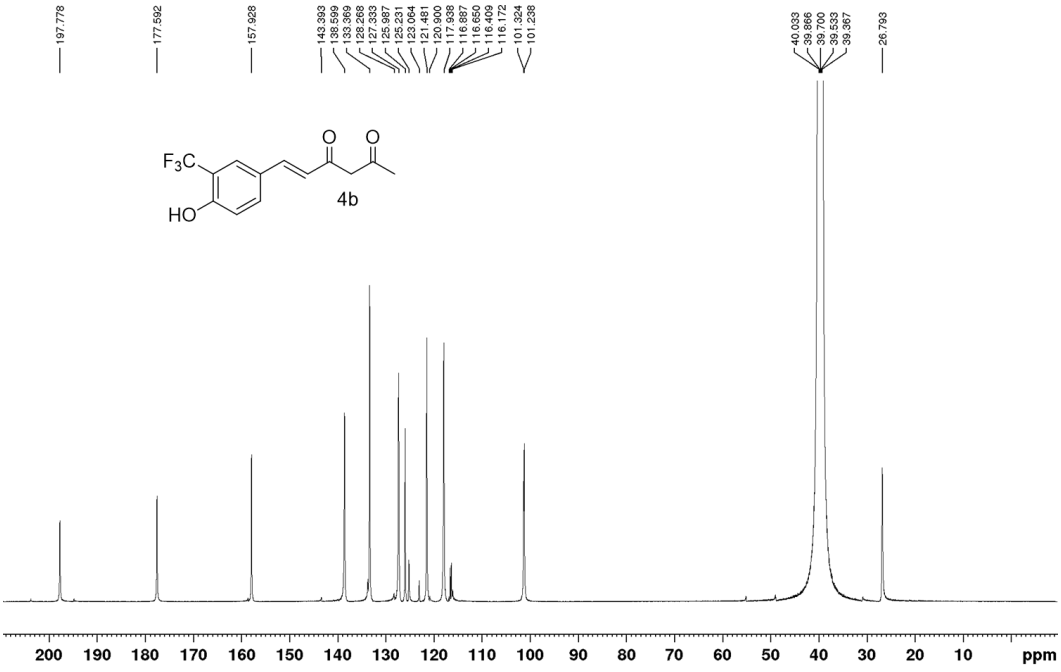

[1]H-NMR Profile of (1E,6E)-1-(4-hydroxy-3-(trifluoromethyl)phenyl)-7-(3-(trifluoromethyl)phenyl)hepta-1,6-diene-3,5-dione (Compound I)

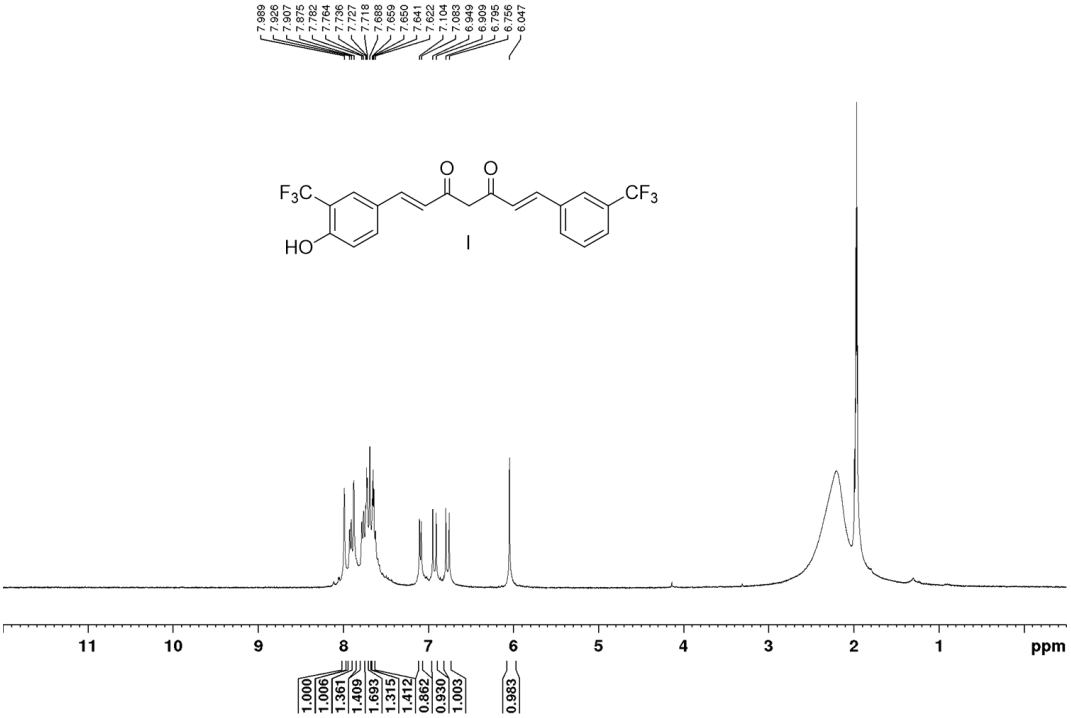

[13]C-NMR Profile of (1E,6E)-1-(4-hydroxy-3-(trifluoromethyl)phenyl)-7-(3-(trifluoromethyl)phenyl)hepta-1,6-diene-3,5-dione (Compound I)

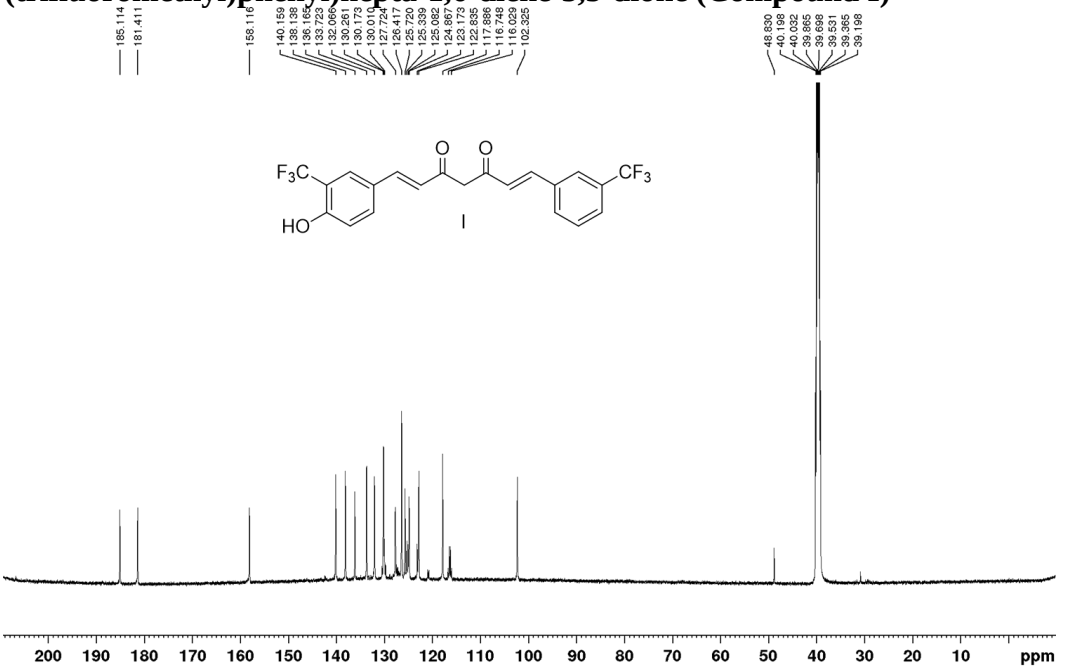

^{19}F-NMR Profile of (1E,6E)-1-(4-hydroxy-3-(trifluoromethyl)phenyl)-7-(3-(trifluoromethyl)phenyl)hepta-1,6-diene-3,5-dione (Compound I)

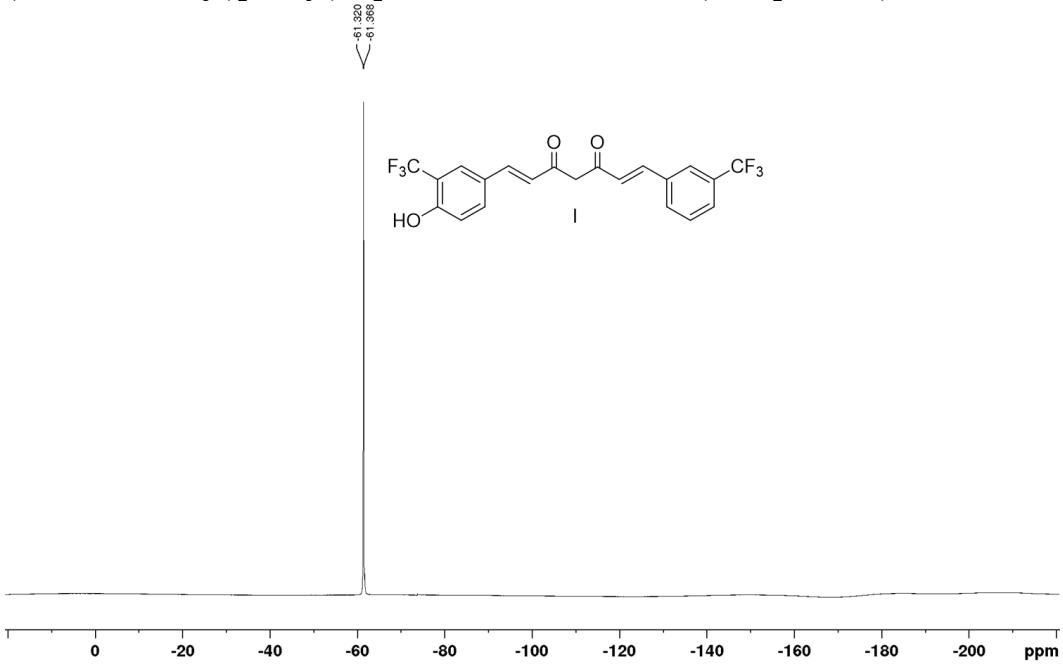

[1]H-NMR Profile of methyl 2-(4-((1E,6E)-7-(4-hydroxy-3-(trifluoromethyl)phenyl)-3,5-dioxohepta-1,6-dien-1-yl)-2-(trifluoromethyl)phenoxy)acetate (Compound J)

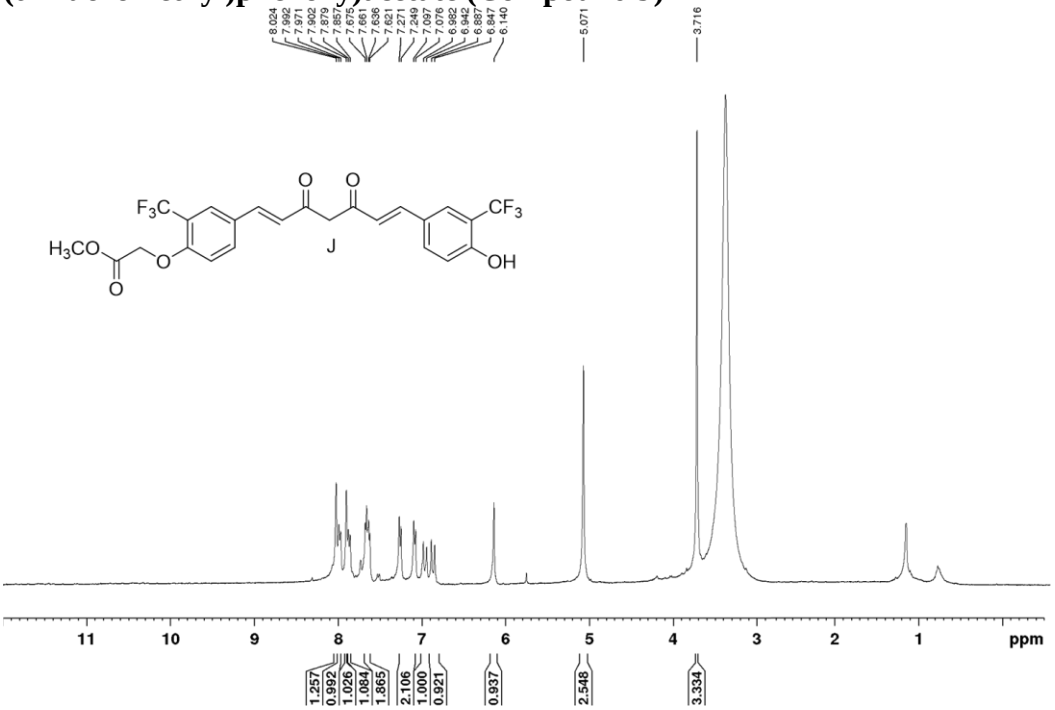

[1]H-NMR Profile of methyl 2-(4-((1E,6E)-7-(4-hydroxy-3-(trifluoromethyl)phenyl)-3,5-dioxohepta-1,6-dien-1-yl)-2-(trifluoromethyl)phenoxy)acetate (Compound J)

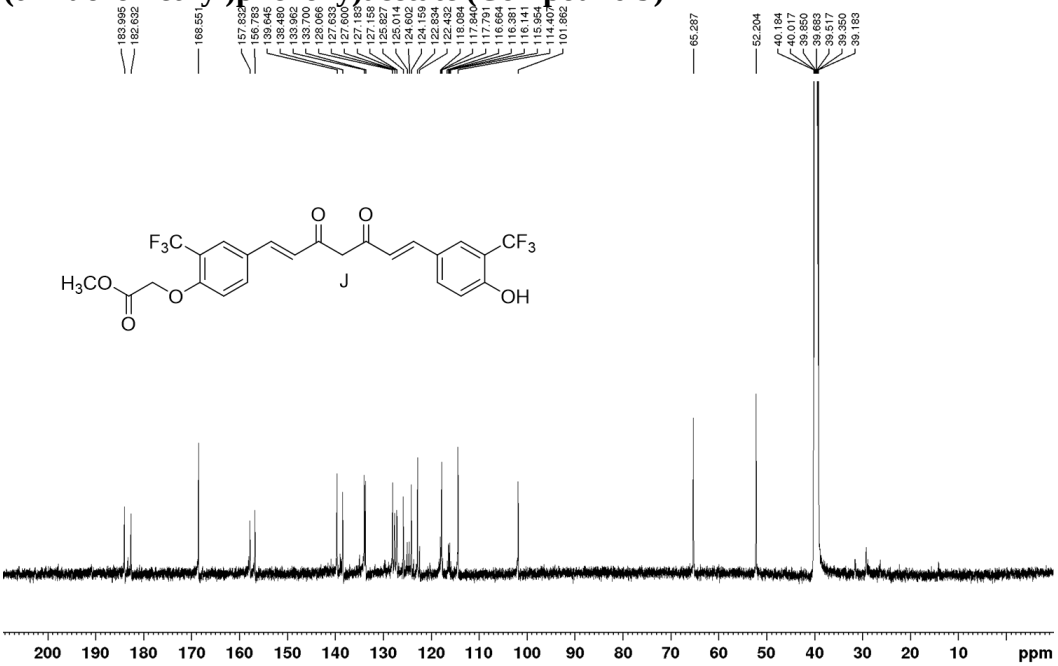

^{19}F-NMR Profile of methyl 2-(4-((1E,6E)-7-(4-hydroxy-3-(trifluoromethyl)phenyl)-3,5-dioxohepta-1,6-dien-1-yl)-2-(trifluoromethyl)phenoxy)acetate (Compound J)

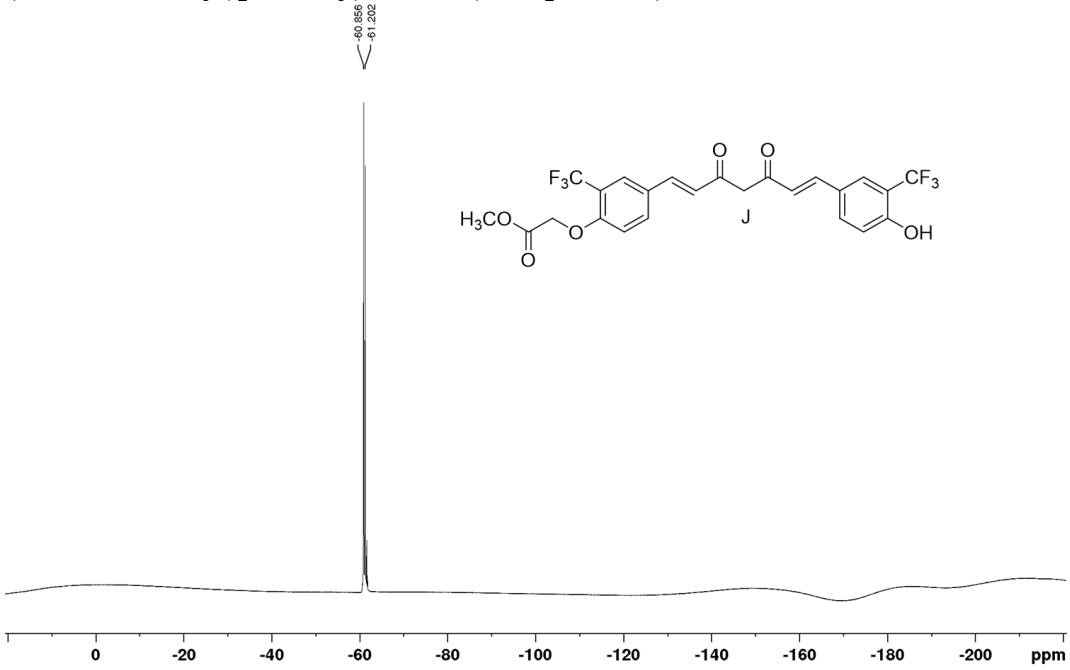

[1]H-NMR Profile of tert-butyl 2-(4-formyl-2-(trifluoromethyl)phenoxy)acetate

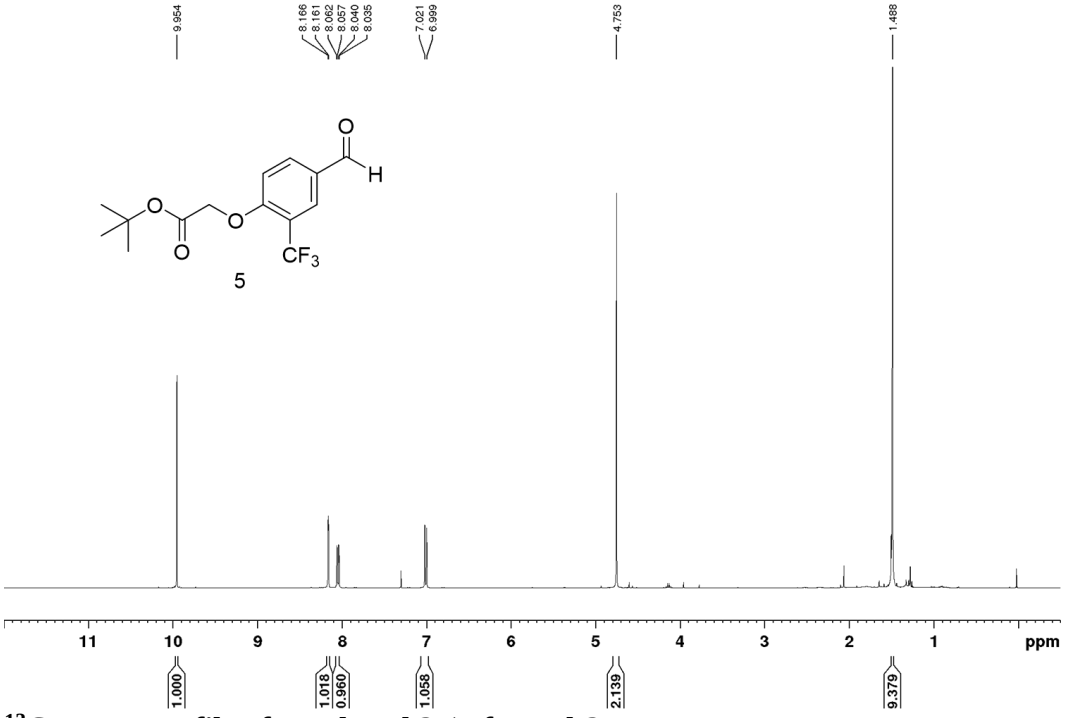

[13]C-NMR Profile of tert-butyl 2-(4-formyl-2-(trifluoromethyl)phenoxy)acetate

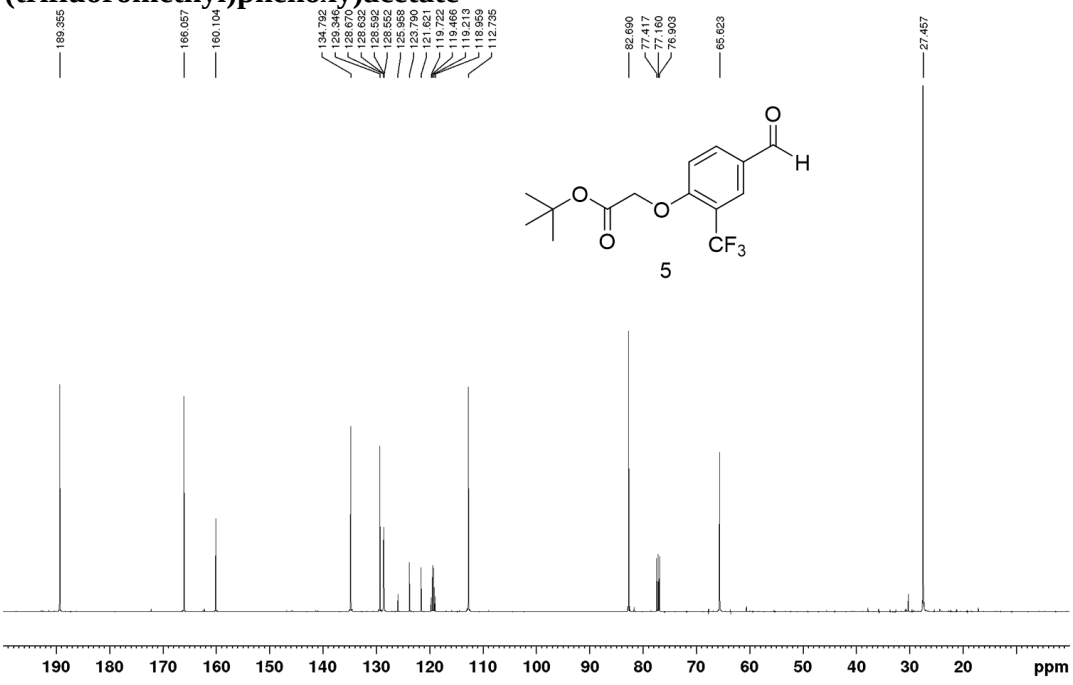

[1]H-NMR Profile of tert-butyl 2-(4-((1E,6E)-7-(4-hydroxy-3-methoxyphenyl)-3,5-dioxohepta-1,6-dien-1-yl)-2-(trifluoromethyl)phenoxy)acetate (Compound K)

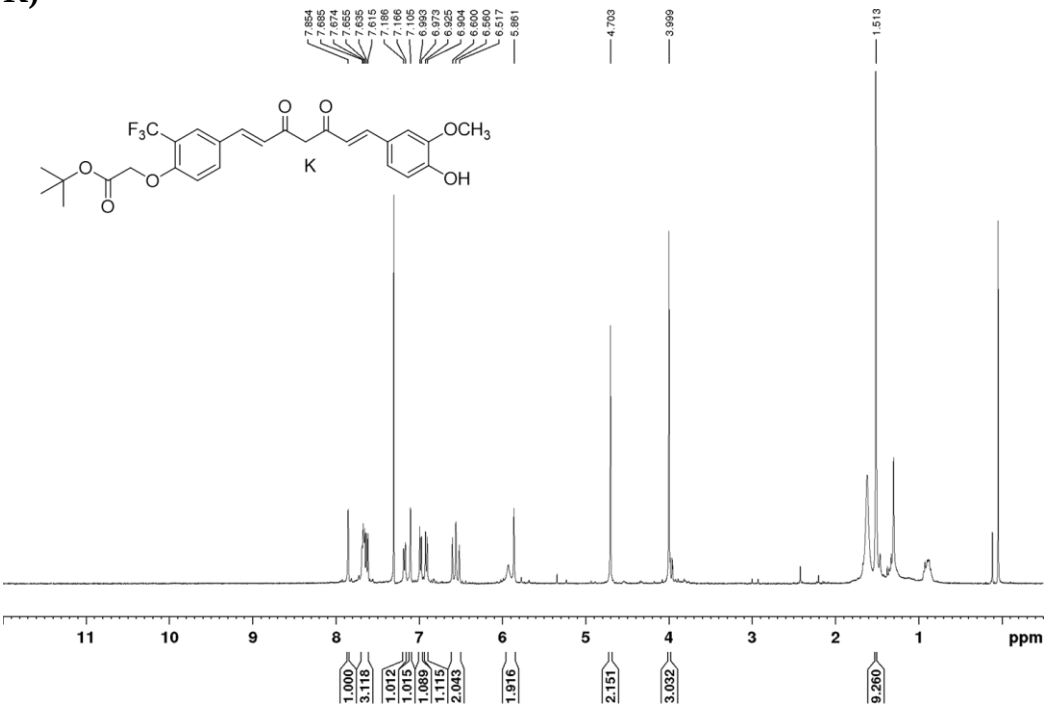

[13]C-NMR Profile of tert-butyl 2-(4-formyl-2-(trifluoromethyl)phenoxy)acetate (Compound K)

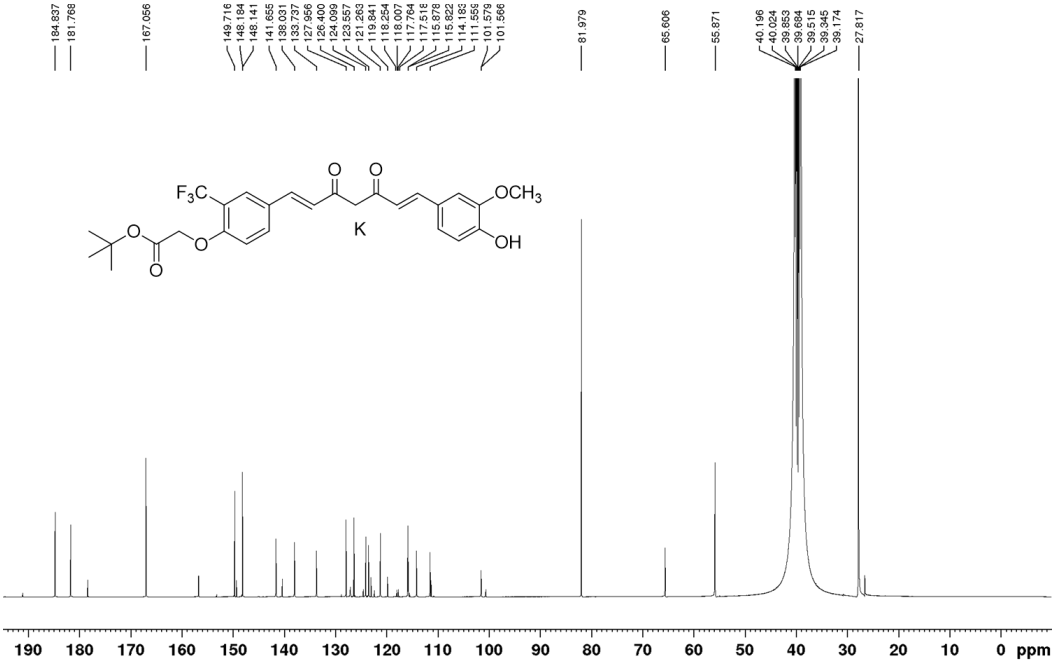

^{19}F-NMR Profile of tert-butyl 2-(4-formyl-2-(trifluoromethyl)phenoxy)acetate (Compound K)

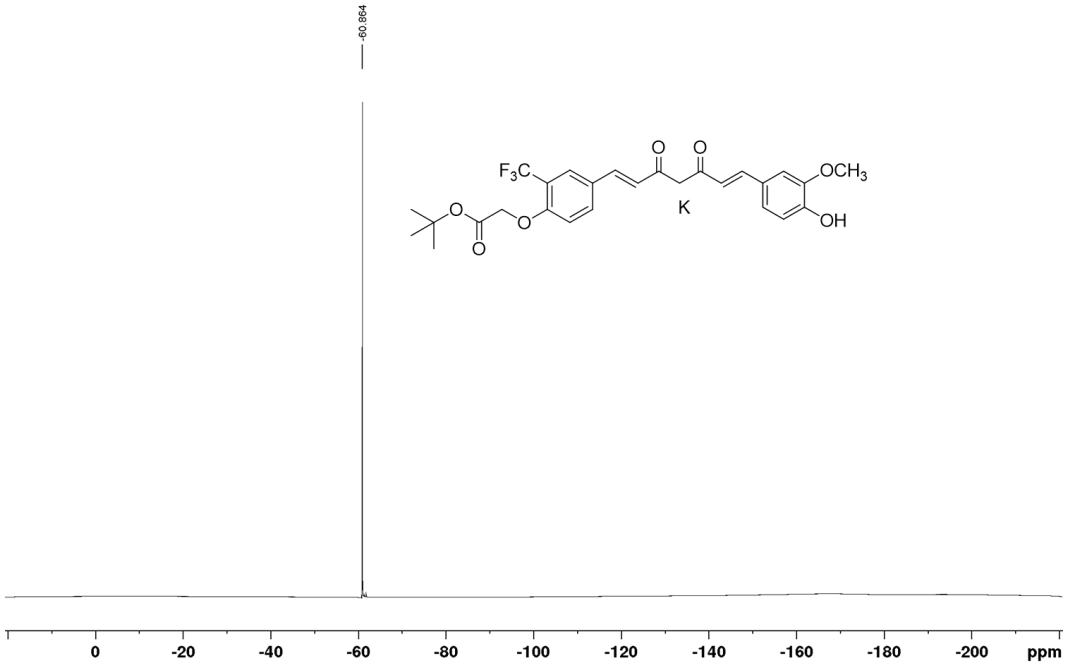

^{1}H-NMR Profile of (1E,6E)-1,7-bis(4-hydroxy-3-methoxyphenyl)hepta-1,6-diene-3,5-dione (Curcumin)

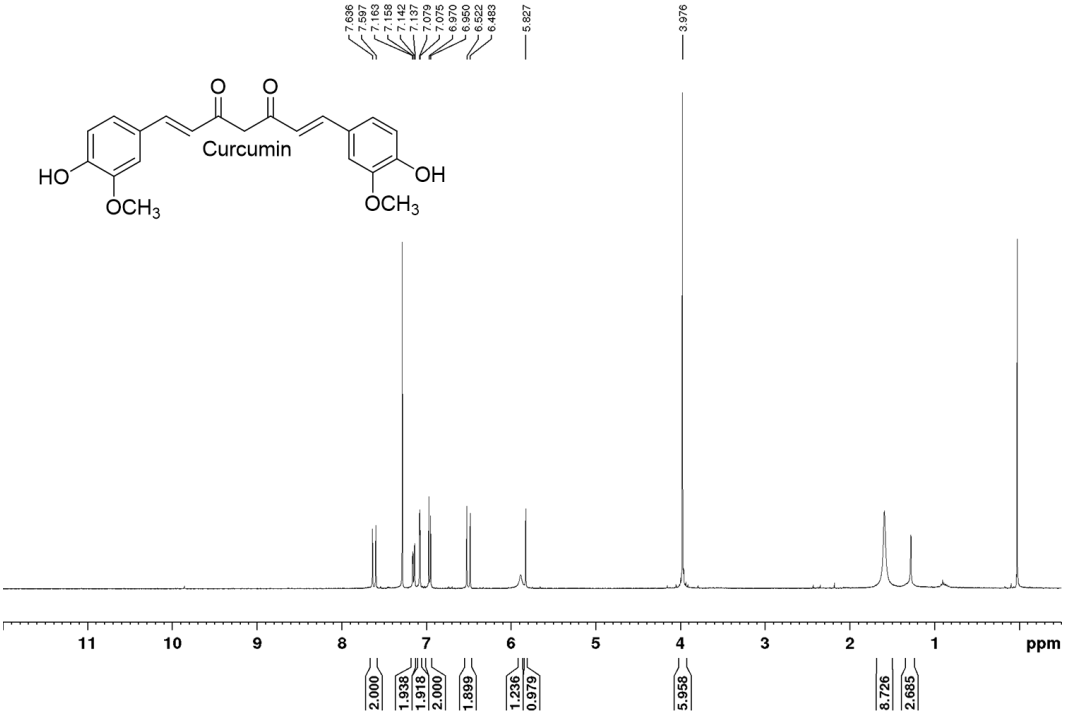

Purity Analysis of Compounds A-K by HPLC

Each peak was represented by retention time (tR) and % area under curve (%AUC)

Compound **A**

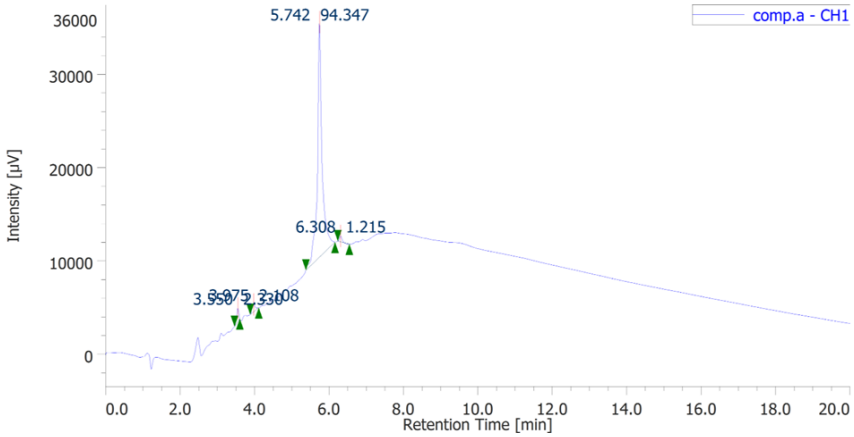

Compound **B**

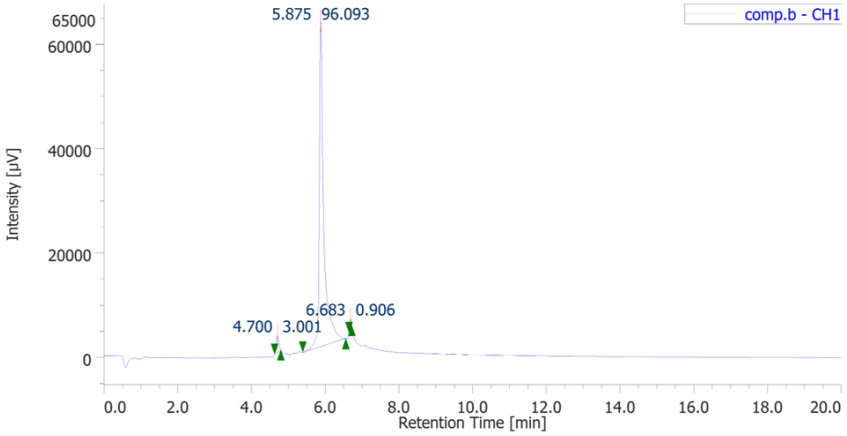

Compound **C**

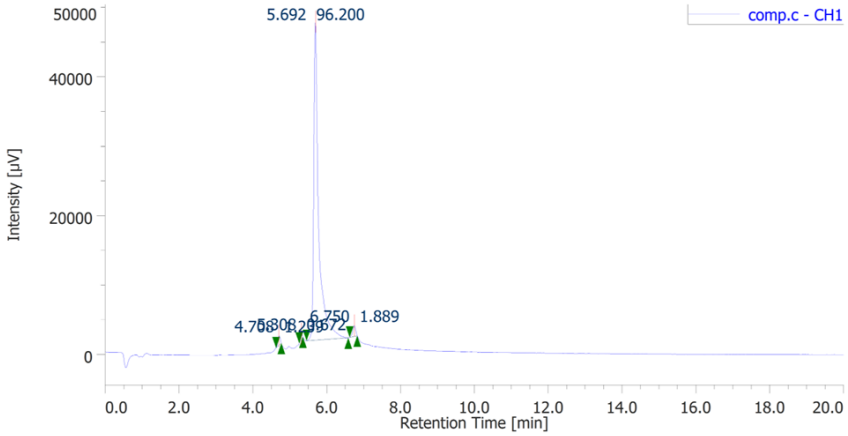

Compound **D**

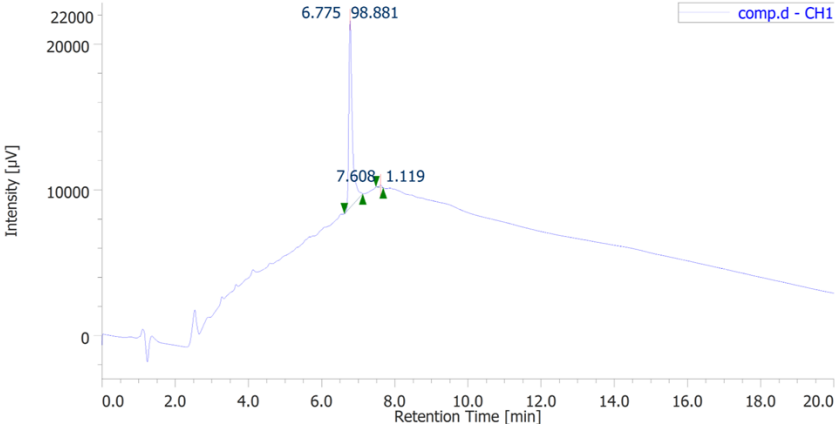

Compound **E**

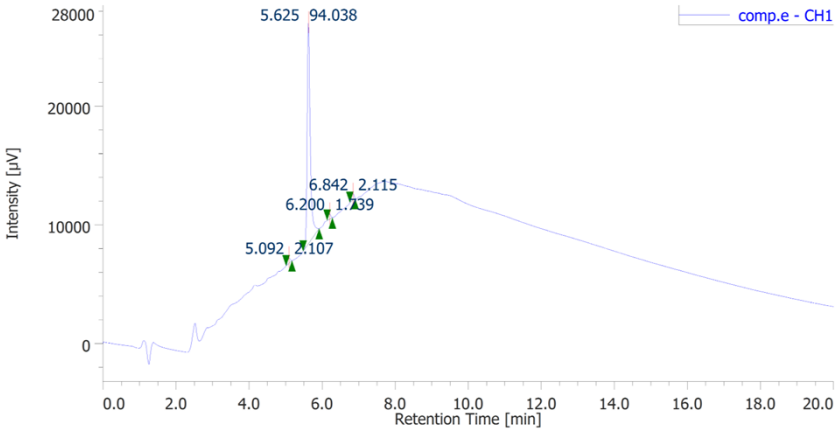

Compound **F**

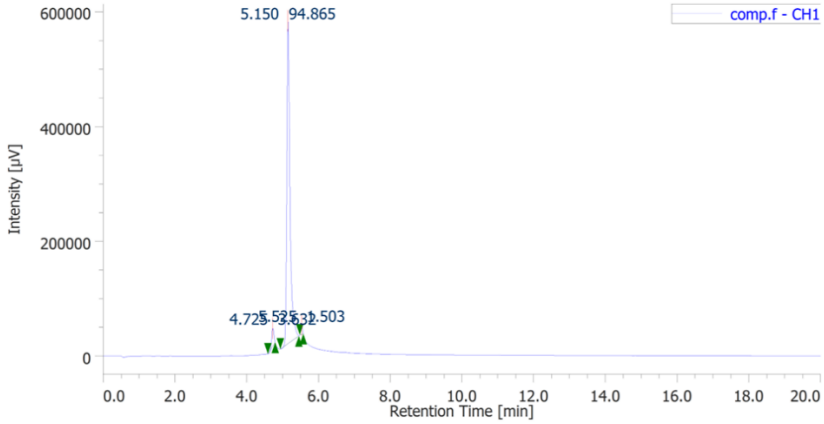

Compound **G**

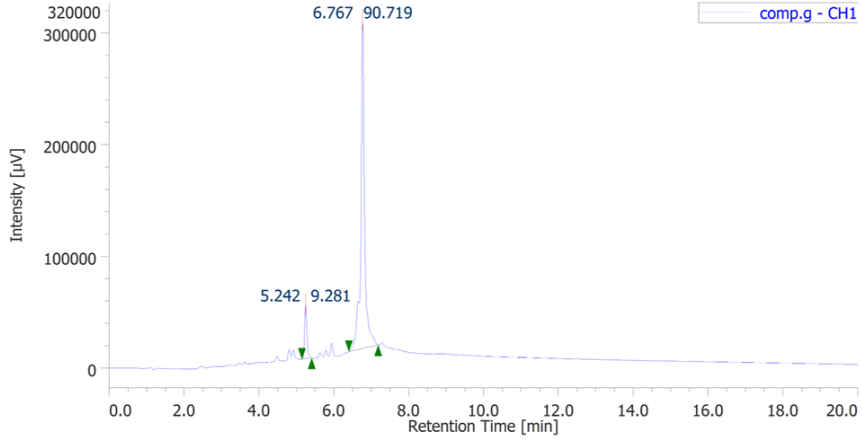

Compound **H**

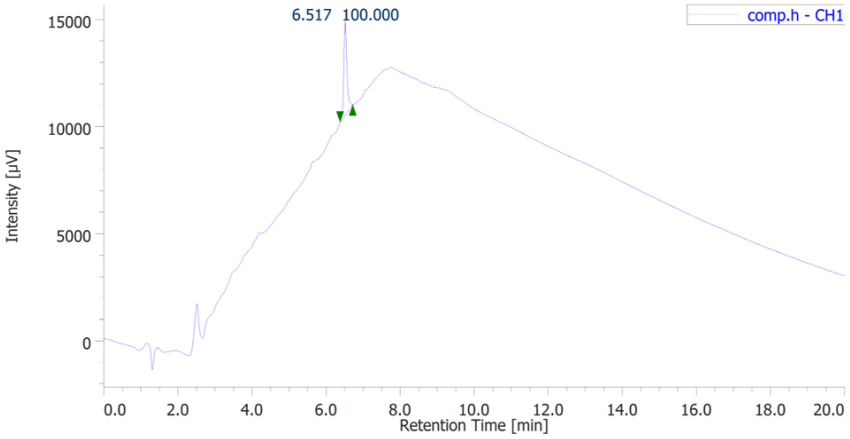

Compound **I**

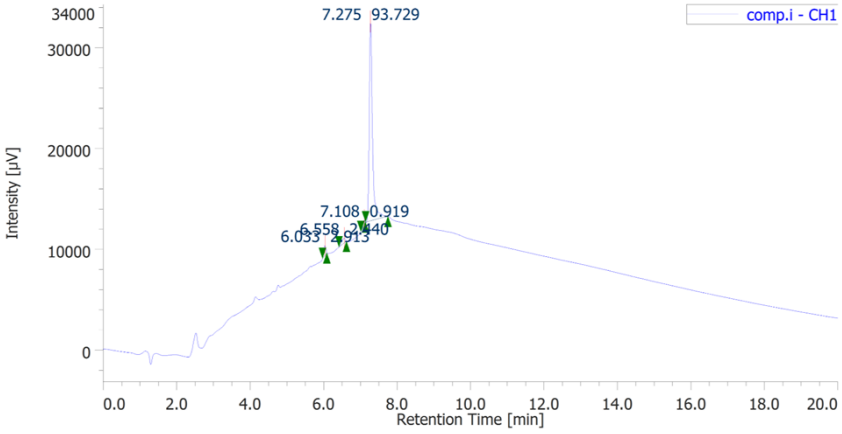

Compound **J**

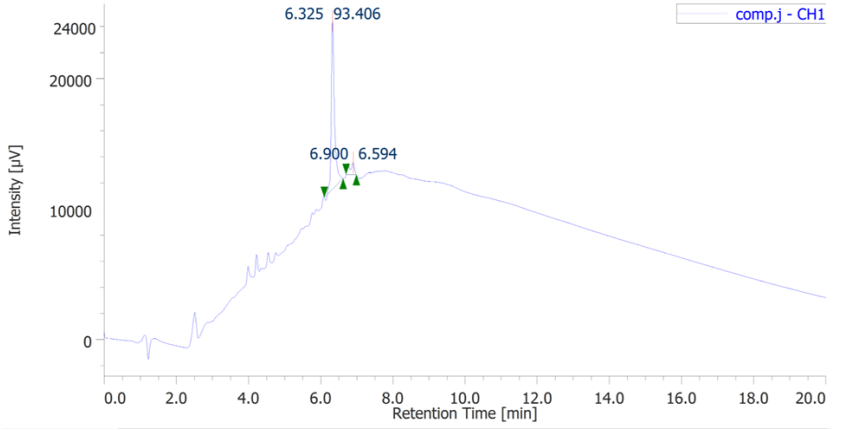

Compound **K**

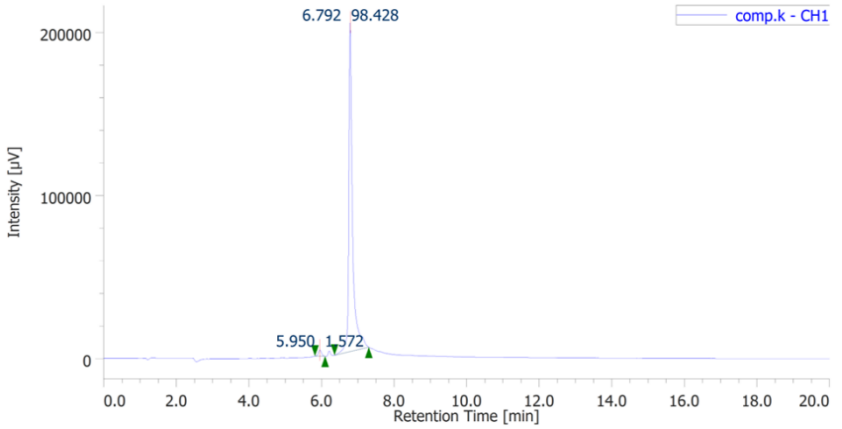

Curcumin

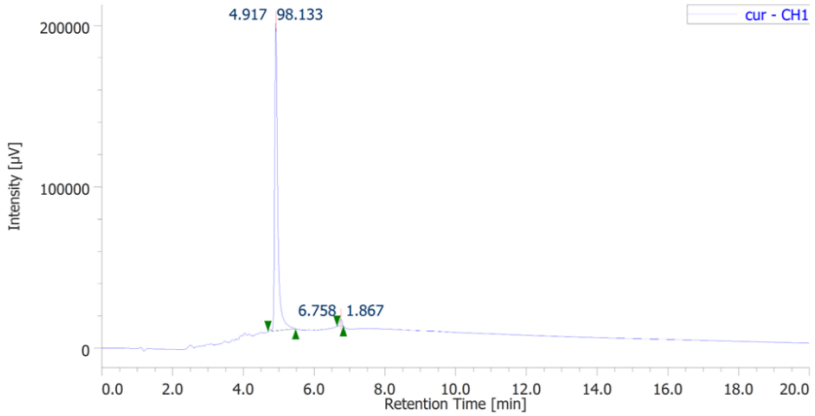
4.917 98.133
cur - CH1
200000
100000
0
Intensity [µV]
6.758 1.867
0.0 2.0 4.0 6.0 8.0 10.0 12.0 14.0 16.0 18.0 20.0
Retention Time [min]

Chapter 3
Development of an MRI Contrast Agent for Both Detection and Inhibition of the Amyloid-β Fibrillation Process

Chapter 3. Development of an MRI Contrast Agent for Both Detection and Inhibition of The Amyloid-β Fibrillation Process

3.1. Introduction

Significant increases in Alzheimer`s disease (AD) patients urge the development of therapeutic and diagnostic technology.[1] As with therapeutic development, diagnostic technology also faces several obstacles. As mentioned in Chapter 1.3, the definite diagnosis of AD currently relies on the histopathological data of postmortem.[2,3] The non-invasive imaging technology targeting AD biomarkers such as amyloid β (Aβ) could provide phenotypical diagnostics, although the development of Aβ probes remains challenging.

Magnetic resonance imaging (MRI) contrast agents could quantify the Aβ accumulation in the anatomic brain image.[4] Several reported MRI contrast agents using gadolinium (Gd) complexes demonstrate the potential use of Aβ detection. A clinically approved contrast agent, Gd (III) diethylenetriaminepentaacetic acid (Gd-DTPA) complex, accumulates in the brain after opening the blood-brain barrier (BBB) by using mannitol and detects Aβ deposits in the AD-model mice.[5] To improve the selectivity, Gd complexes were conjugated with compounds binding to Aβ, such as Pittsburgh compound B (Gd-DO3A-PiB), which could increase MRI sensitivity.[6,7] An α,β-unsaturated ketone compound, curcumin, has been widely reported as an Aβ probe due to its ability to bind the hydrophobic site of Aβ (see in Chapter 1.4).[8,9] Allen et al. first reported the direct conjugation of curcumin with Gd-DTPA which binds to Aβ with four times higher relaxivity than free Gd-DTPA.[10] Furthermore, a polymalic acid-based nanoparticle covalently linked with curcumin and Gd-DOTA could also detect Aβ in human brain specimens by MRI.[11] These previous studies demonstrate that the curcumin structure has significant potential for the development of MRI contrast agents for AD diagnosis.

From SARM prediction, a curcumin derivative, compound **B**, possesses 100-times stronger inhibitory activity of Aβ aggregation than curcumin based on thioflavin T (ThT) competitive binding assay (see in Chapter 2.2). According to this result, this study aims to design curcumin-based Gd probes to detect and inhibit Aβ

aggregation (Figure 3-1A–C). It is expected that these probes could accelerate proton longitudinal relaxation depending on the fibrillation stage of Aβ because the molecular tumbling rate of the Gd complexes becomes slower (Figure 3-1A).[12] As a result, the probes permit the detection of Aβ by longitudinal relaxation time (T_1)-weighted imaging. This mechanism could also be utilized to estimate the inhibitory activity of the probes by T_1-based analysis (Figure 3-1B). The curcumin and compound B were directly conjugated with the macrocyclic DO3A ligand through the propylamine linker to obtain Gd-DO3A-Cur and Gd-DO3A-Comp.B, respectively (Figure 3-1C).

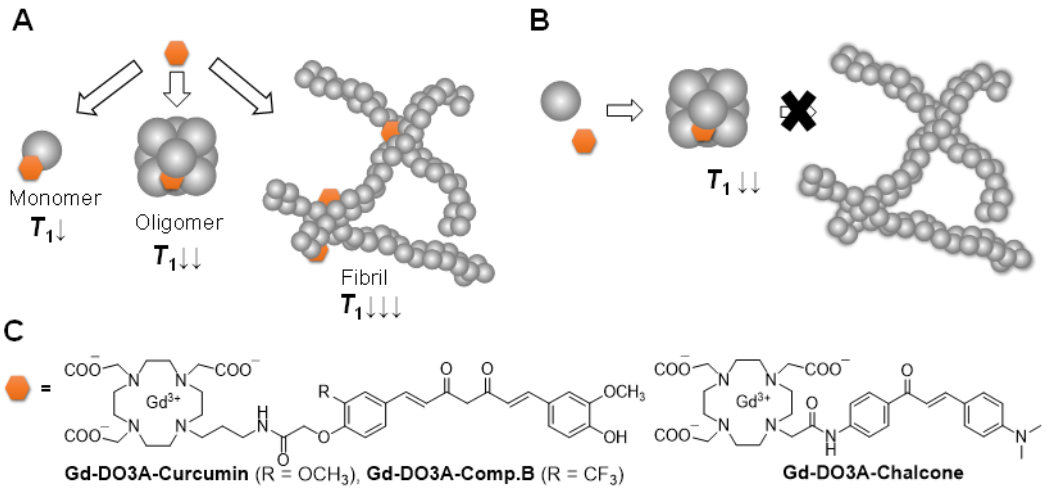

Figure 3-1. (A) The probe concept that produces T_1 in a dependent manner of the Aβ fibrillation process. (B) Inhibitor-based probes that cause moderate T_1 decreases due to inhibitory activity of fibrillation. (C) The chemical structures of the synthesized Gd probes for Aβ detection and inhibition.

3.2. Results and Discussion

3.2.1. Synthesis of Gd Compounds

Gd-DO3A-Cur and Gd-DO3A-Comp.B were synthesized according to Scheme 3-1. The compounds **5a** and **5b**, which have asymmetric curcumin derivatives containing carboxylic acid groups, were synthesized by three-step reactions. Amide bond formation with DO3A(*t*Bu)$_3$-propylamine ligand[13] by condensation reaction afforded compounds **7a** and **7b**. The *tert*-butyl groups were deprotected by trifluoroacetic acid, producing compounds **8a** and **8b**. The

complexation was performed with $GdCl_3 \cdot 6H_2O$ by adjusting the reaction pH to 7, giving **Gd-DO3A-Cur** and **Gd-DO3A-Comp.B** in 43 and 41% yields, respectively.

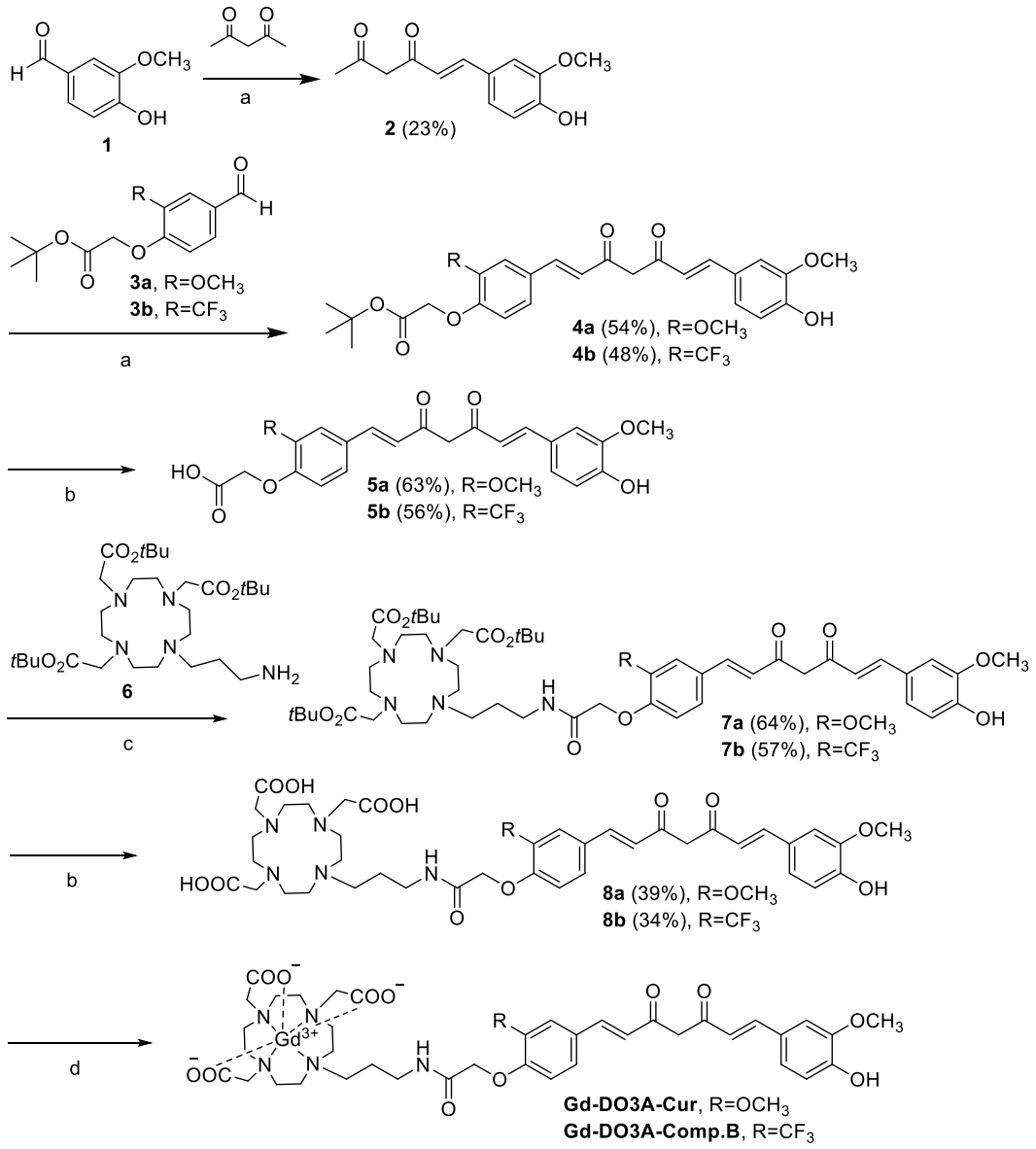

Scheme 3-1. Synthetic scheme of Gd compounds. Reaction conditions: (a) DMF, $B(OH)_3$, morpholine, MW 100 °C, 10 min; (b) DCM, TFA, 2 h; (c) DMF, PyBOP, HOBt, Et_3N, RT, overnight; (d) $GdCl_3 \cdot 6H_2O$, NaOH, H_2O.

3.2.2. Relaxation Rate Profile of Gd Compounds

The T_1 relaxivities (r_1) of the curcumin-based Gd probes were estimated by T_1 measurement using a 1 tesla NMR relaxometry (Figure 3-2). For the comparison,

a reported probe for Aβ, **Gd-DO3A-Chal** was synthesized.[14] The r_1 of **Gd-DO3A-Comp.B**, **Gd-DO3A-Cur**, and **Gd-DO3A-Chal** were 7.1, 6.1, and 5.3 mM^{-1} s^{-1}, respectively. These r_1 values are higher than clinically approved Gd-DOTA (3.9 mM^{-1} s^{-1}).[15] The molecular weight of **Gd-DO3A-Comp.B** and **Gd-DO3A-Cur** is almost two times larger than Gd-DOTA. Because the r_1 increases approximately linearly with molecular weight in the low magnetic field,[17] the high r_1 values of **Gd-DO3A-Comp.B** and **Gd-DO3A-Cur** might be mainly attributed to their high rotational correlation time, rather than the high number of coordinated water molecules. The r_1 of **Gd-DO3A-Chal** was comparable to the value reported previously.[14]

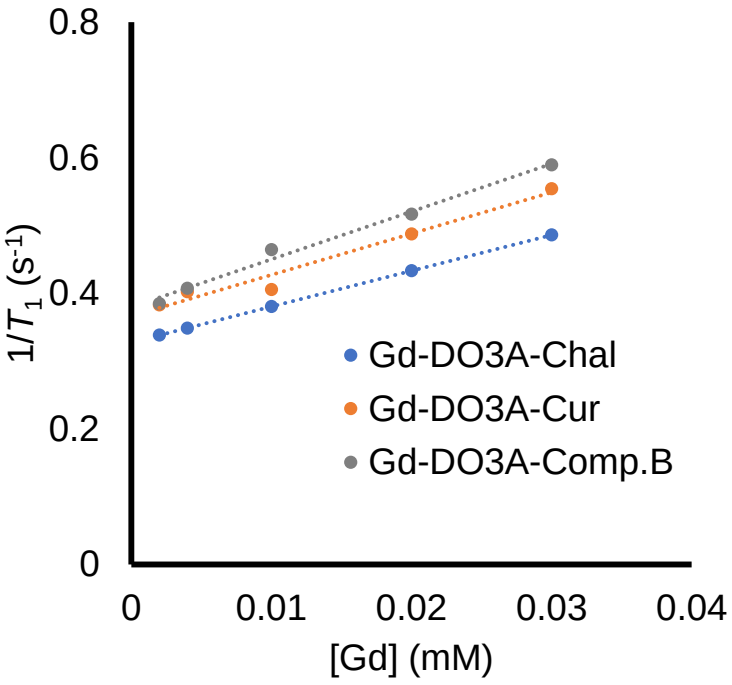

Figure 3-2. Relaxation rate profile of the Gd probes.

3.2.3. Evaluation of Inhibitory Activity toward Aβ Aggregation and Cytotoxicity Study

Gd compounds were further evaluated for the inhibitory activity against Aβ aggregation by ThT assay.[16] After 24 h incubation of 20 μM Aβ with 10 μM Gd compounds, **Gd-DO3A-Comp.B** showed the lowest fluorescence intensity,

indicating the strongest inhibitory activity followed by **Gd-DO3A-Cur** (Figure 3-3A). As a comparison, the reported MRI agents, **Gd-DO3A-Chal**, showed slight inhibitory activity. The inhibitory effect was also assessed by a fluorescence dye with longer fluorescence absorption, congo red (CR) which could bind to the hydrophobic site of Aβ.[17] Based on CR assay, similar patterns were also obtained in which **Gd-DO3A-Comp.B** was the strongest inhibitor followed by **Gd-DO3A-Cur** and **Gd-DO3A-Chal** confirming the results from ThT assay (Figure 3-3B).

The inhibitory effect was further evaluated by TEM with negative staining (Figure 3-3C) to confirm the morphological change of Aβ after treatment. In the absence of the Gd compounds, Aβ formed huge and massive fibrils similar to the typical morphology of Aβ fibril.[18] The TEM images of Aβ with **Gd-DO3A-Comp.B** showed the presence of white spheres below 10 nm, demonstrating that **Gd-DO3A-Comp.B** strongly inhibits Aβ aggregation. In fact, the fibril growth stopped at a stage of oligomer formation. Lower inhibitory activity of **Gd-DO3A-Cur** was also found to provide a shortened worm-like fibril, which is the typical morphology of Aβ exposed to curcumin.[19] In contrast, small numbers of white spheres and partial fibril disruption were found in the image of Aβ with **Gd-DO3A-Chal**. Compared with a reported Gd-DTPA-Curcumin that possessed inhibitory activity starting at 50 μM, **Gd-DO3A-Comp.B** possessed stronger inhibition of Aβ aggregation at 10 μM.[20] The MTT assay using N2a cells showed that IC_{50} of **Gd-DO3A-Cur** and **Gd-DO3A-Comp.B** were more than 500 μM, indicating that these compounds did not possess significant cytotoxicity (Figure 3-3D).

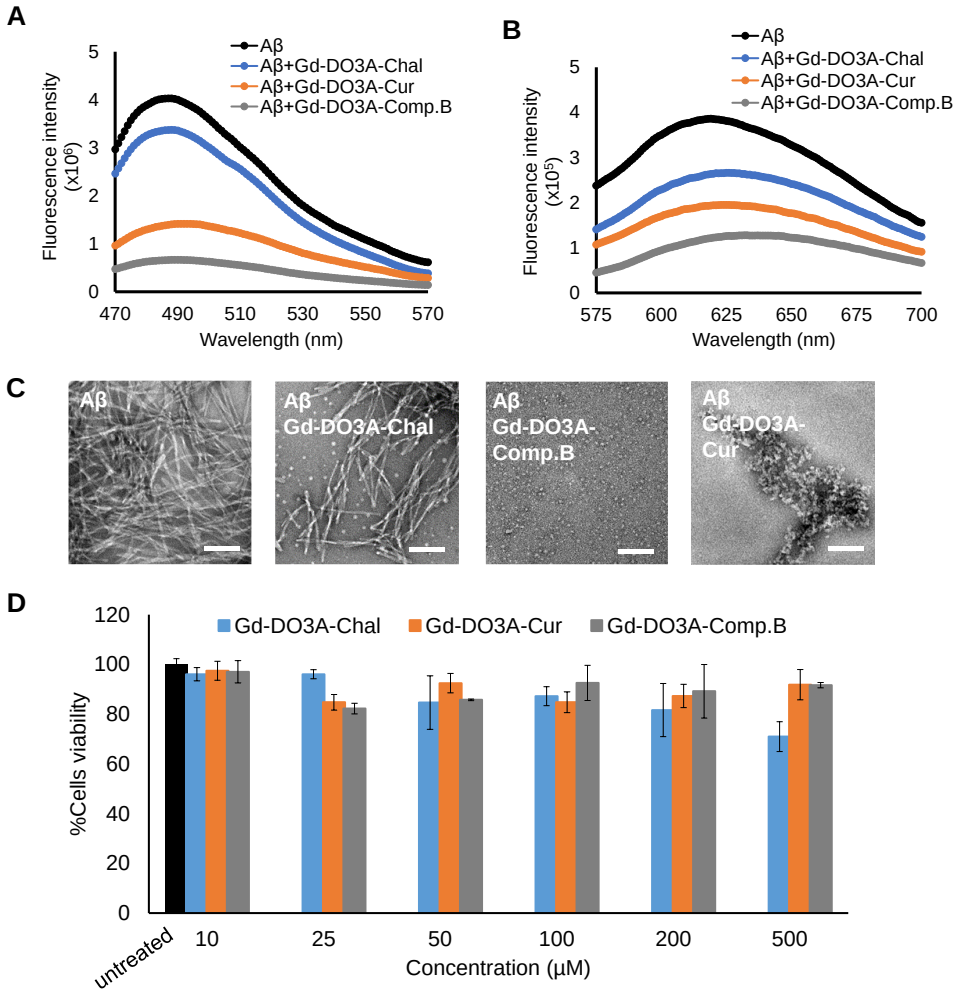

Figure 3-3. Inhibitory effect of the Gd probes toward Aβ aggregation measured by ThT assay (A) Congo Red assay (B) and negative staining TEM images (C). The Gd probes were co-incubated with monomeric Aβ for 24 h in PBS at pH 7.4. [Gd] = 10 μM, [Aβ] = 20 μM. Scale bars = 100 nm. (D) Effect of Gd compounds against cells viability of N2a cells.

3.2.4. Detection of Aβ based on T_1 Change by NMR

The ability of Gd compounds to detect the fibrillation process was assessed based on the T_1 change by NMR relaxometry. The Aβ was pre-incubated at 1, 3, 6, 12, and 24 h to make it form the fibrils of different growth stages (Figure 3-4A). The T_1 of **Gd-DO3A-Comp.B** solution decreased with pre-incubation time of Aβ, demonstrating that the **Gd-DO3A-Comp.B** can detect Aβ fibril depending on the

growth stage (Figure 3-4A). Lower T_1 involved with Aβ growth could be caused by the reduction in the tumbling rate of the Gd complex.[21] In addition, the Gd compounds were also co-incubated with the Aβ monomer and monitored T_1 changes over the incubation time (Figure 3-4B). Interestingly, the **Gd-DO3A-Comp.B** did not cause significant T_1 decreases even after 24 h co-incubation with Aβ monomers, demonstrating that **Gd-DO3A-Comp.B** has a strong inhibitory effect on fibril formation, and the inhibition can be by T_1 measurement (Figure 3-4B). On the other hand, the time-dependent increases of T_1 were observed in **Gd-DO3A-Chal** and **Gd-DO3A-Cur**. This might be because these two probes were buried in the hydrophobic pocket as Aβ fibril grew up and fewer water molecules permitted access to the Gd ions. It is also possible that these probes have a lower binding affinity, especially for matured fibril, and require higher concentrations to produce significant T_1 changes.[22] These probes did not produce the significant ΔT_1 between monomer and fibril samples (Figure 3-4B), although they showed little inhibition.

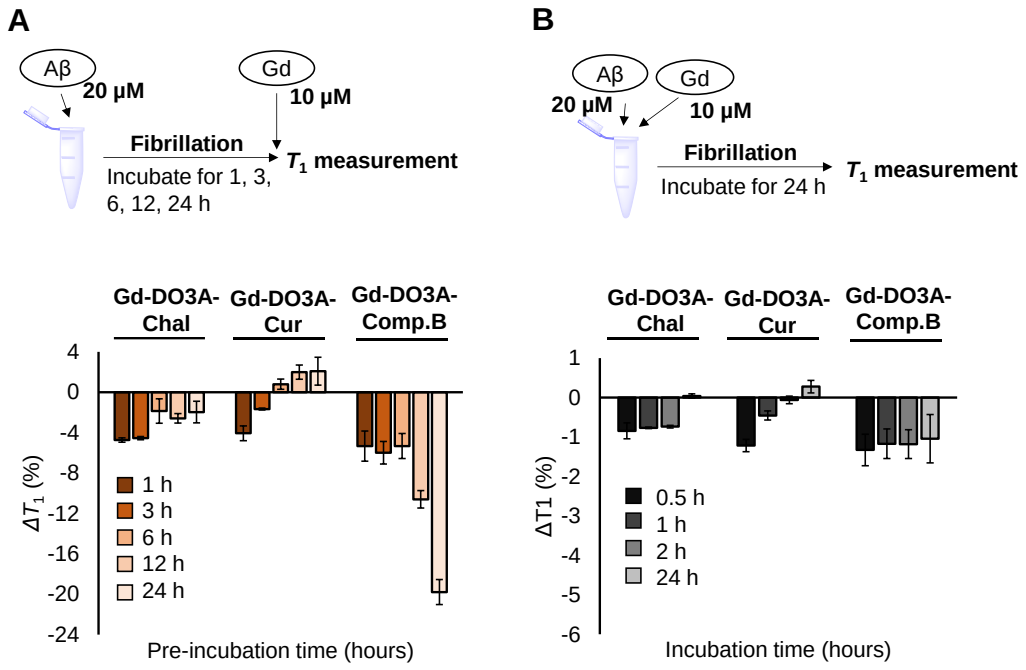

Figure 3-4. (A) T_1 changes of the Gd compounds with pre-incubated fibrils and monomers in PBS at pH 7.4. (B) T_1 changes of Gd compounds co-incubated with Aβ monomer for 0.5, 1, 2, and 24 h at 37 ºC (mean ± SEM, n = 3). [Gd] = 10 μM, [Aβ] = 20 μM.

3.2.5. Detection of Aβ by *In Vitro* MRI

The feasibility of the Gd compounds was further evaluated by *in vitro* MRI measurement using a 1 tesla scanner. The T_1-weighted images showed that **Gd-DO3A-Comp.B** produced slight T_1 signal increases with Aβ monomers for 2 and 24 h (Figure 3-5A and 3-5B). More significant signal increases were observed in the **Gd-DO3A-Comp.B** with Aβ fibril pre-incubated for 24 h (Figure 3-5C). In contrast, **Gd-DO3A-Chal** and **Gd-DO3A-Cur** did not show significant signal changes in the presence of Aβ monomers or fibrils (Figure 3-5A–C). These results were consistent with the T_1 profile measured by NMR (Figure 3-4A and 3-4B). Compared to the previously reported **Gd-DO3A-Chal** that required 100 μM of the probe concentration to detect the equimolar Aβ,[14] **Gd-DO3A-Comp.B** could detect five-times lower concentration of Aβ (20 μM) with ten-times lower probe concentration (10 μM). Therefore, **Gd-DO3A-Comp.B** could be promising further to develop highly sensitive diagnostic MRI contrast agents of AD.

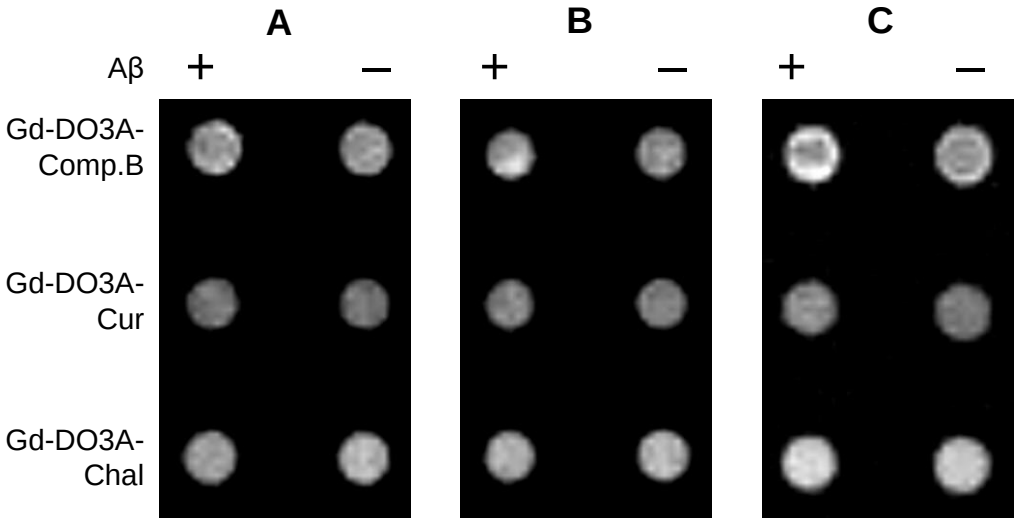

Figure 3-5. T_1-weighted images of the Gd probe solutions in the presence of monomeric Aβ at 2 h incubation (A), monomeric Aβ at 24 h incubation (B), and Aβ fibrils pre-incubated for 24 h (C). Incubation was conducted in PBS at pH 7.4.

3.3. Summary of Chapter 3

A curcumin-based Gd probe, **Gd-DO3A-Comp.B**, enabled the detection and inhibition of Aβ fibril formation. **Gd-DO3A-Comp.B** also allowed for the highly sensitive detection of Aβ fibril by the T_1 measurement. Moreover, the inhibitory

activity could be estimated by the T_1 measurement because **Gd-DO3A-Comp.B** decreased T_1 depending on the growth stage of Aβ fibril formation.

3.4. Experimental Section

All solvents used were in analytical standard grade. The NMR spectra were measured on a Bruker biospin AVANCE II (400 MHz for ^{1}H and 100 MHz for ^{13}C) or a Bruker biospin AVANCE III (500 MHz for ^{1}H, 125 MHz for ^{13}C, and 470 MHz for ^{19}F). Chemical shift (δ) was reported in ppm relative to internal tetramethylsilane. The HRMS data were recorded on the Bruker ESI-TOF-MS micrOTOF II instrument with sodium formate as the calibration standard. Vanillin, 3-bromopropylamine hydrobromide, potassium carbonate, potassium bicarbonate, morpholine, boric acid, and 10% Pd/C were purchased from Wako Chemical (Japan). The 1,4,7,10-tetraazacyclododecane were purchased from Accela (USA). Benzyl chloroformate, *tert*-butyl bromoacetate, PyBOP, and HOBt were purchased from Tokyo Chemical Industry (Japan). Microwave for synthesis was conducted on Biotage® Initiator+ instrument. Column chromatography was performed on silica gel Chromatorex (Japan). Purity analysis was determined by HPLC analysis using Inertsil ODS-3 5 μm (4.6 × 75 mm; GL Science) with a linear gradient of 0.1% formic acid in water/0.1% formic acid in MeCN detected by a UV lamp for 20 min. Amyloid β ($A\beta_{42}$) peptide was purchased from Peptide Institute (Japan). Thioflavin T (ThT) for fluorescence detection of $A\beta_{42}$ was purchased from Sigma (USA).

Synthesis of compound 2. Acetylacetone (10 mmol) and boric acid (10 mmol) were suspended in DMF. Compound **7** (2 mmol) was added, followed by morpholine (2 mmol). The mixture was irradiated in the microwave at 100 ^{o}C for 10 min. The reaction mixture was quenched by HCl 0.1 N and extracted using ethyl acetate. The organic phase was dried using $MgSO_4$. The crude product was purified by column chromatography (silica gel, hexane:ethyl acetate 4:1) to obtain the desired compound.

(4-hydroxy-3-methoxyphenyl) hex-5-ene-2,4-dione (2). Yield: 65%. ^{1}H-NMR (400 MHz, $CDCl_3$): δ (ppm) 2.20 (-CH_3, s, 3H), 3.98 (-OCH_3, s, 3H), 5.68 (=CH, s, 1H), 5.87 (=CH, s, 1H), 6.37 (=CH, *J*=15.8, d, 1H), 6.97 (=CH, *J*=8.2, d, 1H), 7.06

(=CH, *J*=1.8 Hz, d, 1H), 7.13 (=CH, *J*=8.2, 1.8 Hz, dd, 1H), 7.58 (=CH, *J*=15.8 Hz, d, 1H). ^{13}C-NMR (125 MHz, $CDCl_3$): δ (ppm) 26.59, 55.86, 100.69, 111.39, 115.88, 119.87, 123.09, 126.55, 140.47, 148.19, 149.41, 178.48, 196.85. LRMS-ESI (*m/z*): calcd for $C_{13}H_{15}O_4^+$ $[M+H]^+$ 235.10; found 235.13.
Compound 2 was synthesized as described in Chapter 2.4.

Synthesis of compounds 3a or 3b. Vanillin or 4-hydroxy 3-trifluoromethyl benzaldehyde (6 mmol) and potassium carbonate (18 mmol) were dissolved in acetone 10 mL. The tert-butyl bromoacetate (7.5 mmol) was added then the mixture was refluxed for 2 h. After removing inorganic salt, the organic solvent was filtered and evaporated without further purification.
tert-butyl 2-(4-formyl-2-methoxyphenoxy)acetate (3a). Yield: 92%. ^{1}H-NMR (400 MHz, $CDCl_3$): δ (ppm) 1.42 (-CH_3, s, 9H), 3.88 (-OCH_3, s, 3H), 4.63 (-CH_2, s, 2H), 6.82 (=CH, *J*=8.6, d, 1H), 7.35-7.37 (m, 2H), 9.79 (-CHO, s, 1H). ^{13}C-NMR (100 MHz, $CDCl_3$): δ (ppm) 27.93, 55.98, 66.01, 82.66, 109.79, 112.03, 126.01, 130.84, 149.81, 152.62, 166.69, 190.72. HRMS-ESI (*m/z*): calcd for $C_{14}H_{17}O_5^-$ $[M-H]^-$ 265.1081; found 265.1145.
tert-butyl 2-(4-formyl-2-(trifluoromethyl)phenoxy)acetate (3b). Yield: 97%. ^{1}H-NMR (400 MHz, $CDCl_3$): δ (ppm) 1.48 (3x-CH_3, s, 9H), 4.75 (-CH_2, s, 2H), 7.02 (=CH, *J*=8.6 Hz, d, 1H), 8.05 (=CH, *J*=8.6, 2.0 Hz, dd, 1H), 8.16 (=CH, *J*=1.8 Hz, d, 1H), 9.95 (-CHO, s, 1H). ^{13}C-NMR (125 MHz, $CDCl_3$): δ (ppm) 27.46, 65.62, 82.69, 112.74, 119.34 (J_{C-F}=31.6 Hz, q), 122.71 (J_{C-F}=271.1 Hz, q), 128.61 (J_{C-F}=5.0 Hz, q), 134.79, 160.10, 166. 06, 189.36. HRMS-ESI (*m/z*): calcd for $C_{14}H_{15}F_3O_4Na^+$ $[M+Na]^+$ 327.0815; found 327.0827.
Compound 3b was synthesized as described in Chapter 2.4.

Synthesis of compound 4a and 4b. Compound **2** (0.5 mmol) and boric acid (0.5 mmol) were suspended in DMF. Compound **3a** or 3b (0.5 mmol) was added, followed by morpholine (0.5 mmol). The mixture was irradiated in the microwave at 100 °C for 10 min. The reaction mixture was quenched by HCl 0.1 N and extracted using ethyl acetate. The organic phase was dried using $MgSO_4$. The crude

product was purified by column chromatography (silica gel, hexane:ethyl acetate 2:1) to obtain the desired compound.

tert-butyl 2-(4-((1E,6E)-7-(4-hydroxy-3-methoxyphenyl)-3,5-dioxohepta-1,6-dien-1-yl)-2-methoxyphenoxy)acetate (4a). Yield: 54%. ^{1}H-NMR (400 MHz, $CDCl_3$): δ (ppm) 1.48 (-CH_3, s, 9H), 3.93 (-OCH3, s, 6H), 4.62 (-CH_2, s, 2H), 5.8-6.0 (-CH_2, s, 2H), 6.48 (=CH, *J*=15.8 Hz, d, 1H), 6.49 (=CH, *J*=15.8 Hz, d, 1H), 6.78 (=CH, *J*=8.4 Hz, d, 1H), 6.92 (=CH, *J*=8.1, 1.0 Hz, dd, 1H), 7.01-7.12 (m, 4H), 7.57 (=CH, *J*=15.7Hz d, 1H), 7.59 (=CH, *J*=15.7 Hz, d, 1H). ^{13}C-NMR (125 MHz, DMSO-d_6): δ (ppm) 27.94, 55.91, 66.15, 82.44, 101.37, 109.98, 110.66, 113.09, 115.18, 121.39, 120.02, 122.39, 122.89, 127.24, 129.06, 139.92, 140.86, 147.25, 148.46, 149.14, 149.46, 167.55, 182.66, 183.79. LRMS-ESI (*m/z*): calcd for $C_{27}H_{30}O_8Na^+$ $[M+Na]^+$ 505.18; found 505.12.

tert-butyl 2-(4-((1E,6E)-7-(4-hydroxy-3-methoxyphenyl)-3,5-dioxohepta-1,6-dien-1-yl)-2-(trifluoromethyl)phenoxy)acetate (4b). Yield: 48%. ^{1}H-NMR (400 MHz, $CDCl_3$): δ (ppm) 1.51 (-CH_3, s, 9H), 3.99 (-OCH_3, s, 3H), 4.70 (-CH_2, s, 2H), 5.86 (-CH_2, S, 2H), 6.53 (=CH, *J*=16.0 Hz, d, 1H), 6.57 (=CH, *J*=16.0 Hz, d, 1H) 6.92 (=CH, *J*=8.6 Hz, d, 1H), 6.99 (=CH, *J*=8.0 Hz, d, 1H), 7.11 (=CH, s, 1H), 7.19 (=CH, *J*=7.9 Hz, d, 1H), 7.61-7.69 (=CH, m, 3H), 7.85 (=CH, s, 1H). ^{13}C-NMR (125 MHz, DMSO-d_6): δ (ppm) 28.09, 56.15, 65.89, 82.26, 101.86, 111.83, 114.46, 116.16, 118.19 (J_{C-F}=30.7 Hz, q), 121.54, 123.80 (J_{C-F}=271.1 Hz, q), 123.82, 124.37, 126.69, 127.38 (J_{C-F}=4.1 Hz, q), 128.24, 133.99, 138.31, 141.93, 148.47, 150.01, 157.06, 167.32, 182.04, 185.11. ^{19}F NMR (470 MHz, DMSO-d_6): δ 60.9. HRMS-ESI (*m/z*): calcd for $C_{27}H_{26}F_3O_7^-$ $[M-H]^-$ 519.1636; found 519.1702.

Compound **4b** was synthesized as described in Chapter 2.4.

Synthesis of compound 5a and 5b. Compound **4a** or **4b** (0.41 mmol) was dissolved in dichloromethane 10 mL. Trifluoroacetic acid (8 mL, excess) was added then stirred for 2 h under argon gas in RT. The solvent was removed by evaporation, and the product was purified by preparative HPLC (MeCN/water).

2-(4-((1E,6E)-7-(4-hydroxy-3-methoxyphenyl)-3,5-dioxohepta-1,6-dien-1-yl)-2-methoxyphenoxy)acetic acid (5a). Yield: 63%. ^{1}H-NMR (400 MHz, CD_3CN): δ (ppm) 3.92 (-CH_3, s, 3H), 3.94 (-OCH_3, s, 3H), 4.73 (-CH_2, s, 2H), 5.96 (-CH_2, s,

2H), 6.71 (=CH, *J*=15.7 Hz, d, 1H), 6.75 (=CH, *J*=15.7 Hz, d, 1H) 6.89 (=CH, *J*=8.1 Hz, d, 1H), 6.91 (=CH, *J*=8.1 Hz, d, 1H), 7.17 (=CH, *J*=8.3 Hz, d, 1H), 7.19 (=CH, *J*=8.3 Hz, d, 1H), 7.29 (=CH, *J*=8.2 Hz, d, 1H), 7.61 (=CH, *J*=15.8 Hz, d, 1H), 7.62 (=CH, *J*=15.8 Hz, d, 1H). ^{13}C-NMR (125 MHz, DMSO-d_6): δ (ppm) 49.07, 56.08, 65.54, 101.51, 111.38, 113.25, 116.19, 121.55, 122.73, 122.89, 123.61, 126.77, 128.59, 140.47, 141.45, 148.46, 149.51, 149.81, 149.91, 162.79, 170.54, 183.06, 184.25. HRMS-ESI (m/z): calcd for $C_{23}H_{21}O_8^-$ [M-H]$^-$ 425.1242; found 425.1215

2-(4-((1E,6E)-7-(4-hydroxy-3-methoxyphenyl)-3,5-dioxohepta-1,6-dien-1-yl)-2-(trifluoromethyl)phenoxy)acetic acid (5b). Yield: 56%. ^{1}H-NMR (400 MHz, CD_3CN): δ (ppm) 3.98 (-OCH_3, s, 3H), 4.84 (-CH_2, s, 2H), 5.98 (=CH, s, 1H), 6.72 (=CH, *J*=16.0 Hz, d, 1H), 6.78 (=CH, *J*=16.0 Hz, d, 1H), 6.89 (=CH, *J*=8.0 Hz, d, 1H), 7.10 (=CH, *J*=8.8 Hz, d, 1H), 7.18 (=CH, *J*=8.2, 1.9 Hz, dd, 1H), 7.29 (=CH, *J*=1.8 Hz, d, 1H), 7.65 (=CH, *J*=15.6 Hz, d, 2H), 7.84 (=CH, *J*=8.6 Hz, d, 1H), 7.94 (=CH, *J*=1.9 Hz, d, 1H). ^{13}C-NMR (125 MHz, DMSO-d_6): δ (ppm) 55.92, 66.81, 101.58, 111.59, 114.52, 115.99, 117.66 (J_{C-F}=30.2 Hz, q), 121.29, 122.67, 123.58, 123.74 (J_{C-F}=270.7 Hz, q), 126.40, 126.62, 126.74, 127.04 (J_{C-F}=4.7 Hz, q), 127.22, 127.49 (J_{C-F}=5.2 Hz, q), 133.61, 138.37, 141.62, 141.98, 148.28, 157.84, 170.25, 182.01, 184.68, 198.26. ^{19}F NMR (470 MHz, DMSO-d_6): δ 60.8. HRMS-ESI (*m/z*): calcd for $C_{23}H_{18}F_3O_7^-$ [M-H]$^-$ 463.1010; found 463.1087.

Synthesis of compound 6. Synthesis of compound **6** followed the reported method with slight modification.[13] The 3-bromopropylamine hydrobromide (2.05 g, 10 mmol) and NaOH 2M (10 mL, 20 mmol) were dissolved in cold dioxane, then benzyl chloroformate (1.43 mL, 10 mmol) was added dropwise. The reaction was mixed and stirred at room temperature. After overnight stirring, dioxane was removed by evaporation, then the remaining residue was extracted by ethyl acetate. The organic layer was washed by $NaHCO_3$ aq., water, brine, then was dried by Na_2SO_4 and evaporated to obtain the crude product for the next steps without further purification. The crude product (0.5 g, 2.1 mmol) was added dropwise in the 1,4,7,10-tetraazacyclododecane (0.5 g, 2.9 mmol) dissolved in toluene, then refluxed overnight under argon gas. The mixture was extracted with water, then separated by dichloromethane, washed with brine, dried with Na_2SO_4, and

evaporated to obtain the crude product for the next steps without further purification. The crude product (0.5 g, 1.4 mmol) and $KHCO_3$ (1.1g, 14 mmol) were dissolved in acetonitrile. Tert-butyl bromoacetate (0.81g, 4.2 mmol) was added dropwise and refluxed overnight under argon gas. The $KHCO_3$ was filtered, and the filtrate was evaporated. The crude product (0.2 g, 0.1 mmol) and Pd/C 10% (20 mg) were dissolved in ethanol then stirred overnight under hydrogen gas. After filtration, the filtrate was evaporated to get white solid powder products.

Benzyl (3-(1,4,7,10-tetraazacyclododecan-1-yl)propyl)carbamate (6). Yield: 61%. ^{1}H-NMR (400 MHz, CD_3CN): δ (ppm) 1.44 (-CH_3, s, 27H), 1.72 (-CH_2, broad s, 2H), 2.51-3.51 (m, 24H), 3.92 (-NH_2, broad s, 2H). ^{13}C-NMR (100 MHz, CD_3CN): δ (ppm) 24.21, 28.09, 39.48, 50.58, 50.81, 51.31, 53.23, 57.52, 57.79, 82.22, 82.61, 171.76, 173.21. HRMS-ESI (*m/z*): calcd for $C_{29}H_{58}N_5O_6^+$ $[M+H]^+$ 572.4382; found 572.4355.

Synthesis of compounds 7a and 7b. Compounds **5a** or **5b** (0.18 mmol), HOBt (0.18 mmol) and PyBOP (0.18 mmol) were dissolved in DMF (3 mL). Compound **6** (0.22 mmol) and triethylamine (0.54 mmol) in DMF 2 mL were added, followed by stirring for 24 h. The desired product was purified by column chromatography (silica gel, dichloromethane/methanol).

tri-tert-butyl 2,2',2''-(10-(3-(2-(4-((1E,6E)-7-(4-hydroxy-3-methoxyphenyl)-3,5-dioxohepta-1,6-dien-1-yl)-2-methoxyphenoxy)acetamido)propyl)-1,4,7,10-tetraazacyclododecane-1,4,7-triyl)triacetate (7a). Yield 64%. ^{1}H-NMR (400 MHz, CD_3CN): δ (ppm) 1.46 (-CH_3, s, 27H), 2.70-3.80 (m, 24h), 3.93 (-OCH_3, s, 6h), 4.55 (-CH_2, s, 1H), 4.78 (-CH_2, s, 1H), 5.96 (-CH_2, s, 1H), 6.69 (=CH, *J*=15.7 Hz, d, 1H), 6.75 (=CH, *J*=15.7 Hz, d, 1H), 6.89 (=CH, *J*=8.1 Hz, d, 1H), 6.98 (=CH, *J*=8.2 Hz, d, 1H), 7.16 (=CH, *J*=8.1 Hz, d, 1H), 7.21 (=CH, *J*=8.8 Hz, d, 1H), 7.27-7.32 (m, 2H), 7.60 (=CH, *J*=15.7 Hz, d, 1H), 7.61 (=CH, *J*=15.7 Hz, d, 1H). ^{13}C-NMR (125 MHz, DMSO-d_6): δ (ppm) 28.24, 28.27, 46.97, 49.26, 51.99, 52.30, 52.53, 55.91, 56.13, 68.57, 81.15, 101.50, 111.41, 111.83, 113.59, 114.44, 116.18, 121.53, 122.87, 122.97, 123.10, 123.67, 126.71, 129.34, 140.21, 141.59, 148.46, 149.57, 149.67, 149.86, 149.95, 168.19, 169.44, 170.52, 170.71, 182.82, 184.48. HRMS-ESI (m/z): calcd for $C_{52}H_{78}N_5O_{13}^+$ $[M+H]^+$ 980.5591; found 980.5518.

tri-tert-butyl 2,2',2''-(10-(3-(2-(4-((1E,6E)-7-(4-hydroxy-3-methoxyphenyl)-3,5-dioxohepta-1,6-dien-1-yl)-2-(trifluoromethyl)phenoxy)acetamido)propyl)-1,4,7,10-tetraazacyclododecane-1,4,7-triyl)triacetate (7b). Yield 57%. ^{1}H-NMR (500 MHz, DMSO-d_6): δ (ppm) 1.41 (-CH_3, s, 27H), 2.6-3.8 (m, 24h), 3.84 (-OCH_3, s, 3h), 4.73 (-CH_2, s, 2H), 6.1 (-CH_2, s, 1H), 6.77 (=CH, *J*=15.7 Hz, d, 1H), 6.84 (=CH, *J*=8.1, d, 1H), 6.91 (=CH, *J*=15.6, d, 1H), 7.13 (=CH, *J*=8.4, d, 1H), 7.33 (=CH, s, 1H), 7.58 (=CH, *J*=15.7 Hz, d, 1H), 7.62 (=CH, *J*=15.3 Hz, d, 1H), 7.93 (=CH, *J*=8.6 Hz, d, 1H), 7.97 (=CH, s, 1H), 8.06 (=CH, *J*=8.1 Hz, d, 1H). ^{13}C-NMR (125 MHz, DMSO-d_6): δ (ppm) 27.90, 28.22, 30.34, 52.46, 56.14, 56.26, 65.56, 66.56, 68.98, 70.27, 81.11, 101.79, 111.83, 114.66, 116.20, 117.95 (J_{C-F}=30.5 Hz, q), 121.51,123.79, 123.93 (J_{C-F}=270.7 Hz, q), 124.01, 126.62, 127.29 (J_{C-F}=5.2 Hz, q), 127.64, 128.32, 133.88, 138.51, 141.86, 148.49, 150.12, 157.82, 170.10, 182.18, 184.98. ^{19}F NMR (470 MHz, DMSO-d_6): δ 60.8. HRMS-ESI (m/z): calcd for $C_{52}H_{75}F_3N_5O_{12}^+$ $[M+H]^+$ 1018.5359; found 1018.5384.

Synthesis of compound 8a and 8b. Compounds **7a** or **7b** (0.18 mmol) was dissolved in dichloromethane 10 mL. Trifluoroacetic acid (8 mL, excess) was added then stirred for 2 h under argon gas in RT. The solvent was removed by evaporation, and the product was purified by preparative HPLC (MeCN/water).

2,2',2''-(10-(3-(2-(4-((1E,6E)-7-(4-hydroxy-3-methoxyphenyl)-3,5-dioxohepta-1,6-dien-1-yl)-2-methoxyphenoxy)acetamido)propyl)-1,4,7,10-tetraazacyclododecane-1,4,7-triyl)triacetic acid (8a). Yield 39%. ^{1}H-NMR (400 MHz, CD_3CN): δ (ppm) 3.3-4.0 (m, 24H), 3.93 (-OCH_3, s, 6H), 4.61 (-CH_2, s, 2H), 5.99 (=CH, s, 1H), 6.69 (=CH, *J*=15.8 Hz, d, 1H), 6.76 (=CH, *J*=15.9 Hz, d, 1H), 6.91 (=CH, *J*=8.1 Hz, d, 1H), 6.99 (=CH, *J*=8.8 Hz, d, 1H), 7.27 (=CH, s, 1H), 7.33 (=CH, s, 1H), 7.62 (=CH, *J*=15.8 Hz, d, 2H), 8.04 (=CH, s, 1H). LRMS-ESI (m/z): calcd for $C_{40}H_{52}N_5O_{13}^-$ $[M-H]^-$ 810.36; found 810.76.

2,2',2''-(10-(3-(2-(4-((1E,6E)-7-(4-hydroxy-3-methoxyphenyl)-3,5-dioxohepta-1,6-dien-1-yl)-2-(trifluoromethyl)phenoxy)acetamido)propyl)-1,4,7,10-tetraazacyclododecane-1,4,7-triyl)triacetic acid (8b). Yield 34%. ^{1}H-NMR (500 MHz, DMSO-d_6): δ (ppm) 2.6-3.7 (m, 24H), 3.84 (-OCH_3, s, 3H), 4.65 (-CH_2, s, 2H) 6.77 (=CH, *J*=15.6 Hz, d, 1H), 6.88 (=CH, *J*=15.7 Hz, d, 1H), 7.09 (=CH, *J*=7.8

Hz, d, 1H), 7.15 (=CH, *J*=7.7 Hz, d, 1H), 7.2-7.4 (m, 2H) 7.57 (=CH, *J*=15.4 Hz, d, 1H), 7.61 (=CH, *J*=15.4 Hz, d, 1H), 7.79 (=CH, *J*=7.9, 2.7 Hz, dd, 1H), 7.91 (=CH, *J*=7.7 Hz, d, 1H), 7.95 (=CH, s, 1H). ^{19}F NMR (470 MHz, DMSO-d_6): δ 60.81. LRMS-ESI (m/z): calcd for $C_{40}H_{49}F_3N_5O_{12}^-$ [M-H]$^-$ 848.3335; found 848.3722.

Preparation of Gd-DO3A-Cur and Gd-DO3A-Comp.B. Compounds **8a** and **8b** were mixed with equimolar quantities of $GdCl_3$ in Milli-Q water. The pH of the solution was adjusted to **7** by adding NaOH 2 mM. The solution was allowed to react for 1 h at 60 °C by regularly controlling the pH. The absence of free metal was checked in each sample using the xylenol orange test and purified by preparative HPLC (MeCN/water).

Gd-DO3A-Cur. LRMS-ESI (m/z): calcd for $C_{40}H_{49}GdN_5O_{13}^-$ [M-H]$^-$ 965.26; found 965.32.

Gd-DO4A-Comp.B. LRMS-ESI (m/z): calcd for $C_{40}H_{47}F_3GdN_5O_{12}Cl^-$ [M+Cl]$^-$ 1039.21; found 1038.82.

Aβ Preparation for Aggregation Study

To prepare the Aβ monomer stock, 0.5 mg of the lyophilized $Aβ_{42}$ (Peptide Institute) was dissolved in DMSO by gently mixing without vortexing to obtain 500 µM as the final concentration. The solution was centrifuged at 13,200 rpm at 4 °C for 10 min. The supernatant was collected and stored at −80 °C until used. The Aβ stock was diluted into 100 µM in 2 mM NaOH freshly before being used.

Congo Red and Thioflavin T Assay

Congo Red or Thioflavin T stock at concentration 2 mM was freshly prepared in tris glycine 10 mM pH 8.5, then diluted in PBS at pH 7.4 to reach a final concentration of 40 µM. Gd probes were added at the final concentration of 10 µM followed by Aβ to reach the final concentration of 20 µM then were incubated at 37 °C. After 24 h, the mixture was transferred in 384-well plate black bottom non-binding to be scanned the fluorescence intensity with an excitation of 430 nm and emission range from 450 to 600 nm using a microplate reader (SpectraMax iD5, Molecular Device, USA).

Negative-Staining TEM Imaging

Elastic carbon grids (ELS-C10, STEM, Japan) was hydrolyzed by ion coater (IB-2, Eiko, Japan) with 3 mA of plasma current for 40 s before applying sample solution. Briefly, 5 μL of the Aβ only or containing Gd probes after 24 h incubation was applied to a hydrophilic grid and incubated for 1 min at RT. After gently drying with filter paper, the grid sample was washed with Milli-Q water and dried again with filter paper two times. Finally, the grid was incubated with 5 μL of 1% Nano-W negative staining solution (NY, USA) for 1 min followed by complete drying using filter paper. The negative stained sample was observed using TEM H-8100 (Hitachi) operated at 200 kV.

Cell Culture

The N2a cells were suspended in Dulbecco's Modified Eagle Medium (DMEM) medium supplemented with 10% fetal bovine serum. Briefly, N2a cells ($5x10^3$ cells/well) were grown on a 96-well plate overnight at 37 ^oC CO_2 5%. For the cytotoxicity study, cells were treated with Gd compounds at serial concentrations (10, 25, 50, 100, 200, 500 μM) for 24 h.

MTT Assay

An MTT reduction assay was conducted as described previously.[23] Briefly, MTT powder was dissolved in PBS pH 7.4 to obtain 5 mg/mL concentration stock, then was diluted into 0.5 mg/mL in DMEM medium. After removing the medium on a 96-well plate containing-treated cell, each well was added by 100 μL MTT 0.5 mg/mL and incubated at 37 ^oC CO_2 5%. After 3 h incubation, 100 μL DMSO was added following the absorbance measurement at a wavelength of 550 nm using a microplate reader (Tecan Infinite F200, Tecan, Switzerland). Calculation of % cells viability was measured by dividing the absorbance of untreated cells with the absorbance of curcumin-treated cells.

Nuclear Magnetic Resonance (NMR) Relaxometry

Longitudinal relaxation time (T_1) was measured using a Spinsolve ULTRA 43 MHz ^{1}H-NMR (Magritek Ltd., Wellington, New Zealand) in PBS at pH 7.4. The inversion-recovery (IR) was used to measure T_1. The parameters in the IR pulse sequence were as follows: number of scans = 2, acquisition time = 1.6 s, repetition time = 7 s, maximum inversion time = 5 s, number of steps = 21. To confirm the inhibitory effect on fibril growth, 20 μM of monomeric Aβ was mixed with 10 μM Gd probes at 37 ^{o}C, and the T_1 was measured at 0.5, 1, 2, and 24 h after preparing the samples. The fibrillation growth was detected as follows: 20 μM of monomeric Aβ was pre-incubated at 37 ^{o}C for 1, 3, 6, 12, and 24 h to cause the fibril formation in different growth stages. Then the 10 μM Gd probes were added into the fibril at each incubation time, and T_1 was measured without further incubation. The T_1 change (ΔT_1) was calculated by the equation as follow;

$$\Delta T_1 = \frac{(T_{1,(t)} - T_{1,(0)})}{T_{1,(0)}} \times 100\ (\%)$$

where $T_{1,(t)}$ is T_1 of the Gd probe solution with Aβ at t h while $T_{1,(0)}$ was T_1 of the Gd probe solution without Aβ at 0 h.

***In Vitro* MRI Imaging**

MRI was performed with a benchtop 1 tesla MRI scanner (ICON, Bruker BioSpin, Ettlingen, Germany). A 100 μL of each sample was added into 0.2 mL PCR tubes and imaged using a solenoid volume coil for transmission and reception. An inversion recovery rapid acquisition with relaxation enhancement (IR-RARE) sequence was used to obtain multi-inversion time images, with parameters including matrix size = 100 × 50, field of view = 4.0 cm × 2.0 cm, slice thickness = 3 mm, repetition time = 10,000 ms, effective echo time (TE) = 10 ms, RARE factor = 4, the number of excitations = 1, inversion time = 100, 300, 500, 700, 900, 1100, 1300, 1500, 1700, 1900, 2100, 2300, 2500, 2700, 2900, 3100, 3300, 3500, 3700, 3900 ms.

3.5. References

(1) Batsch, N. L.; Mittelman, M. S. *World Alzheimer Report 2012: Overcoming the Stigma of Dementia*; London, 2012; pp 1–80.

(2) McKhann, G.; Drachman, D.; Folstein, M.; Katzman, R.; Price, D.; Stadlan, E. M. Clinical Diagnosis of Alzheimer's Disease: Report of the NINCDS-ADRDA Work Group* under the Auspices of Department of Health and Human Services Task Force on Alzheimer's Disease. *Neurology* **1984**, *34* (7), 939–939.

(3) Dubois, B.; Feldman, H. H.; Jacova, C.; DeKosky, S. T.; Barberger-Gateau, P.; Cummings, J.; Delacourte, A.; Galasko, D.; Gauthier, S.; Jicha, G.; Meguro, K.; O'Brien, J.; Pasquier, F.; Robert, P.; Rossor, M.; Salloway, S.; Stern, Y.; Visser, P. J.; Scheltens, P. Research Criteria for the Diagnosis of Alzheimer's Disease: Revising the NINCDS–ADRDA Criteria. *Lancet Neurol* **2007**, *6* (8), 734–746.

(4) Sedgwick, A. C.; Brewster, J. T.; Harvey, P.; Iovan, D. A.; Smith, G.; He, X.-P.; Tian, H.; Sessler, J. L.; James, T. D. Metal-Based Imaging Agents: Progress towards Interrogating Neurodegenerative Disease. *Chem. Soc. Rev.* **2020**, *49* (10), 2886–2915.

(5) Wadghiri, Y. Z.; Sigurdsson, E. M.; Sadowski, M.; Elliott, J. I.; Li, Y.; Scholtzova, H.; Tang, C. Y.; Aguinaldo, G.; Pappolla, M.; Duff, K.; Wisniewski, T.; Turnbull, D. H. Detection of Alzheimer's Amyloid in Transgenic Mice Using Magnetic Resonance Microimaging. *Magn Reson Med* **2003**, *50* (2), 293–302.

(6) Martins, A. F.; Morfin, J.-F.; Kubíčková, A.; Kubíček, V.; Buron, F.; Suzenet, F.; Salerno, M.; Lazar, A. N.; Duyckaerts, C.; Arlicot, N.; Guilloteau, D.; Geraldes, C. F. G. C.; Tóth, É. PiB-Conjugated, Metal-Based Imaging Probes: Multimodal Approaches for the Visualization of β-Amyloid Plaques. *ACS Med. Chem. Lett.* **2013**, *4* (5), 436–440.

(7) Bort, G.; Catoen, S.; Borderies, H.; Kebsi, A.; Ballet, S.; Louin, G.; Port, M.; Ferroud, C. Gadolinium-Based Contrast Agents Targeted to Amyloid Aggregates for the Early Diagnosis of Alzheimer's Disease by MRI. *Eur J Med Chem* **2014**, *87*, 843–861.

(8) Rao, P. P. N.; Mohamed, T.; Teckwani, K.; Tin, G. Curcumin Binding to Beta Amyloid: A Computational Study. *Chem Biol Drug Des* **2015**, *86* (4), 813–820.

(9) Garcia-Alloza, M.; Borrelli, L. A.; Rozkalne, A.; Hyman, B. T.; Bacskai, B. J. Curcumin Labels Amyloid Pathology in Vivo, Disrupts Existing Plaques, and Partially Restores Distorted Neurites in an Alzheimer Mouse Model. *J Neurochem* **2007**, *102* (4), 1095–1104.

(10) Vithanarachchi, S. M.; Allen, M. J. A Multimodal, β-Amyloid-Targeted Contrast Agent. *Chem. Commun.* **2013**, *49* (39), 4148–4150.

(11) Patil, R.; Gangalum, P. R.; Wagner, S.; Portilla-Arias, J.; Ding, H.; Rekechenetskiy, A.; Konda, B.; Inoue, S.; Black, K. L.; Ljubimova, J. Y.; Holler, E. Curcumin Targeted, Polymalic Acid-Based MRI Contrast Agent for the Detection of Aβ Plaques in Alzheimer's Disease. *Macromol Biosci* **2015**, *15* (9), 1212–1217.

(12) Wahsner, J.; Gale, E. M.; Rodríguez-Rodríguez, A.; Caravan, P. Chemistry of MRI Contrast Agents: Current Challenges and New Frontiers. *Chem. Rev.* **2019**, *119* (2), 957–1057.
(13) Pazos, E.; Goličnik, M.; Mascareñas, J. L.; Vázquez, M. E. Detection of Phosphorylation States by Intermolecular Sensitization of Lanthanide–Peptide Conjugates. *Chem. Commun.* **2012**, *48* (76), 9534–9536.
(14) Choi, G.; Kim, H.-K.; Baek, A. R.; Kim, S.; Kim, M. J.; Kim, M.; Cho, A. E.; Lee, G.-H.; Jung, H.; Yang, J.; Lee, T.; Chang, Y. Multifunctional Imaging of Amyloid-Beta Peptides with a New Gadolinium-Based Contrast Agent in Alzheimer's Disease. *J Ind Eng Chem* **2020**, *83*, 214–223.
(15) Shen, Y.; Goerner, F. L.; Snyder, C.; Morelli, J. N.; Hao, D.; Hu, D.; Li, X.; Runge, V. M. T_1 Relaxivities of Gadolinium-Based Magnetic Resonance Contrast Agents in Human Whole Blood at 1.5, 3, and 7 T. *Invest Radiol* **2015**, *50* (5), 330–338.
(16) Hudson, S. A.; Ecroyd, H.; Kee, T. W.; Carver, J. A. The Thioflavin T Fluorescence Assay for Amyloid Fibril Detection Can Be Biased by the Presence of Exogenous Compounds. *FEBS J* **2009**, *276* (20), 5960–5972.
(17) Frieg, B.; Gremer, L.; Heise, H.; Willbold, D.; Gohlke, H. Binding Modes of Thioflavin T and Congo Red to the Fibril Structure of Amyloid-β(1–42). *Chem. Commun.* **2020**, *56* (55), 7589–7592.
(18) Xiao, Y.; Matsuda, I.; Inoue, M.; Sasahara, T.; Hoshi, M.; Ishii, Y. NMR-Based Site-Resolved Profiling of β-Amyloid Misfolding Reveals Structural Transitions from Pathologically Relevant Spherical Oligomer to Fibril. *J. Biol. Chem.* **2020**, *295* (2), 458–467.
(19) Thapa, A.; Jett, S. D.; Chi, E. Y. Curcumin Attenuates Amyloid-β Aggregate Toxicity and Modulates Amyloid-β Aggregation Pathway. *ACS Chem. Neurosci.* **2016**, *7* (1), 56–68.
(20) Kochi, A.; Lee, H.; Vithanarachchi, S.; Padmini, V.; Allen, M.; Lim, M. Inhibitory Activity of Curcumin Derivatives Towards Metal-Free and Metal-Induced Amyloid-β Aggregation. *Curr Alzheimer Res* **2015**, *12* (5), 415–423.
(21) Lauffer, R. B. Paramagnetic Metal Complexes as Water Proton Relaxation Agents for NMR Imaging: Theory and Design. *Chem. Rev.* **1987**, *87* (5), 901–927.
(22) Majdoub, S.; Garda, Z.; Oliveira, A. C.; Relich, I.; Pallier, A.; Lacerda, S.; Hureau, C.; Geraldes, C. F. G. C.; Morfin, J.-F.; Tóth, É. Concentration-Dependent Interactions of Amphiphilic PiB Derivative Metal Complexes with Amyloid Peptides Aβ and Amylin**. *Chemistry – A European Journal* **2021**, *27* (6), 2009–2020.
(23) Mosmann, T. Rapid Colorimetric Assay for Cellular Growth and Survival: Application to Proliferation and Cytotoxicity Assays. *J Immunol Methods* **1983**, *65* (1), 55–63.

^{1}H-NMR Profile of tri-tert-butyl 2,2',2''-(10-(3-aminopropyl)-1,4,7,10-tetraazacyclododecane-1,4,7-triyl)triacetate

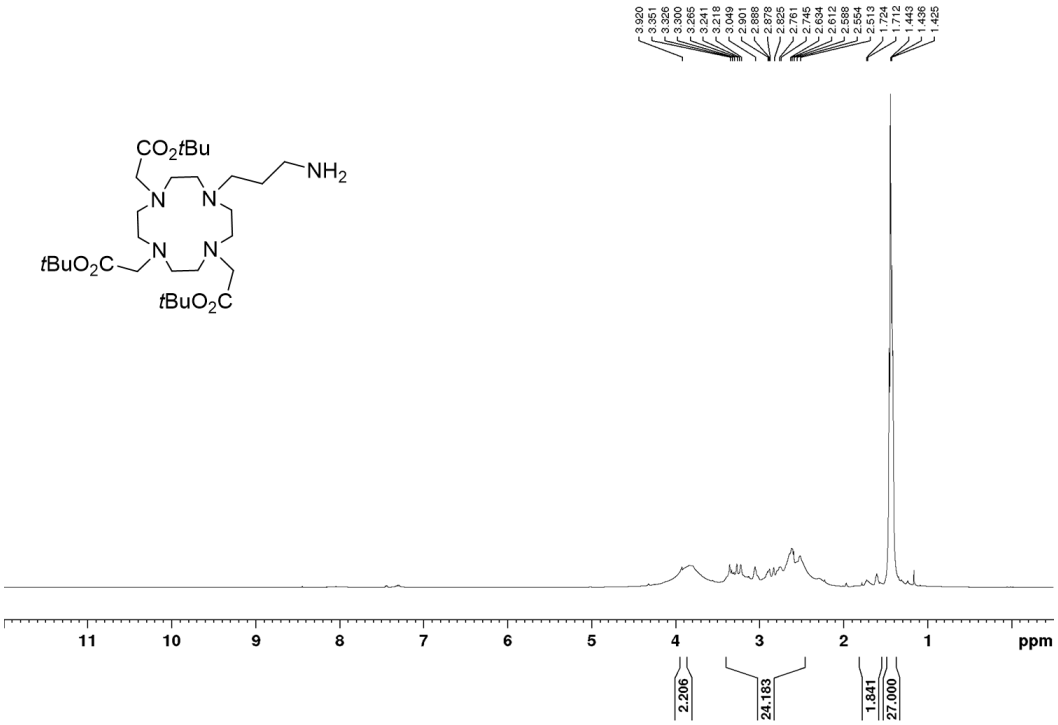

^{13}C-NMR Profile of tri-tert-butyl 2,2',2''-(10-(3-aminopropyl)-1,4,7,10-tetraazacyclododecane-1,4,7-triyl)triacetate

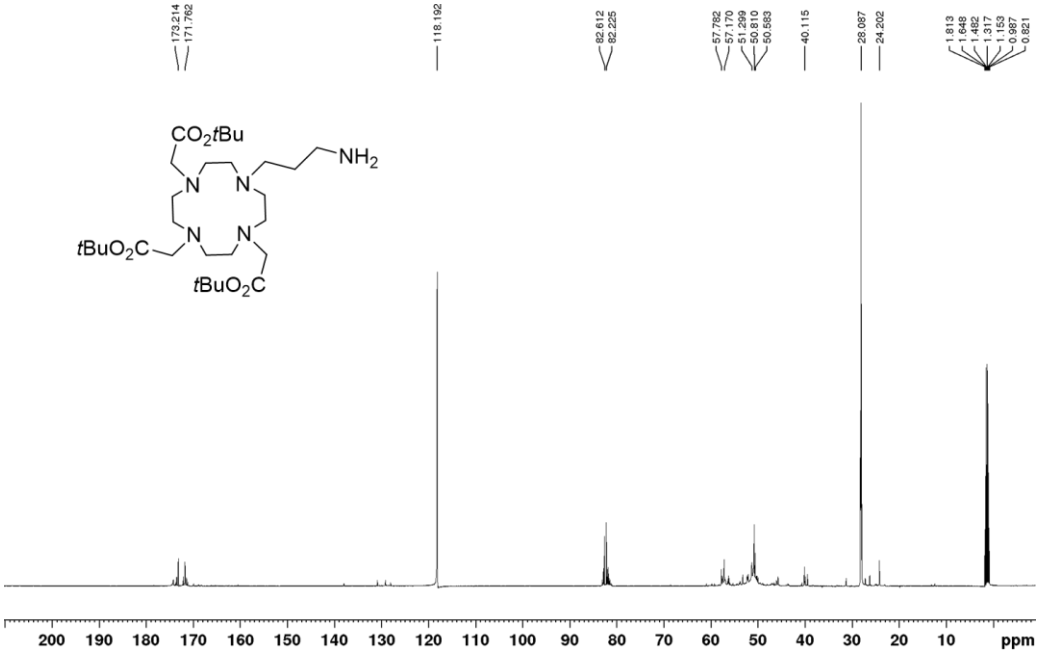

^{1}H-NMR Profile of tert-butyl 2-(4-formyl-2-methoxyphenoxy)acetate

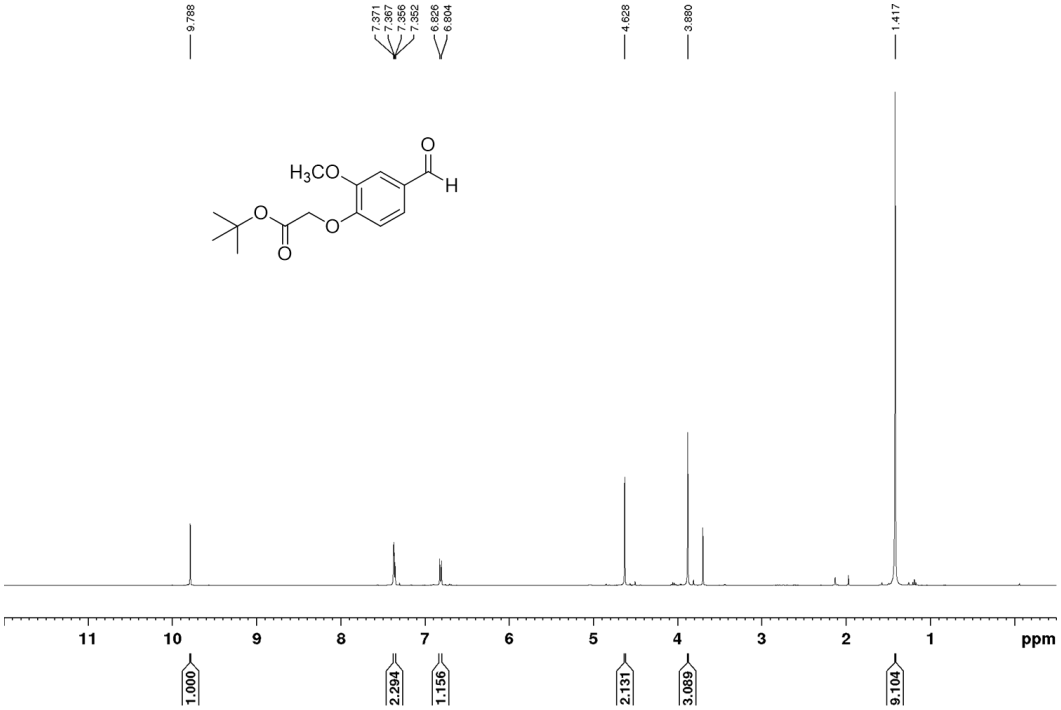

^{13}C-NMR Profile of tert-butyl 2-(4-formyl-2-methoxyphenoxy)acetate

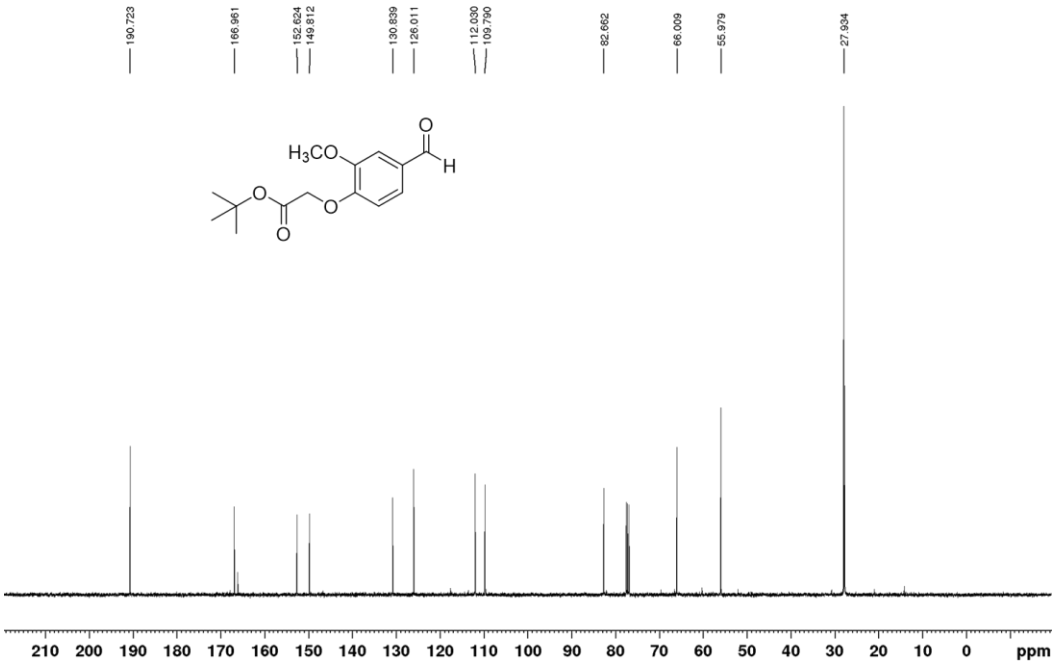

[1]H-NMR Profile of tert-butyl 2-(4-((1E,6E)-7-(4-hydroxy-3-methoxyphenyl)-3,5-dioxohepta-1,6-dien-1-yl)-2-methoxyphenoxy)acetate

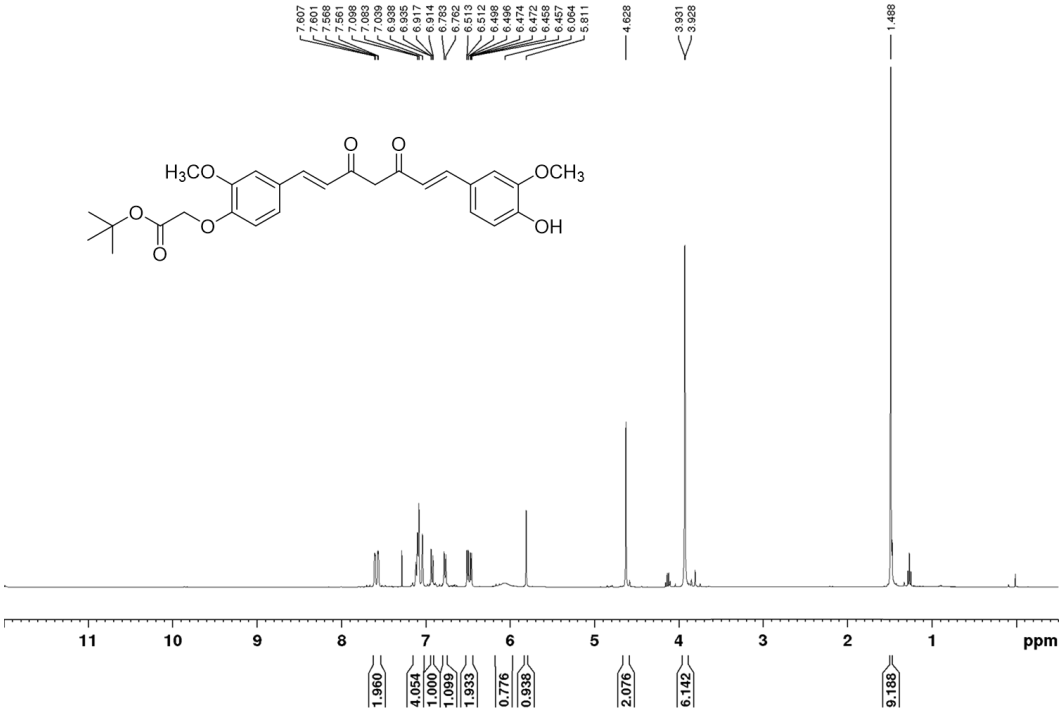

[13]C-NMR Profile of tert-butyl 2-(4-((1E,6E)-7-(4-hydroxy-3-methoxyphenyl)-3,5-dioxohepta-1,6-dien-1-yl)-2-methoxyphenoxy)acetate

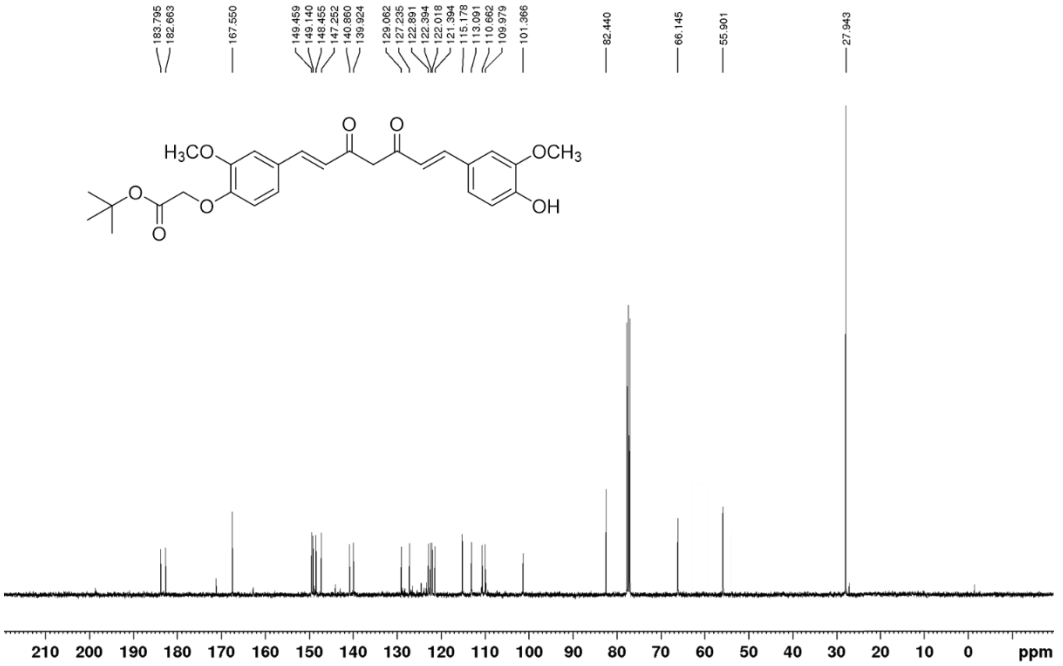

[1]H-NMR Profile of 2-(4-((1E,6E)-7-(4-hydroxy-3-methoxyphenyl)-3,5-dioxohepta-1,6-dien-1-yl)-2-methoxyphenoxy)acetic acid

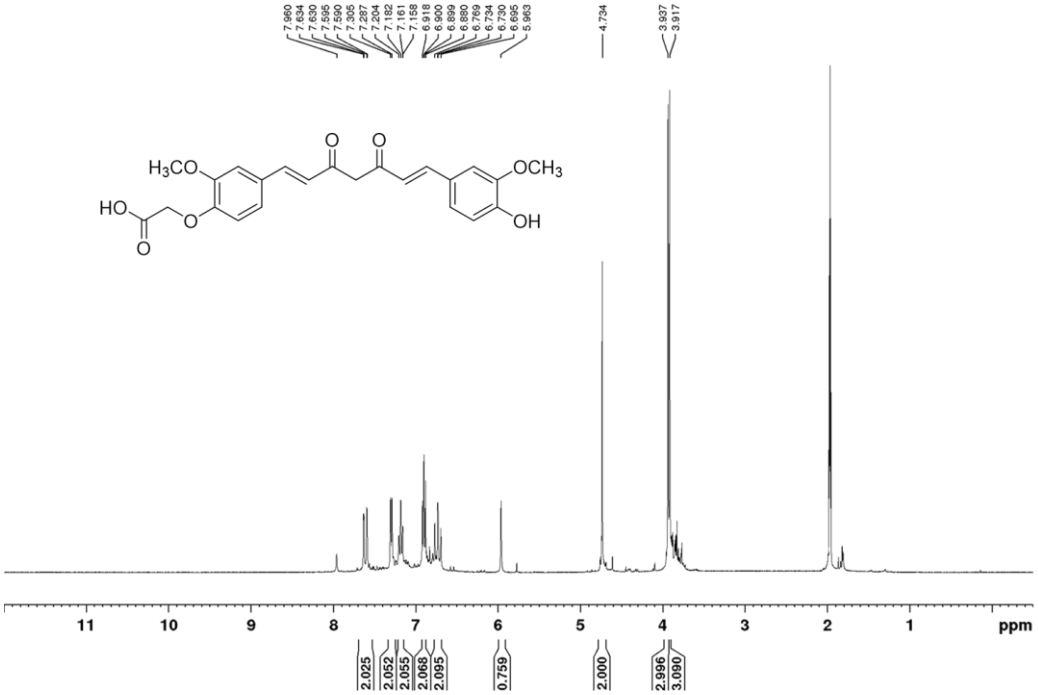

[13]C-NMR Profile of 2-(4-((1E,6E)-7-(4-hydroxy-3-methoxyphenyl)-3,5-dioxohepta-1,6-dien-1-yl)-2-methoxyphenoxy)acetic acid

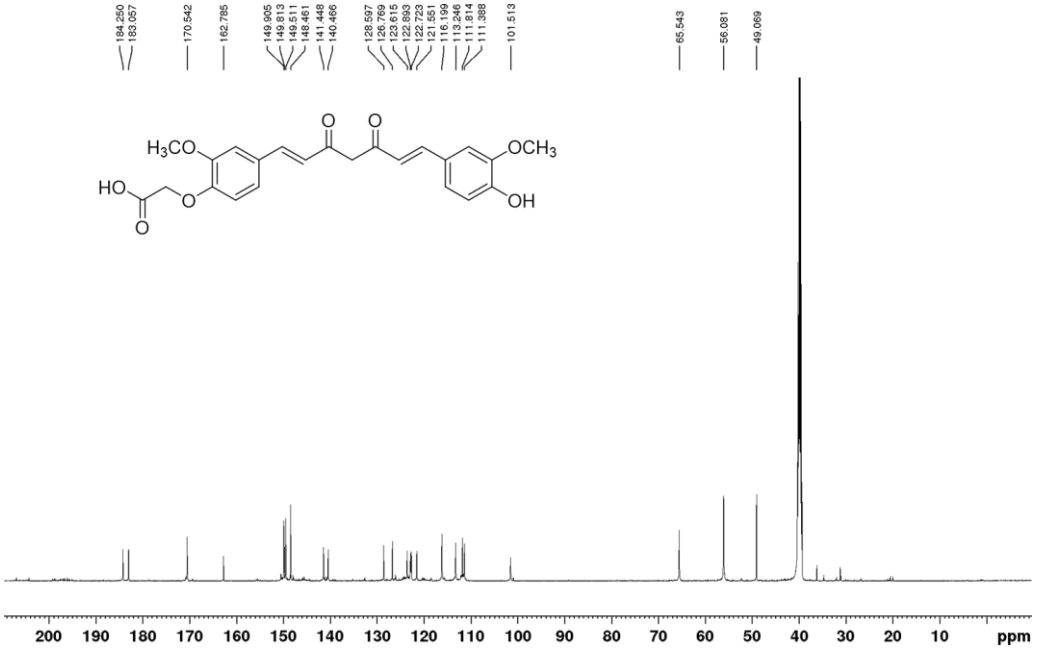

[1]H-NMR Profile of tri-tert-butyl 2,2',2''-(10-(3-(2-(4-((1E,6E)-7-(4-hydroxy-3-methoxyphenyl)-3,5-dioxohepta-1,6-dien-1-yl)-2-methoxyphenoxy)acetamido)propyl)-1,4,7,10-tetraazacyclododecane-1,4,7-triyl)triacetate

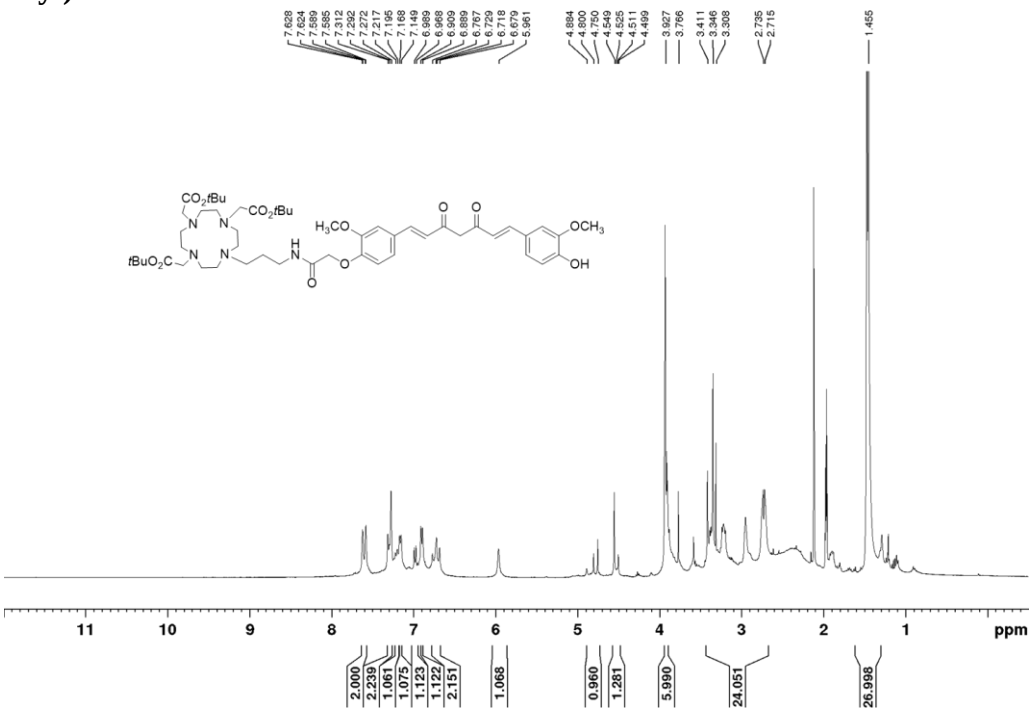

[13]C-NMR Profile of tri-tert-butyl 2,2',2''-(10-(3-(2-(4-((1E,6E)-7-(4-hydroxy-3-methoxyphenyl)-3,5-dioxohepta-1,6-dien-1-yl)-2-methoxyphenoxy)acetamido)propyl)-1,4,7,10-tetraazacyclododecane-1,4,7-triyl)triacetate

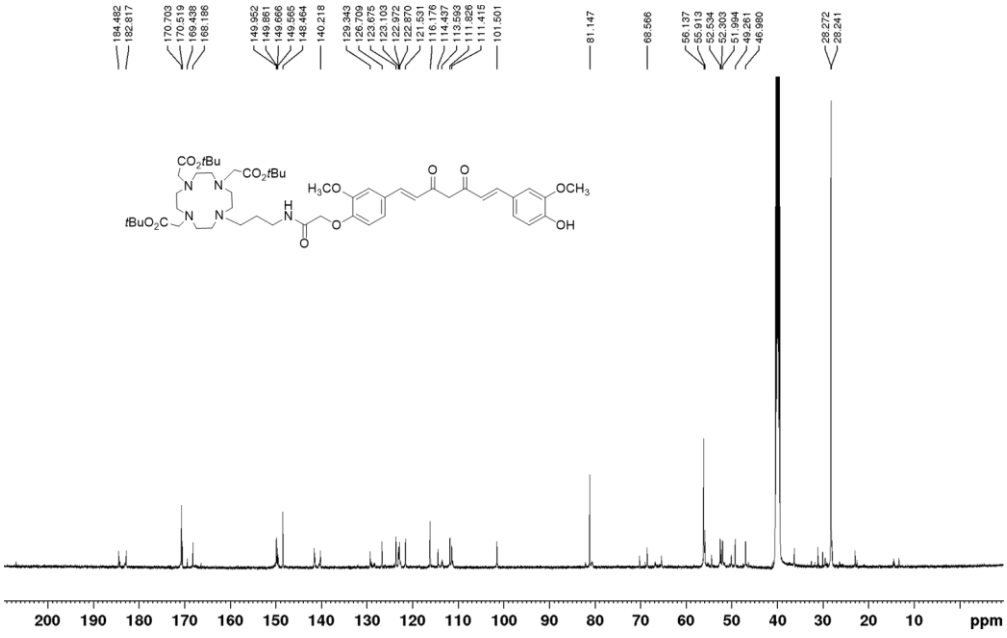

^{1}H-NMR Profile of tri-tert-butyl 2,2',2''-(10-(3-(2-(4-((1E,6E)-7-(4-hydroxy-3-methoxyphenyl)-3,5-dioxohepta-1,6-dien-1-yl)-2-(trifluoromethyl)phenoxy)acetamido)propyl)-1,4,7,10-tetraazacyclododecane-1,4,7-triyl)triacetate

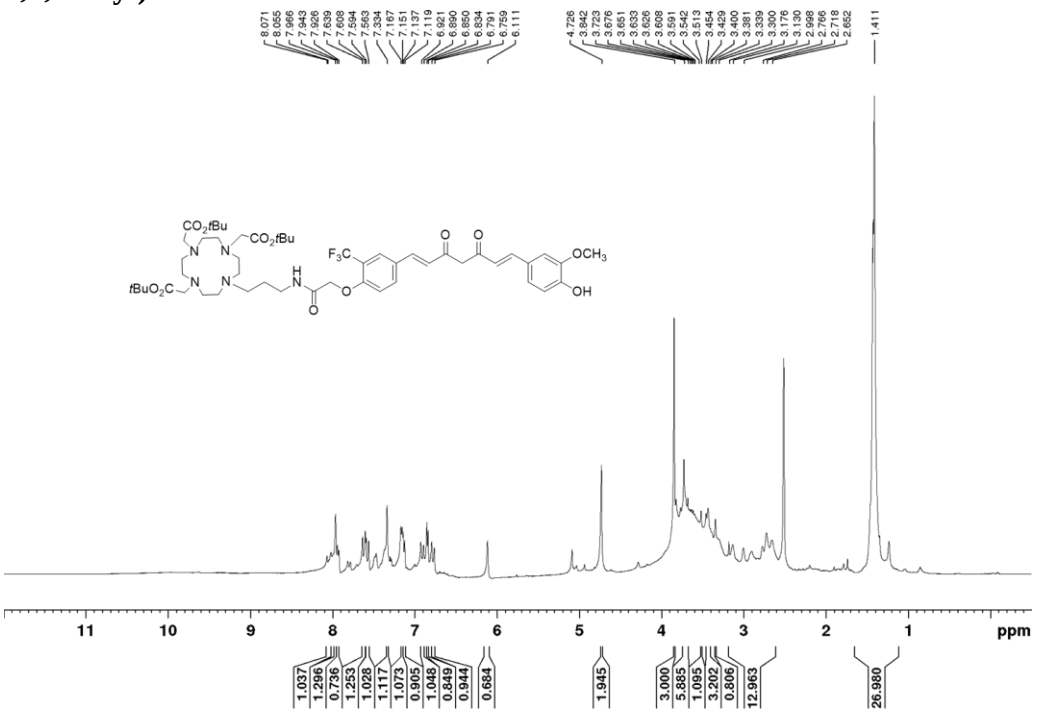

^{13}C-NMR Profile of tri-tert-butyl 2,2',2''-(10-(3-(2-(4-((1E,6E)-7-(4-hydroxy-3-methoxyphenyl)-3,5-dioxohepta-1,6-dien-1-yl)-2-(trifluoromethyl)phenoxy)acetamido)propyl)-1,4,7,10-tetraazacyclododecane-1,4,7-triyl)triacetate

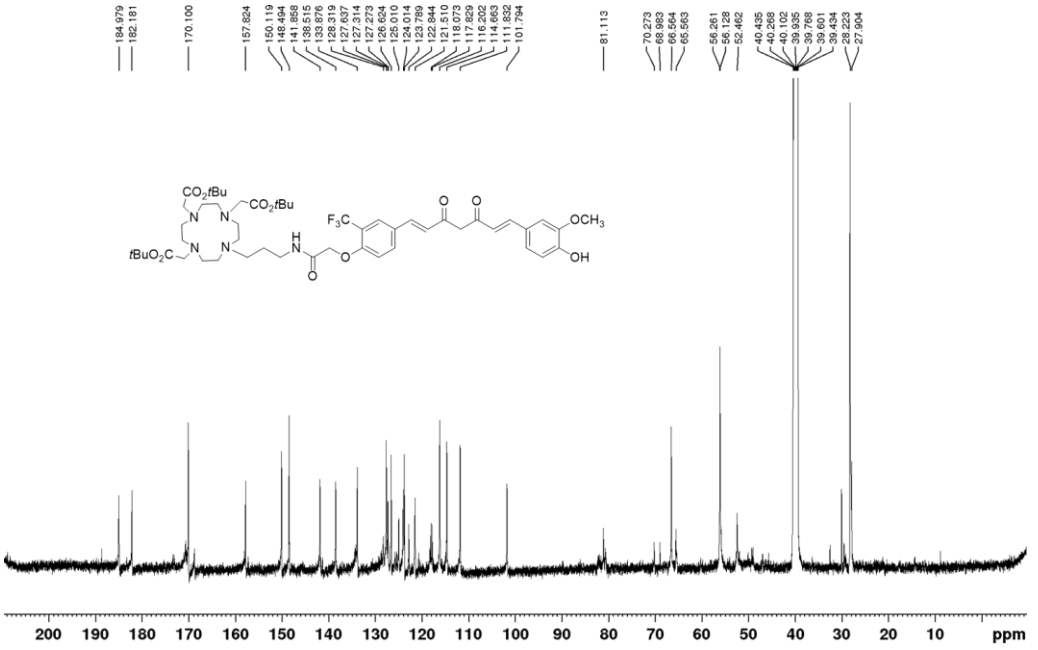

^{19}F-NMR Profile of tri-tert-butyl 2,2',2''-(10-(3-(2-(4-((1E,6E)-7-(4-hydroxy-3-methoxyphenyl)-3,5-dioxohepta-1,6-dien-1-yl)-2-(trifluoromethyl)phenoxy)acetamido)propyl)-1,4,7,10-tetraazacyclododecane-1,4,7-triyl)triacetate

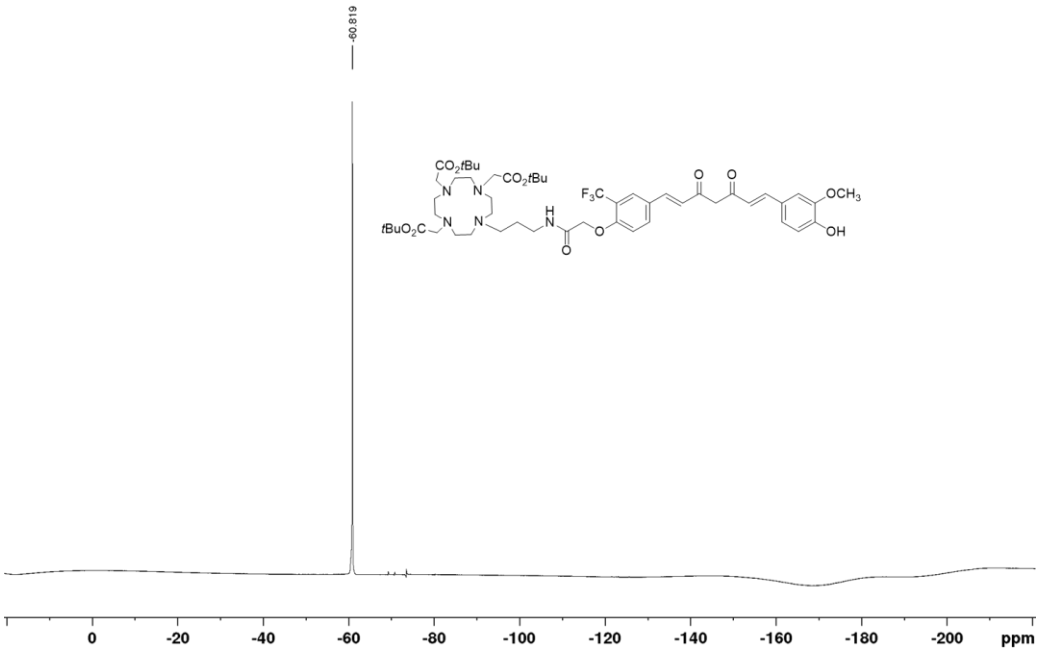

^{1}H-NMR Profile of 2,2',2''-(10-(3-(2-(4-((1E,6E)-7-(4-hydroxy-3-methoxyphenyl)-3,5-dioxohepta-1,6-dien-1-yl)-2-methoxyphenoxy)acetamido)propyl)-1,4,7,10-tetraazacyclododecane-1,4,7-triyl)triacetic acid

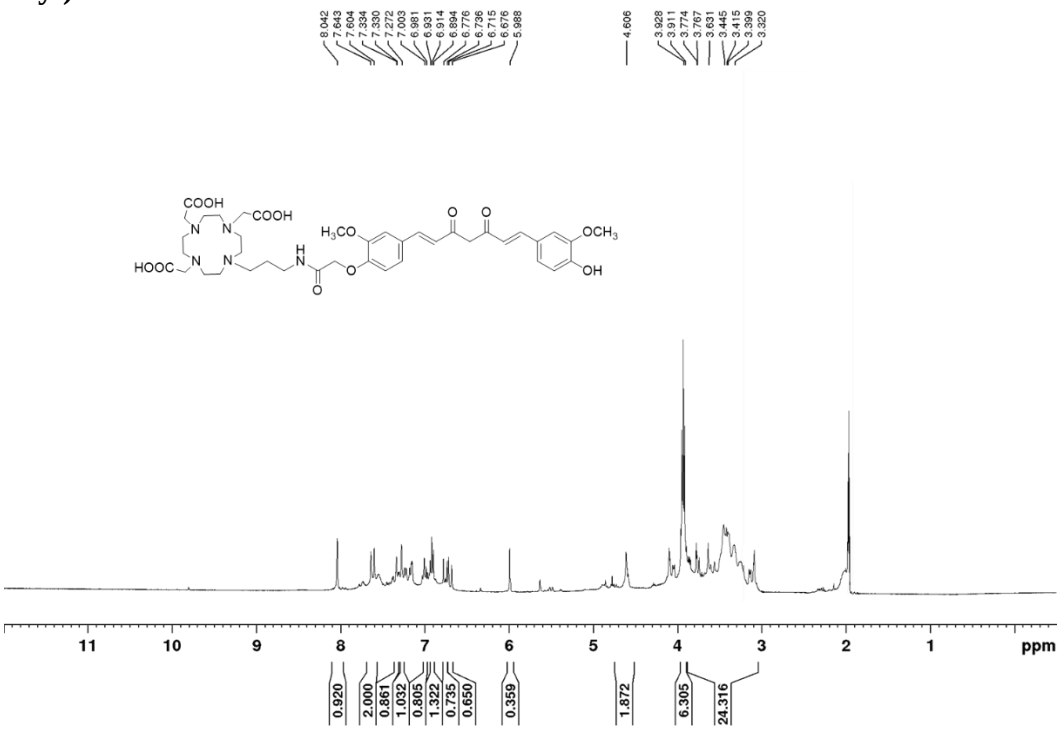

^{1}H-NMR Profile of 2,2',2''-(10-(3-(2-(4-((1E,6E)-7-(4-hydroxy-3-methoxyphenyl)-3,5-dioxohepta-1,6-dien-1-yl)-2-(trifluoromethyl)phenoxy)acetamido)propyl)-1,4,7,10-tetraazacyclododecane-1,4,7-triyl)triacetic acid

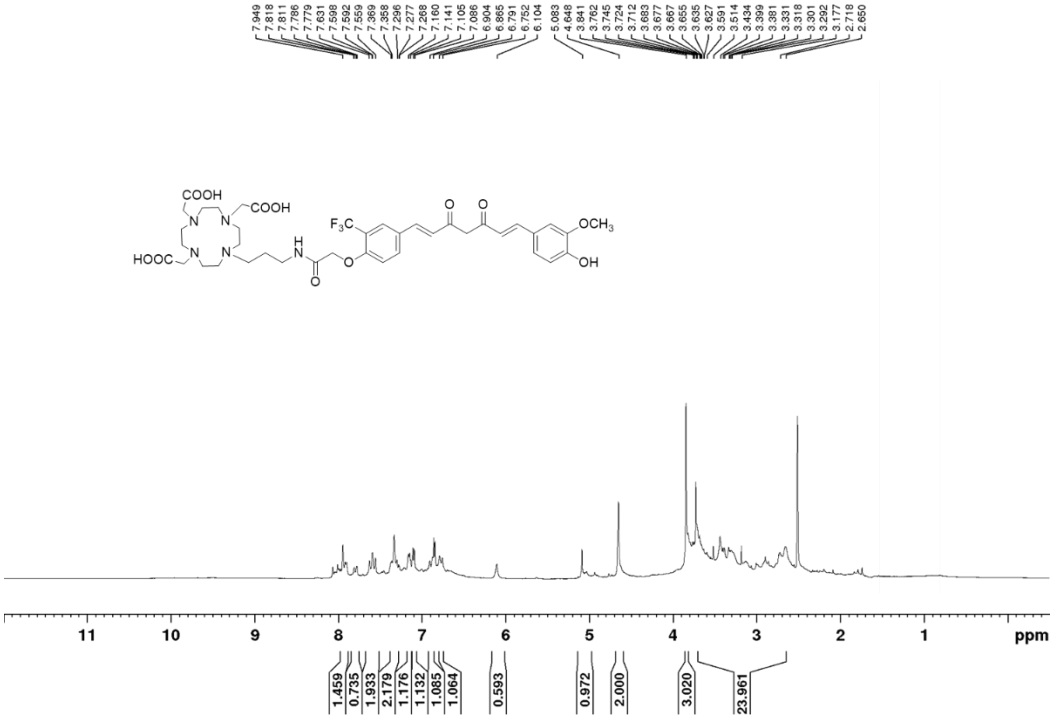

^{19}F-NMR Profile of 2,2',2''-(10-(3-(2-(4-((1E,6E)-7-(4-hydroxy-3-methoxyphenyl)-3,5-dioxohepta-1,6-dien-1-yl)-2-(trifluoromethyl)phenoxy)acetamido)propyl)-1,4,7,10-tetraazacyclododecane-1,4,7-triyl)triacetic acid

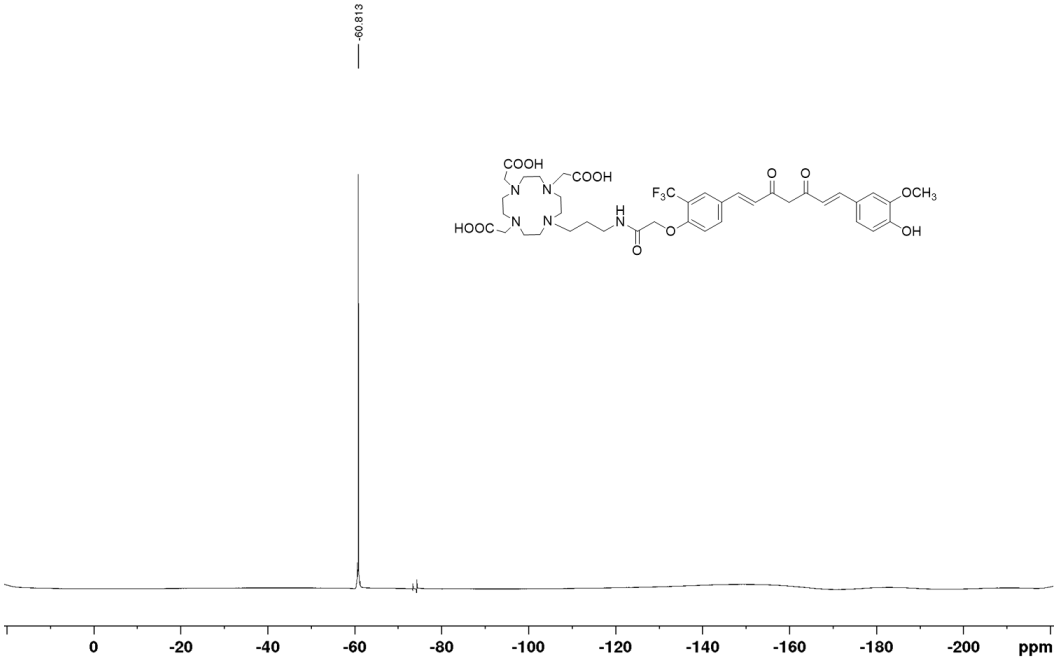

Purity Analysis of Gd-DO3A-Comp.B

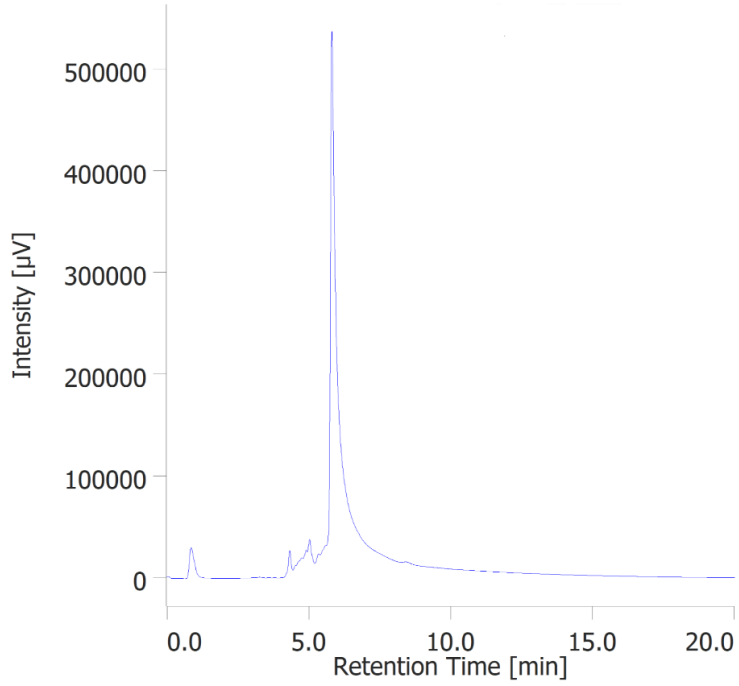

Purity Analysis of Gd-DO3A-Cur

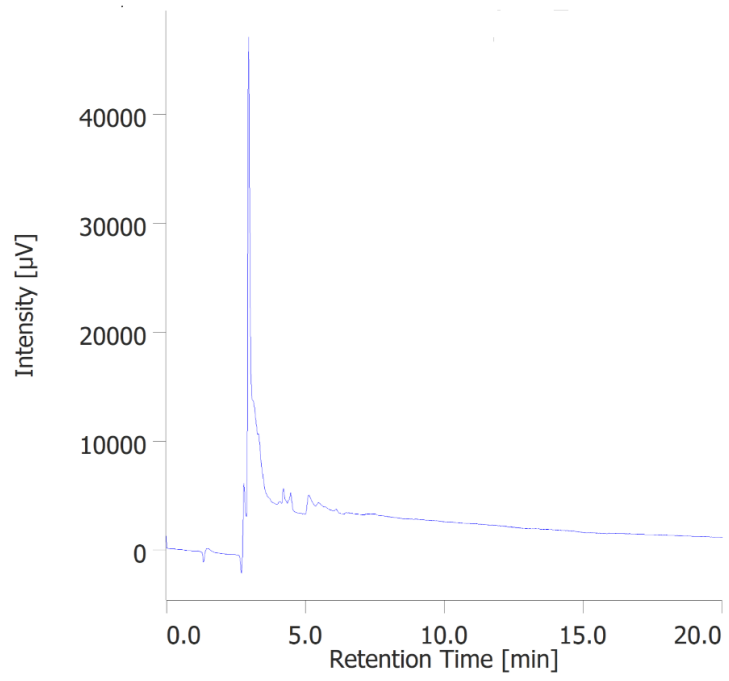

Chapter 4
Detoxification by Curcumin Derivative via Dissociation of Amyloid β Fibrils and its Verification in Drosophila Alzheimer's Model

Chapter 4. Detoxification by Curcumin Derivative via Dissociation of Amyloid β Fibrils and its Verification in *Drosophila* Alzheimer's Model

4.1. Introduction

The promising clinical results of Aducanumab highlight two important points: aggregated Aβ, such as fibrils or plaques, is a major pathological target for the treatment of AD, and its removal is expected to improve cognitive function clinically.[1,2] However, due to their enormous size, antibodies have limited permeability of the blood-brain barrier (BBB), which may affect their effectiveness.[3] Compared to antibodies such as aducanumab, small molecule drugs are considered to be more economical and thus suitable the for long-time treatment of AD (see in Chapter 1.2).

Small molecule compounds may exhibit the related effects by inducing the disaggregation of Aβ fibrils. The typical compounds can bind to Aβ fibrils and break them down into very low-toxic aggregates.[4] Curcumin has been reported to possess an amyloid disaggregation activity by reducing the amount of pre-existing plaques *in vivo*, in addition to its ability to inhibit the Aβ aggregation.[5] In clinical trials, formulated curcumins (Longvida and Theracurmin) improved cognitive behaviour and reduced amyloid deposition in non-demented adults over 60 years old, despite gastrointestinal side effects (see in Chapter 1.4).[6,7] Based on the previous studies, the structure of curcumin has great potential as a compound that can induce disaggregation of amyloid fibrils and improve physiological conditions.

Drosophila is widely used as a simple *in vivo* model for the molecular pathogenesis of AD.[8,9] Among the various *Drosophila* models, flies that express Aβ are the most commonly utilized as AD models. Although there are no peptides homologous to Aβ in *Drosophila*, the human Aβ-expressing fly has been shown to have reduced learning function, accumulation of amyloid plaques, neurodegeneration, and shortened lifespan, as observed in patients with AD.[10–12] Although the main feature of AD is a cognitive dysfunction, patients sometimes show symptoms from motor deterioration to behavioral alterations.[13,14] Decreased

motor performance has also been demonstrated in the Aβ-expressing fly models, and the severity of cognitive impairment is closely correlated with the level of motor dysfunction.[10] Therefore, *Drosophila* enables low-cost drug screening by feeding and thus an effective option in the drug discovery process.[15]

Previously, the SARM study discovered an asymmetrical curcumin derivative, compound **B**, which possesses an IC_{50} value 100 times lower than curcumin (see in Chapter 2.2). Compound **B** inhibited the Aβ aggregation and attenuated the Aβ-stimulated cytotoxicity in neuroblastoma cells. Since compound **B** has a similar structural backbone to curcumin, it is suspected that it could strongly inhibit Aβ aggregation and induce disaggregation of amyloid fibrils. This study also developed a novel curcumin derivative, compound **N**, in which the methoxy ester in compound **B** was replaced by benzylamide to improve its bioavailability and evaluated whether compounds **B** and **N** could rescue the Aβ fibril-induced toxicity in neuroblastoma cells and *Drosophila* AD models (Figure 4-1).

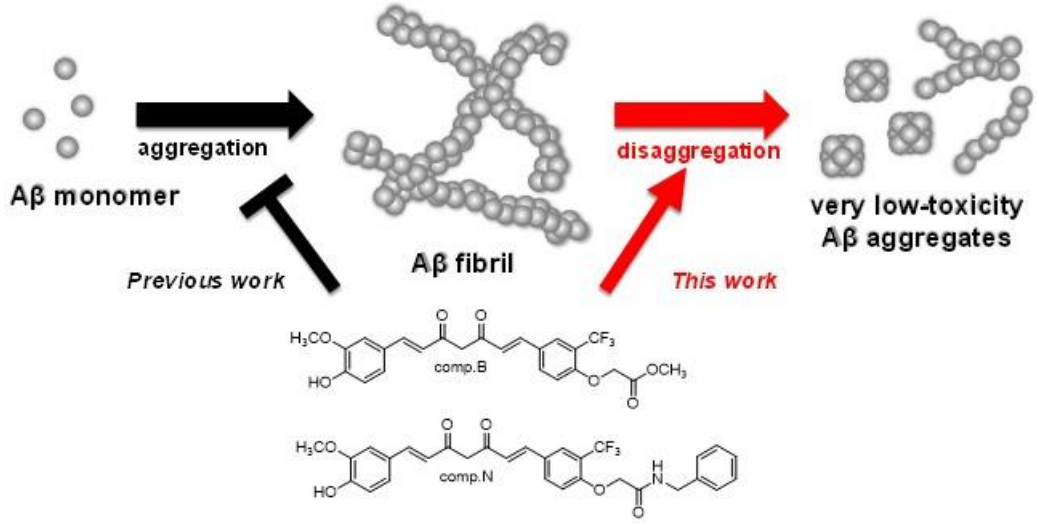

Figure 4-1. Design of compounds **B** and **N**, and their application to Aβ disaggregation.

4.2. Results and Discussion

4.2.1. Synthesis of Curcumin Derivative

Compound **N** was synthesized as described in Scheme 4-1. Methyl bromoacetate was introduced at the hydroxyl group of aldehyde **1** to give compound **2**. The methoxy group of **2** was deprotected under basic conditions, and the resulting carboxylic acid **3** was treated with benzylamine to produce compound **4**. The

Knoevenagel condensation reaction of compound **4** with α,β-unsaturated diketone **5** under microwave irradiated conditions afforded compound **N**.

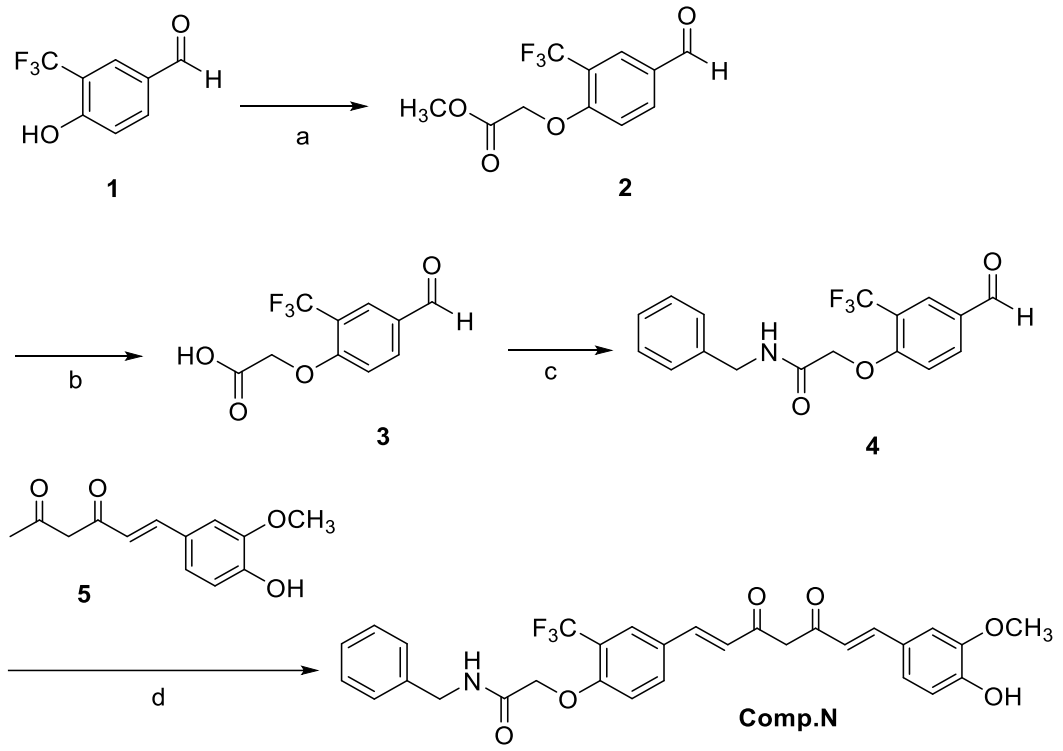

Scheme 4-1. Synthesis of compound **N**. Reaction condition: (a) acetone, methyl bromoacetate, K_2CO_3, 80 °C, 94%; (b) NaOH 1 M, 100 °C, 41%; (c) benzylamine, DMF, HOBt, DCC, DMAP, RT 24 h, 58%; (d) DMF, $B(OH)_3$, morpholine, MW 150 °C, 15 min, 47%.

4.2.2. Evaluation of *In Vitro* Amyloid Disaggregation

Previous inhibitory screening of curcumin and compound **B** toward Aβ aggregation using ThT assay demonstrated IC_{50} values of 0.693 ± 0.013 and 0.007 ± 0.001 μM, respectively (see in Chapter 2.2.3). Using the same method, compound **N** performed IC_{50} of 0.015 ± 0.023 μM, indicating that the benzylamide modification also retains a considerable inhibitory activity. Before evaluating the amyloid disaggregation effect, the complete formation of Aβ fibrils was monitored by ThT assay. After 6 h incubation in PBS, the fluorescence reached a plateau, and a sigmoidal curve was observed as a profile of Aβ aggregation, and Aβ fibrils were completely formed after 24 h incubation (Figure 4-2A).

To confirm disaggregation activities of the compounds, Congo Red (CR) assay was used using Aβ fibrils formed by 24 h incubation instead of ThT assay,[16] because compounds **B** and **N** quenched the fluorescence of ThT but not CR (Figure 4-2B and 4-2C). The compounds **B** and **N** were added into Aβ fibrils with CR and incubated for 2 h. The lowest fluorescence was observed in the presence of compounds **B** and **N**, followed by curcumin (Figure 4-2B). These results demonstrated that compounds **B** and **N** destructed Aβ fibrils more effectively than curcumin. To obtain direct proof of fibril deconstruction, the morphological changes of Aβ fibrils were observed by negative stain transmission electron microscopy (TEM). The abundant long rods, which are the typical morphology of Aβ fibrils, were observed in Aβ incubated for 24 h (Figure 4-2C).[17] In contrast, the addition of compounds **B** and **N** at the same concentration as the CR assay disaggregate the Aβ fibrils into smaller aggregated species. Compound **B** broke up the fibrils to a shortened form while the compound **N** disrupted the fibrils to oligomer-like granular species (Figure 4-2C), indicating the different role of methyl ester on compound **B** and benzylamide moiety on compound **N**. In contrast, a moderate effect was found in the treatment with curcumin. While the previously reported compounds act on amyloid disaggregation at 5−10 μM, compounds **B** and **N** acted at only 1 μM.[18–20]

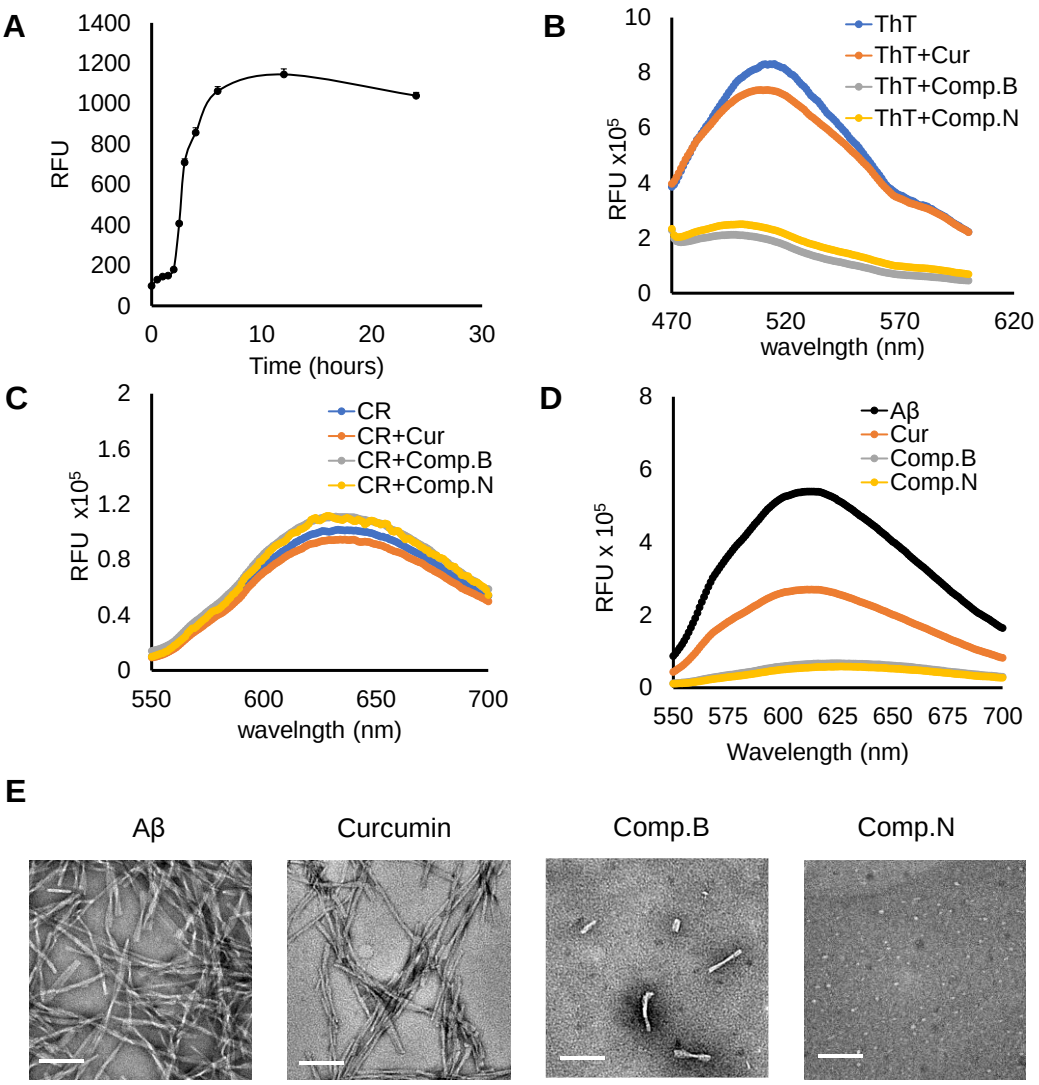

Figure 4-2. (A) Aggregation profile of Aβ monitored by ThT assay. Quenching study of in the presence of Thioflavin T (B) and Congo Red (C). (D) Amyloid disaggregation effect of curcumin derivatives measured by CR Assay. Aβ (20 μM) was incubated with CR (20 μM) in PBS (pH 7.4) at 37 °C for 24 h before adding curcumin derivatives (1 μM) and incubating for further 2 h. (E) Negative staining TEM images showed morphological changes of Aβ in the absence or presence of curcumin derivatives. Scale bars are 100 nm.

4.2.3. Detoxification effect in cells

In addition to the amyloid disaggregation effect, it is also important to evaluate the toxicity of smaller aggregated species produced by disaggregation, as protofibrils and oligomers contribute to neurotoxicity.[21] Therefore, the cytotoxicity of Aβ monomers and fibrils with or without curcumin derivatives were evaluated

on N2a mouse neuroblastoma cells. Incubation of 20 μM monomeric Aβ with N2a cells decreased the cell viability up to 30%. This was restored to 60-70% by adding 1 μM of curcumin and compounds **B** and **N** (Figure 4-3A). The co-incubation of Aβ fibril with compounds **B** and **N** attenuated the toxicity of Aβ fibril and increased the cell viability up to 60−70% (Figure 4-3B). In contrast, curcumin did not increase the cell viability, indicating that curcumin is less effective on fibril than monomers. In fact, curcumin required higher concentration to reduce the fibril cytotoxicity, according to previous studies.[22]

The effect of curcumin derivatives on intracellular amyloid disaggregation was further evaluated by visualizing the Aβ fibrils in N2a cells using a confocal laser scanning microscopy. N2a cells were incubated with 1 μM curcumin derivatives in the presence of 20 μM Aβ fibril. The presence of Aβ fibril was detected by an anti-Aβ fibril antibody conjugated with ATTO594 fluorescence dye. After 24 h treatment of the curcumin derivatives, Aβ fibrils were localized in the cytoplasm and slightly surrounding the nucleus, as reported (Figure 4-3C).[18,23] Aβ fibrils also disrupted actin and reduced the fluorescent signals corresponding to actin.[24] The curcumin treatment resulted in the actin disruption and a slight decrease of the Aβ fibrils, whereas compounds **B** and **N** completely eliminated the intracellular Aβ fibrils. Interestingly, only compound **N** could restore the actin cytoskeleton in N2a cells. The ability of curcumin derivatives to retain the actin cytoskeleton is supported by the results obtained from the TEM measurements (Figure 4-2E). Compound **N** produced small spherical aggregates as a product of the amyloid disaggregation effect, while curcumin and compound **B** still produced short Aβ fibrils, which could affect the actin cytoskeleton, as previously reported.[25] These results demonstrate that compound **N** retains the actin cytoskeleton by suppressing Aβ fibrils.

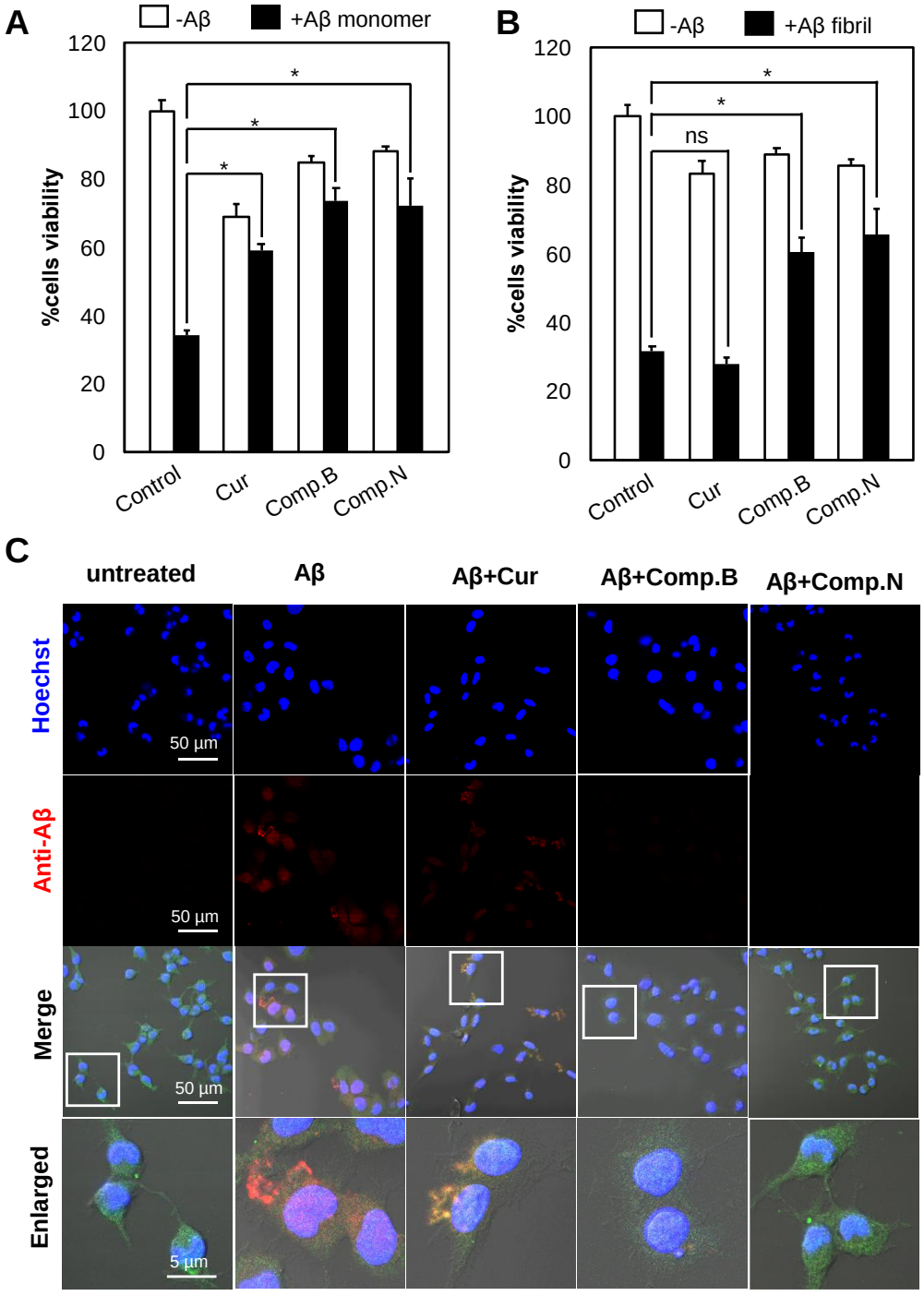

Figure 4-3. The effect of curcumin derivatives on attenuating the toxicity of Aβ and amyloid disaggregation. N2a cells were treated with monomeric Aβ (A) or pre-formed fibril (B) at a concentration of 20 μM in the absence or presence of curcumin derivatives (1 μM) for 24 h incubation. Data were expressed in mean ± SEM from three independent experiments. *P <0.01 by two-sided Student's t-test, ns = not significant. (C) Immunofluorescence microscopy analysis of N2a cells exposed to the Aβ fibril (10 μM) in the absence or presence of curcumin derivatives (1 μM). After 24 h incubation, these cells were fixed and stained then visualized under confocal microscope (original magnification x400). (Red): mAb amyloid fibril OC, (*Blue*): Hoechst staining, (*Green*): Actin.

4.2.4. Evaluation of Brain Accumulation and Detoxification Effect in Animal

One of the important requirements for the AD drug candidates is their ability to be distributed in the brain through the BBB. This study evaluated brain penetration ability by intravenously injecting curcumin or compound **N** in healthy mice at 1 mM using a reported protocol.[26] All protocols for *in vivo* mice study were approved by the Institutional Animal Care and Use Committee of Tokyo Institute of Technology. The biodistribution was evaluated by the intrinsic fluorescence profile of each compound measured by the IVIS imaging system. The results confirmed the wide distribution of curcumin, such as in the liver, lung, and kidney, besides its distribution in the brain as previously reported.[27,28] Interestingly, compound **N** showed a more selective distribution, mainly in the brain, and was only slightly detected in the liver, a non-target organ (Figure 4-4). The distribution of compound **N** in the liver was higher than that in other organs, consistent with the extensive biotransformation profile of curcumin derivatives.[29]

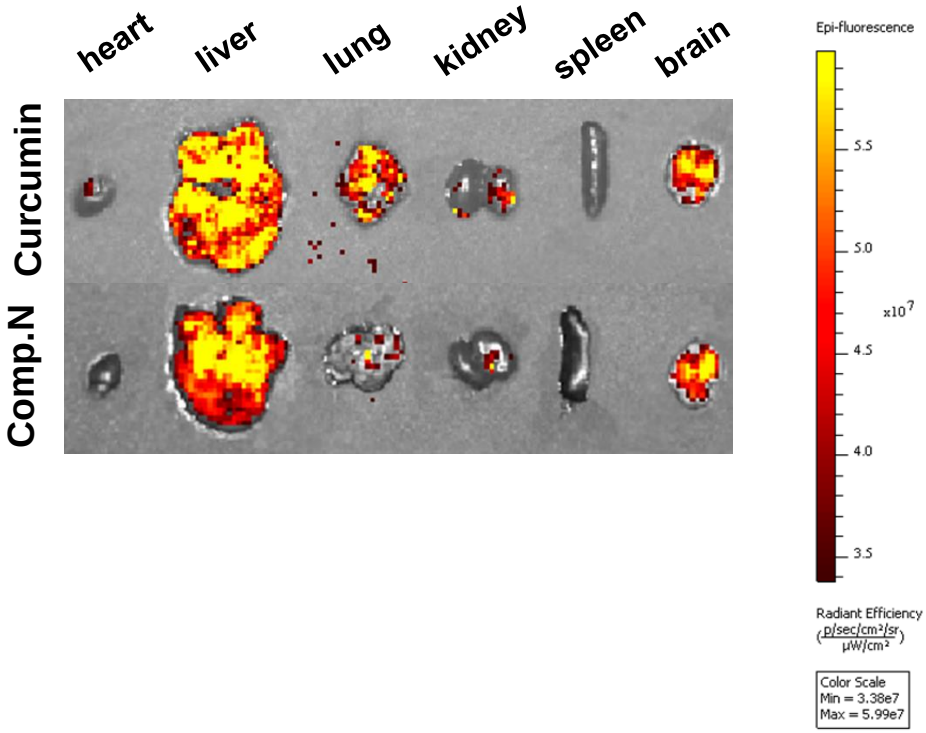

Figure 4-4. *Ex vivo* fluorescence images of the heart, liver, lung, kidney, spleen, and brain of mice after 1 h injection. Three mice were used for each imaging experiment.

To evaluate the effect of curcumin derivatives **B** and **N** against the toxicity of amyloid β *in vivo,* this study used Aβ expression *Drosophila* model. The *Drosophila* that expressed Aβ in all neurons from developmental stages was supplied with curcumin and compounds **B** and **N** in the food. After one day or two weeks, the locomotor function was measured by climbing assay (Figure 4-5A). The results showed that the locomotor function of both control and Aβ-expressing flies was comparable after one day (Figure 4-5B). After two weeks, the Aβ-expressing flies showed a significant decrease in motor function (Figure 4-5C). Importantly, feeding of compounds **B** and **N** significantly rescued locomotor dysfunction in Aβ-expressing flies after two weeks (Figure 4-5C). These results suggest that the toxicity of Aβ is mitigated by feeding compounds **B** and **N**.

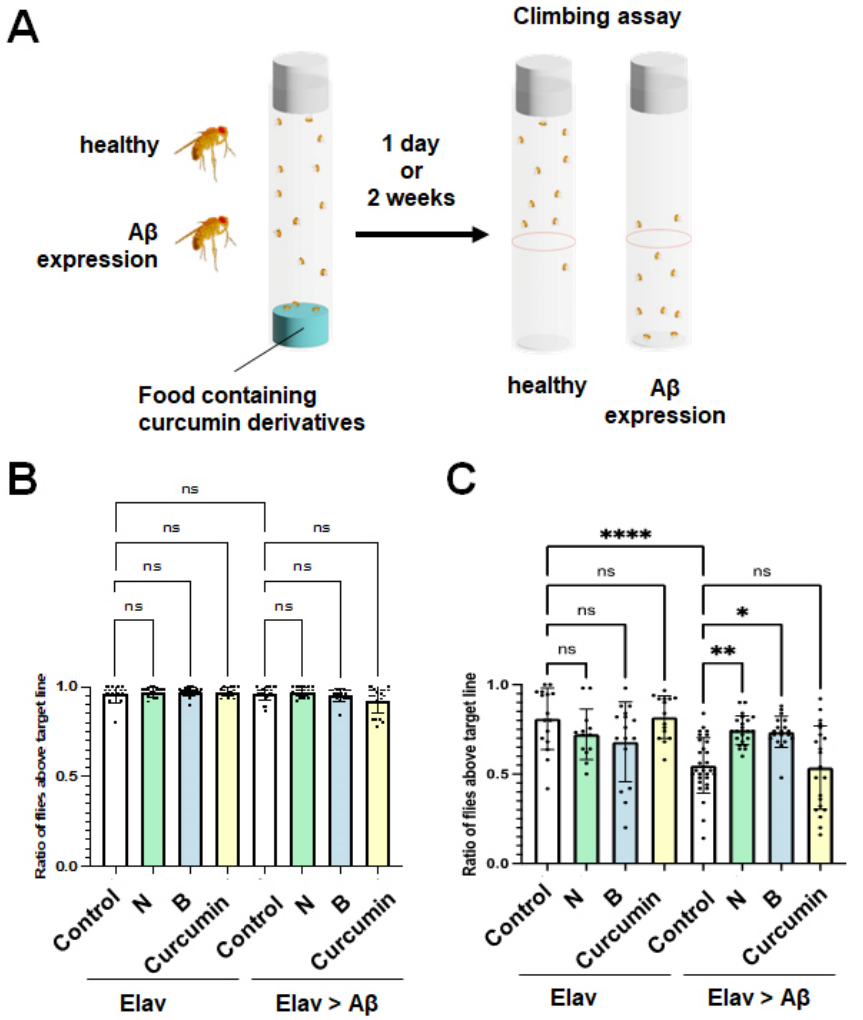

Figure 4-5. (A) Schematic diagram of feeding and climbing assays of curcumin derivatives in *Drosophila*. The quantification results of the climbing assay at one day (B) and two weeks (C) after the administration of the curcumin derivative were shown. Compound **N** was represented by green bar, compound **B** by blue bar, and curcumin by yellow bar. The control (white) contained no compound. Reduced locomotor function in *Drosophila* expressing amyloid β was attenuated by curcumin derivatives. ****$P < 0.0001$, ** < 0.01, * < 0.05 by two-sided Student's *t*-test, ns = not significant. The number of experimental samples is as follows. (B) Elav control (n = 17), Elav N (n = 15), Elav B (n = 20), Elav Curcumin (n = 14), Elav>Aβ (n = 21), Elav>Aβ N (n = 20), Elav>Aβ B (n = 18), and Elav>Aβ Curcumin (n = 19). (C) Elav control (n = 16), Elav N (n = 13), Elav B (n = 16), Elav Curcumin (n = 15), Elav>Aβ (n = 30), Elav>Aβ N (n = 23), Elav>Aβ B (n = 19), and Elav>Aβ Curcumin (n = 21). The fly genotypes were *Elav/Y; UAS-Aβ1-42#1/+; UAS-Aβ1-42#3/+* for Elav> Aβ and *Elav/Y; +/+; +/+* (control) for Elav.

4.3. Summary of Chapter 4

Curcumin derivatives **B** and **N** inhibit fibril formation and induce amyloid disaggregation at low concentrations, thus alleviating Aβ fibril-induced toxicity in neuroblastoma cells. Both compounds could also accumulate in the brain and rescue AD-model flies from Aβ toxicity.

4.4. Experimental Section

All the solvents used were in analytical standard grade. The NMR spectra were measured on a Bruker biospin AVANCE II (400 MHz for ^{1}H and 100 MHz for ^{13}C) or a Bruker biospin AVANCE III (500 MHz for ^{1}H, 125 MHz for ^{13}C, and 470 MHz for ^{19}F). Chemical shifts (δ) was reported in ppm relative to internal tetramethylsilane. The HRMS data were recorded on the Bruker ESI-TOF-MS micrOTOF II instrument with sodium formate as the calibration standard. The negative stain transmission electron microscopy (TEM) images were measured using TEM H-8100 (Hitachi) operated at 200 kV. Vanillin, potassium carbonate, morpholine, and boric acid were purchased from Wako Chemical (Japan). Acetylacetone, benzylamine, 4-dimetylaminopyridine, methyl bromoacetate, and hydroxybenzotriazole were purchased from Tokyo Chemical Industry (Japan). Microwave for synthesis was conducted on Biotage® Initiator+ instrument. Column chromatography was performed on silica gel Chromatorex (Japan). Purity analysis was determined by HPLC analysis using Inertsil ODS-3 5 μm (4.6 × 75 mm; GL Science) with a linear gradient of 0.1% formic acid in water/0.1% formic acid in MeCN detected by a UV lamp for 30 min. Amyloid β ($A\beta_{42}$) peptide was purchased from Peptide Institute (Japan). Thioflavin t and congo red for fluorescence detection of Aβ was purchased from Wako Chemical (Japan) and Sigma (USA), respectively.

General Procedure to Synthesis Compound 2

Compound **2** was synthesized as described in Chapter 2.4. 4-hydroxy 3-trifluoromethyl benzaldehyde (1 mmol) and potassium carbonate (3 mmol) were dissolved in DMF 10 mL. Methyl bromoacetate (1.1 mmol) was added then the mixture was refluxed for 2 h at 80 ^{o}C in oil bath. After filtration to remove the salt,

the organic solvent was removed then the mixture was purified by column chromatography (silica gel, hexane:ethyl acetate 2:1).

Methyl 2-(4-formyl-2-(trifluoromethyl)phenoxy)acetate (2). Yield: 94%. ^{1}H-NMR (400 MHz, $CDCl_3$): δ (ppm) 3.82 (-OCH_3, s, 3H), 4.01 (-OCH_3, s, 3H), 4.76 (-CH_2, s, 2H), 6.88 (=CH, *J*=8.8, d, 1H), 8.05 (=CH, *J*=8.4, d, 1H), 8.18 (=CH, s, 1H), 9.96 (-CHO, s, 1H). ^{13}C-NMR (125 MHz, $CDCl_3$): δ (ppm) 52.50, 65.46, 68.01, 112.86, 120.18, 121.39, 129.35, 134.95, 160.15, 167.76, 189.64. HRMS-ESI (m/z): calcd for $C_{11}H_{10}F_3O_4^+$ 263.0526; found 263.0535 $[M+H]^+$.

General Procedure to Synthesis Compound 3

Compound **3** was synthesized as described in Chapter 2.4. Compound **2** (0.26 mmol) was dissolved in 0.5 mL methanol, then 2 mL of NaOH 1 M was added. The mixture was stirred for 30 min at 100 ºC. The reaction was quenched by adding HCl 0.1 M, then was extracted using ethyl acetate. The desired compound was purified by column chromatography (silica gel, hexane:ethyl acetate 2:1).

2-(4-formyl-2-(trifluoromethyl)phenoxy)acetic acid (3). Yield: 41%. ^{1}H-NMR (400 MHz, $CDCl_3$): 7.08 (=CH, *J*=8.6, d, 1H), 8.09 (=CH, *J*=8.7, d, 1H), 8.21 (=CH, d, 1H), 9.99 (-CH, s, 1H). ^{13}C-NMR (125 MHz, $CDCl_3$): δ (ppm) 64.91, 102.02, 112.68, 122.27, 125.09, 131.19, 131.59, 156.05, 170.16. HRMS-ESI (*m/z*): calcd for $C_{10}H_6F_3O_4^-$ 247.0224; found 247.0217 $[M-H]^-$.

General Procedure to Synthesis Compound 4

Compound **3** (0.5 mmol) was dissolved in DMF. To that solution, dicyclohexylcarbodiimide (1.5 mmol), hydroxybenzotriazole (0.5 mmol), 4-dimethylaminopyridine (0.05 mmol) was added. Benzylamine (0.6 mmol) was added, followed by stirring for 24 h. The white precipitate obtained was filtered and evaporated. The desired compound was purified by column chromatography (silica gel, hexane:ethyl acetate 2:1).

***N*-benzyl-2-(4-formyl-2-(trifluoromethyl)phenoxy)acetamide (4).** Yield: 58%. ^{1}H-NMR (400 MHz, $CDCl_3$): δ (ppm) 4.67 (-CH_2, d, 2H), 4.82 (-CH_2, s, 2H), 5.41 (-NH, s, 1H), 7.12 (=CH, d, 2H), 7.24 (=CH, d, 1H), 7.31 (=CH, d, 2H), 7.45 (=CH, d, 1H), 8.20 (=CH, d, 1H), 8.26 (=CH, s, 1H), 10.01 (-CHO, s, 1H). ^{13}C-NMR (125

MHz, $CDCl_3$): δ (ppm) 43.54, 67.96, 113.49, 127.77, 128.05, 129.13, 129.35, 130.52, 135.97, 137.53, 166.35, 189.61. HRMS-ESI (*m/z*): calcd for $C_{17}H_{14}F_3O_3Na^+$ 360.0818; found 360.0814 $[M+Na]^+$.

General Procedure to Synthesis Compound 5. Compound **5** was synthesized as described in Chapter 2.4. Acetylacetone (10 mmol) and boric acid (10 mmol) were suspended in DMF. Vanillin (2 mmol) was added, followed by morpholine (2 mmol). The mixture was irradiated in the microwave at 100 ^oC for 10 min. The reaction mixture was quenched by HCl 0.1 N and extracted using ethyl acetate. The organic phase was dried using $MgSO_4$. The crude product was purified by column chromatography (silica gel, hexane:ethyl acetate 4:1) to obtain the desired compound.

(4-hydroxy-3-methoxyphenyl) hex-5-ene-2,4-dione (5). Yield: 65%. ^{1}H-NMR (400 MHz, $CDCl_3$): δ (ppm) 2.20 (-CH_3, s, 3H), 3.98 (-OCH_3, s, 3H), 5.68 (=CH, s, 1H), 5.87 (=CH, s, 1H), 6.37 (=CH, *J*=15.8, d, 1H), 6.97 (=CH, *J*=8.2, d, 1H), 7.06 (=CH, *J*=1.8 Hz, d, 1H), 7.13 (=CH, *J*=8.2, 1.8 Hz, dd, 1H), 7.58 (=CH, *J*=15.8 Hz, d, 1H). ^{13}C-NMR (125 MHz, $CDCl_3$): δ (ppm) 26.59, 55.86, 100.69, 111.39, 115.88, 119.87, 123.09, 126.55, 140.47, 148.19, 149.41, 178.48, 196.85. LRMS-ESI (*m/z*): calcd for $C_{13}H_{14}O_4$ 234.09; found 235.13 $[M+H]^+$

General Procedure to Synthesis Compound N

Compound **5** (0.26 mmol) and boric acid (0.26 mmol) were suspended in DMF. Compound **4** (0.26 mmol) was added, followed by morpholine (0.1 mmol). The mixture was irradiated by microwave at 150 ^oC for 10 min. The HCl 0.1 N was added to quench the reaction. The crude product was extracted by ethyl acetate then dried using $MgSO_4$. The desired compound was purified by column chromatography (silica gel, hexane:ethyl acetate 2:1).

N-benzyl-2-(4-((1E,6E)-7-(4-hydroxy-3-methoxyphenyl)-3,5-dioxohepta-1,6-dien-1-yl)-2-(trifluoromethyl)phenoxy)acetamide (N). Yield: 47%. ^{1}H-NMR (400 MHz, CD_2Cl_2): δ (ppm) 3.97 (-CH_3, s, 3H), 4.56 (-CH_2, d, 2H), 4.69 (-CH_2, s, 2H), 5.89 (-CH_2, s, 2H), 6.57 (=CH, d, 1H), 6.64 (=CH, d, 2H), 6.92 (=CH, d, 2H), 7.09 (=CH, d, 1H), 7.14 (=CH, d, 1H), 7.17 (=CH, d, 1H), 7.19 (=CH, d, 1H) 7.3-

7.4 (=CH, d, 5H), 7.62 (=CH, d, 1H), 7.65 (=CH, d, 2H), 7.75 (=CH, d, 1H), 7.85 (=CH, s, 1H), 8.01 (-NH, s, 1H). ^{13}C-NMR (125 MHz, DMSO-d_6) 42.46, 56.19, 68.02, 101.89, 111.89, 115.01, 116.15, 118.24 ($J_{c\text{-}f}$= 30, q), 121.55, 123.88, 124.36 ($J_{c\text{-}f}$= 270.8, q), 124.39, 126.69, 127.37 ($J_{c\text{-}f}$= 4.2, q), 127.71, 128.33, 128.79, 134.15, 138.36, 139.39, 141.97, 148.47, 150.01, 157.41, 167.16, 182.04, 185.15. ^{19}F-NMR (475 MHz, DMSO-d_6): δ (ppm) 60.68. HRMS-ESI: *m/z* calcd for $C_{30}H_{25}F_3NO_6^-$ 552.1639; found 552.1630 $[M-H]^-$. HPLC Purity 98.1%, retention time 6.20 min.

Preparation of Aβ monomer and fibril

The procedure for solubilizing the Aβ was slightly modified according to the known literature.[30] Isoform of Aβ used in this study is the Aβ with 42-amino acid residue. To prepare the Aβ monomer stock, 0.5 mg of the lyophilized Aβ (Peptide Institute) was dissolved in NaOH 2 mM by gently mixing without vortexing to obtain 500 µM as the final concentration. The solution was centrifuged at 13,200 rpm, 4^{o}C, and 10 min. Aβ fibril was prepared by incubating Aβ monomer at concentration 20 µM in PBS pH 7.4 for 24 h at 37 ^{o}C.

Thioflavin T Assay

The Thioflavin T (ThT) stock at 2 mM was freshly prepared in tris glycine 10 mM pH 8.5. To observe the aggregation kinetics of Aβ, ThT was diluted by PBS pH 7.4 to reach a final concentration of 40 µM. The Aβ was added to get a final concentration of 20 µM then incubated at 37 ^{o}C to stimulate the aggregation process, monitored based on the fluorescence intensity measured at Ex/Em 430/480 nm using a microplate reader (Tecan Infinite F200, Tecan, Switzerland). This assay was conducted in 384-well plate full black non-binding with frequent 15s of linear shaking every 5 min. To the determination the inhibitory activity of aggregation process, curcumin derivatives in serial concentrations was added and incubated along with Aβ following the procedure in Chapter 2.4.

Congo Red Assay

Congo Red (CR) stock at concentration 2 mM was freshly prepared in tris glycine 10 mM pH 8.5, then diluted in PBS at pH 7.4 to reach a final concentration of 40 µM. Curcumin derivatives were added at final concentration of 10 µM followed by Aβ to reach the final concentration of 20 µM then was incubated at 37 ^{o}C. After 24 h, the mixture was transferred in 384-well plate black bottom non-binding to be scanned the fluorescence intensity with an excitation of 490 nm and emission range from 510 to 700 nm using a microplate reader (SpectraMax iD5, Molecular Device, USA).

Quenching Study

The ThT or CR stock at concentration 2 mM was diluted into 40 µM in PBS at pH 7.4. Curcumin derivatives (1 µM) were added to the mixture, then fluorescence spectra were recorded with excitation of 430 nm and emission range from 450 to 500 nm for ThT and excitation of 490 nm and emission range from 510 to 700 nm for CR.

Negative Stained TEM

Elastic carbon grids (ELS-C10, STEM, Japan) was hydrolyzed by ion coater (IB-2, Eiko, Japan) with 3 mA of plasma current for 40 s before applying sample solution. Briefly, 5 µL of Aβ solution with or without curcumin derivatives was applied to a hydrophilic grid and incubated for 1 min at RT. After gently drying with filter paper, the grid sample was washed with Milli-Q water and dried again two times. Finally, the grid was incubated with 5 µL of 1% Nano-W negative staining solution (NY, USA) for 1 min followed by complete drying using filter paper. The negative stained sample was observed using TEM H-8100 (Hitachi) operated at 200 kV.

Cell Culture

The N2a cells were cultured in Dulbecco's Modified Eagle Medium (DMEM) medium supplemented with 10% fetal bovine serum. Briefly, N2a cells (5 x 10^3 cells/well) were grown overnight on a 96-well plate overnight at 37 ^{o}C CO_2 5%. The evaluation of protective effect was conducted by treating the N2a cells with

monomeric Aβ (20 μM) and pre-formed Aβ fibril in the absence or presence of curcumin derivatives 1 μM.

MTT Assay

An MTT reduction assay was conducted as described previously.[31] Briefly, MTT powder was dissolved in PBS pH 7.4 to obtain 5 mg/mL concentration stock, then was diluted into 0.5 mg/mL in DMEM medium. After removing the medium on a 96-well plate containing-treated cell, each well was added by 100 μL MTT 0.5 mg/mL and incubated at 37 ºC CO_2 5%. After 3 h incubation, the medium was removed, and 100 μL DMSO was added following the absorbance measurement at wavelength of 550 nm using a microplate reader (Tecan Infinite F200, Tecan, Switzerland). Calculation of % cells viability was measured by dividing the absorbance of untreated cells with the absorbance of curcumin-treated cells after absorbance correction.

Immunofluorescence Staining

N2a (1 x 10^4 cells/well) was cultured on cover glass in a 6-well plate overnight at 37 ºC CO_2 5%. Cells were treated with Aβ fibril (10 μM) and curcumin derivatives (1 μM) and incubated for 24 h. After washing with PBS, cells were fixed by 4% paraformaldehyde for 20 min. Cells were rewashed by PBS before permeabilizing by 0.1% Triton X-100 in PBS for 10 min. After additional washing by PBS, cells were blocked by 2% BSA in PBS for 30 min. After further washing by PBS, it was followed by incubation with primary anti-Aβ fibril (OC) monoclonal antibody conjugated with fluorescence dye ATTO594 (1:100 in 2% BSA, StressMarq; SPC-507D) for 1 h. Non-specifically bound primary antibody was washed by PBS before the incubation with primary anti-β-actin monoclonal antibody (1:300 in 2% BSA, santa cruz; sc-47778) for 1 h followed by 1 h incubation with secondary antibody anti-mouse IgG (1:300 in 2% BSA, santa cruz: sc-2010). Cells were rewashed by PBS, and the nucleus was stained by Hoechst 33342 (dojindo; 346-07951). All images were recorded by a Zeiss LSM 780 confocal microscope.

Brain Permeability Study

Curcumin and Compound **N** were dissolved in DMSO followed by kolliphor, then stirred for 30 min. The mixture was added by PBS until the concentration of curcumin, DMSO, and kolliphor reached 1 mM, 1%, and 15%, respectively. After stirring for 15 min, the mixture was sonicated for 15 min to homogenize the emulsion. The emulsion was sterilized by filtration and stored at room temperature until used. The Slc:ddY mice were injected intravenously from the tail with emulsion. After 1 h, mice were sacrificed and collected their heart, liver, lung, kidney, spleen, and brain. After gently washing the organs with saline, the fluorescence profile was measured by IVIS imaging with Ex/Em 430/520 for curcumin and 430/540 for compound **N**. All protocols for *in vivo* study were approved by the Institutional Animal Care and Use Committee of Tokyo Institute of Technology.

Fly Strains

Flies were maintained at 25°C on standard fly food. Male flies were used in the experiment. *Elav-Gal* (#458) was obtained from the Bloomington *Drosophila* Stock Center (BDSC, Bloomington, IN, USA). *UAS-Aβ1-42#1* and *UAS-Aβ1-42#3* were kindly provided by Dr. Tsuda.[3]

Locomotor behavior

The climbing assay was based on a method previously described.[32] In brief, flies were reared at 25 °C, and adult flies one to five days old were collected and placed in a vial containing a compound. The compounds were 25 μM of curcumin, compound **B**, or compound **N** in Formula 4-24 Blue *Drosophila* Medium (Fujifilm Wako Pure Chemical Corporation, Osaka, Japan). After one day or two weeks at 25 °C, locomotor behavior was measured by climbing assay. Ten flies were distributed in an empty vial and allowed to adapt for 5 min at room temperature. The flies were tapped down to the bottom. Then flies climbed above 4 cm in 10 s were counted, and the percentage was calculated. This ratio was defined as the climbing index in this study. After resting for 1 min, the above procedure was performed 5 times per vial, and the average was obtained. Statistical analyses were

performed using Prism 9 (GraphPad Software, San Diego, CA, USA). Data were analyzed using multiple comparison ANOVA with the Kruskal-Wallis test and Dunn's multiple comparisons between groups. The null hypothesis was rejected at a 0.05 level of significance.

4.5. References

(1) Sevigny, J.; Chiao, P.; Bussière, T.; Weinreb, P. H.; Williams, L.; Maier, M.; Dunstan, R.; Salloway, S.; Chen, T.; Ling, Y.; O'Gorman, J.; Qian, F.; Arastu, M.; Li, M.; Chollate, S.; Brennan, M. S.; Quintero-Monzon, O.; Scannevin, R. H.; Arnold, H. M.; Engber, T.; Rhodes, K.; Ferrero, J.; Hang, Y.; Mikulskis, A.; Grimm, J.; Hock, C.; Nitsch, R. M.; Sandrock, A. The Antibody Aducanumab Reduces Aβ Plaques in Alzheimer's Disease. *Nature* **2016**, *537* (7618), 50–56.

(2) Cummings, J.; Aisen, P.; Lemere, C.; Atri, A.; Sabbagh, M.; Salloway, S. Aducanumab Produced a Clinically Meaningful Benefit in Association with Amyloid Lowering. *Alzheimers Res Ther* **2021**, *13* (1), 98.

(3) Lemere, C. A. Immunotherapy for Alzheimer's Disease: Hoops and Hurdles. *Mol Neurodegener* **2013**, *8* (1), 36.

(4) Low, K. J. Y.; Venkatraman, A.; Mehta, J. S.; Pervushin, K. Molecular Mechanisms of Amyloid Disaggregation. *J Adv Res* **2022**. 36, 113-132

(5) Yang, F.; Lim, G. P.; Begum, A. N.; Ubeda, O. J.; Simmons, M. R.; Ambegaokar, S. S.; Chen, P. P.; Kayed, R.; Glabe, C. G.; Frautschy, S. A.; Cole, G. M. Curcumin Inhibits Formation of Amyloid β Oligomers and Fibrils, Binds Plaques, and Reduces Amyloid in Vivo. *J. Biol. Chem.* **2005**, *280* (7), 5892–5901.

(6) Small, G. W.; Siddarth, P.; Li, Z.; Miller, K. J.; Ercoli, L.; Emerson, N. D.; Martinez, J.; Wong, K.-P.; Liu, J.; Merrill, D. A.; Chen, S. T.; Henning, S. M.; Satyamurthy, N.; Huang, S.-C.; Heber, D.; Barrio, J. R. Memory and Brain Amyloid and Tau Effects of a Bioavailable Form of Curcumin in Non-Demented Adults: A Double-Blind, Placebo-Controlled 18-Month Trial. *Am J Geriatr Psychiatry* **2018**, *26* (3), 266–277.

(7) Cox, K. H.; Pipingas, A.; Scholey, A. B. Investigation of the Effects of Solid Lipid Curcumin on Cognition and Mood in a Healthy Older Population. *J Psychopharmacol* **2015**, *29* (5), 642–651.

(8) Bouleau, S.; Tricoire, H. Drosophila Models of Alzheimer's Disease: Advances, Limits, and Perspectives. *J Alzheimers Dis* **2015**, *45* (4), 1015–1038.

(9) Jeon, Y.; Lee, J. H.; Choi, B.; Won, S.-Y.; Cho, K. S. Genetic Dissection of Alzheimer's Disease Using Drosophila Models. *Int J Mol Sci* **2020**, *21* (3), 884.

(10) Iijima, K.; Liu, H.-P.; Chiang, A.-S.; Hearn, S. A.; Konsolaki, M.; Zhong, Y. Dissecting the Pathological Effects of Human Aβ40 and Aβ42 in Drosophila: A Potential Model for Alzheimer's Disease. *PNAS* **2004**, *101* (17), 6623–6628.

(11) Finelli, A.; Kelkar, A.; Song, H.-J.; Yang, H.; Konsolaki, M. A Model for Studying Alzheimer's Aβ42-Induced Toxicity in Drosophila Melanogaster. *Mol Cell Neurosci* **2004**, *26* (3), 365–375.

(12) Crowther, D. C.; Kinghorn, K. J.; Miranda, E.; Page, R.; Curry, J. A.; Duthie, F. A. I.; Gubb, D. C.; Lomas, D. A. Intraneuronal Aβ, Non-Amyloid Aggregates and Neurodegeneration in a Drosophila Model of Alzheimer's Disease. *Neuroscience* **2005**, *132* (1), 123–135.

(13) McKhann, G.; Drachman, D.; Folstein, M.; Katzman, R.; Price, D.; Stadlan, E. M. Clinical Diagnosis of Alzheimer's Disease: Report of the NINCDS-

ADRDA Work Group* under the Auspices of Department of Health and Human Services Task Force on Alzheimer's Disease. *Neurology* **1984**, *34* (7), 939–939.
(14) Carrillo, M. C.; Rowe, C. C.; Szoeke, C.; Masters, C. L.; Ames, D.; O'Meara, T.; Macaulay, S. L.; Milner, A.; Ellis, K. A.; Maruff, P.; Rainey-Smith, S. R.; Martins, R. N.; Bain, L. J.; Head, R. J. Research and Standardization in Alzheimer's Trials: Reaching International Consensus. *Alzheimers Dement* **2013**, *9* (2), 160–168.
(15) Pandey, U. B.; Nichols, C. D. Human Disease Models in Drosophila Melanogaster and the Role of the Fly in Therapeutic Drug Discovery. *Pharmacol Rev* **2011**, *63* (2), 411–436.
(16) Hudson, S. A.; Ecroyd, H.; Kee, T. W.; Carver, J. A. The Thioflavin T Fluorescence Assay for Amyloid Fibril Detection Can Be Biased by the Presence of Exogenous Compounds. *FEBS J* **2009**, *276* (20), 5960–5972.
(17) Wickramasinghe, A.; Xiao, Y.; Kobayashi, N.; Wang, S.; Scherpelz, K. P.; Yamazaki, T.; Meredith, S. C.; Ishii, Y. Sensitivity-Enhanced Solid-State NMR Detection of Structural Differences and Unique Polymorphs in Pico- to Nanomolar Amounts of Brain-Derived and Synthetic 42-Residue Amyloid-β Fibrils. *J. Am. Chem. Soc.* **2021**, *143* (30), 11462–11472.
(18) Bieschke, J.; Russ, J.; Friedrich, R. P.; Ehrnhoefer, D. E.; Wobst, H.; Neugebauer, K.; Wanker, E. E. EGCG Remodels Mature α-Synuclein and Amyloid-β Fibrils and Reduces Cellular Toxicity. *PNAS* **2010**, *107* (17), 7710–7715.
(19) Ladiwala, A. R. A.; Lin, J. C.; Bale, S. S.; Marcelino-Cruz, A. M.; Bhattacharya, M.; Dordick, J. S.; Tessier, P. M. Resveratrol Selectively Remodels Soluble Oligomers and Fibrils of Amyloid Aβ into Off-Pathway Conformers. *J Biol Chem* **2010**, *285* (31), 24228–24237.
(20) Du, W.-J.; Guo, J.-J.; Gao, M.-T.; Hu, S.-Q.; Dong, X.-Y.; Han, Y.-F.; Liu, F.-F.; Jiang, S.; Sun, Y. Brazilin Inhibits Amyloid β-Protein Fibrillogenesis, Remodels Amyloid Fibrils and Reduces Amyloid Cytotoxicity. *Sci Rep* **2015**, *5*, 7992.
(21) Ono, K.; Tsuji, M. Protofibrils of Amyloid-β Are Important Targets of a Disease-Modifying Approach for Alzheimer's Disease. *Int J Mol Sci* **2020**, *21* (3), 952.
(22) Thapa, A.; Jett, S. D.; Chi, E. Y. Curcumin Attenuates Amyloid-β Aggregate Toxicity and Modulates Amyloid-β Aggregation Pathway. *ACS Chem. Neurosci.* **2016**, *7* (1), 56–68.
(23) Ochiishi, T.; Doi, M.; Yamasaki, K.; Hirose, K.; Kitamura, A.; Urabe, T.; Hattori, N.; Kinjo, M.; Ebihara, T.; Shimura, H. Development of New Fusion Proteins for Visualizing Amyloid-β Oligomers in Vivo. *Sci Rep* **2016**, *6* (1), 22712.
(24) Lee, H. N.; Sim, K. M.; Kim, H.; Ju, J.; Pae, A. N.; Park, J.-B.; Ryu, H.; Seong, J. Aβ Modulates Actin Cytoskeleton via SHIP2-Mediated Phosphoinositide Metabolism. *Sci Rep* **2019**, *9* (1), 15557.
(25) Song, C.; Perides, G.; Wang, D.; Liu, Y. F. β-Amyloid Peptide Induces Formation of Actin Stress Fibers through P38 Mitogen-Activated Protein Kinase. *J Neurochem* **2002**, *83* (4), 828–836.

(26) Nagashima, N.; Ozawa, S.; Furuta, M.; Oi, M.; Hori, Y.; Tomita, T.; Sohma, Y.; Kanai, M. Catalytic Photooxygenation Degrades Brain Aβ in Vivo. *Sci. Adv.* **2021**, *7* (13).
(27) Kang, Y. Y.; Choi, I.; Chong, Y.; Yeo, W.-S.; Mok, H. Complementary Analysis of Curcumin Biodistribution Using Optical Fluorescence Imaging and Mass Spectrometry. *Appl Biol Chem* **2016**, *59* (2), 291–295.
(28) Kang, Y. Y.; Song, J.; Kim, J. Y.; Jung, H.; Yeo, W.-S.; Lim, Y.; Mok, H. Byakangelicin as a Modulator for Improved Distribution and Bioactivity of Natural Compounds and Synthetic Drugs in the Brain. *Phytomedicine* **2019**, *62*, 152963.
(29) Dei Cas, M.; Ghidoni, R. Dietary Curcumin: Correlation between Bioavailability and Health Potential. *Nutrients* **2019**, *11* (9), 2147.
(30) Mohamed, T.; Shakeri, A.; Tin, G.; Rao, P. P. N. Structure–Activity Relationship Studies of Isomeric 2,4-Diaminoquinazolines on β-Amyloid Aggregation Kinetics. *ACS Med. Chem. Lett.* **2016**, *7* (5), 502–507.
(31) Mosmann, T. Rapid Colorimetric Assay for Cellular Growth and Survival: Application to Proliferation and Cytotoxicity Assays. *J Immunol Methods* **1983**, *65* (1), 55–63.
(32) Cunningham, P. C.; Waldeck, K.; Ganetzky, B.; Babcock, D. T. Neurodegeneration and Locomotor Dysfunction in Drosophila Scarlet Mutants. *J Cell Sci* **2018**, *131* (18), jcs216697.

^{1}H-NMR Profile of N-benzyl-2-(4-formyl-2-(trifluoromethyl)phenoxy)acetamide

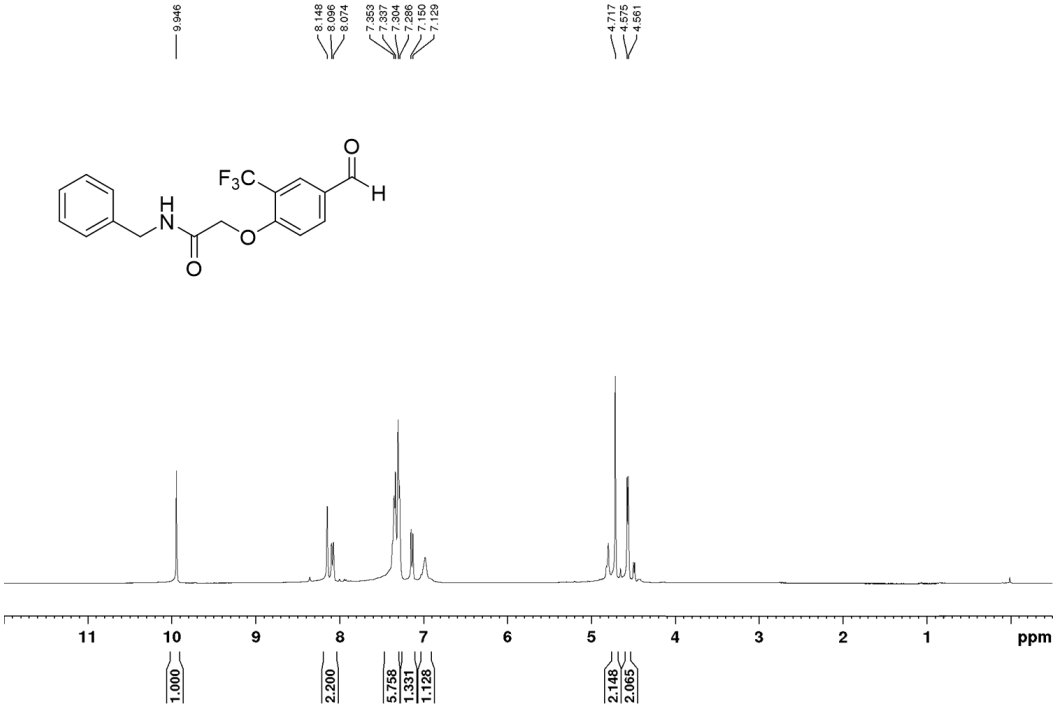

^{13}C-NMR Profile of N-benzyl-2-(4-formyl-2-(trifluoromethyl)phenoxy)acetamide

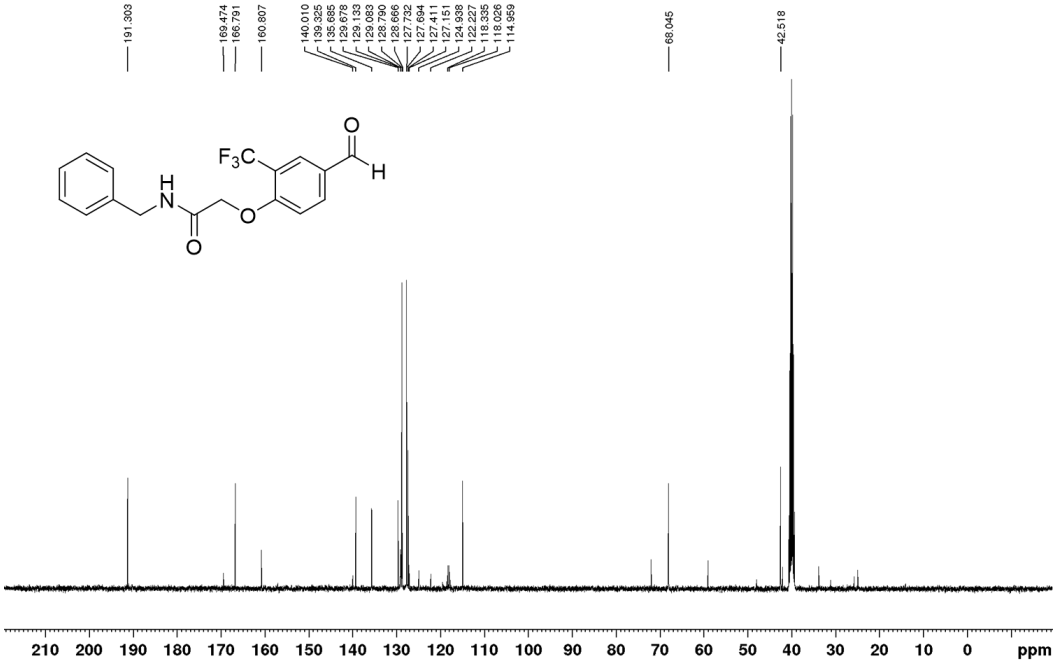

^{19}F-NMR Profile of N-benzyl-2-(4-formyl-2-(trifluoromethyl)phenoxy)acetamide

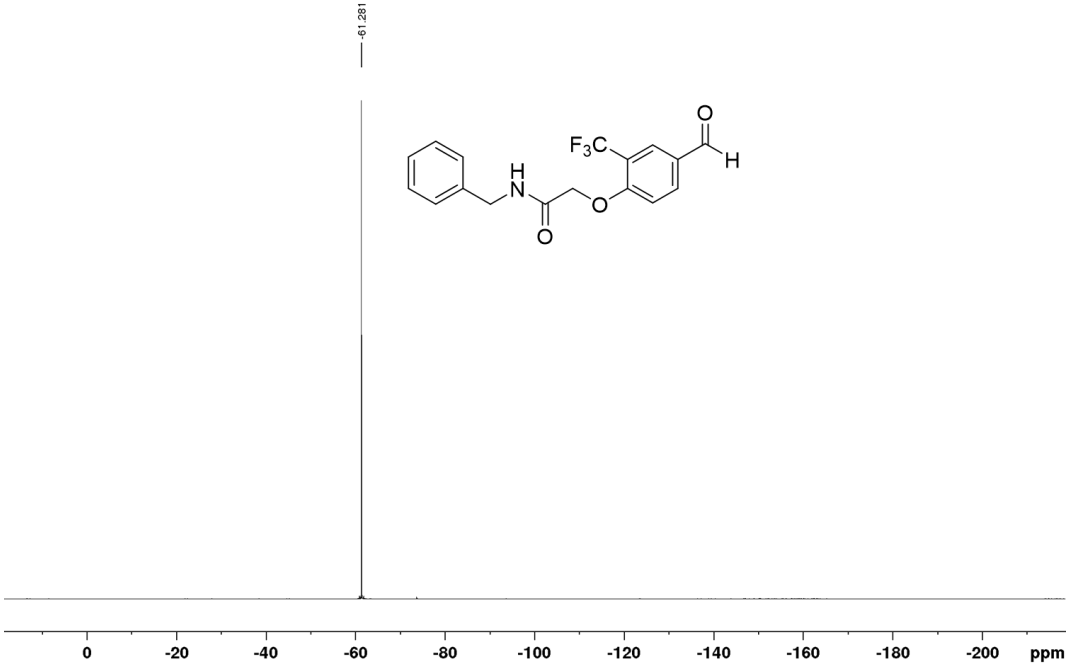

^{1}H-NMR Profile of N-benzyl-2-(4-((1E,6E)-7-(4-hydroxy-3-methoxyphenyl)-3,5-dioxohepta-1,6-dien-1-yl)-2-(trifluoromethyl)phenoxy)acetamide

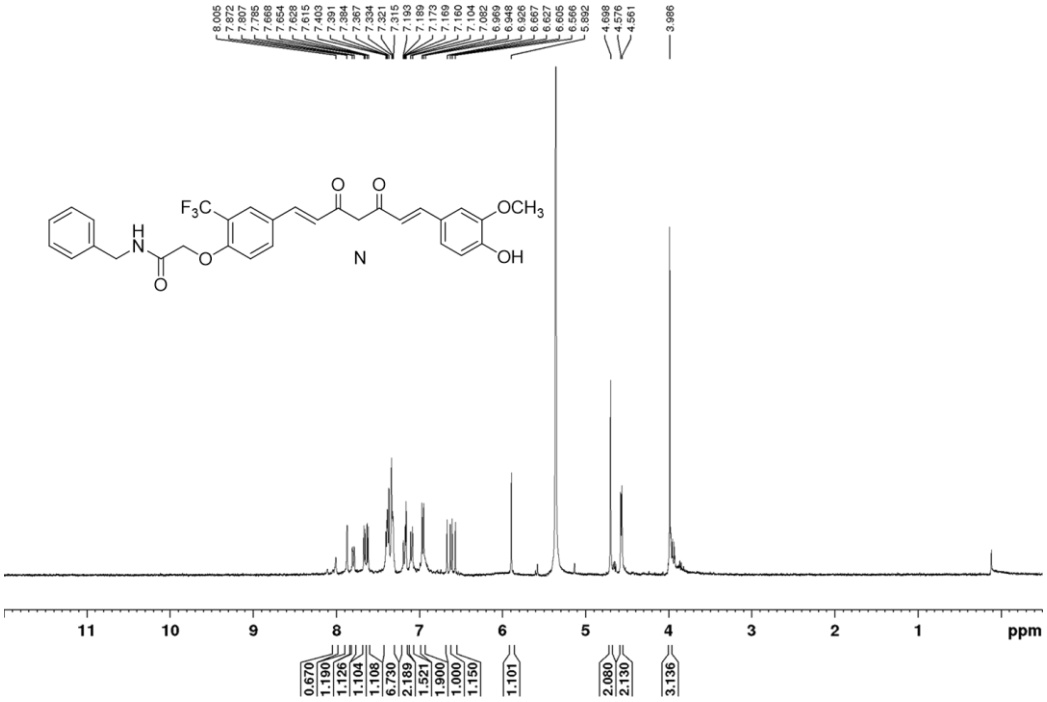

^{13}C-NMR Profile of N-benzyl-2-(4-((1E,6E)-7-(4-hydroxy-3-methoxyphenyl)-3,5-dioxohepta-1,6-dien-1-yl)-2-(trifluoromethyl)phenoxy)acetamide

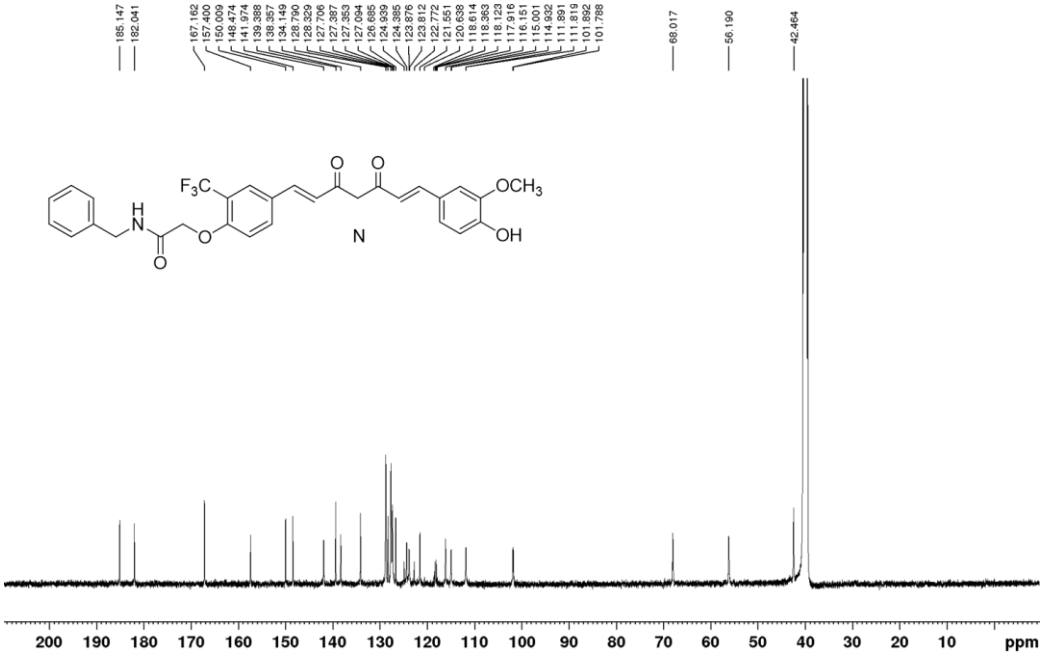

^{19}F-NMR Profile of N-benzyl-2-(4-((1E,6E)-7-(4-hydroxy-3-methoxyphenyl)-3,5-dioxohepta-1,6-dien-1-yl)-2-(trifluoromethyl)phenoxy)acetamide

HPLC Profile of Compound **N**

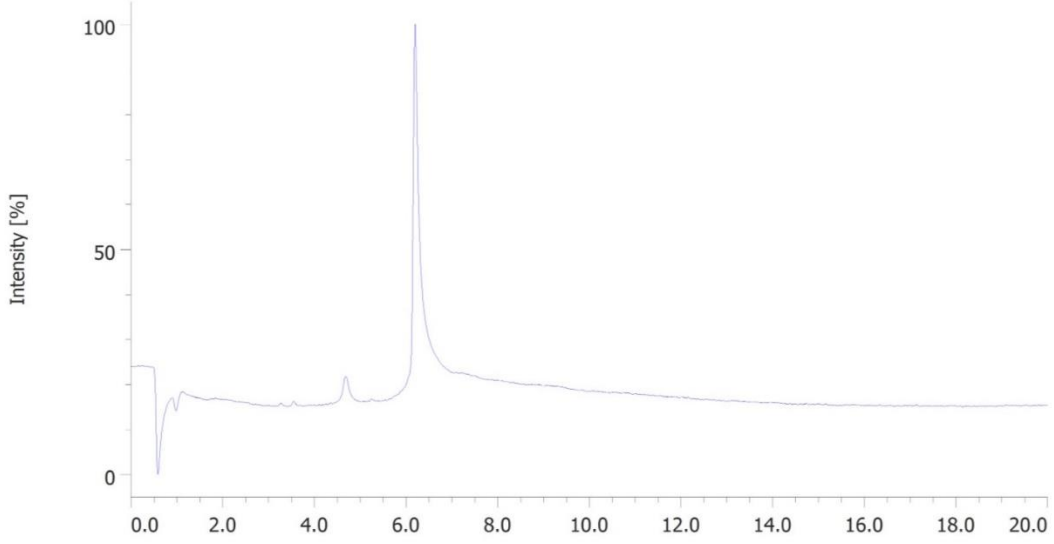

Chapter 5
Conclusion

Chapter 5. Conclusion

This study aims to utilize SARM for developing Aβ inhibitors and their further application on designing Gd-based MRI contrast agent targeting Aβ. In chapter 1, the importance of Aβ as the target of drug and biomarker of AD is discussed. This chapter also describes the progress of drug candidates targeting Aβ, especially curcumin, which shows promising results in preclinical studies but has limitations in the clinical study mainly due to the requirement of high dose and side effects. The preclinical study about the application of curcumin structures to MRI contrast agents targeting Aβ is also discussed.

Chapter 2 introduces the successful application of SARM on designing curcumin derivatives and avoiding the possible compounds with PAINS profiles. Based on curcumin derivatives-activity cliff and MGM analysis, compound **B** was identified as a potent Aβ inhibitor. Inhibition of Aβ aggregation by compound **B** caused the increase of Aβ oligomers in a concentration-dependent manner so that it attenuated Aβ-induced cytotoxicity. In chapter 2 also introduces compound **K**, in which the *tert*-butyl ester replaced the methyl ester of compound **B**. Compound **K** also showed considerable inhibitory activity and attenuated the cytotoxicity of Aβ, suggesting the possibility of further optimization by modifying the ester group of compound **B**.

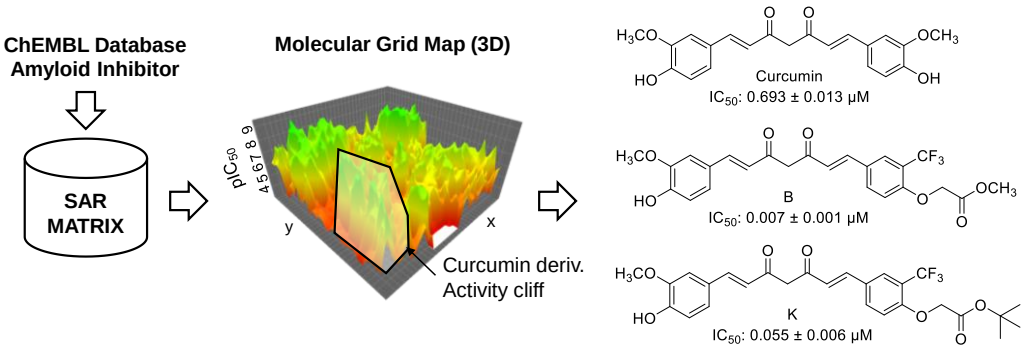

Figure 5-1. Summary of Chapter 2

Chapter 3 demonstrates the further application of a curcumin derivative generated from SARM, compound **B** as the ligand for Gd-based MRI contrast agent (**Gd-DO3A-Comp.B**). **Gd-DO3A-Comp.B** sensitively detected Aβ fibril based on T_1 measurement, and the inhibitory activity could be estimated by T_1 change

depending on the growth stage of Aβ fibril formation. Such unique modalities would be useful for diagnostics and for the direct evaluation of the therapeutic efficacy *in vivo*.

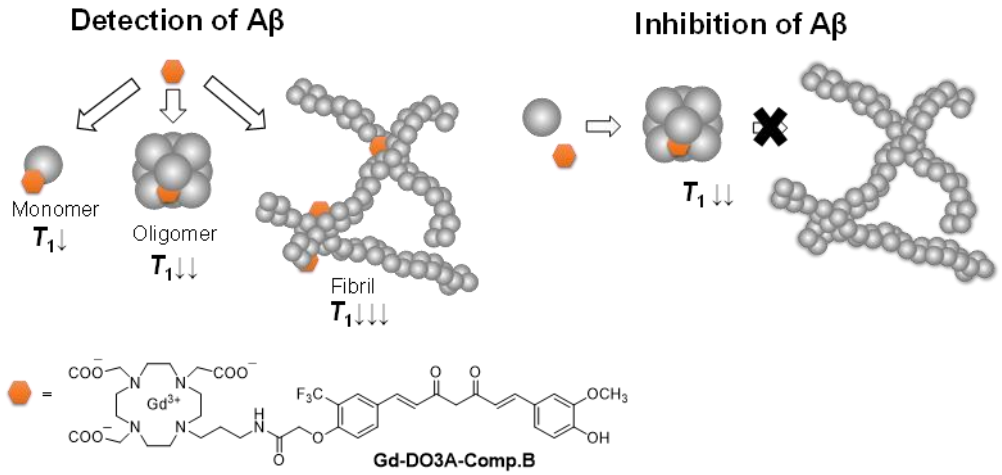

Figure 5-2. Summary of Chapter 3

In chapter 4, compound **B** and its derivative, compound **N**, were proposed as the inducer of Aβ fibril disaggregation. Besides strongly inhibiting the fibril formation, both compounds also induced amyloid disaggregation at low concentrations, allowing the alleviation of Aβ fibril-induced toxicity in neuroblastoma cells. By their ability to accumulate in the brain, both compounds rescued the locomotor dysfunction of AD-model flies caused by Aβ toxicity. These results suggested that compounds **B** and **N** might be promising for clinical applications, considering the problem of BBB permeability common to AD therapeutic candidates.

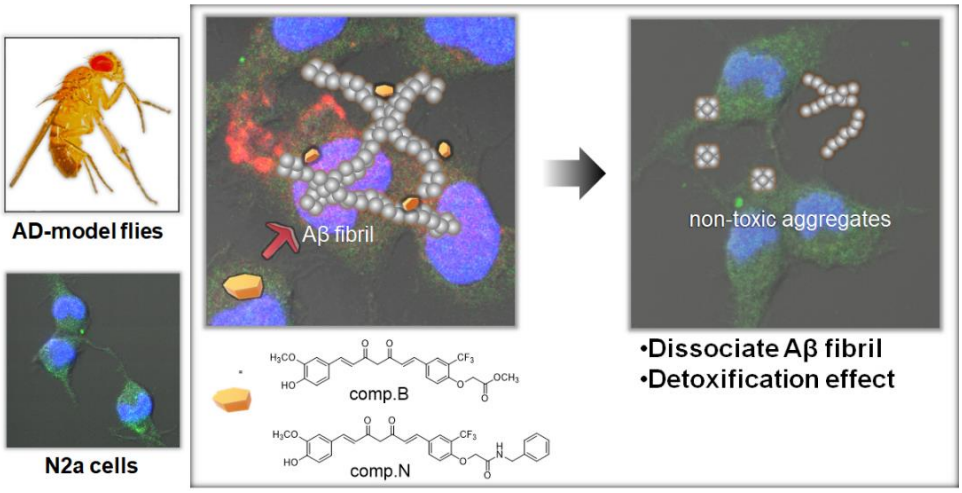

Figure 5-3. Summary of Chapter 4

Acknowledgment

Alhamdulillah, all praise to the Most Gracious, the Most Merciful, Allah.

I would like to express my sincere respect and gratitude to Prof. Hiroyuki Nakamura for his excellent supervision, invaluable support, patience, motivation, and sincere care during my study in the Tokyo Institute of Technology.

My sincere thanks and gratitude go to Assoc. Prof. Satoshi Okada for his support, sharing, and patience about my research and social life during my stay on the lab.

I would like to thank to Assist. Prof. Dr. Taiki Morita, Dr. Kazuki Miura for the discussion and invaluable guidance for my research project.

I would like to the thank former staff in our lab, Prof. Shinichiro Fuse and Dr. Shinichi Sato, for supporting me with many research experiences and kindness during my first year in this lab.

My gratitude also goes to Ms. Toshie Matsumoto and former secretary Ms. Junko Ikeda for their endless help supporting my study.

I would like to thank all the collaborators, Dr. Atsushi Yoshimori (ITM, Japan) and Prof. Jürgen Bajorath (Univ. Bonn, Germany) for supporting the SARM study, Dr. Hyun Seung Ban (KRIBBS, Korea) for establishing the ThT Assay, Dr. Akira Sumiyoshi & Prof. Ichio Aoki (QST, Japan) for facilitating MRI experiments, and Dr. Atsushi Sugie (Univ. Niigata, Japan) for providing Drosophila studies.

I would like to send my gratitude to my doctoral thesis review committee: Prof. Katsunori Tanaka, Prof. Nobuhiro Nishiyama, Dr. Hiroshi Tsusumi, Dr. Toshinori Fujie, and Dr. Hiroyuki Akama, for their constructive comments and encouragements.

I also would like to thank my fellow Doctoral students, Dr. Yasunobu Asawa, and Dr. Hiroki Ueda, for their friendly atmosphere and scientific discussions.

I thank the former Doctoral students Dr. Yuma Otake and Dr. Michihiko Tsushima for their valuable experience and help in my research and life.

I thank Mr. Masato Tsuda and Mr. Kohei Umedera for their friendship and priceless help.

I thank Mr. Hiroki Murakami, Mr. Kai Nishimura, Mr. Aaron Chang, Ms. Ayana Uehara, Ms. Qarri Ainaya, and Ms. Yijin Wen for their kindness and inspiring works.

I thank Mr. Tomoyuki Araki, Ms. Yuka Takashima, Ms. Yuka Muto, Ms. Non Ito, Mr. Shota Saiki, Mr. Tomoya Doi, Mr. Kentaro Makino, Mr. Akito Mochizuki, Ms. Dhina Fitriastuti, Ms. Yujie Shao, Mr. Shunya Kitahara, Mr. Kakeru Miyamoto, and Mr. Nao Yamamoto.

I also thank to other former member in our labs Dr. Somaraju Yugandar, Dr. Joshi Manjusha, Mr. Kazuki Kawai, Mr. Koshiro Masuda, Mr. Wataru Moriya, Ms. Shangze Wu, Mr. Naoto Sugisawa, Mr. Keiji Komuro, Mr. Keita Nakane, Mr. Jeff Deloso Dela Cruz, Mr. Hiroshi Kitamura, Mr. Takumi Ogawara, Mr. Kiyotaka Dohmae, Mr. Manchun Wong, Mr. Jun-Sik Kim, and Ms. Suzanna Harrison.

I would like to thank my former research supervisor in Indonesia, Prof. Edy Meiyanto, for the discussion, kind guidance, help, patience, and encouragement during my study.

I thank the Directorate General of Higher Education, Ministry of Education and Culture of the Republic of Indonesia and the Faculty of Pharmacy Universitas Gadjah Mada (UGM) for permitting me to study abroad. I received support from UGM during my early period in Japan.

I thank Ajinomoto for supporting me with a scholarship during my study and for their continuous support in general.

This dissertation is dedicated to my beloved family, alma mater, and country.